Institute of Geophysics
Polish Academy of Sciences

PUBLICATIONS
OF THE INSTITUTE OF GEOPHYSICS
POLISH ACADEMY OF SCIENCES

Geophysical Data Bases, Processing and Instrumentation

438 (P-3)

MONOGRAPHIC VOLUME

The Influence of Topography and Vegetation on the Snow Cover in Tundra: Case Study from the Southern Spitsbergen Area

Daniel Dawid Kępski

Warsaw 2021 (Issue 4)

INSTITUTE OF GEOPHYSICS
POLISH ACADEMY OF SCIENCES

PUBLICATIONS
OF THE INSTITUTE OF GEOPHYSICS
POLISH ACADEMY OF SCIENCES

Geophysical Data Bases, Processing and Instrumentation

438 (P-3)

MONOGRAPHIC VOLUME

The Influence of Topography and Vegetation on the Snow Cover in Tundra: Case Study from the Southern Spitsbergen Area

Daniel Dawid Kępski

Warsaw 2021

ISBN 978-83-66254-09-1 eISSN-2299-8020
DOI: 10.25171/InstGeoph_PAS_Publs-2021-041

Editorial Office
Instytut Geofizyki Polskiej Akademii Nauk
ul. Księcia Janusza 64, 01-452 Warszawa

C O N T E N T S

Editorial note

The present publication is a revised version of the Author's PhD thesis defended at the Institute of Geophysics, Polish Academy of Sciences, under supervision of Prof. Krzysztof Migała and Dr. Bartłomiej Luks.

Acknowledgments

This work has been (partially) financed from the funds of the Leading National Research Centre (KNOW) received by the Centre for Polar Studies for the period 2014–2018. The author was awarded in the 7th edition of Anna Pasek Scientific Grant Program and would like to thank the foundation for their support in 2015/2016. Time-lapse camera imagery were collected during Snow Monitoring Using Automatic Camera Systems at Svalbard Key Sites project (project No. 236768/E10; Svalbard Science Forum, Research Council of Norway) and Landsat 8 images were available by courtesy of the U.S. Geological Survey. Fieldworks were possible thank to Svalbard Science Forum funds in form of Arctic Field Grant No. 257119/E10 "Evolution of spatial variability and physico-chemical properties of snow on coastal tundra of the Hornsund fjord during the spring season". I wish also to thank the Norwegian Polar Institute for sharing their cartographic resources via npolar.no website.

I would also like to thank all those who helped in the formation of this work, in particular to:

Supervisor Prof. Krzysztof Migała for introducing me to the polar world and for recommending me as a candidate for the 36th polar expedition of the Polish Academy of Sciences, as well as for all advice and assistance during my research work at doctoral studies;

Dr. Bartłomiej Luks for his patience and help in all matters (especially concerning the English language), and for being a "good cop";

The whole overwinter crew of the 36th PAS Polar Expedition for a wonderful year spent together, and in particular to the expedition leader, Dr. Piotr Dolnicki, for choosing me to the wintering team. This work would certainly not have been written without "polar fever", that I got on our expedition;

Participants of the 37th–40th polar expeditions overwintering in Hornsund station, for collecting data used in this study. Especially to meteorologists, who, partly because of me, got extremely tedious work of weekly snow measurements in the Fuglebekken catchment area. Special thanks to the members of the 38th expedition for warmly welcoming me to the station and spending 2 months together in spring 2016;

PhD students of the Center for Polar Studies for a fantastic time together and a joint exploration of Silesian, Tri-City or Warsaw pubs at monthly KNOW conventions;

Employees of the Polar and Marine Research Department for any substantive help and a warm atmosphere at the workplace;

Co-authors of all scientific papers and presentations for their persistence in enduring my sloppy writing technique. In particular, to Dr. Sebastian Westermann for his great commitment and all help in obtaining Norwegian funds for field research through the Arctic Field Grant;

To everyone who helped me with my frequent and unfortunate relocations in Warsaw: Krzysztof Mitelsztedt, Szymon Szyszko, Dr. Adam Nawrot and Dr. Mateusz Moskalik. Thanks for providing shelter in difficult times and for help with move my belongings from place to place;

At the end, to my parents for providing decent learning conditions, thanks to which I managed to start higher education and finally obtain a doctoral degree.

List of symbols and abbreviations

ANOVA	ANalysis Of VAriance
AO	Arctic Oscillation
ARPS	Advanced Regional Prediction System
AWS	Automatic Weather Station
UAV	Unmanned Aerial Vehicle
CAAML	Canadian Avalanche Association Markup Language
CFMask	C function of Mask
CLM	Climate Limited-area Model
CORDEX	COordinated Regional climate Downscaling EXperiment
COSMO	The Consortium for Small-scale Modeling
DBSM	Distributed Blowing Snow Model
DN	Digital Number
DOS	Dark Object Subtraction
GCP	Ground Control Points
GPR	Ground Penetrating Radar
GPS	Global Positioning System
HS	Snow depth
IPCC	Intergovernmental Panel on Climate Change
MPI-ESM	Max Planck Institute Earth System Model
NAO	North Atlantic Oscillation
NDSI	Normalized Difference Snow Index
NDVI	Normalized Difference Vegetation Index
DEM	Digital Elevation Model
NPI	Norwegian Polar Institute
OLI	Operational Land Imager
PBSM	Prairie Blowing Snow Model
PREVAH	Precipitation-Runoff-Evapotranspiration-Hydrotope
PPS	Polish Polar Station
RCP	Representative Concentration Pathways
RMSE	Root Mean Square Error
SCE	Snow Cover Extent
SWE	Snow Water Equivalent
SLF WSL	Swiss Federal Institute for Snow and Avalanche Research
SURF	Speeded-Up Robust Features
Sv	Sverdrup [1 Sv = 10^6 m^3 s^{-1}]
TIRS	Thermal Infrared Sensor
TOA	Top-Of-Atmosphere reflectance
TPI	Topographic Position Index
TRI	Terrain Ruggedness Index
TWI	Topographic Wetness Index
USGS	United States Geological Survey
WMO	World Meteorological Organization

Abstract

The aim of the study was to identify the snow cover distribution in the southern Spitsbergen tundra environment and to quantify its relationship with the topography and land cover. This was achieved by correlating vectorized cartographic materials, modeled climatic parameters and calculated topographic indices with snow cover properties measured in the field and obtained using remote sensing techniques. An important source of information used in the analyzes was time-lapse photography, which, thanks to the developed methodology and created tools, allowed to obtain snow cover extent data characterized by high temporal and spatial resolution. Snow cover distribution in the immediate vicinity of the Polish Polar Station obtained from time-lapse material was related to the results of satellite image classification from the 2014 ablation season. The field data was used to validate the SNOWPACK (predicting snow cover structure) and Alpine3D (predicting snow spatial distribution) models developed by SLF-WSL. They were implemented for the first time in the tundra environment of Svalbard. The models were also used to simulate snow conditions in the vicinity of the Polish Polar Station at the end of the twenty-first century. For this purpose, data from climate projections of the Polar CORDEX initiative were adopted. The worst-case climate change scenario (RCP8.5) was assumed.

The obtained results point to an increased snow deposition during the winter season in the western parts of the valleys, related to the snow redistribution by the dominant eastern wind. However, on a macroscale, the snow cover duration and depth increase eastward with growing distance to the open Greenland Sea. The snow cover extent in the ablation phase shows a relatively strong correlation with the modeled average annual air temperature ($r = –0.78$), precipitation total ($r = 0.57$) and, to a much lesser extent, with the potential insolation ($r = –0.24$). Topographic indices turned out to be important primarily on a local scale. In the Fuglebekken catchment, the strongest impact on the snow cover duration was found for the Terrain Ruggedness Index and Wind Exposition Index, especially for the NE wind. This proves the dominant influence of wind activity on the local snow cover distribution, which is less visible on a larger scale of the entire fiord.

Significant relationships were found between the duration and thickness of the snow cover with the land cover. The longest snow cover persistence was in places devoid of vegetation. On the opposite side there was a plant formation, the tallest of the local vascular plants being the polar willow (Salix polaris). The observed difference in snow ablation time between these two land-cover formations, rock debris and lichen-herb-heath tundra, was approximately two weeks. On the other hand, a greater snow cover thickness during the winter season was found on wet moss tundra. This class is characterized by the highest value of the normalized differential vegetation index (NDVI), which is an indicator of biological productivity. This means complex relationhips between the snow cover and the vegetation, where the development of flora is hindered in accumulation places, with prolonged snow persistence. However, some plant species are well adapted to living under a thicker layer of snow.

The presented results of snow cover modeling did not take into account its redistribution under the influence of wind. Consequently, the snow thickness in the Fuglebekken catchment area was overestimated by an average of 50%. This is the potential amount of snow removed from the tundra by wind activity and associated sublimation. Under changed climatic conditions, with an air temperature increase of about 6.5 °C at the end of the 21st century, the models show a significant reduction of the snow cover period in the tundra. In the projections for 2089-2100, snowfall occurs only in November–May, and in the winter season thaws strong enough to melt completely the snow cover in the middle of winter take place. Additionally, climate projections indicate development of thick ice layers in the future tundra snowpack, which could cause severe environmental effects on both plants and animals.

WPŁYW RZEŹBY I POKRYCIA TERENU NA POKRYWĘ ŚNIEŻNĄ TUNDRY POŁUDNIOWEGO SPITSBERGENU

Streszczenie

Celem pracy było rozpoznanie rozkładu pokrywy śnieżnej w środowisku tundry południowego Spitsbergenu oraz określenie w sposób ilościowy jej związku z topografią i pokryciem terenu. Osiągnięto go porównując zwektoryzowane materiały kartograficzne, modelowane parametry klimatyczne i obliczone indeksy topograficzne ze zmierzonymi w terenie i otrzymanymi dzięki technikom teledetekcyjnym właściwościami pokrywy śnieżnej. Ważnym źródłem danych wykorzystanych w analizach była fotografia poklatkowa, która dzięki opracowanej metodyce i stworzonym narzędziom, pozwoliła pozyskać dane o zasięgu pokrywy śnieżnej charakteryzujące się wysoką rozdzielczością czasową i przestrzenną. Informacje o rozmieszczeniu śniegu w najbliższej okolicy Polskiej Stacji Polarnej otrzymane z obróbki zdjęć z aparatu odniesiono do wyników klasyfikacji zdjęć satelitarnych z sezonu ablacyjnego z 2014 roku. Dane terenowe (sondowania pokrywy śnieżnej i obserwacje cech fizycznych w szurfach) wykorzystano do walidacji wyników modeli: struktury pokrywy śnieżnej SNOWPACK i rozmieszczenia pokrywy śnieżnej Alpine3D (SLF-WSL). Po raz pierwszy zaimplementowano je do działania w środowisku tundry na Svalbardzie. Powyższe modele wykorzystano także do symulacji warunków śnieżnych w okolicy Polskiej Stacji Polarnej pod koniec XXI wieku. Wykorzystano do tego dane z projekcji klimatycznych inicjatywy Polar CORDEX, zakładających brak walki z emisją gazów cieplarnianych (scenariusz RCP8.5).

Otrzymane wyniki wskazują na zwiększone odkładanie się śniegu w ciągu sezonu zimowego w zachodnich częściach dolin związane z redystrybucją śniegu przez dominujący wiatr z kierunku wschodniego. W skali całego wybrzeża fiordu Hornsund stwierdzono natomiast wydłużenie zalegania pokrywy śnieżnej, połączone ze zwiększaniem jej grubości, w kierunku wschodnim, wraz z oddalaniem się od otwartego Morza Grenlandzkiego. Pokrycie terenu śniegiem w fazie ablacyjnej wykazuje stosunkowo silną korelację z modelowanymi średnimi rocznymi temperaturami powietrza ($r = –0,78$), sumami opadów ($r = 0,57$) oraz w znacznie mniejszym stopniu z potencjalnym usłonecznieniem ($r = –0,24$). Zależności między indeksami topograficznymi mają znaczenie przede wszystkim w skali lokalnej. W zlewni Fuglebekken najsilniejszy związek długości zalegania pokrywy śnieżnej znaleziono ze wskaźnikiem szorstkości terenu (*Terrain Ruggedness Index*) oraz jego ekspozycją na wiatr, przede wszystkim z kierunku północno-wschodniego. Świadczy to o dominującym oddziaływaniu przewiewania na lokalne rozmieszczenie pokrywy śnieżnej, które przestaje mieć znaczenie w skali większej – na wybrzeżach fiordu traktowanych jako całość.

Wykazano istotne związki między długością zalegania pokrywy śnieżnej i jej grubością a pokryciem terenu. Miejsca odsłaniające się spod śniegu najpóźniej charakteryzowały się brakiem roślinności, natomiast teren na którym śnieg zalegał najkrócej pokrywał się z występowaniem formacji roślinnej (tundra porostowo-zielno-krzewinkowa) tworzonej przez, m.in., najwyższą z roślin naczyniowych – wierzbę polarną (*Salix polaris*). Zaobserwowana różnica w czasie ablacji śniegu pomiędzy tymi dwoma typami terenu, wyniosła około dwóch tygodni. Większą grubość pokrywy śnieżnej w ciągu sezonu zimowego stwierdzono natomiast

na wilgotnych tundrach mszystych, klasie reprezentowanej przez najwyższą wartość znormalizowanego różnicowego wskaźnika wegetacji (NDVI), świadczącego o bioproduktywności. Oznacza to skomplikowane powiązania między pokrywą śnieżną a roślinną, gdzie rozwój flory jest utrudniony w miejscach o zbyt długim zaleganiu śniegu, przy czym niektóre gatunki roślin charakteryzują się bardzo dobrą kondycją pod grubszą jego warstwą.

Przedstawione wyniki modelowania pokrywy śnieżnej nie uwzględniały jej przewiewania. Skutkowało to przeszacowaniem miąższości śniegu w zlewni Fuglebekken o średnio 50%. Jest to potencjalna ilość śniegu usuwana z terenu tundry przez działalność wiatru i związaną z nią sublimację. W zmienionych warunkach klimatycznych, przy prognozowanym ociepleniu o 6,5 °C do końca XXI wieku, modele wskazują na znaczne skrócenie okresu z pokrywą śnieżną na tundrze. W symulacjach dla lat 2089–2100 opady śniegu występują jedynie w miesiącach listopad–maj, a w trakcie sezonu zimowego pojawiają się odwilże na tyle silne, by doprowadzać do całkowitej ablacji pokrywy śnieżnej w środku zimy. Wyniki modeli dla końca XXI wieku wskazują też na rozwój w pokrywie znacznych warstw lodoszreni, które mogą wywołać poważne skutki środowiskowe zarówno dla roślin jak i zwierząt.

1. INTRODUCTION

Snow cover plays a crucial role in the Arctic ecosystem, where it persists most of the year. On southern Spitsbergen it is present on the ground usually from the first decade of October to the mid-June (Luks 2012). Although most (~60%) of the Svalbard archipelago is glaciated and only about 10% of its surface is covered by tundra vegetation (Hagen et al. 1993; Johansen et al. 2012), the tundra is a living part of this ecosystem and the habitat of most of the terrestrial flora and fauna. Despite this, research on the distribution of snow cover in this part of the Arctic focuses primarily on the glacial zone and is mainly devoted to the issue of the glacier mass balance (Winther et al. 2003). This also applies to the Hornsund area, where snow studies have been carried out since 1957, but the research activity on non-glaciated areas was often only a supplement to hydrochemical studies and concerned mainly individual winter seasons (Migała et al. 1988; Luks 2012).

Despite the generally flat nature of the area covered by tundra vegetation, the distribution of snow cover in this type of area is extremely diverse and depends, above all, on the terrain's micro relief (Sturm and Holmgren 1994). On the other hand, local differences in snow depth affect the spatial differentiation of many elements of the environment: thickness of the active layer (Johansson et al. 2013), ground temperature variability (Dolnicki 2002; Zhang 2005), soil moisture (Williams et al. 2009), length of vegetation season (Cooper et al. 2011), and also the growth and health of plants (Wahren et al. 2005; Wipf 2010). In addition to the snow cover depth, its density and internal structure are also important. Those snow properties determine, e.g., the availability of food for reindeer and thus their numbers, which also influences the abundance of other animals due to trophic relationships (Hansen et al. 2013). In the tundra, areas with very thick snow cover may be adjacent to completely snow-free places due to high wind activity (Gisnås et al. 2014). This results in high variability in the snow cover melting time, followed by irregular absorption of solar radiation by the ground (Hinkler et al. 2003) and disturbance of the heat flow between the ground and the atmosphere (Liston 1995; Marsh et al. 1997; Granger et al. 2002). The time of snow cover disappearance is also an important factor influencing the choice of nesting sites by birds and their reproductive success (Madsen et al. 2007; Moe et al. 2009).

In light of all these issues, a thorough knowledge of the distribution of snow cover becomes a key factor in understanding the functioning of the tundra ecosystem. Recognition of the relationships between the topographical relief, land coverage, and snow cover distribution will allow for the improvement of existing hydrological, permafrost, and energy balance models. The Arctic, with a particular emphasis on Svalbard, is one of the fastest-warming areas on Earth (Wei et al. 2016). This makes monitoring changes in the distribution of snow cover particularly important, without which it would be difficult to understand the future of this part of the world.

2. AIM AND SCOPE OF THE STUDY

The main aim of the study is to **identify temporal and spatial distribution of snow cover in the vicinity of the Polish Polar Station Hornsund and attempt to quantify its relationship with topography and land cover**. The detailed dynamics of the development and disappearance of snow on the tundra was presented on the basis of data collected since the 2013/2014 winter season in the Fuglebekken catchment area. Additional data comes from the Hornsund weather station, part of the WMO network (no. 01003), which has been observing snow on the ground since 1982. The dynamics of changes in snow cover in the immediate vicinity of the Polish Polar Station (PPS) was used as a reference point for the measurements carried out at the time of maximum accumulation on the coast of the Hornsund Fiord in spring 2014 and 2016. Satellite images from the ablation periods 2014–2016 supported the study, allowing for the determination of the large-scale course of snow disappearance from the coast of the

Hornsund Fiord. Rich resource of meteorological data was used to feed the SNOWPACK model in order to try recreate metamorphic processes taking place inside the snow cover in selected measurement sites. The collected materials were also used to try to determine the depth and snow water equivalent (SWE) at each point in space using the Alpine3D model. Finally, the aforementioned software, along with the output of global climate models, was used to forecast local snow conditions in southern Spitsbergen at the end of the twenty-first century.

3. STUDY AREA

Research were performed on unglaciated coast of the Hornsund Fiord, located in the southern part of the Spitsbergen island (Fig. 1). The fiord itself is 30 km long and up to 15 km wide at its widest point, while its maximum depth exceeds 250 m (Swerpel 1985; Rudowski and Marsz 1996; Moskalik et al. 2013). This allows for a fairly intense inflow of warm Atlantic water carried by the Gulf Stream branch, the West Spitsbergen Current, that according to the name runs poleward just west of Spitsbergen. The inflow of Atlantic water to the fiord is on average 20 mSv (1 mSv = 1000 $m^3 s^{-1}$) (Promińska et al. 2017), which hinders the freezing of the sea and strongly affects the temperature and rainfall in the Hornsund area, especially in the cold season (Walczowski and Piechura 2011). Recent research results indicate that Hornsund is not a fiord *sensu stricto*, but a strait blocked from the eastern side by the Hornbreen-Hambergbreen glacial system (Grabiec et al. 2018). Due to the progressing rapid retreat of Svalbard glaciers related to global warming (Błaszczyk et al. 2013; Nuth et al. 2013), it is estimated that Hornsund will become a strait connecting the Greenland Sea with the Barents Sea in 2055–2065, which is likely to completely change the oceanic circulation and thus the climate of the area (Grabiec et al. 2018).

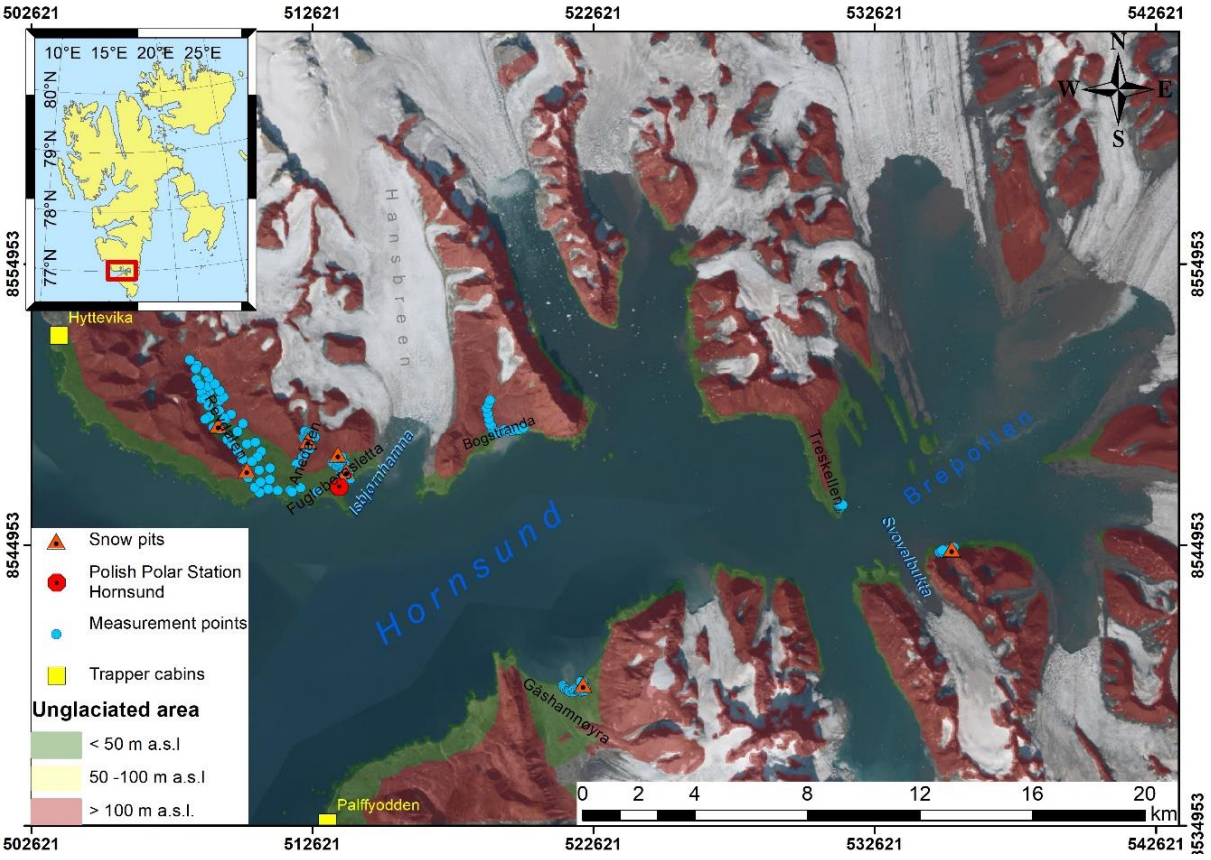

Fig. 1. Location of the study area (background map: http://toposvalbard.npolar.no/).

Given the location of the measurement points, the study area extends from Revdalen area on northwest to the Gåshamnøyra plain in the south and the coast of Svovelbukta in the east. The shores where measurements were taken are part of the physico-geographical units: Wedel Jarlsberg Land (north-west part with PPS Hornsund station), Torell land (Treskelen Peninsula) and South Cape Land (nor. *Sørkapp Land;* southern coast of Hornsund fiord). The coastal zone treated as a terrain up to 50 m a.s.l., a maximum of 5 km from the sea line and in the fiord, considering the Palffyoden and Hyttevika trapper cabins as the entrance to the fiord, covers 47 km^2 (Fig. 1).

The *Stanisław Siedlecki* Polish Polar Station in Hornsund (77°00′04″N, 15°33′37″E) is situated on the northern shore of the Hornsund Fiord near the outlet into the Greenland Sea (Fig. 1). The station is located about 200 m from the shore at an altitude of 10 m above sea level in the Fuglebergsletta area, which is a raised marine terrace that slopes gently towards the sea. In its eastern part, limited by the moraine of the Hansbreen glacier, located is a small (~1.5 km^2) unglaciated catchment of the Fuglebekken stream. This area was selected as the site of extended snow monitoring, implemented in the program of permanent observations at PPS Hornsund starting from the season 2013/2014. Due to the continuity, the measurements from the Fuglebekken catchment served as a reference for all other measurements carried out in the Hornsund Fiord area. In the study, spatial analyzes were performed on a lowland fragment of the catchment area covering 0.72 km^2, for which information on soil and plant communities was available. Correlations between snow cover and geomorphological forms were studied for a larger area of 1.8 km^2.

3.1 Relief and land coverage

The Hornsund Fiord area is mostly glaciated. Glaciers in whole Svalbard cover around 57% of the surface (Nuth et al. 2013). However, in southern Spitsbergen their share reaches 67% (Błaszczyk et al. 2013; Johansen et al. 2012). Despite this, **about 20% of the area is made up of flat, non-glaciated plains** (Zwoliński et al. 2013), which are the nesting place of some of the largest bird populations in Svalbard (Isaksen 1995). Bird droppings are one of the main sources of minerals for the Svalbard's poor soils (Zwolicki et al. 2013) increasing abundance of vegetation in the tundra (Wojciechowska et al. 2015). This makes the coasts of Hornsund an area of increased biodiversity.

The relief of the coasts of the Hornsund Fiord and the entire Spitsbergen is the result of geological processes shaping the study area from the Precambrian period. Geological formations have a meridional course, where the oldest rock outcrops are found on the western shores of the Hornsund Fiord, while further east, the younger rock formations create the surface. However, for the topography of the tundra area, the most important were the processes that took place in the immediate geological past, especially the isostatic movements. In the Hornsund region, these led to the creation of a system of several raised marine terraces. The youngest terrace is located 2 m a.s.l. while the oldest ones are elevated even more than 200 m a.s.l. (Karczewski 2004).

The most thoroughly studied area in terms of topographical relief, land coverage, soil and plant distribution is the closest vicinity of PPS (Fig. 2). A large part of the catchment area is made up of slopes covered with the coarse weathered material from Fugleberget-Ariekammen mountain ridge (569–513 m a.s.l.), which forms its border on the north side. The lower part, covered with tundra, consist of the plains of raised marine terraces (Fig. 2b), with southern exposure and a gentle slope, not exceeding 5°. The study area is diversified by several meters high abrasive outliers and the moraine of the Hansbreen glacier created during maximum Holocene extent (Błaszczyk et al. 2013), which limits the catchment from the east.

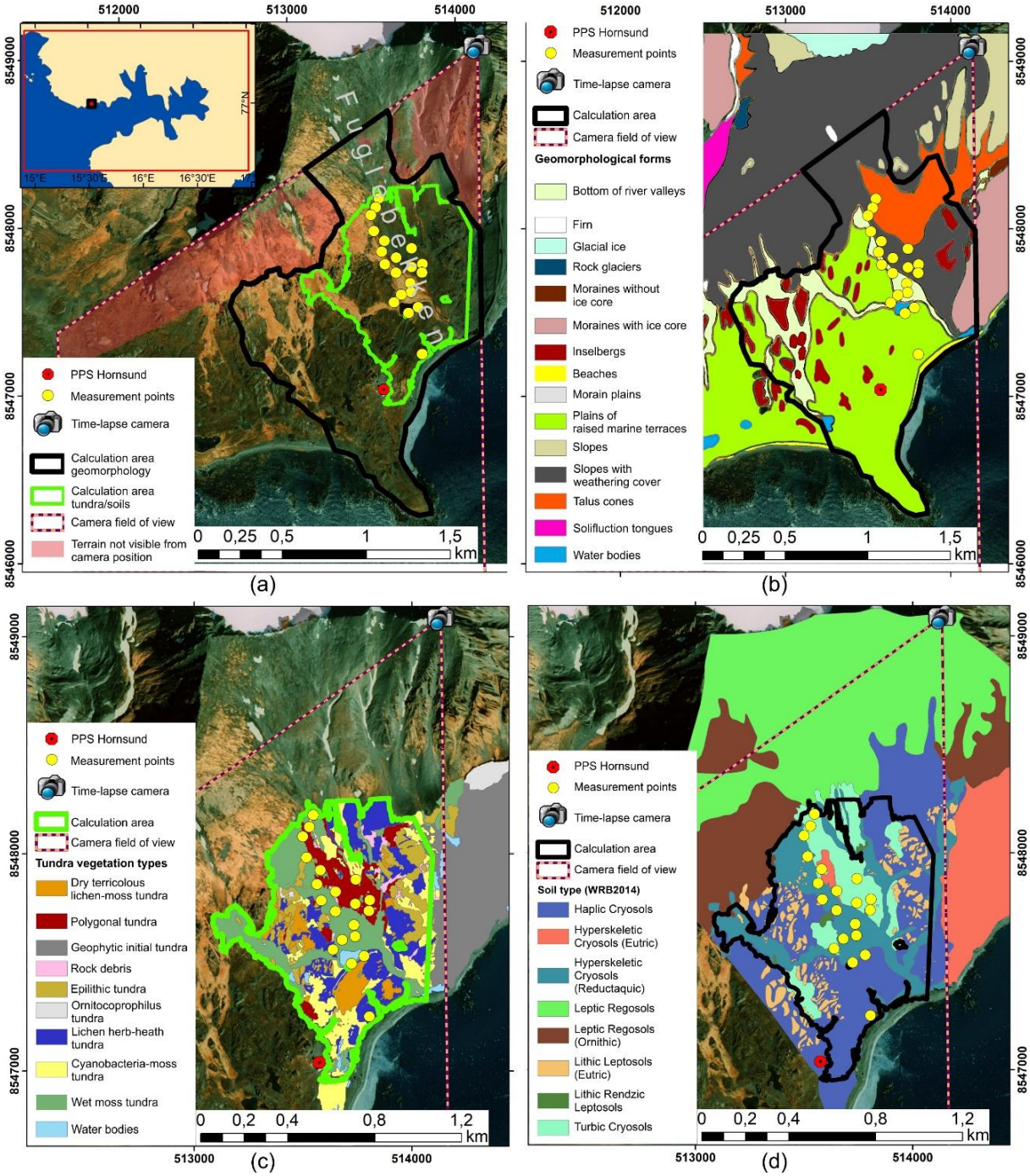

Fig. 2. The vicinity of the Polish Polar Station. (a) orthofotomap (after Kolondra 2003), (b) geomorfological map (after Traczyk and Kasprzak 2008), (c) tundra vegetation map (after Migała et al. 2014), and (d) soil types map (after Szymański et al. 2013). The points of weekly snow thickness and density measurements, location of time-lapse camera, its field of view and surfaces used for spatial analysis are shown (see the Data and Methods section).

In the catchment area, 10 land coverage classes were distinguished, based on the occurrence of vegetation species (Migała et al. 2014). The largest share on the study area covers wet moss tundra (26.2%), followed by lichen-herb-heath tundra (24.2%), cyanobacteria-moss tundra (15.4%), epilithic tundra (12.1%), polygonal tundra (10.7%), dry terricolous lichen-moss tundra (7.5%), geophytic initial tundra (0.5%) and ornitocoprophilus tundra (0.2%). Apart from plant

communities, on the study area there were also distinguished the vegetation-free land coverage classes: rock debris (1.9%) and lakes and water bodies (1.3%) (Fig. 2c). Except of wet moss tundra, all other vegetation formations belong to dry plant communities. Each of the separated classes is characterized by a specific species composition and occurs on a slightly different type of ground (Wojtuń et al. 2013). It is worth noting that **wet mosses tundra is considered to be the most biologically productive class**, due to significantly higher values of the normalized differential vegetation index (NDVI) obtained from the analysis of satellite images (Hobbler 2011). The NDVI index (Rouse et al. 1974) is commonly used to assess the condition of vegetation and the intensity of photosynthesis in plants in remote sensing studies (Gamon et al. 1995), also in the arctic tundra environment (Raynolds et al. 2012).

The local flora grows on poor, weakly developed soils with shallow-lying perennial permafrost (Szymański et al. 2013). Permafrost layer itself can be over 100 meters thick here (Christiansen et al. 2010; Wawrzyniak et al. 2016), although in the zone of direct land contact with the sea, it is limited to an average of 40 m (Strzelecki et al. 2017). Frozen ground at the end of summer may thaw locally to a depth of more than 2 meters (Dolnicki et al. 2013; Chmal et al. 1988). The typical thickness of active layer in the Hornsund area is 1–1.15 m (Kasprzak et al. 2017), but this value varies greatly on the type of land cover and the distribution of snow cover. The most common soils (using the 2014 WRB soil classification) in the study area are cryosols, together with leptosols and regosols (Szymański et al. 2013; WRB Group 2014). In addition, in the area of the Hornsund coast there is a limited amount of other soil types: histosols, gleysols, fluvisols and cambisols (de Kleijjn 2016; Borysiak and Ratyńska 2004).

The harsh climate, resulting in the presence of permafrost, a short growing season and poorly developed soils, makes it difficult for plants to develop in Svalbard. Nevertheless, the flora of this area can be considered quite rich and varied (Jónsdóttir 2005). The number of vascular plant species in the Hornsund region is estimated at 92 (Kuc and Dubiel 1995), while on the whole Svalbard archipelago there are at least 164 such species (Rønning 1996). More common are lichens, with nearly 600 species identified there, bryophytes with almost 400 representatives, algae with cyanobacteria (almost 800 species) or fungi represented by over 550 varieties (Elvebakk and Prestrud 1996). From the plants kingdom, special attention should be given to woody plants, the most common representative of which is the polar willow (*Salix Polaris*) (Rønning 1996). Despite its small size, rarely exceeding 8 cm (Påhlsson 1985), this long living plant is used in dendrochronological research and can serve as an indicator of past climatic conditions (Owczarek and Opała 2016). The oldest dwarf shrubs found so far from the Hornsund region were almost 100 years old (Owczarek 2010a).

3.2 Climate

The study area is located in the tundra climate zone (ET) according to the Köppen classification, which means that the average temperature of the warmest month does not exceed 10 °C, and only in 2–3 months the monthly mean value exceeds 0 °C (Köppen and Geiger 1936). Due to the location of Spitsbergen beyond the Arctic Circle, the phenomenon of polar day and night occurs there, and the radiation balance of the surface is negative for most of the year (Raschke et al. 1973). In Hornsund, the polar night period lasts from October 31 to February 11, which means 104 days without sun, while the polar day occurs for 118 days from April 24 to August 18 (Marsz and Styszyńska 2013). These phenomena cause huge disproportions in surface energy balance. Only the summer months (June–August) in Hornsund are characterized by a clearly positive radiation balance, while September and May have a balance close to zero, and in the rest of the year negative values prevail (Budzik et al. 2009). Nevertheless, the total annual energy balance of the area is positive (Baranowski 1968; Budzik et al. 2009).

In addition to the insolation conditions, the climate of Hornsund is strongly influenced by the atmospheric circulation, which is responsible for the extremely mild temperatures in this part of the Arctic. For example, high cloudiness limiting the heat radiation in winter months is caused by the location of Spitsbergen on the route of the Atlantic cyclones (Brümmer et al. 2000). The observed increase in cyclonic activity, accompanied by growth of cloudiness, is largely responsible for the faster warming of this part of the Arctic (Serreze and Francis 2006). The increase in temperatures noticeable in recent years (see Fig. 6) is additionally related to the influx of warmer and warmer Atlantic water masses towards Hornsund, which additionally hinders the formation of sea ice and contribute to further climate warming (Kruszewski 2004; Kruszewski et al. 2003; Styszyńska 2011). However, despite reports of decreasing activity of the Gulf Stream (Rahmstorf et al. 2015), the current series of measurements point to an increase in the amount of heat transported by the West Spitsbergen current (Piechura and Walczowski 2009; Walczowski and Piechura 2011; Styszyńska 2011).

3.2.1 Selected meteorological parameters on PPS Hornsund

Insolation and cloudiness

The average annual cloudiness measured at the station in Hornsund is 5.8 octants (for comparison, the average values recorded in the Polish lowlands are 5–5.6 octants (Błażejczyk 2004)).The most cloudy skies are observed in summer months, where mean values reach 6.4 octants (Fig. 3). For this reason, higher insolation is recorded in spring than in summer, and May and April are the sunniest (Fig. 4). In May the sun shines for an average of 204 hours. Taking into account the proportion of actually measured insolation to the maximum possible to obtain in that place, April is statistically the sunniest, reaching an average of 41% of potential insolation. The least sunny is September, where only 18% of the potential insolation is achieved on average. These values are reflection of the course of cloud coverage observed in Hornsund. However, the amount of energy reaching the ground is greatest in the summer months, despite the prevailing overcast condition. This is an effect of greater solar zenith angle (reaching a maximum of 36.5° on the day of the summer solstice) and the reduced ground albedo due to the lack of snow cover (Głowicki 1985; Budzik et al. 2009). The mean annual total sunshine duration is 1031 hours, while the potential total is 3542 hours.

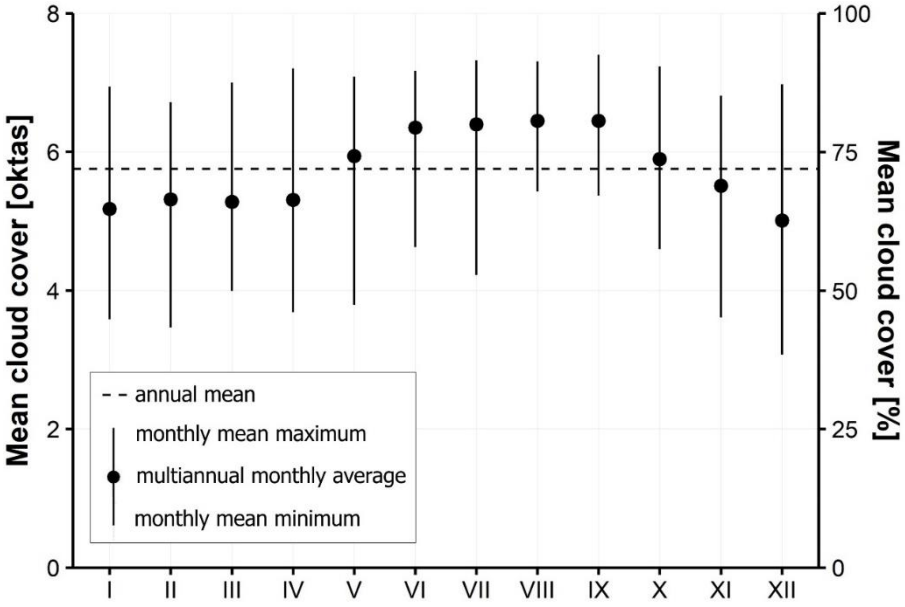

Fig. 3. Monthly cloudiness distribution in 1979–2017 in PPS.

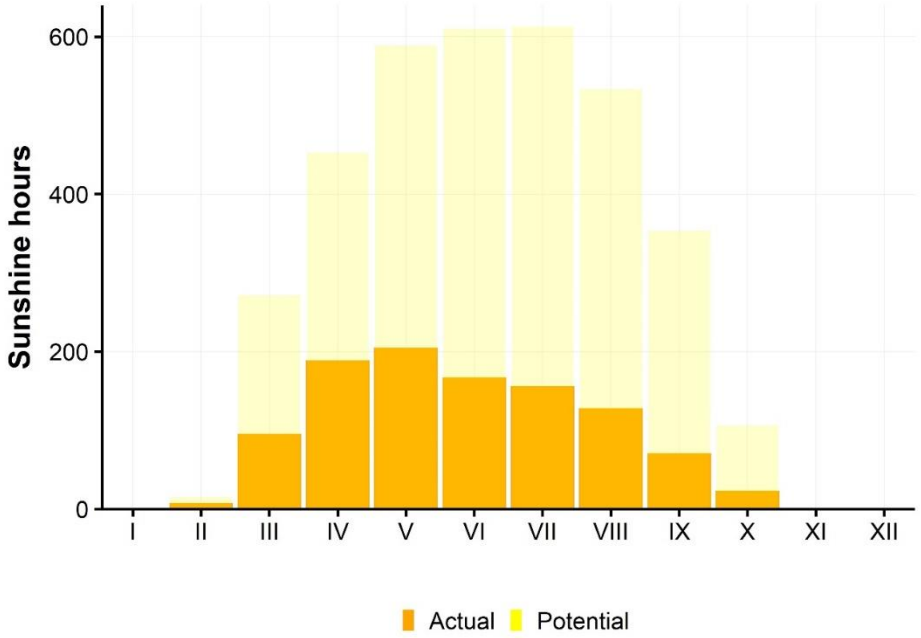

Fig. 4. Average monthly sunshine duration in PPS in 1979–2017. The potential insolation duration takes into account the influence of the local topography.

Air temperature

The average annual temperature in the Hornsund station for the period 1979–2017 was –3.7 °C. Mean annual temperatures during this time varied from –7.2 °C in 1988 to +0.3 °C in 2016. The air temperature distribution in PPS Hornsund is presented in Fig. 5 in the form of a box plot. The middle line marks out the median value, the lower and upper sides of the box are the first and third quartiles, and the points represent the outliers (exceeding 1.5 interquartile range [the difference between quartile 3 and 1]) (Williamson et al. 1989).

As in the entire Arctic, also in Svalbard, the greatest variability of temperatures is observed in the winter months (Przybylak 2016). In Hornsund, the coldest of these is March with an

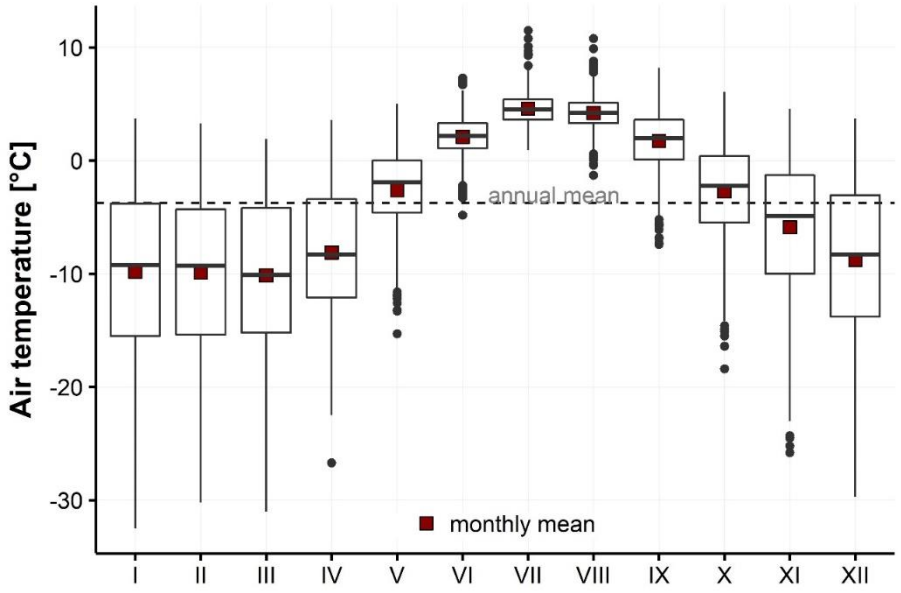

Fig. 5. Air temperature distribution measured in PPS in 1979–2017.

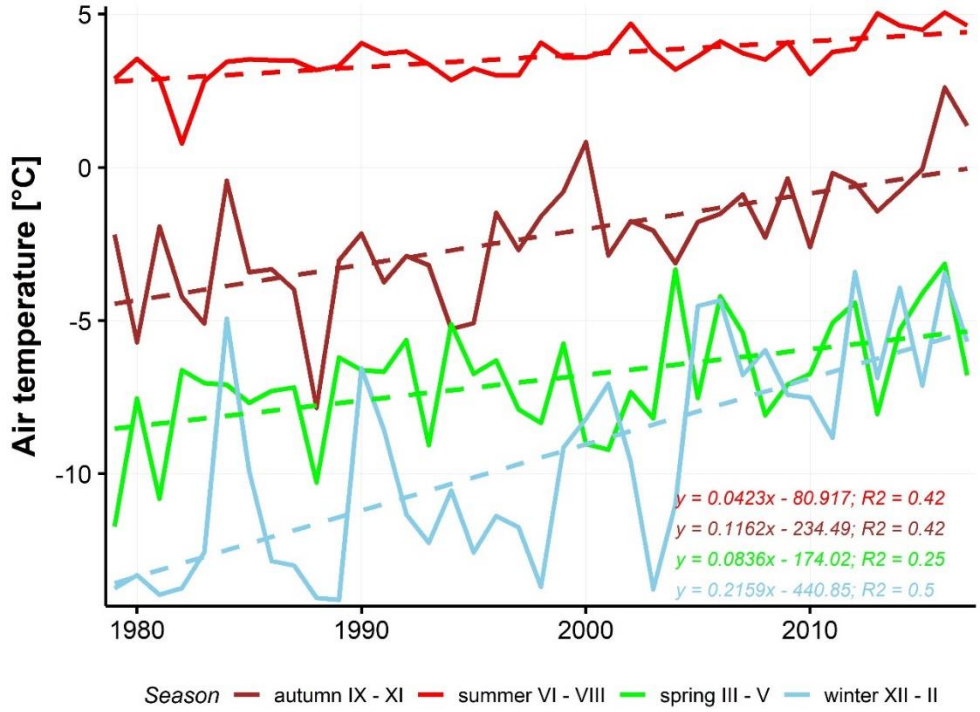

Fig. 6. The average air temperature of seasons in PPS with linear trends outlined.

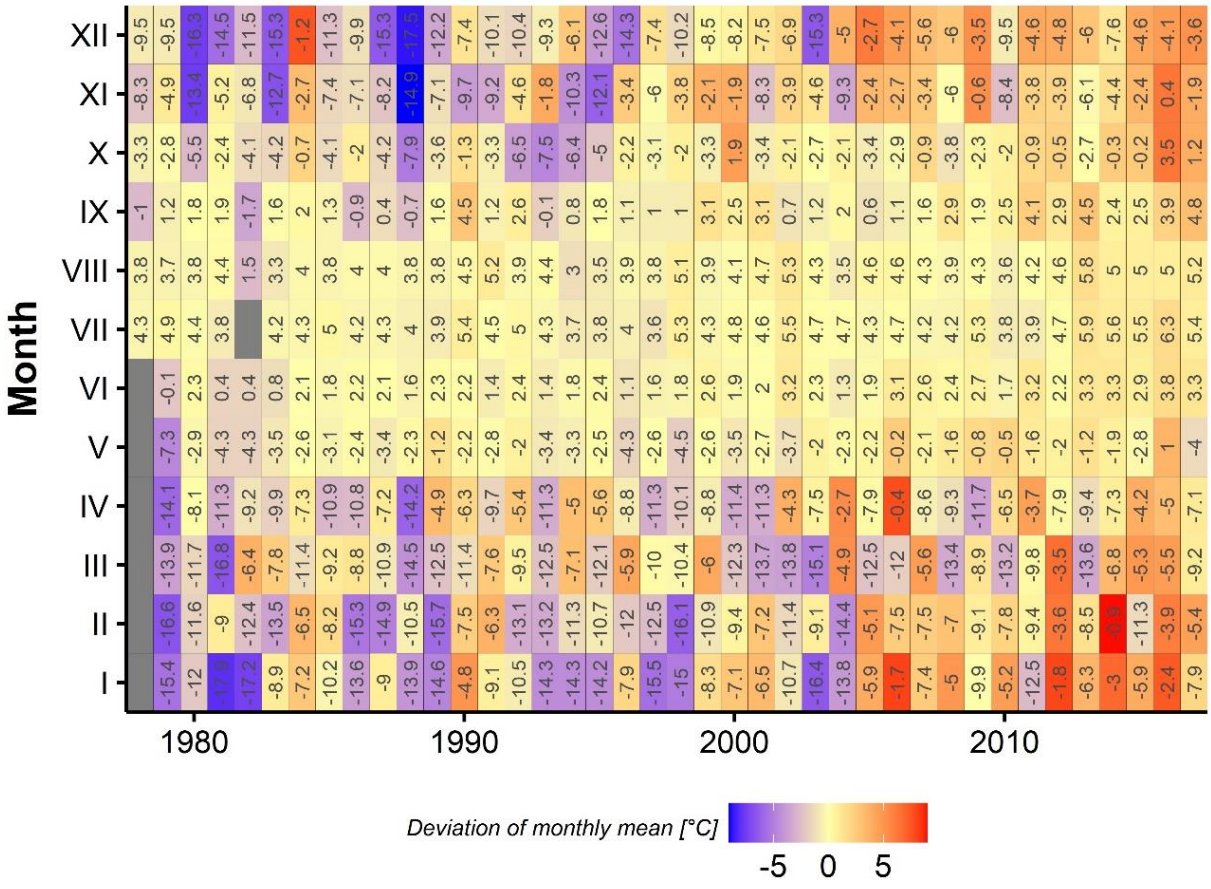

Fig. 7. Mean monthly air temperatures in PPS (text) and their deviation from the long-term averages (color) from 1979–2017 period.

average temperature of –10.1 °C (Fig. 5). This is due to the maximum extent of sea ice this month (Peterson et al. 2015), with a simultaneous little inflow of solar radiation. In summer, temperature variability is minimal. The average temperature of the warmest July is +4.6 °C.

Global climate warming is clearly visible in the measurement series from the Polish Polar Station. The fastest temperature increase is recorded in the winter months (Fig. 6). In winter, the temperatures grow **2.16 °C per decade.** For autumn, spring and summer, the temperature increases are 1.16 °C, 0.84 °C, and 0.42 °C per decade, respectively. The trend for the whole year reaches 1.17 °C per decade. Similar values were obtained for the entire land area of Svalbard using climate reanalyses for the period 1961–2012, where the warming trend achieved 0.8 °C per decade, with much faster warming in winter than in summer (1.6 °C per decade against 0.2 °C per decade) (van Pelt et al. 2016). Due to the rapid warming, months colder than the long-term norm have become extremely rare in recent years. Usually only 1 or 2 months in a year turn out to be warmer than multiannual average (Fig. 7). The greatest temperature anomalies take place in winter months (December–February), when, for example, in February 2014 the average temperature was 9 °C higher than the long-term norm. On the other hand, in the 1980s, winter temperatures could be even 9 °C lower than the average values (e.g. in December 1988). Single months colder than the average have recently been recorded in the spring period. The last winter with an average monthly temperature below –10 °C took place in 2004 and, since then, it is spring (March–May) that often turns out to be cooler than winter (Fig. 6).

Precipitation

The average annual sum of precipitation in Hornsund from 1979 to 2017 was just over 450 mm. There is a noticeable disproportion between the annual sums of precipitation in particular years. Until 1988 they oscillated around 300 mm, while recently they often exceed 500 mm, reaching even over 800 mm in 2016 (Fig. 8). The determined linear trend indicates an exceptionally fast increase in the total annual precipitation amounting to 55.5 mm per decade. At the same time, the proportion of snowfall is decreasing. The amount of precipitation in solid form has remained at a similar level from the beginning of the observation; however, with rapidly increasing rainfall, **the share of snow in the total sum dropped from 40% in the 1980s to less than 30% in the second decade of twenty-first century** (2010–2017). This can be explained by the rising sum of the most efficient liquid precipitation in the autumn and summer period (Fig. 9). However, also in winter, the rain-on-snow events occur more and more often, altering the properties of the snow cover and causing serious environmental effects.

In a word of explanation, it should be added here that some studies indicate a different distribution of precipitation forms in Hornsund, where the share of the solid, liquid and mixed fractions in total sum is similar (Łupikasza 2003, 2008). This is a result of different methodology, where the precipitation form is assigned according to the air temperature. In this study, the division into the fraction of solid, mixed and liquid precipitation was made taking into account the duration of meteorological phenomena (drizzle, snowfall, etc.) between the observation times at the synoptic station (6, 12, 18, and 24 UTC). Types of precipitation are presented in Fig. 8 since 1983, as such information began to be collected in the summer of 1982.

Precipitation totals are unevenly distributed throughout the year. The highest rainfalls are recorded in September, where the average precipitation sum amounts to about 70 mm. In the spring months, April and May, the average monthly sum is the lowest: around 20 mm (Fig. 9). Taking into account long-term changes, most months are characterized by an increase in the sum of precipitation, however, in early spring, and especially in April, their decrease is noted (Łupikasza 2002). Spring precipitation is also characterized by the lowest year-to-year variability. Snowfall predominates in the period from December to May, but practically does not occur in summer. The annual course of precipitation is closely related to the circulation conditions. The highest totals are recorded during cyclonic situations with the influx of warmer air

from the south or south-west. Such situations are uncommon in the driest spring season (Marsz and Styszyńska 2013).

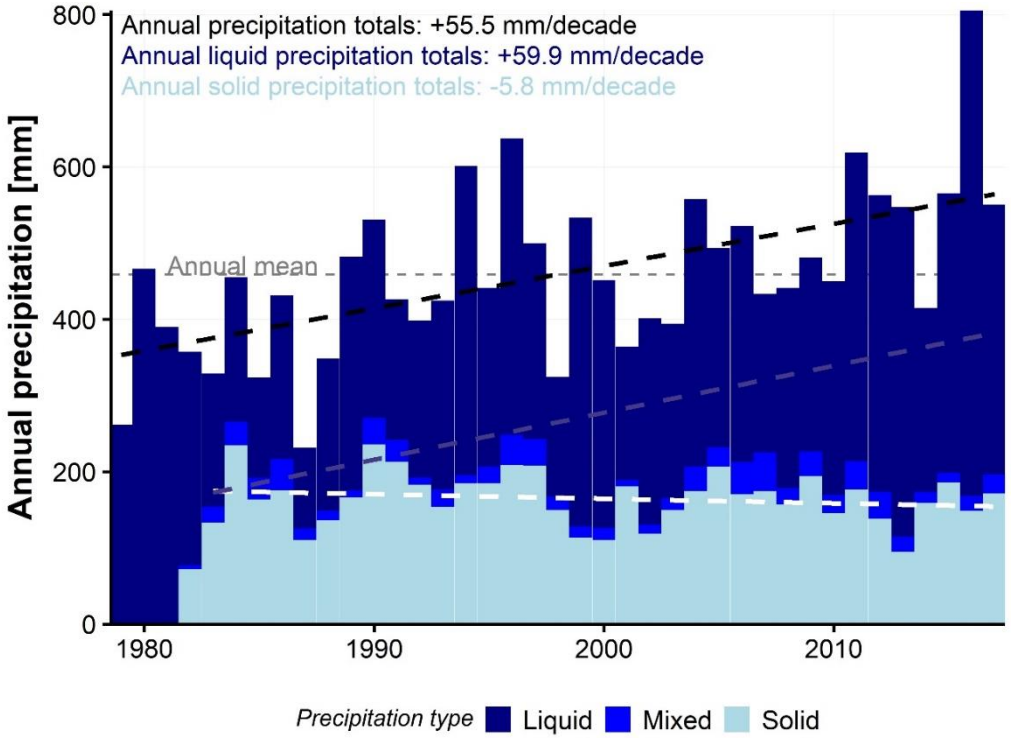

Fig. 8. Annual precipitation totals measured in PPS Hornsund meteorological site.

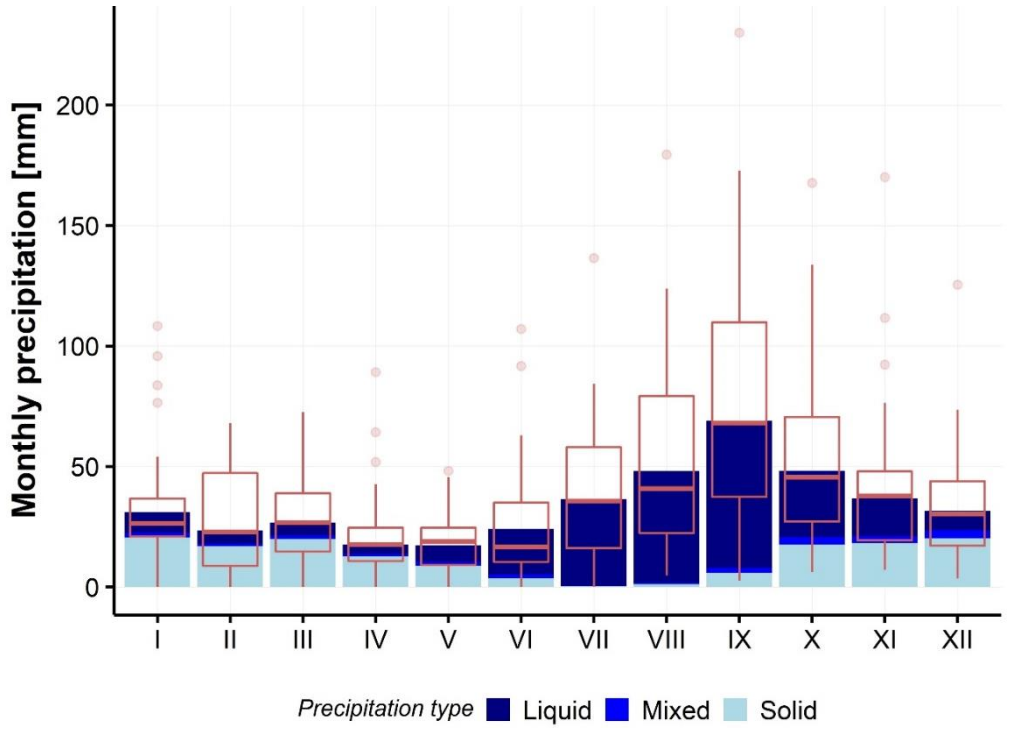

Fig. 9. Mean monthly precipitation totals in PPS with the presentation of the inter-season variability in the form of a box plot.

Considering the precipitation values measured at the Hornsund station, it should be remembered that the wind-induced measurement errors were not taken into account, so the actual total sums in this area are certainly higher. The study carried out in Ny-Alesund shows that the actual annual rainfall is about 50% greater than the measured values (Hanssen-Bauer et al. 1996). **The difference between measured and actual precipitation totals is the highest for snowfall and can even exceed 70%**. The underestimation of liquid precipitation is smaller, around 15% (Hanssen-Bauer et al. 1996). This means that as the climate warms up and the share of rain in the annual rainfall total increases, the measurement error decreases, and the annual precipitation sums are closer to the real values.

Wind speed and direction

Due to the latitudinal course of the fiord axis and the general location of Svalbard in the circumpolar zone with prevailing east wind, this direction is dominant in the Hornsund region (Fig. 10). **Overall, air inflow from the 45–135° sector accounts for 61% of all situations**, and from the western sector (225–315°) for almost 19%. Wind weaker than 0.5 m/s is observed in 6% of observations. **Meridional circulation is rare**. Northern wind is observed in 9% of cases and southern in 6% of cases. Noteworthy, the highest wind speeds are recorded from the dominant direction. The mean wind speed from the east is 7 m/s, while the annual average for the period 1979–2017 is 5.5 m/s. Taking into account seasons, much higher wind speeds are recorded in the winter than in the summer months. In winter, the averages are close to 7 m/s, while in summer they oscillate around 4 m/s. This is consequence of greater air pressure fluctuations in the winter (Marsz and Styszyńska 2013). In that season, the wind speed often exceeds 20 m/s, while in summer it only occasionally breaks the 12 m/s limit (Fig. 11).

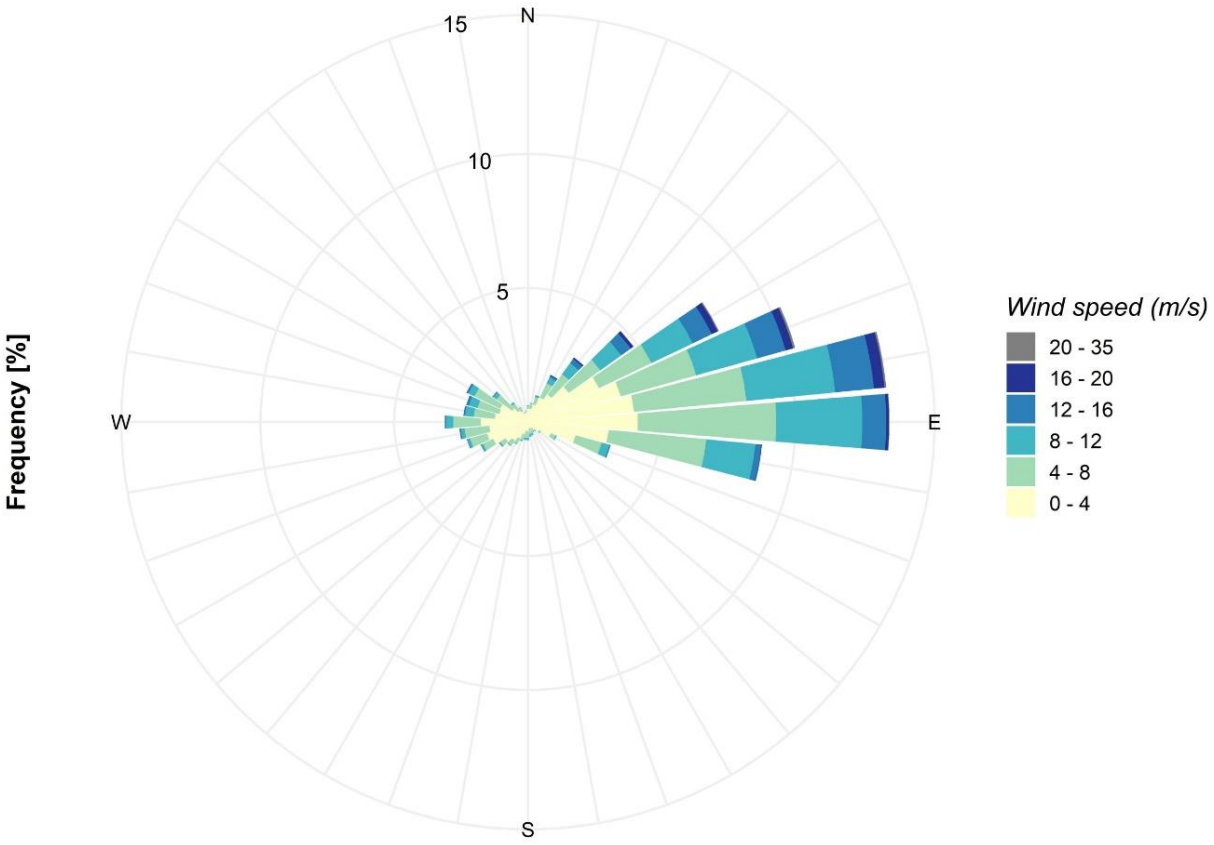

Fig. 10. Distribution of wind speed and direction in PPS in the 1979–2017 period.

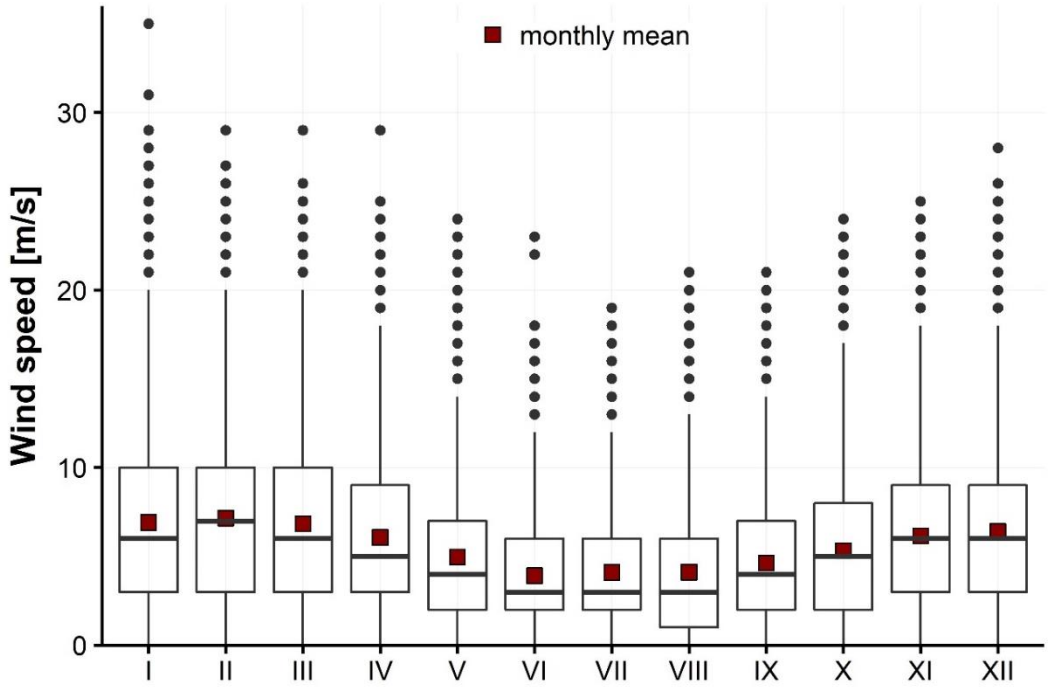

Fig. 11. Wind speed distribution for individual months in PPS in 1979–2017.

Relative humidity

One of the most important factors influencing metamorphism (Kaempfer and Plapp 2009) and melting (Zuzel and Cox 1975) of snow cover is the humidity deficiency above it, which is the difference between the saturated water vapor pressure at a given temperature and the actual

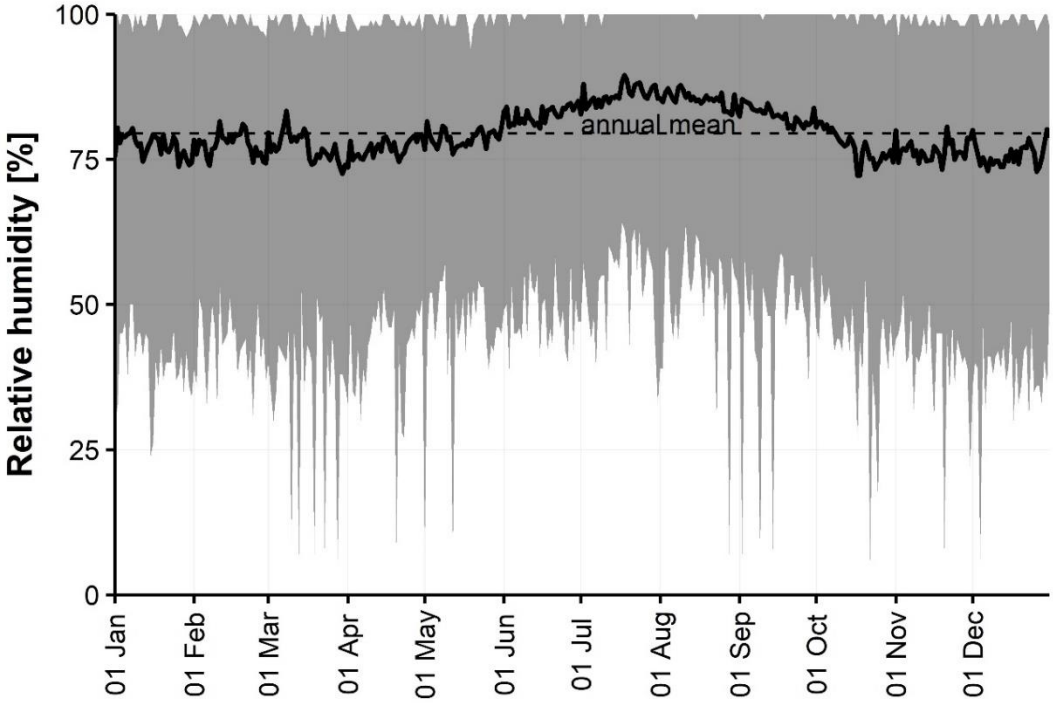

Fig. 12. Average course of the daily air relative humidity during the year (black line) and the range of its occurrence determined by the maximum and minimum daily averages obtained in the years 1979–2017 (gray ribbon).

water vapor pressure. This value can be indirectly inferred from the relative air humidity. This parameter is particularly important, especially in places where snow is often redistributed by wind. The relative air humidity determines the snow sublimation rate, which can be very high, especially during blowing snow events (Schmidt 1982). The amount of water vapor in the air also affects the longwave radiation flux, an important component of the energy balance in the polar regions (Sicart et al. 2006; Ruckstuhl et al. 2007).

At the Polish Polar Station, the average annual relative humidity is 79.4% and its inter-season variability should be considered as low. Only in the summer months, the humidity is higher, reaching an average of slightly above 85% in July and August. It is related to the increased advection of the air from the west in this period, which also results in an increase in cloudiness and the number of fogs (Marsz and Styszyńska 2013). In the period from October to May, the average daily relative humidity is in the range of 72–82% (Fig. 12). Drops below 50% are incidental, and their occurrence is associated with the occurrence of strong anticyclonal situations or sporadic episodes in which the *foehn* wind reaches the level of the station (Marsz and Styszyńska 2013).

3.2.2 Spatial distribution of meteorological parameters

Snow cover properties on the coast of southern Spitsbergen are affected by the variability of meteorological conditions in this region. Due to the flat, lowland nature of the area and its

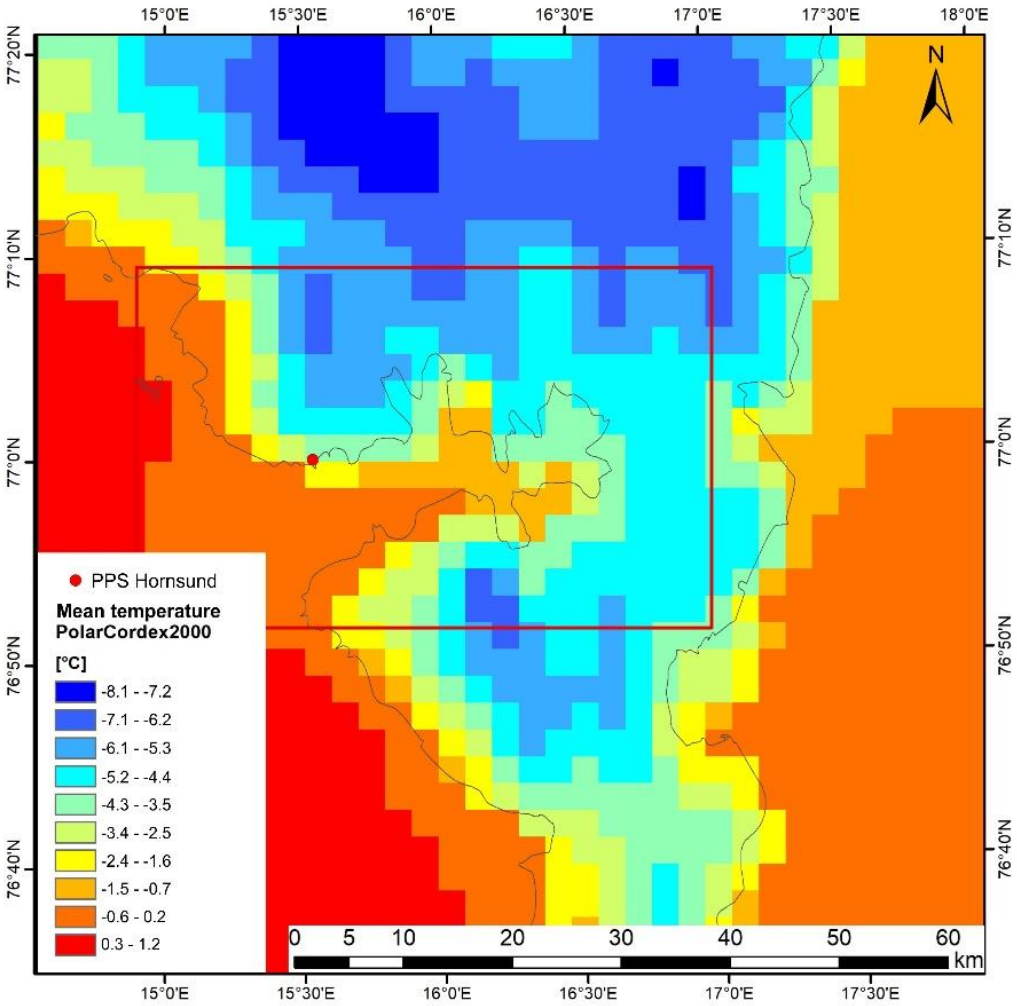

Fig. 13. Mean annual air temperatures – Polar CORDEX reanalysis for 2000.

the Hornsund Fiord showed that the air temperature drops quite quickly with increasing distance from the open Greenland Sea. Data from the 2014/2015 season show that **the warmest zone of the Hornsund is its north-western part** (near Hyttevika), where the average annual temperature can be over 2 °C higher than on the coasts in the inner part of the fiord (Treskelodden) (Araźny et al. 2017). In particular days, the relative humidity also can vary considerably in this region, and their mean annual values may differ by even 15 percentage points between measurement sites (Araźny et al. 2017). The assessment of precipitation spatial variability is very difficult. It can only be estimated on the basis of the snow cover thickness due to the lack of reliable measurements outside the meteorological site of the Polish Polar Station.

Additional information on the spatial variability of meteorological parameters in the study area is provided by high-resolution climate models. For the southern Spitsbergen, one of the best of its kind is available thanks to Polar CORDEX initiative from the COSMO-CLM model nested in global MPI-ESM-LR model (Dobler and Haugen 2016; Isaksen et al. 2017). However, the projection series with a spatial resolution of 0.022° (approximately 2.5 km × 2.5 km) are still too inaccurate to properly reflect the conditions in the narrow coastal zone of Hornsund. Nevertheless, its outcome clearly shows a slight **decrease in the annual mean air temperature with growing distance from the open Greenland Sea** (Fig. 13) together with simultaneous **increase in annual precipitation totals towards the inner part of the fiord** (Fig. 14). This result is generally in line with data from automatic weather sensors installed on the coast

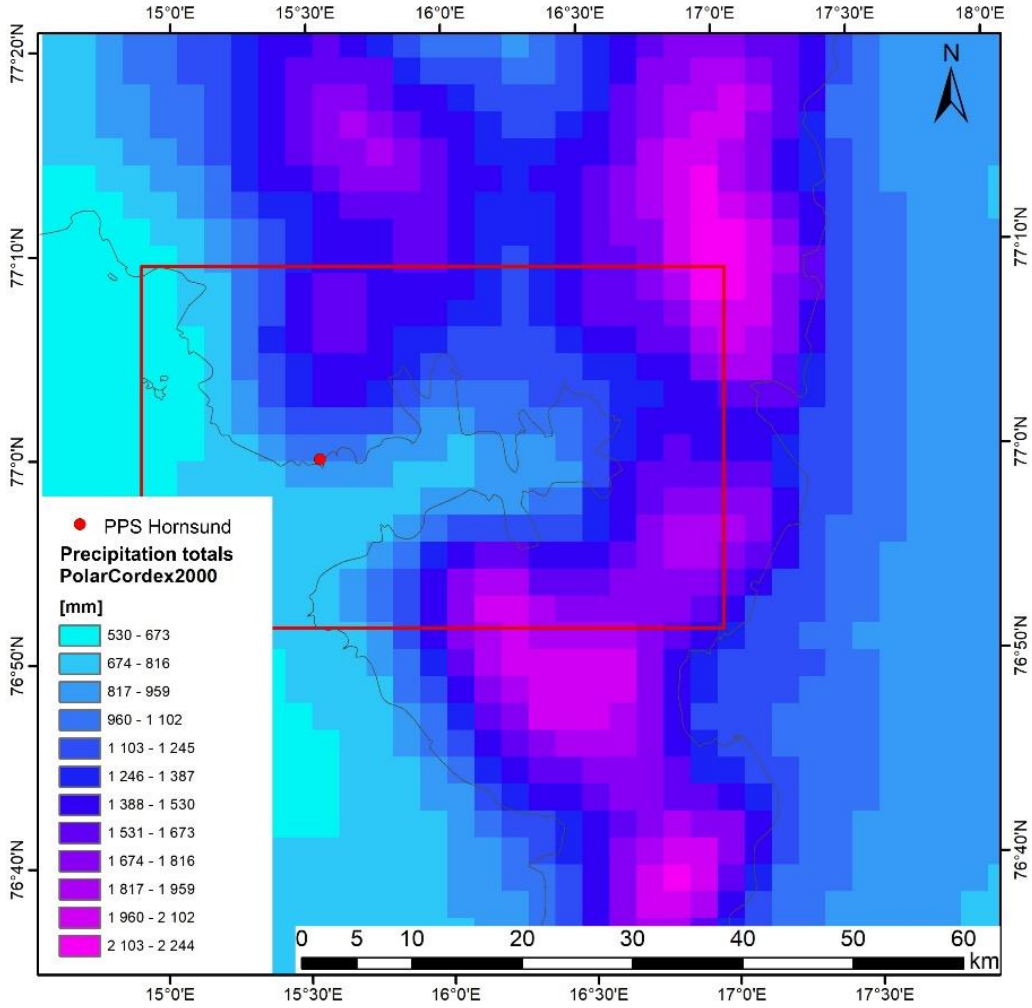

Fig. 14. Annual precipitation sum – Polar CORDEX reanalysis for 2000.

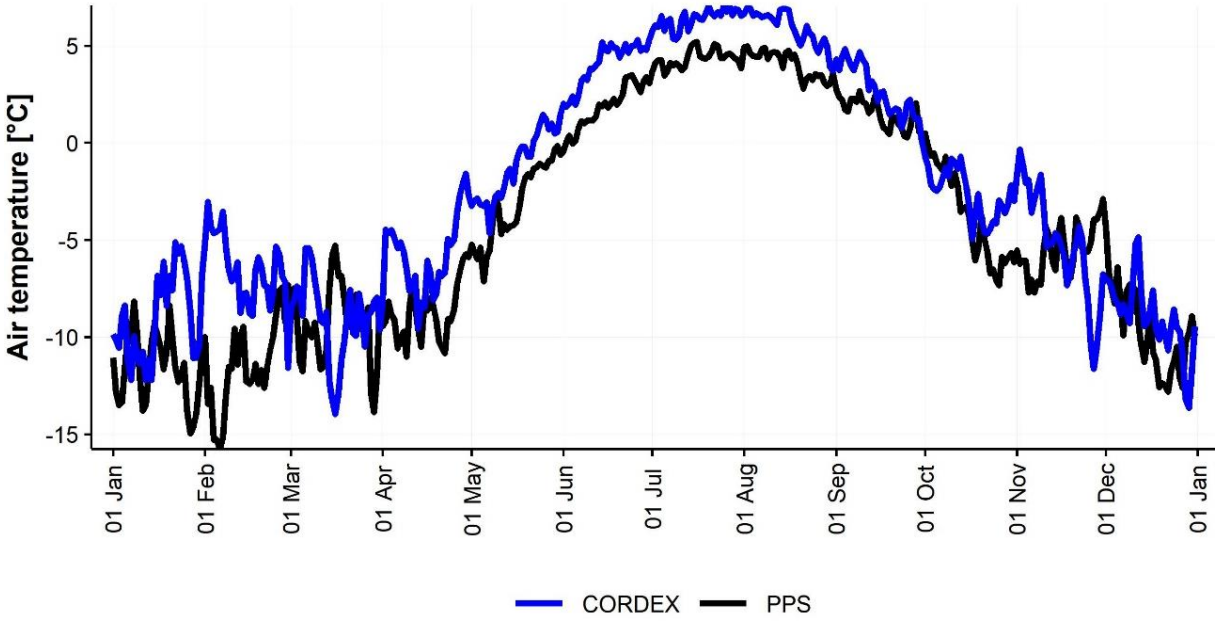

Fig. 15. The average daily air temperatures in the years 1991–2000 measured at PPS Hornsund paired with results of COSMO-CLM nested in MPI-ESM-LR model reanalysis.

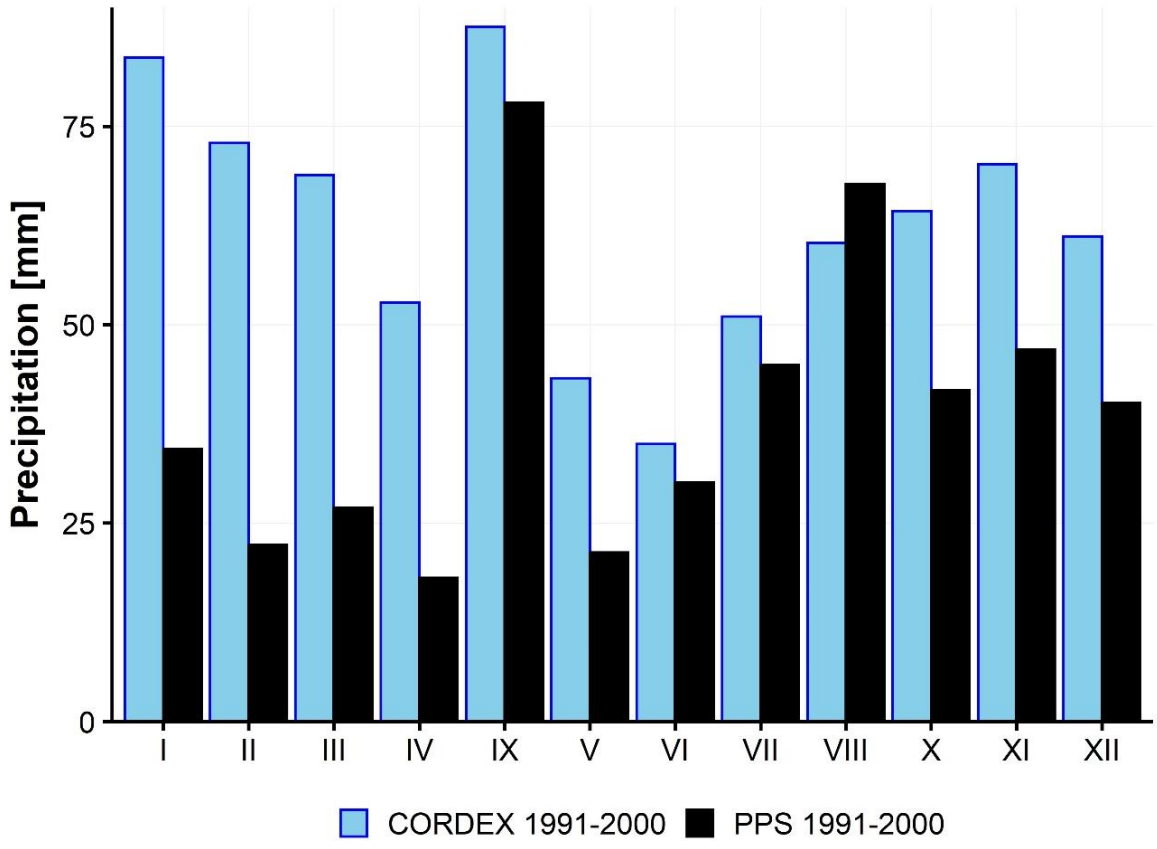

Fig. 16. Average monthly sums of precipitation obtained in the years 1991–2000 at PPS Hornsund and modeled from the COSMO-CLM climate reanalysis nested in MPI-ESM-LR.

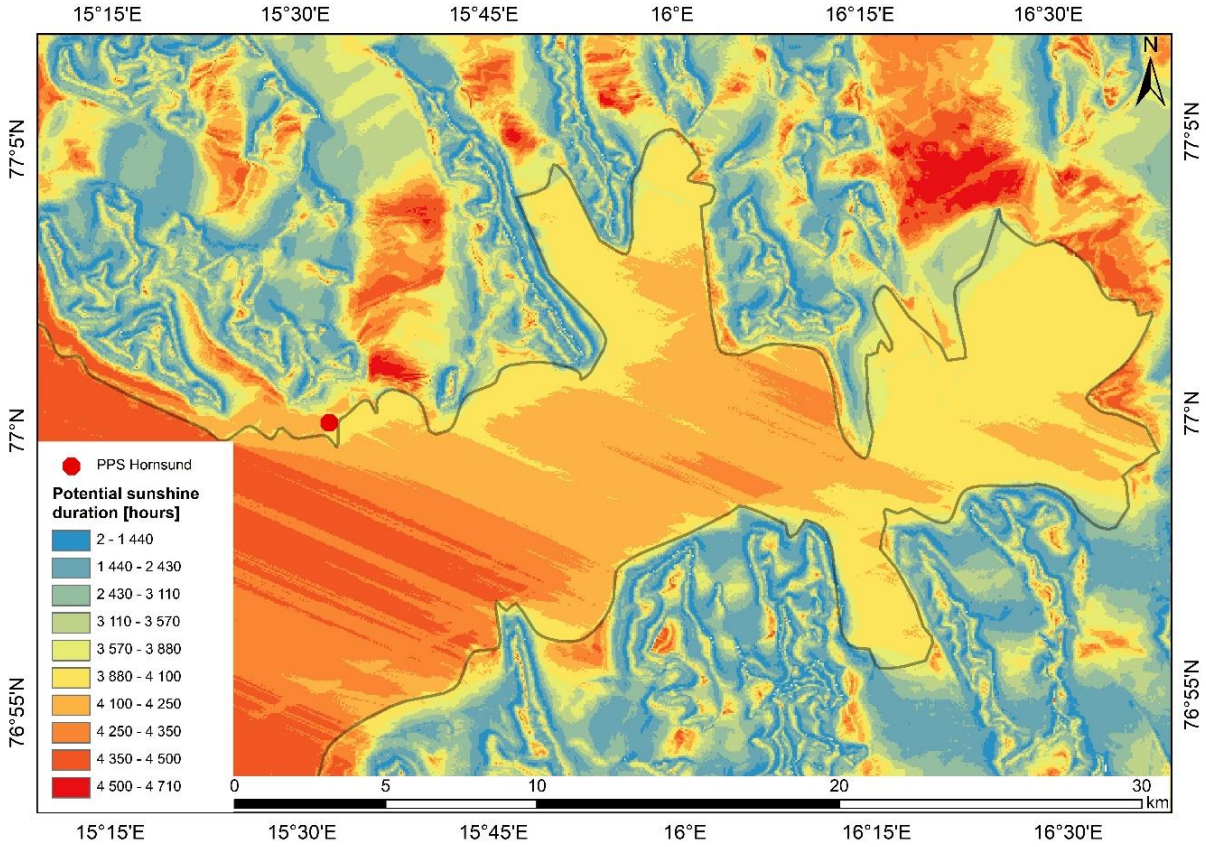

Fig. 17. Annual potential sunshine duration in the area of Hornsund Fiord.

proximity to the fiord water, spatial differences in air temperature, precipitation or relative humidity should be small. However, the results from automatic weather stations installed around (Araźny et al. 2017). However, the climate reanalysis with the use of the above-mentioned model overestimates the air temperature for the recent past (end of the twentieth century). For example, for a cell with the Polish Polar Station, the average annual temperature is 1.8 °C higher than the average from the measurements for the same period (–4.3 °C) (Fig. 15). Despite this, the long-term course of the daily temperatures from the observations and from the model is very consistent (r = 0.91). The precipitation amount is also overestimated. In the model results, the average annual sum reached 796 mm, while in the same period the average measured at the station was 472 mm (Fig. 16). Considering the precipitation measurement error which reduces the actual totals by about 50% in Svalbard (Hanssen-Bauer et al. 1996), the model results can be quite close to the actual sums of precipitation that fall on the ground. Even taking this effect into account, we can indicate an overestimation, as the model for the period 1991–2000 shows the precipitation sum 69% higher than that measured at that time on the PPS.

The supply of solar radiation as well as the speed and direction of the wind are characterized by greater spatial differentiation. Shortwave radiation influx is mainly influenced by terrain slope and aspect. Calculations made in SAGA GIS on the basis of 20 m spatial resolution Digital Elevation Model (DEM) (Norwegian Polar Institute 2014) indicate that due to the southern exposure of the area, **the northern side of the Hornsund Fiord is characterized by much better insolation conditions** (Fig. 17). In general, the differences in the potential annual sunshine duration in the coastal strip do not exceed 500 hours. However, locally and on a small scale, the variation can be much greater. For example, the western part of the Treskelen peninsula can be potentially illuminated by the sun for more than 4 000 hours, while the central and

eastern part for no more than 2 500 hours a year (Fig. 17). The factor determining the radiation balance is also cloudiness, which is slightly higher in the inner part of fiord (Araźny et al. 2017). Nevertheless, it should not diametrically differentiate the spatial insolation conditions.

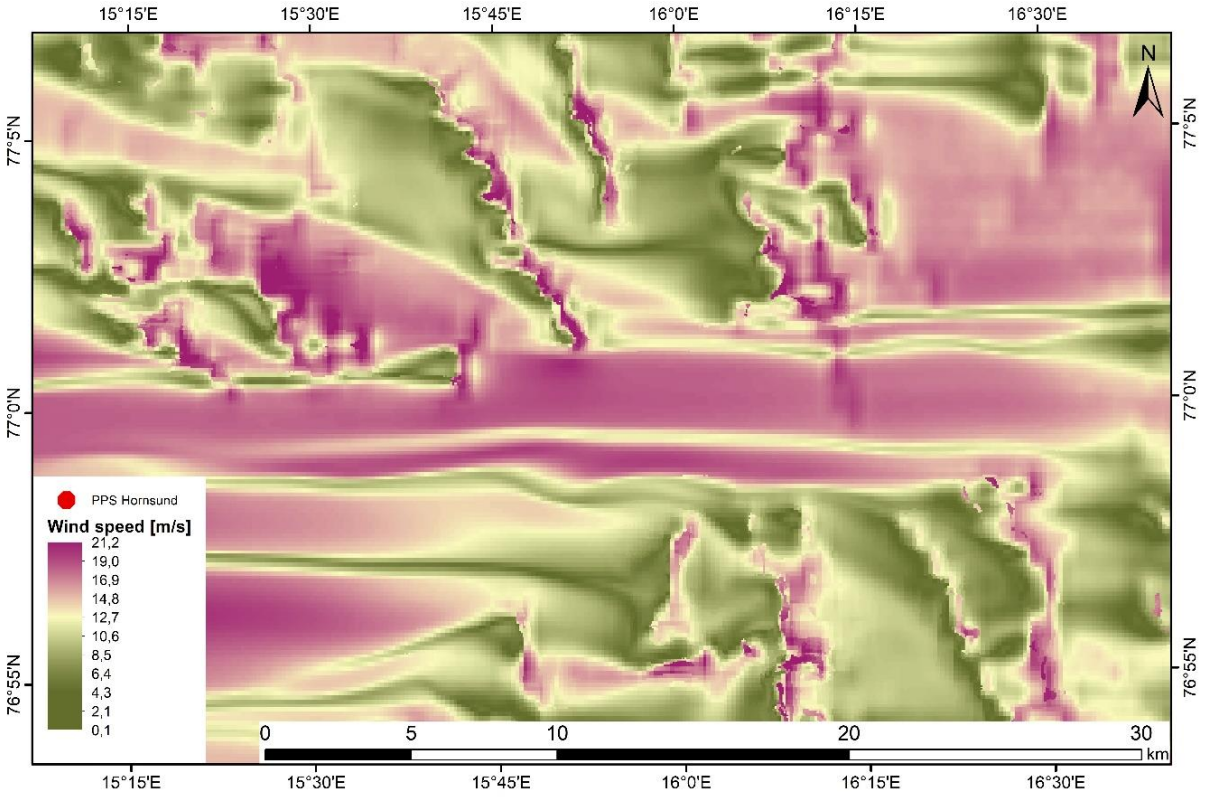

Fig. 18. Wind speed distribution (50 m resolution) around the Hornsund Fiord when an east wind with an average speed of 10 m/s was set over the domain of the WindNinja model.

With a digital terrain model and measurements from the PPS Hornsund, it is possible to simulate wind conditions in other parts of the area (Fig. 18). This was done with the WindNinja software (Forthofer et al. 2017). The obtained results indicate a slight variation in the wind speed and direction on coasts of the Hornsund Fiord. However, due to the enormous computational power requirements, simulations for the entire area were carried out with a spatial resolution of 50 m, which did not allow for mapping many elements of the terrain. In the model results, it is worth to draw attention, among others areas, to the Revdalen valley on the north of the Hornsund Fiord. This region is sheltered from wind activity. When at the Hornsund station and in the coastal zone there is an east wind with a speed of 13 m/s, the air flow in the depths of the Revdalen valley does not exceed 7 m/s. Due to the arrangement of the mountain ridges, the southern shores of the fiord are particularly calm in terms of wind. In the situation mentioned before, the wind speed in Gåshamnøyra does not exceed 5 m/s. Using a DEM with a resolution of 20 m, it was possible to model the wind field with a final spatial resolution of 10 m for the immediate vicinity of the Hornsund station. The Fuglebekken catchment stands out from the flat area, protected from the east by the moraine of the Hansbreen glacier (Fig. 19). The model outcome shows **about two or even three times lower wind speeds in the catchment area in comparison to PPS Hornsund**, when there is an eastern wind of 10 m/s at PPS.

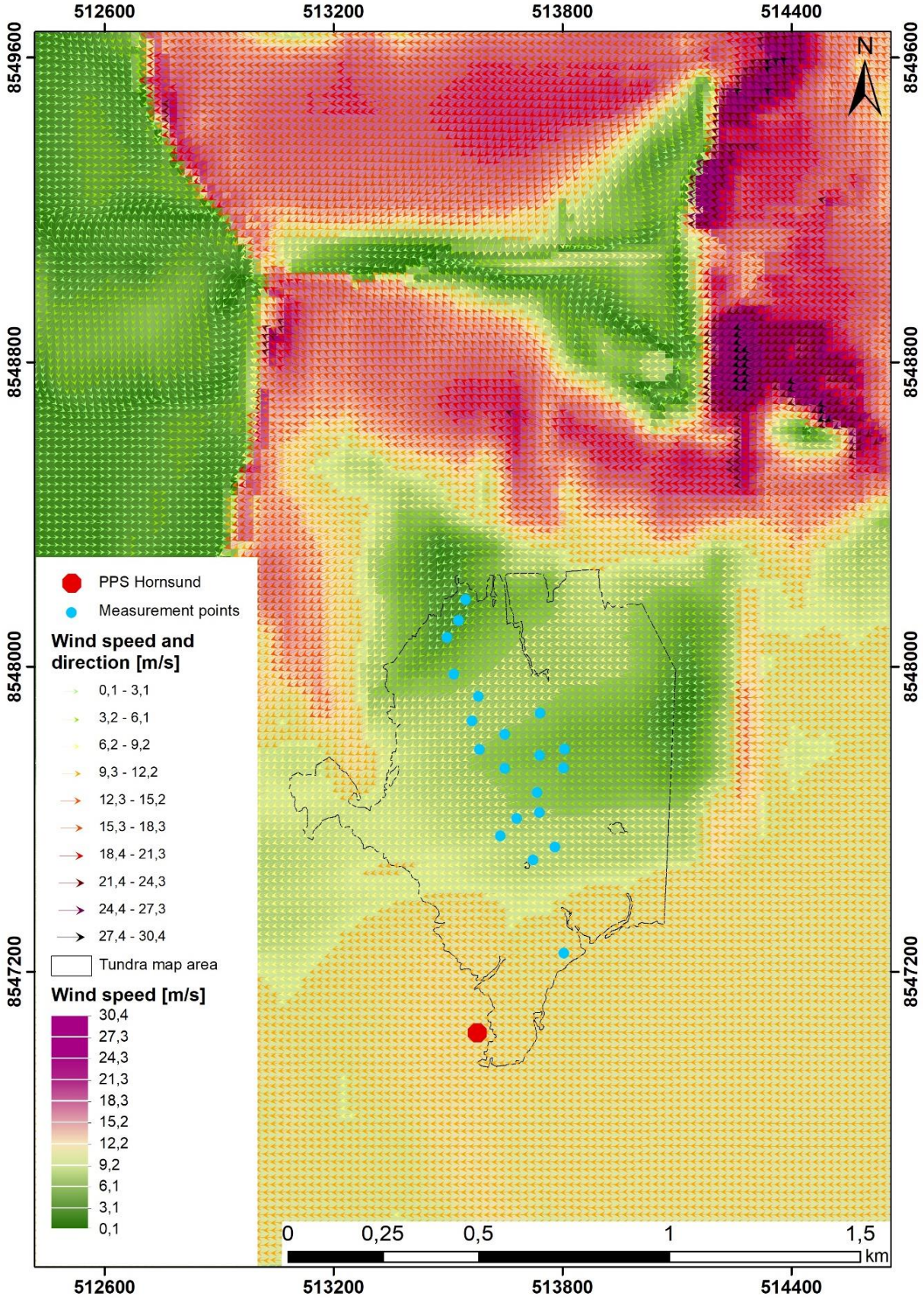

Fig. 19. The wind field (20 m resolution) for the vicinity of PPS Hornsund, when 10 m/s eastern wind speed of is recorded at PPS.

3.2.3 Snow cover at PPS Hornsund meteorological site

Long-term series of measurements carried out at PPS allow to analyse changing conditions of snow cover formation and ablation in the southern Spitsbergen tundra area. **The snow cover persists in the vicinity of the station for an average of 235 days a year**, and their number in individual years varied from 181 in 2012 to 266 in 1988 (Fig. 20). Considering the number of days with snow on the ground in terms of winter seasons, this ranged from 168 in the 1993/1994 season to 275 in the 1982/1983 season. Along with the global warming, **progressive decrease in the length of the snow season in southern Spitsbergen is visible. The delineated linear trend** for the period 1983–2017 **reveals shortening of the snow season by one day for each subsequent year** (Fig. 20). This trend, although not so strong, is observed all over Svalbard. The later formation of snow cover is responsible for this in connection with the significant warming of the autumn period. The slightly earlier onset of ablation contributes to that effect, together with more frequent precipitation in form of rain (Osuch and Wawrzyniak 2017; van Pelt et al. 2016).

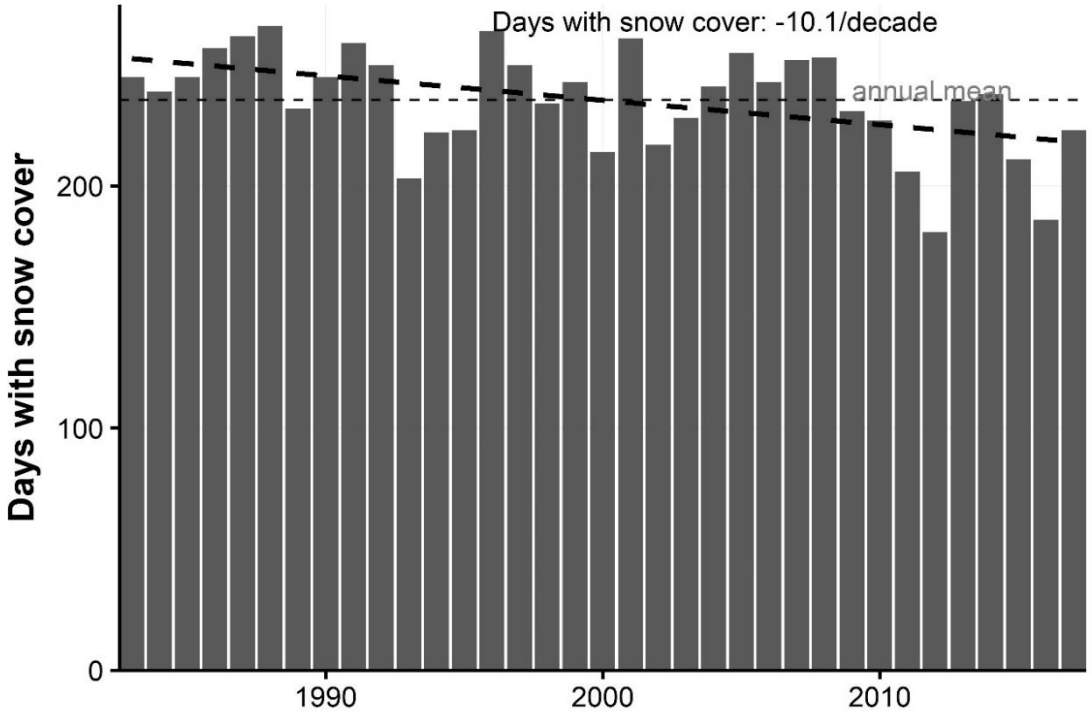

Fig. 20. Number of days with snow cover in individual years 1983–2017 at PPS Hornsund.

During the year, snow lays on the ground practically every day from December to May. However, in the period 1983–2017, April was the only month when a day without snow cover never happened (Fig. 21). It should be remembered that according to meteorological stations regulations, a day with snow cover is recorded when more than half of the ground near the measurement site is under the snow during the observation at 6 UTC (Janiszewski 1962; Doesken and Judson 1997; NOAA 2013). Therefore, snow-free days in winter months may be noted after strong winds, when snow is still not very thick and can be easily redistributed by the wind. On the other hand, July and August can be considered as completely snow-free months on the tundra. In the entire period of 1983–2017, there was only one day with snow in July (in 1996). In August, there were 7 such days, 3 of them in 1994, when the snow cover created on August 29 and remained on the ground for 5 days, until September 2, 1994. Continuous snow cover usually forms in mid-October and melts during the first half of June (Fig. 21).

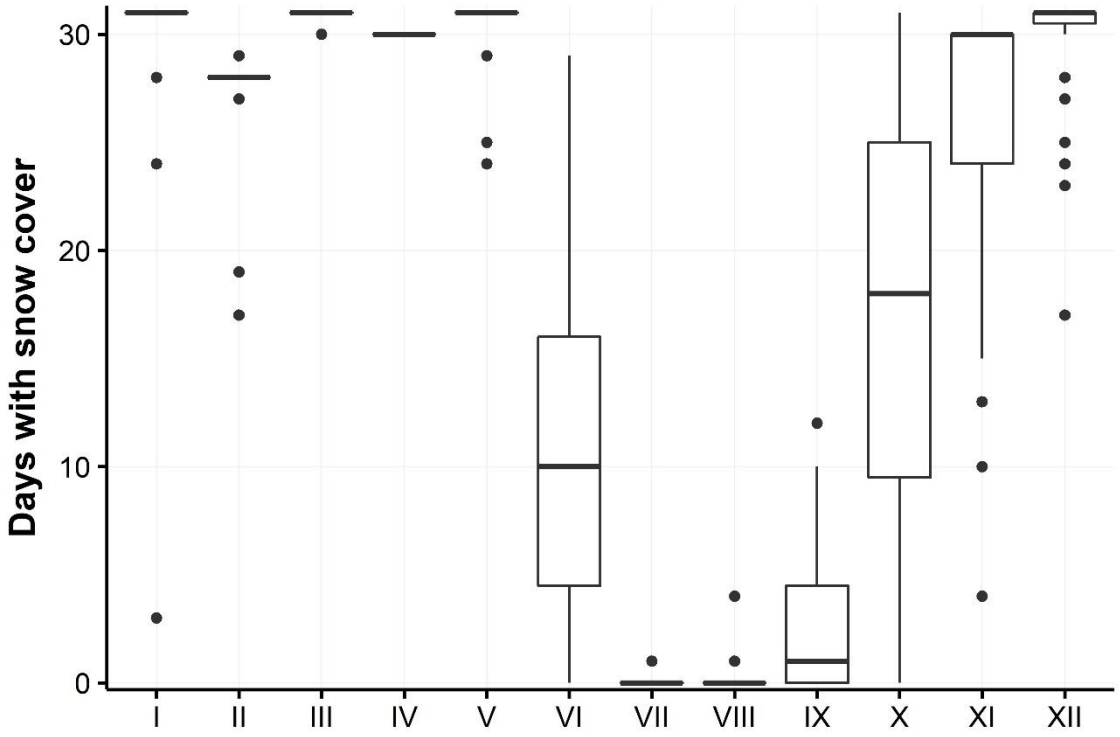

Fig. 21. Distribution of snow cover days in individual months in 1983–2017 at PPS.

The ablation period, understood here as a gradual decrease in snow cover height with the simultaneous lack of significant increases caused by new snowfalls, usually begins in early May (Luks 2012). However, there were years when the ablation began in the first days of April, as well as seasons in which the snow cover increased significantly even at the end of May (e.g. in 2005) (Luks 2012).

The snow cover height measured at the meteorological site of the Polish Polar Station is usually small. The highest average monthly snow thickness on the ground is recorded in April, where it is 28 cm for the years 1983–2017 (Fig. 22). Noteworthy is the difference between the mean and median values, as the median is smaller in all months, e.g. in April it is 24 cm. This means that the average is overstated by the influence of relatively small number of days with thick snow cover. Considering the course of the average diurnal snow heights from the period 1983–2017, it can be seen that the snow accumulates intensively usually until the first days of February. Then comes a period of relative stabilization (Fig. 23). It is followed by a period with a slower snow thickness increase, which lasts until the first days of May. The deepest snowpack ever measured at the PPS meteorological station was 80 cm on May 14, 1998. On average, after May 7, ablation begins. It intensifies significantly at the beginning of June (Fig. 23). In the last decade of this month, the tundra is usually snow-free in the vicinity of the Polish Polar Station meteorological site.

Similarly to the average number of days with snow cover, the **average annual thickness of snow on the ground** also **decreases** (Fig. 24). In this case, the decrease is 3.8 cm per decade. The lowest snow height, both in terms of average and maximum value, was recorded in 2012, where the average annual thickness was only 3.5 cm. At the opposite extreme, there is the year 1998. This year, the average snow thickness amounted 37 cm and the deepest snow in the history of measurements at the Polish Polar Station Hornsund was recorded.

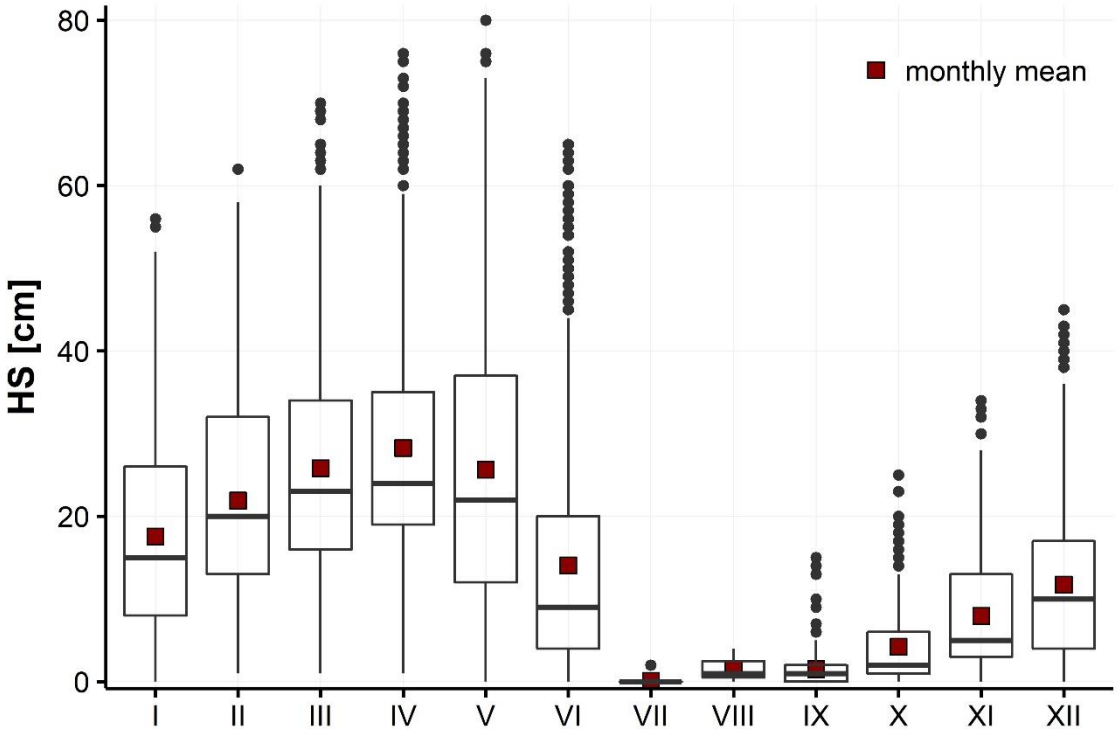

Fig. 22. Distribution of the snow cover depths in individual months of the 1983–2017 at PPS.

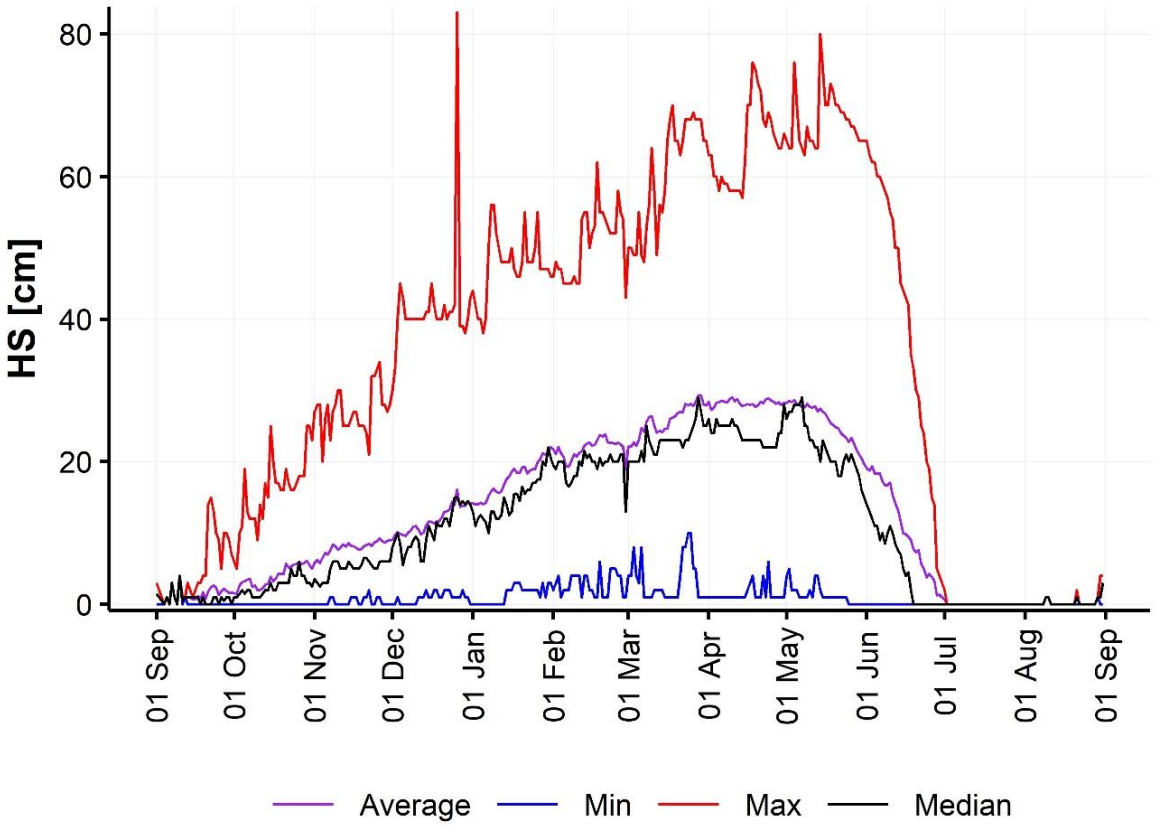

Fig. 23. Summary of the daily snow depths at PPS in years 1983–2017.

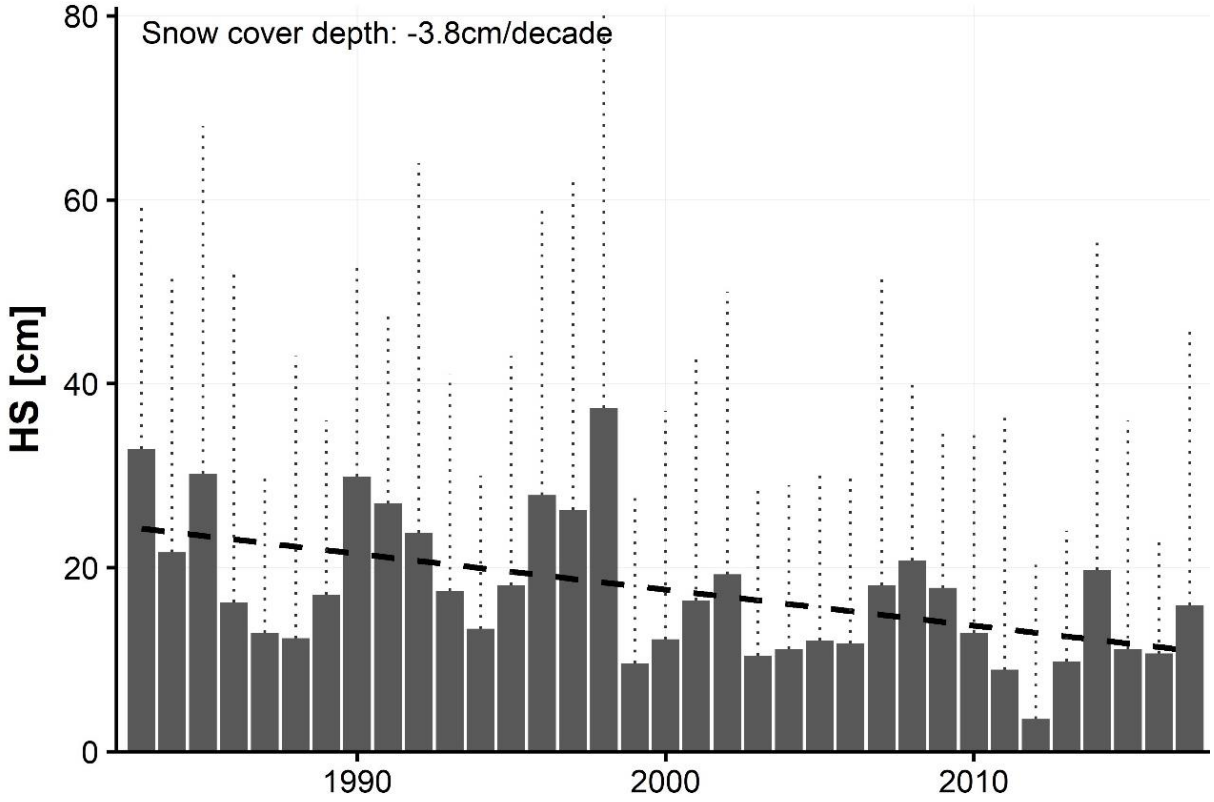

Fig. 24. Average (bar) and maximum (dotted line) annual snow cover thickness at PPS in 1983–2017.

At the end of the accumulation period, in the vicinity of the Polish Polar Station, the snow cover usually accumulates slightly over 100 mm of water equivalent. The highest average monthly water equivalent occurs in April, but more often the maximum values are reached later: in May or June (Fig. 25). This is possible despite the decrease in snow cover height due to the increase in snow density during ablation (Fig. 26). During the accumulation period, the snow cover reaches a density of 250–450 kg/m^3. Values in this range are present in 64% of all measurements (Fig. 27). Situations with lower (mainly in autumn) and higher snow density (mainly in late spring) as in this range occur almost equally often (in 17% and 19% of cases, respectively). During the ablation period, SWE can still increase due to the "soaking" of the snow cover during spring rainfalls. However, it may happen that at the measurement site, water inflows from the melting snow above, which would disturb the SWE values recorded during the ablation period. Nevertheless, the snow water equivalent measured at the station reached its highest value, exceeding 300 mm, in June 1998. A typical course of SWE at Hornsund station is shown in Fig. 28. Due to the irregularity of the measurements of this parameter, the graph shows 14-day moving average. SWE is usually checked every five days, but not regularly on the same days of the year. Such time step allows for averaging the measurements taken at irregular intervals and reflecting the annual variability of this parameter without presenting individual outliers. Figure 28 shows that the maximum amount of water accumulated in snow is recorded in April, followed by a second maximum in last days of May or beginning of June, related to the saturation of snow with rainwater and ablation water.

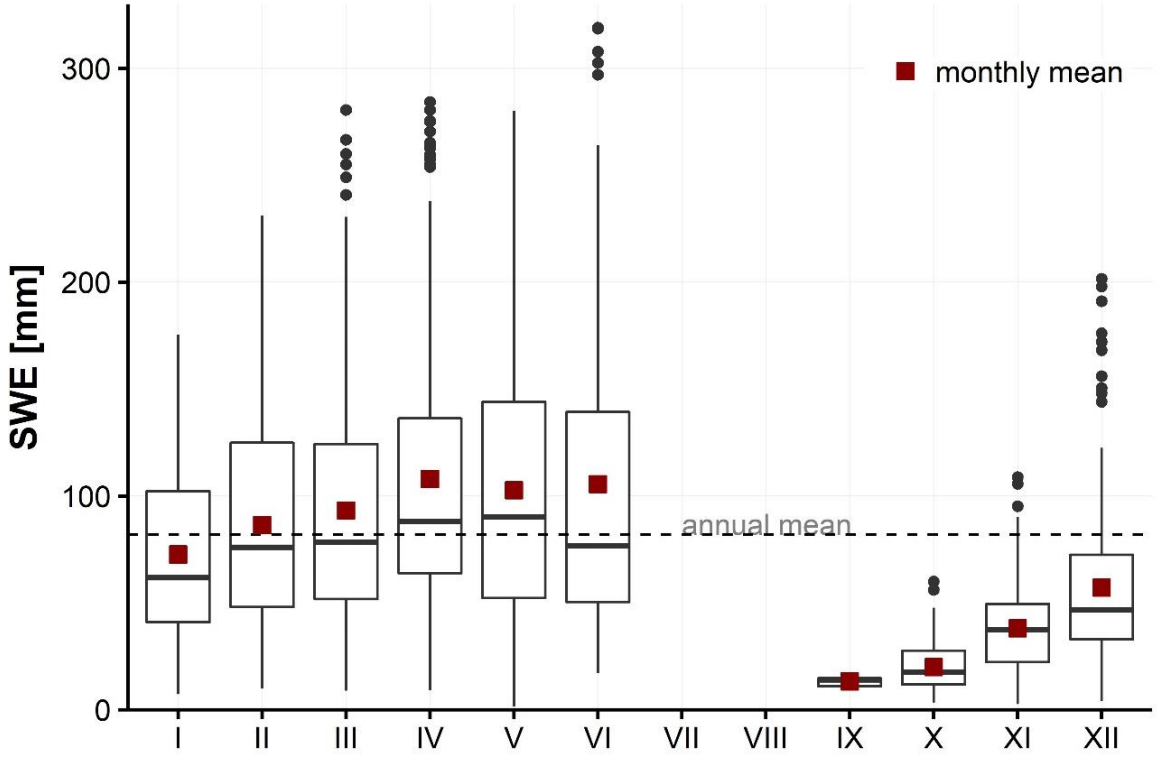

Fig. 25. Distribution of snow water equivalent at PPS in 1983–2017.

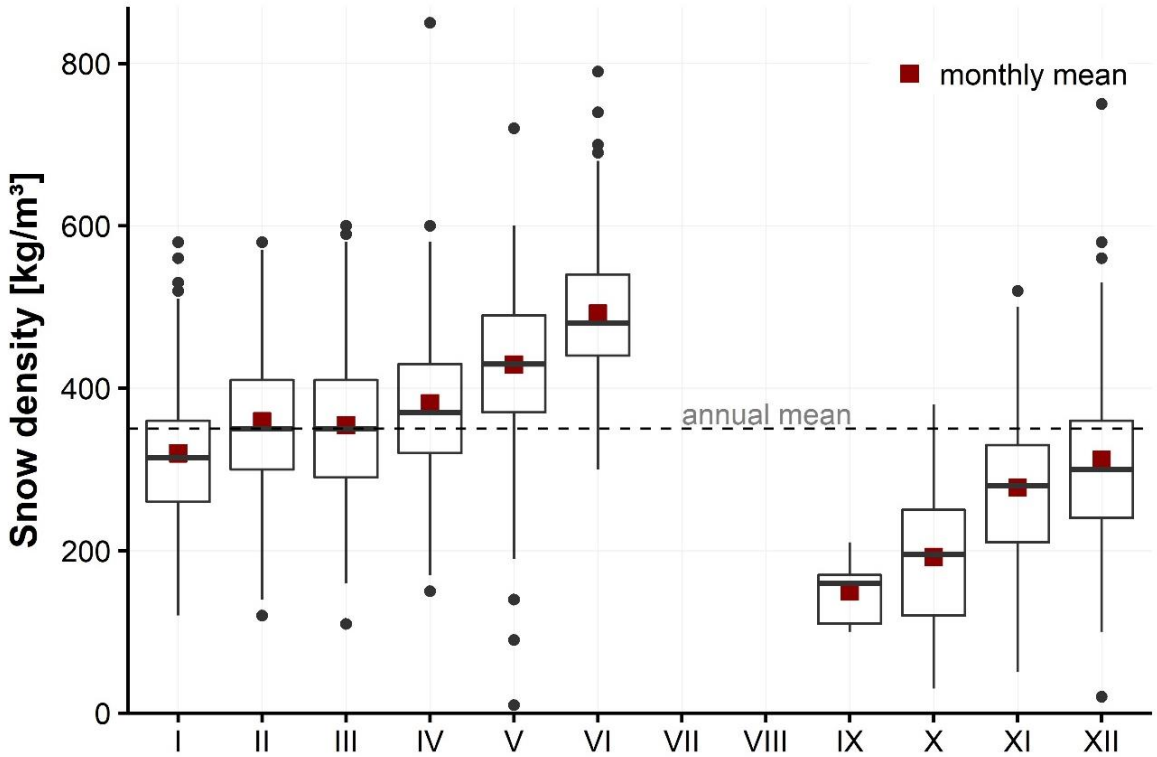

Fig. 26. Distribution of snow density at PPS in 1983–2017.

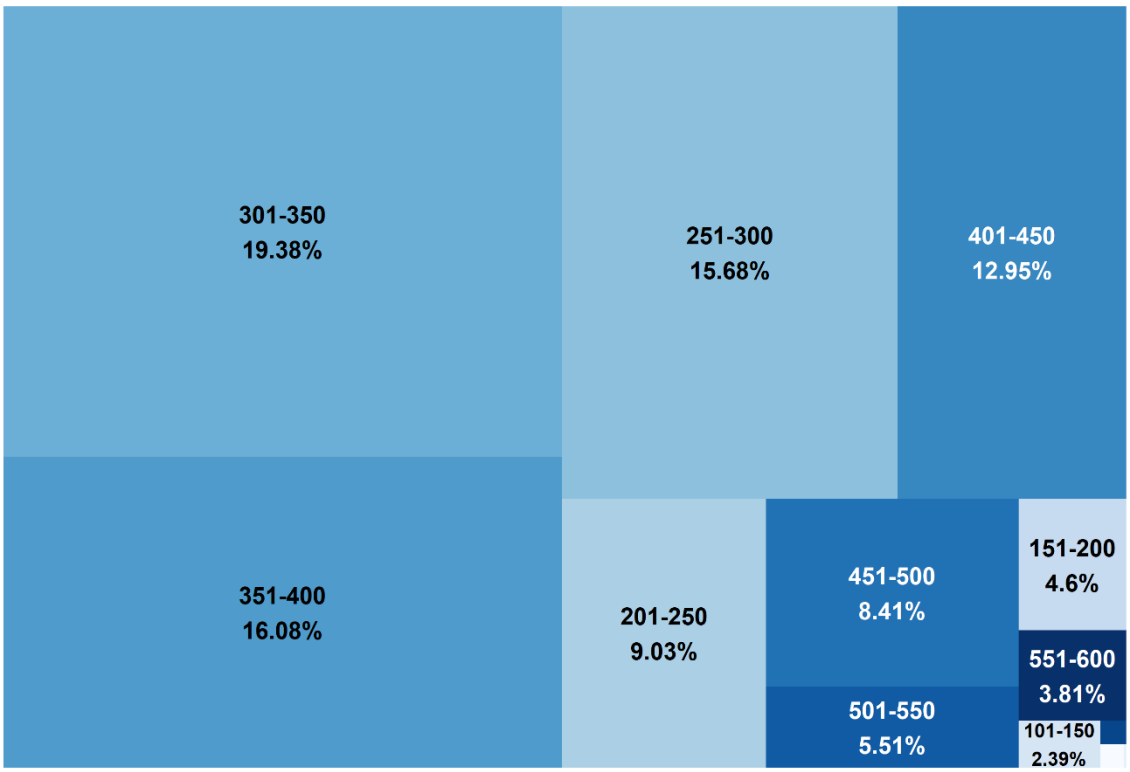

Fig. 27. Share of snow density classes [kg/m^3] at PPS in 1983–2017.

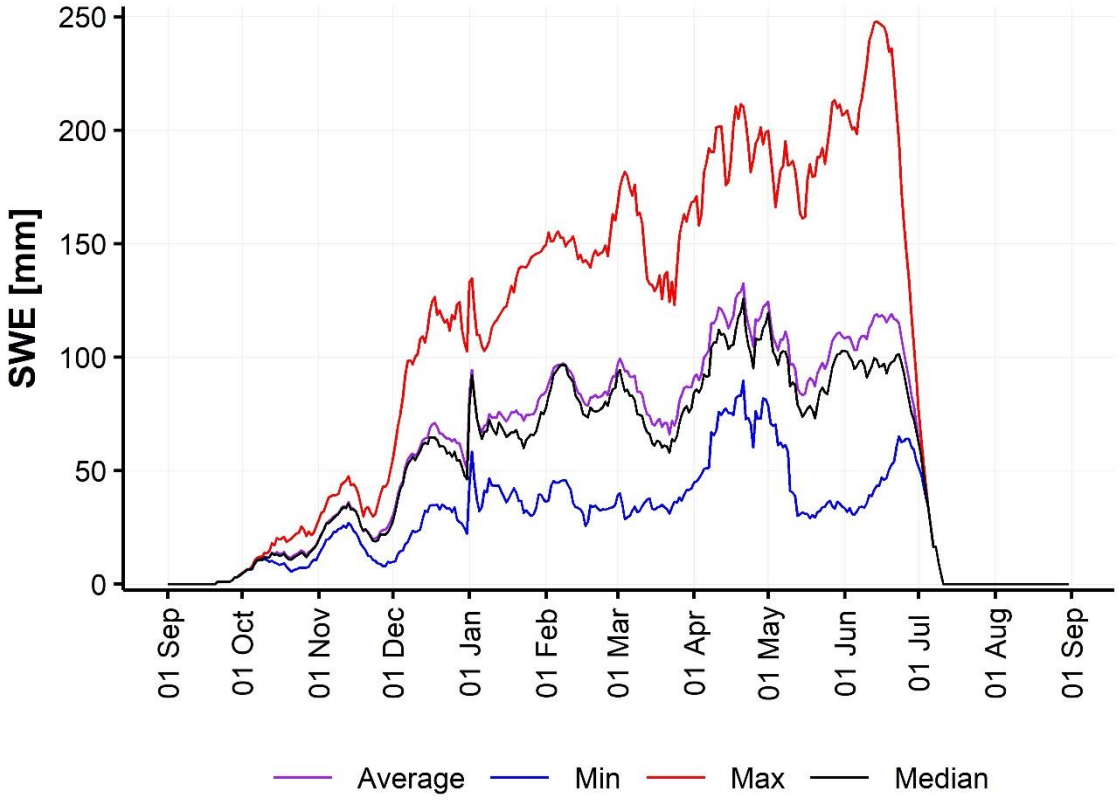

Fig. 28. 14-days moving average of snow water equivalent measurements at PPS in 1983–2017.

4. SNOW COVER OF SVALBARD TUNDRA AREAS IN THE LIGHT OF LITERATURE

4.1 Snow cover relationship with land cover and relief

There is a widespread agreement in the scientific community that in the micro and mesoscale (distances of the order of 100 m – 1 km) (Pomeroy and Gray 1995), topography and land cover are the main factors determining the distribution of snow cover (Walker et al. 2001; Essery and Pomeroy 2004; Ménard et al. 2014). In open terrain such as the tundra, snow is often redistributed by the wind activity (Sturm et al. 1995). The result is an increased deposition on leeward slopes at the expense of windward slopes, as well as the filling of troughs and terrain depressions, thereby smoothing the snow-covered surface (Meister 1989; Benson and Sturm 1993; Mott and Lehning 2010). The relief determines not only the surface roughness, the increase of which reduces the wind speed and, consequently, enhances the snow deposition (Raderschall et al. 2008). It also influences ablation by conditioning, for example, potential incoming solar radiation (Grünewald et al. 2010). The melting of snow cover occurs faster with increasing slope inclination, but also with increasing wind speed (Grünewald et al. 2010), which is indirectly influenced by the topography. This is because topography modifies the wind field, creating various types of effects increasing or decreasing the speed and direction of air flow (Kondo et al. 2002; Hertenstein and Kuettner 2005; Lewis et al. 2008; Fang and Porté-Agel 2016), thus changing the conditions of snow cover deposition and ablation.

The influence of land cover on snow distribution can be equally important. This is especially visible in temperate climates, where, for example, much greater snow thicknesses, are recorded at the forest border than in an open terrain, due to a sharp increase in the surface roughness (Ojrzyńska et al. 2010). In the forest, snow cover also persist longer due to the limitation of the inflow of solar radiation, higher air humidity and lower wind speed (Żarnowiecki 2008). However, the deposition of snow on the branches of trees or shrubs increases the contact area of snow with air, which modifies the size of sublimation in such an environment (Essery et al. 2003; Montesi et al. 2004). In the tundra ecosystem, the importance of land cover will be smaller. In Alaska, for example, 27% greater snow thickness in grasslands (Tussock tundra) was found and this increase was highly correlated with the height of vegetation (McFadden et al. 2001). However, the influence of vegetation on the distribution of snow practically disappears when it completely covers the flora protruding from the ground (Benson and Sturm 1993). In the case of Svalbard, the height of vegetation in the most favorable places for its development reaches a maximum of 25–30 cm (Rønning 1996). In the Hornsund region, the polar willow (Salix Polaris), not exceeding 10 cm in height, belongs to the highest common specimens (Owczarek 2010b). It means a rather negligible direct influence of vegetation on the spatial distribution of the snow cover in this area.

The slight influence of low vegetation on surface roughness does not mean, however, that the relationship between the snow cover and the vegetation is weak. In the high mountains, the interdependencies between the occurrence of snow and the presence of plant communities has been studied since the 19th century (Heer 1836; Vestergren 1902). Since then, plant species associated with long-lasting snow cover have been well recognized all over the world and called snowbed vegetation (see Walker et al. (2001)). Studies carried out in the Arctic Archipelago in Canada explains the richness of plant species with topography and winter snow thickness (Bliss et al. 1984). They show that the vegetation is scarce in places with thin snow cover due to the water deficiency in the soil associated with the low supply of meltwater. On the other hand, research from the Rocky Mountains area shows that the long presence of snow cover is also harmful for plants. The extremely thick snowdrifts that form there significantly shorten the vegetation season, leading to the dying of trees and replacing them with wet meadows. This is caused by the supersaturation of the soil with water from melting snow (Earle 1993). Often, the

impact of snow cover on vegetation is indirect, through changes in moisture and the amount of minerals in the soil. In places with long-lasting snow cover, the substrate is often acidic and poor in nutrients needed for the development of flora, due to the intensive washing out of the soil by significant amounts of meltwater (Tomaselli 1991; Stanton et al. 1994). On the other hand, high accumulation sites can also more efficiently capture organic and inorganic material carried by the wind. In such places, the soils are additionally enriched, which results in quite a significant development of vegetation (Walker 1985, 1990). Overall, the influence of snow cover on vegetation is ambiguous and may be both positive and negative. It depends on the prevailing meteorological conditions or the mutual relations between the components of the natural environment.

4.2 History of snow research at Svalbard, with particular attention to the Hornsund Fiord area

Snow cover research in Svalbard was initiated in the 1930s as part of pioneering scientific expeditions organized at that time (Ahlmann 1933, 1935). Observations of the snow cover were also provided by Norwegian and Russian meteorological stations established in Svalbard since 1911, or German during World War II (Lüdecke 2001). However, continuous weather observations in this area are available after 1945 (Nordli et al. 1996).

4.2.1 Studies from the vicinity of the Polish Polar Station

In the area of southern Spitsbergen, snow studies began with the establishment of the Polish Polar Station in 1957. The first scientific works concerned the glaciated areas (Kosiba 1958, 1960). One of the first studies dealing with the topic of snow cover on the tundra is the work by Baranowski from 1968. It presents the development and disappearance of snow on the ground in the first year of operation of the Polish Polar Station. Study emphasizes the insulating effect of snow cover on the ground thermal regime as well as its enormous spatial diversity, despite the flat nature of the Fuglebergsletta area (Baranowski 1968).

The subject of spatial variability of snow cover in the vicinity of Hornsund was first taken up in the work from late 1980s (Migała et al. 1988), which aggregated the results of previous snow studies (Pereyma 1981, 1983, 1988a; Rodzik 1985). On the basis of measurements from three winter seasons, it was found, inter alia: (1) the Fuglebekken catchment area has good conditions for snow accumulation compared to the surrounding areas, (2) in the above-mentioned catchment snow water equivalent is even twice as large as it would appear from the precipitation measurements at PPS, (3) snow on the tundra is very dense (400–500 kg/m^3) and its internal structure is characterized by the occurrence of many crusts layers formed during winter thaws, (4) in the lower part of the southern slope of the Fugleberget massif, higher snow thickness is recorded in its western part, while above 100 m a.s.l. in the eastern part (Migała et al. 1988). In addition to this study, several works were published before the year 2000 about the snow cover of the non-glacial areas of Hornsund. They focused on: ablation rate of snow patches on Guliksenfjellet slopes (Głowicki 1975), the influence of snow cover on the permafrost active layer thickness (Grześ 1985; Migała 1988, 1991), snow cover temperatures (Pereyma 1988b), an analysis of the course of the snow seasons 1978–1986 at the PPS, highlighting shorter snow persistence on Spitsbergen by 4–5 decades, as in the Russian part of the Arctic Ocean (Miętus 1991; Vovinckel and Orvig 1973), snow physicochemical properties (Pulina 1991; Głowacki and Pulina 2000) and weather influence on snow stratification (Leszkiewicz and Pulina 1999). After 2000, studies continued the topic of the snow thickness influence on ground thermal regime (Dolnicki 2002, 2005, 2015; Dolnicki et al. 2013; Leszkiewicz and Caputa 2004; Wawrzyniak et al. 2016) and snow physicochemical properties (Leszkiewicz and Głowacki 2001). These works emphasized the large spatial variability of

snow cover in the area of the PPS and presented it as the main factor affecting the differences in active layer thickness.

In Hornsund, the shortening of the snow cover period was also analyzed in connection with the warming observed in the Arctic, which turned out to be more intense compared to other areas of Spitsbergen (Osuch and Wawrzyniak 2017). The relationships between course of snow seasons and values of the AO and NAO indices were also investigated, but no clear correlation was found (Luks 2012; Luks et al. 2011). Moreover, variability of soil moisture and temperature in the Fuglebekken catchment was explained by the uneven distribution of snow cover (Migała et al. 2014). Most studies took into account the spatial variability of snow cover, but all of them were based on point measurements to represent different snow conditions. Until now, there have been no works presenting the distribution of snow cover in a spatial and continuous manner on the tundra.

In this respect, the recognition of snow distribution on the glaciers around Hornsund looks much better. Thanks to the measurement campaigns with numerous snow surveys, e.g. using GPR, it was possible to prove, that: (1) the height above sea level has the most important influence on snow thickness, (2) better conditions for the accumulation of snow occur in the western part of the glaciers due to the deposition of snow blown from the eastern parts in accordance with the prevailing wind direction and thanks to hypothetically increased amounts of precipitation just beyond the terrain obstacle during the most abundant snowfalls related to western circulation, (3) the above pattern of snow distribution is disturbed and more complicated for glaciers that run perpendicular to the prevailing wind directions, (4) the areas with complex topography (the vicinity of non-glacial slopes and the highest parts of glaciers) are characterized by the greatest inter-seasonal variability of snow thickness (Grabiec 2017; Grabiec et al. 2006, 2011), (5) effective transport of dry snow takes place when wind speed exceed 4 m/s (Grześ and Sobota 2000; Laska et al. 2017). For glaciers in the region of central and southern Spitsbergen, a formula was defined that allows to obtain an approximate snow accumulation (with an error not exceeding 25%) for each point on the glacier, based on data from the nearest meteorological stations (Grabiec 2005; Grabiec et al. 2012). Analyzes of snow thickness on glaciers in the macroscale (Spitsbergen as a whole) showed 2.5 to 3 times more snow accumulation in coastal areas compared to the interior of the island (Troitskiy et al. 1980; Guskov and Troitskiy 1984) and 38–49% higher at the eastern coast than at the western coast (Winther et al. 1998). It is believed that the latter regularity is associated with forced precipitation on the orographic barrier due to more frequent influx of air masses from the east (Hisdal 1976).

The first attempts to model snow cover in southern Spitsbergen were made relatively recently (Osuch et al. 2010; Luks et al. 2012; Luks 2012). However, snow conditions were modeled pointwise, based on measurements from the PPS weather station and without taking into account the spatial variability of snow distribution. In recent years, the results of simulations devoted to the variability of meteorological conditions in Svalbard begun to be published, where much attention has been paid to the snow cover (Claremar et al. 2012; Lang et al. 2015; Aas et al. 2016; Dobler and Haugen 2016; van Pelt et al. 2016; Isaksen et al. 2017). However, these models were validated primarily on measurements from glaciers, and their spatial resolution (from 10 km up to 900 m) is not sufficient to reliably present snow conditions in the Spitsbergen coastal zone.

4.2.2 Research from other parts of Spitsbergen

Analyzes of snow cover spatial variability on the tundra are carried out mainly in the Ny-Alesund region in the Bayelva catchment area (Zdanowicz 2015), where 50% of the terrain is glaciated (Nowak and Hodson 2013). Other well studied place is Adventdalen valley near Longyearbyen, where snow cover depths are artificially altered to study its effects on vegetation

(Cooper et al. 2011). Measurements in these locations allowed to conclude, e.g., that late ablation of snow hinders germination and reduces the number of flowers in plants (Cooper et al. 2011) and shortens the vegetation season, thus reducing also the duration of individual stages of plant growth (Semenchuk et al. 2016). It was also found that higher vegetation occurs in places where the snow cover persists for a relatively short time (Bruland and Cooper 2001). Additionally, macroscale satellite studies from central Spitsbergen have shown an increase in the NDVI index in the last 30 years, indicating an improvement of vegetation condition (Vickers et al. 2016). Overall, more research indicates the negative impact of snow cover on Svalbard's vegetation. This is in contrast to the results of studies from the lower latitude Arctic, which quite often refer to greater plant growth under a thick snow cover (Johansson et al. 2013) and the opposite effect under a thin cover, where vegetation may be exposed to water shortages in the summer, and in winter exposed to the destructive influence of strong winds (Walker et al. 2001; Callaghan et al. 2011). In global warming reality, the living conditions for grasses and shrubs are expected to improve, but mosses and lichens situation is likely to deteriorate, leading to an overall impoverishment of the ecosystem (Walker et al. 2006). As the frequency of rain-on-snow events increases during winter periods, there is also a risk that the initial increase in plant productivity, as expressed by NDVI, will be inhibited. This is because winter rainfalls may cause plant deaths by cutting off oxygen source caused by ice layers formation on, inside or beneath the snow cover (Phoenix and Bjerke 2016).

In the Bayelva catchment (Ny-Alesund surroundings) and DeGeerdalen valley (near Longyearbyen), numerous snow soundings were performed to validate the SnowTran-3D model (Bruland et al. 2004). Thanks to them, it was possible to show that the thickest snow cover occurred on the leeward and east-south-eastern slopes exposed to the west-northwest advection, which brought the most abundant precipitation in this area. A time-lapse camera was also installed in the Bayelva catchment, which is used to monitor changes in snow cover extent during ablation period as well as to validate satellite measurements (Westermann et al. 2015; Aalstad et al. 2018). Time-lapse pictures were also used in Ny-Alesund earlier, to monitor snow disappearance and changes in its spectral characteristics during the ablation season in 2002 (Hinkler et al. 2003). In recent years, the snow cover distribution in unglaciated areas of Spitsbergen has been studied using unmanned aerial vehicles (UAV) (Klump et al. 2014; Bernard et al. 2016; Cimoli et al. 2017). It is also worth mentioning the attempts to model the snow cover distribution and the results of measurements of the snow ablation rate on the tundra. In the vicinity of Ny-Alesund, simulations based on (1) thermal coefficient, (2) energy balance and (3) CROCUS physical model have been validated (Brun et al. 1989; Martin 1996). Other studies from this region found the greatest influence of solar radiation on snow melting rate (Harding and Lloyd 1998; Lloyd et al. 2001). In the same region, the snow cover behavior was simulated under climate warming conditions. According to them, each increase in the average annual temperature by 1 °C decreases maximum SWE by 6.9% and reduces the duration of snow cover period on the tundra by 11 days (López-Moreno et al. 2016).

5. DATA AND METHODS

Most of analyses and figures contained in the dissertation were made with the use of free R software language (R Core Team 2018) with help of RStudio Integrated Development Environment (RStudio Team 2016). The following packages were used during work on dissertation: tidyverse (Wickham et al. 2019), stringi (Gagolewski 2018), mosaic (Pruim et al. 2017), raster (Hijmans 2017), sp (Pebesma and Bivand 2005), rgdal (Bivand et al. 2018), plotly (Sievert et al. 2017), maptools (Bivand and Lewin-Koh 2017), corrplot (Wei and Simko 2017), PMCMRplus (Pohlert 2021), agricolae (de Mendiburu 2021), treemap (Tennekes 2017), and ncdf4 (Pierce 2017).

5.1 Fieldwork

The climatic characteristics of the study area presented in Chapter 3 were developed on the basis of meteorological data from the WMO 01003 synoptic station operating at the Polish Polar Station Hornsund. The data collection procedure has changed several times since 1978. In the first two years of operation, observations were carried out four times a day, while from 1980 to the present day weather parameters are recorded eight times a day. Synoptic reports are sent at 00, 03, 06, 09, 12, 15, 18, and 21 UTC. Additionally, since 2004, meteorological data has been recorded automatically every minute (Pętlicki 2012). However, not all data are measured automatically. Cloudiness or horizontal visibility are measured only at the time of observation every 3 hours. In turn, precipitation is measured every 6 hours with a standard Hellman rain gauge.

Regular snow cover measurements at the Hornsund station began in the winter season 1982/1983[1]. The snow depth is measured twice a day, at 6 and 18 UTC, and it is an average taken from five probing in the meteorological garden. Snow depth on a given day comes from measurement at 6 UTC. In addition to the thickness, the density and SWE are also assessed. These measurements are usually performed at five-day intervals using a Chomicz's snow tube sampler (Fig. 29), if the snow depth exceeds 5 cm. Several times, the sounding site of snow depth and SWE changed slightly, due to the PPS building expansion or the installation of new measuring equipment. From the 2013/2014 winter season, thickness measurements are based on snow depth gauges (Fig. 30) installed at fixed positions in meteorological site. Their scale allows to read the snow height with an accuracy of 1 cm.

In the winter season 2013/2014, weekly measurements of SWE and snow depth were initiated at 20 fixed points located in the Fuglebekken catchment area (see Fig. 2). In eight of them, snow depth gauges are installed. The remaining twelve are marked by poles driven into the snow each season. Every year, soundings are performed in the same places, and the position of the measurement points is determined by means of differential GPS. The survey start when a stable snow cover is formed and continue until part of the Fuglebekken catchment is flooded with meltwater. Snow probing is performed every 7 days. However, due to unfavorable weather conditions, the subsequent sounding was often delayed. According to statistics, the observers revisit the measurement sites after 8–11 days on average (Table 1). The SWE measurements were carried out in the same way as in the PPS Hornsund, so using a 60 cm long Chomicz' snow tube with an inlet area of 50 cm^2. This study uses data from the 2013/2014, 2014/2015, and 2015/2016 seasons.

Fig. 29. Chomicz's snow tube sampler.

[1] Measurements were carried out since the station's reopening in 1977 – not all of them, however, are available in the archives of the IG PAS.

Fig. 30. Snow depth gauge used to read the snow cover thickness.

Table 1

Statistics of snow cover probing in the Fuglebekken catchment

Season	First measurements	Last measurements	Number of measurement series	Length of the observation season [days]	Average time between transects [days]
2013/2014	2013-10-02	2014-07-03	31	274	8.8
2014/2015	2014-10-09	2015-07-06	27	270	10
2015/2016	2015-10-01	2016-06-22	25	265	10.6
2016/2017	2016-12-04	2017-06-07	21	185	8.8

In addition to the monitoring in the Fuglebekken catchment area conducted by the employees of the PPS Hornsund, data on the snow cover spatial variability were collected during fieldwork in the spring of 2016. Snow cover probing were made in the period from April 15 to May 24 at 186 points on the unglaciated coast of the Hornsund Fiord (Fig. 1, Table 2). Snow sounding was performed using an avalanche probe, which could reach a depth of up to 330 cm. In eleven points, additional SWE measurements were carried out with the Chomicz' snow tube (Table 2). Sampling was conducted in the same places as in 2014 under the AWAKE-2 project (Nawrot et al. 2015), which allowed comparison of snow accumulation between the two winter seasons. Additionally, in order to check the vertical structure of snow in each location, a single snow profile ("snow pit") was made in accordance with the international instructions (Fierz et

Table 2
Number of snow cover measurements in spring 2016

Place	Date	Depth probing	SWE	Full snowpits
Ariedalen	May 01	26	1	1
Treskelen	May 03	9	–	–
Svovelbukta coast	May 03	17	2	1
Bogstranda	May 24	31	2	–
Gåshamnøyra	May 10	24	1	1
Revdalen	April 15	46	5	2
Fuglebekken	April 18	33	–	2

al. 2009). Snow pit analyses were repeated regularly at 4 points representing different land cover in the Fuglebekken catchment and the Revdalen valley (Fig. 1). This was done to track changes in snow cover structure during ablation. For each layer specified in the snow profile, the following parameters were determined: (1) hardness, (2) temperature (measured in the middle of layer or every 10 cm), (3) density (measured with a 100 cm^3 density cutter), (4) grain size, and (5) grain shape. All measurements were made with standardized equipment and in accordance with the latest procedures developed for the unification of snow measurements in Svalbard (Gallet et al. 2018).

Additionally, in the Revdalen valley and the Fuglebekken catchment area, snow thickness was measured using the Mala GeoScience RAMAC CUII impulse ground penetrating radar (GPR) and a shielded 800 MHz antenna. Radar soundings were carried out on April 19 and May 19 in the Fuglebekken catchment area and on April 21 in the Revdalen valley. To correctly represent the analysed structure and its thickness by GPR, it is necessary to know the speed of electromagnetic wave propagation in the medium (Grabiec 2017; Maurer 2006). Based on the snow density measurements from the Fuglebekken catchment, this speed was determined at 220 m/μs and 180 m/μs for the April and May soundings, respectively. It was assumed that in April the snow was completely dry and the density amounted to 350 kg/m^3, while in May it was wet and the density reached 450 kg/m^3 (Bradford et al. 2009; Grabiec 2017). The GPR signal was recorded together with the location using the differential GPS method. For this, the Leica 1230 receiver operating in RTK mode was used, giving the measurement accuracy of 10 cm (Laska 2017). The length of time window was set to 0.2 s. The obtained radargrams were denoised and processed using the Mala Object Mapper software. The so-called near-field effect was problematic, resulting in poor signal quality at the top of the radargram, equal to approximately 1.5 times the wavelength (λ) emitted by the device (Maurer 2006). As a result, in the first 40 cm of the vertical profile, the signal was practically invisible using an 800 MHz antenna. This results from the wavelength equation:

$$\lambda = \frac{v}{f}$$

where f is the frequency and v the wave propagation velocity. Assuming the wave propagation velocity equal to 220 m/μs, the area affected by the near-field effect will cover about 41 cm of the upper profile, and at a speed of 180 m/μs, about 34 cm. For this reason, the GPR profiling with this antenna frequency makes it possible to determine the snow thickness only in sites with high snow accumulation on the tundra. In places where the signal was invisible, it was assumed

that the snow cover thickness was lower than the near-field effect. Measurements that were significantly different from the results of snow soundings performed simultaneously with the radar profiles were not taken into account.

5.2 Remote sensing data

5.2.1 Time-lapse photography

In spring 2014, the snow cover monitoring program at PPS was expanded. The time-lapse camera was installed to track the ablation of snow cover in the Fuglebekken catchment area. Ready to use Harbortronics time-lapse kits were used (Harbortronics Inc. 2018), consisting a Canon EOS Rebel T3 (1200D) camera with DigiSnap 2000 intervalometer (Fig. 31). The set was sealed in a waterproof case and powered by an 11.1 V lithium-polymer battery with a capacity of 9000 mAh and a 5 Watt solar panel. The set was mounted near the Fugleberget summit at 550 m a.s.l. and oriented towards the lower part of the Fuglebekken catchment (see Fig. 2). It has been programmed to take photo every hour with a constant aperture (f/8), ISO sensitivity (100) and focal length (18–23 mm depending on the season). Only the shutter speed was automatically adjusted to the lighting conditions. Focus of the lens was checked and manually corrected, if necessary, each time the SD card was replaced. Autofocus was not used due to the possibility of dirtying the viewing window, which could mistakenly become the focus point. The camera recorded an image in a resolution of 4272 by 2848 pixels (12.2 Mpix) and 8 bit color depth, which means that each pixel is characterized by 3 values from the range 0–255 in the following bands: red, green, and blue (RGB), where 0 is black and 255 is the full color intensity.

It was assumed that changes in the snow cover extent will be analyzed in a daily step. Due to the weather conditions (cloudiness, ice formation on the window of the camera system) data from about 25% of days were discarded (Table 3). Ultimately, 203 photos from the 3 ablation

Fig. 31. Internal view of the Harbortronics system.

Table 3
Statistics of snow cover monitoring with a time-lapse camera

Year	Date of initial deployment	Date of last processed picture	Days between dates (demanded amount of pictures)	Number of processed pictures	Success rate [%]	Date of deinstallation
2014	8.04	25.07	108	81	75	17.10
2015	23.04	5.07	73	60	82	5.11
2016	20.04	18.07	89	62	70	29.07

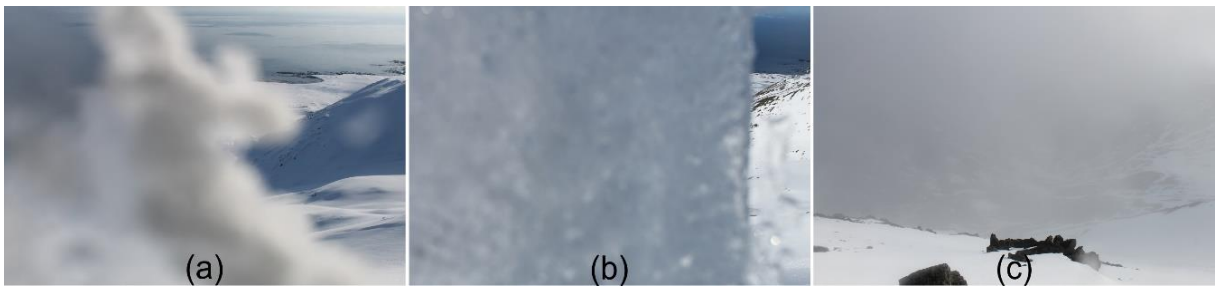

Fig. 32. Examples of photos not suitable for further analysis. From the left: (a) snow on the window, (b) ice after freezing rain, (c) fog.

seasons 2014–2016 were selected. The most common reason for rejecting the pictures for further processing was low cloud cover: Stratus in the catchment area below or low-hanging Stratocumulus at the camera level. Gaps in the data were also due to the formation of ice on the camera's housing window after episodes of freezing rain, or adhering snow after snowfall at temperatures close to 0 °C (Fig. 32). Among the photographs sufficient for further processing, those with similar lighting conditions were preferred. In the first place, the most desirable photos were from the afternoon hours, when the rock formations on the tundra cast the shortest shadow. If at that time the catchment area was poorly visible, e.g. due to low-lying clouds or precipitation events, photographs were selected from a different time of day. Those from 23 UTC were preferred, as the study area is entirely in the shadow casted by the Fuglebergет-Ariekammen massif at that time (which also means even illumination).

Raw camera photos provide a lot of information about snow cover, but cannot be analyzed spatially. This is caused by a perspective distortion, so that the image distant from the camera is perceived as small, and the one located close appears relatively large (Fig. 33). This does not allow determining the actual surface area in the photograph. In order to compare the information contained in the image cells, the previously selected 203 photos were orthorectified. This was done in MATLAB environment with "Camera Calibration Toolbox" package (Bouguet 2015) using 1 m spatial resolution DEM interpolated from original 20 m DEM (Norwegian Polar Institute 2014). For this purpose, 17 to 20 characteristic spots evenly distributed in the area were used as ground control points (GCPs) for images transformation (Fig. 34). The average root mean square error (RMSE) of the fit was in the range of 58 to 63 m for the entire camera scene, with a smaller RMSE of 39 m for the study area. In theory, once recognized GCPs should allow for orthorectification of all available photographs. However, due to strong winds and ground thawing, the camera position and its view angle have slightly changed within each season. That is why the orthorectification was performed independently for subperiods without substantial camera shifts. Although this minimized errors, it was not possible to avoid minor image shifts

between sets, which have been attempted to correct using automatic alignment algorithms. For this purpose, the "Speeded-Up Robust Features" (SURF) technique available in the MATLAB Computer Vision toolkit was used. It consists in matching images on the basis of characteristic patterns that repeat in the compared scenes (Bay et al. 2008). The technique worked fairly well for images with similar land cover, i.e. at the beginning or end of the ablation period. Unfortunately, the algorithm often selected snowdrifts changing with time as characteristic patterns in the pictures, which did not allow for the correct automatic alignment of all pictures.

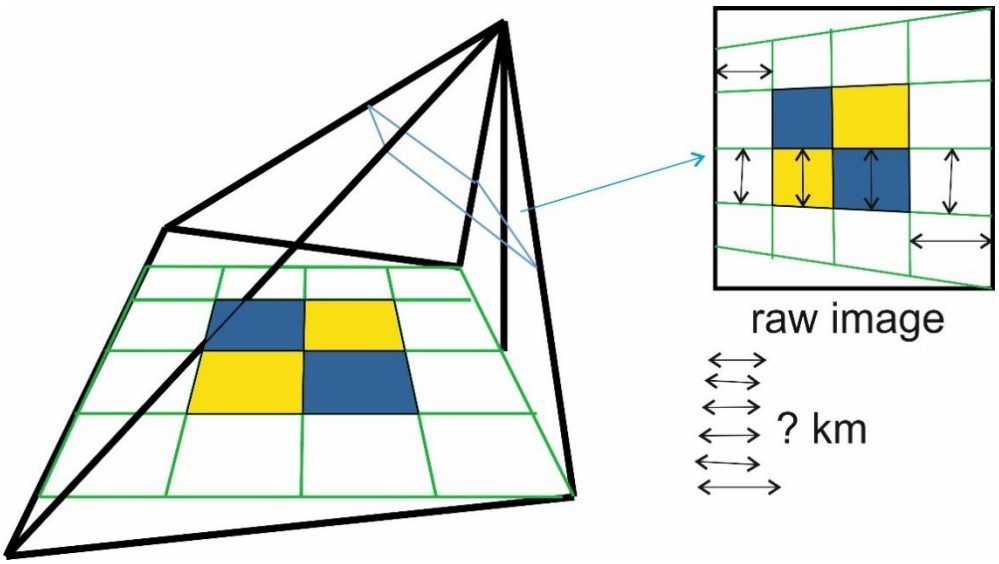

Fig. 33. Visualization of the perspective distortion problem. Modified after: http://www.cardiofx.com/media/img/perspectiveDistortion.gif.

Fig. 34. Photo from the camera mounted on top of Fugleberget with marked location of all the GCP used in the orthorectification process.

The final correction of the shifts was made in the ArcGIS environment, where the images were georeferenced using the "spline" method. It allows for the compensation of nonlinear distortions arising during orthorectification and the perfect superimposition of control points on the processed image on the target points at the reference surface (Affek 2013). A high-resolution (0.8 × 0.8 m) orthophotomap of the Polish Polar Station surroundings was used as such a reference surface (Kolondra 2003). The deviation of RMSE of the points after georeferencing using a spline transformation was always close to 0, which does not mean, however, that the entire plane is perfectly mapped. The area between the reference points may have been significantly distorted. In order to estimate the real RMSE, the matching error was checked for the first order polynomial technique in ArcGIS environment. In that case, depending on the image, RMSE was in the range of 13–55 m for the entire area, but did not exceed 21 m for the surface subjected to later spatial analyzes. The spline georeferencing of images was performed on at least 16 reference points. When automatic georeferencing was successful in ArcGIS (working similarly to the aforementioned SURF method – based on finding characteristic patterns common on the compared images), the number of reference points exceeded 100. This allowed to obtain a very high mapping accuracy, but it did not completely eliminate shifts between individual images, which could be the cause of errors in spatial analyzes.

After the aforementioned transformations, each pixel of the image represented an equal space of approximately 1 m^2. In order to determine area covered by snow (SCE – snow cover extent), a binary classification was made, dividing the surface into snow-covered and snow-free areas. In all images where snow or other high-albedo material covers part of the terrain, the pixel brightness histogram should follow a bimodal pattern. In such pictures, high values represent high-albedo surfaces such as snow (Fig. 35). The images can therefore be easily divided into 2 parts by looking for the least frequent value between two modal values and selecting it as the threshold value. This method allows for relatively easy automatic processing of many photos at the same time, which was used in snow cover studies in various locations (Salvatori et al. 2011; Härer et al. 2013). In this work, snow classification was performed using threshold value in blue band. As in previous studies, it turned out that it is best to distinguish the snow cover from other surfaces with values of about 150 in this band (see Fig. 35c). In the above-mentioned works, the value of 127 was adopted as the minimum value, which should be used for the snow cover classification (Salvatori et al. 2011; Härer et al. 2013). In the present study, threshold values in the range of 115–200 of the blue band were used, depending on the prevailing lighting conditions. In a single case (this occurred on May 23, 2016), the threshold value was lowered to 92 to correctly separate the snow on the image. This exception was made due to the appearance of brownish melt water on the surface of the snow cover (Fig. 36). A fully automated approach was not used due to the frequent misclassification of shaded or wet snow surfaces as snow-free surfaces. Instead, images after a preliminary binary classification using a threshold value of 150 were visually compared to the original image and, in the event of unacceptable results, corrected by changing the threshold value until satisfactory results were obtained. Due to the time-consuming nature of such a procedure, a model was created in ArcGIS 10.5 that allows for processing many images at the same time. The model requires preliminary sorting of RGB rasters into individual folders in terms of threshold values, which will be used to separate the desired surface (in this case, snow cover) from the surrounding area. After determining the threshold value and an optional mask indicating the study area, the model classifies all pictures and calculates the extent covered by the two outcome surfaces. The result is automatically saved in the spreadsheet. The tool is available for download from the supplementary materials to the article (Kępski et al. 2017a).

The classification was performed from the maximum accumulation period to the complete ablation of the snow cover. Within the analyzed extent there is a white environmental house

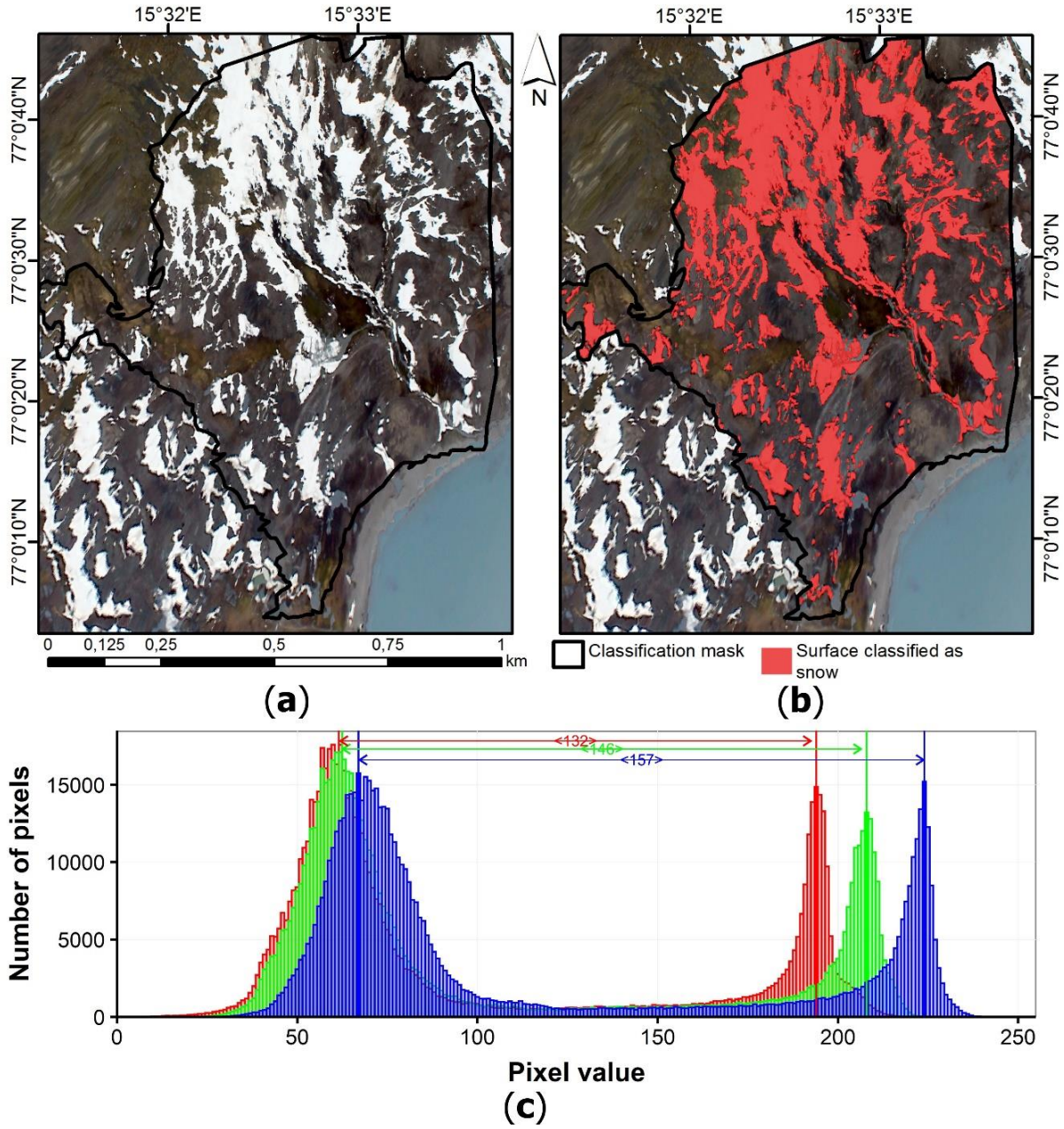

Fig. 35. Classification example for June 5, 2016: (a) orthoimage zoomed to classification area; (b) classification result with threshold value in blue band set to 140; (c) frequency histogram of RGB values with characteristic bimodal distribution. Visible is the largest distance between modal values for the blue band.

and some areas covered by water that can reflect solar radiation directly to the camera, which, under the adopted method, were often classified as snow surfaces. Therefore, the moment of snow cover complete disappearance was assumed to be the first day when the SCE in the study area fell below 2%.

The total camera field of view installed on Fugleberget is approximately 5.7 km^2. The final area subjected to spatial analyzes was limited to the size of the available maps overlapping the camera's field of view: geomorfological (analyzed area: 1.8 km^2), vegetation (0.72 km^2), and soil type (0.72 km^2). Additionally, the surface obscured by topographic obstacles (determined by Visibility tool in ArcGIS software) and the most distorted during the orthorectification pro-

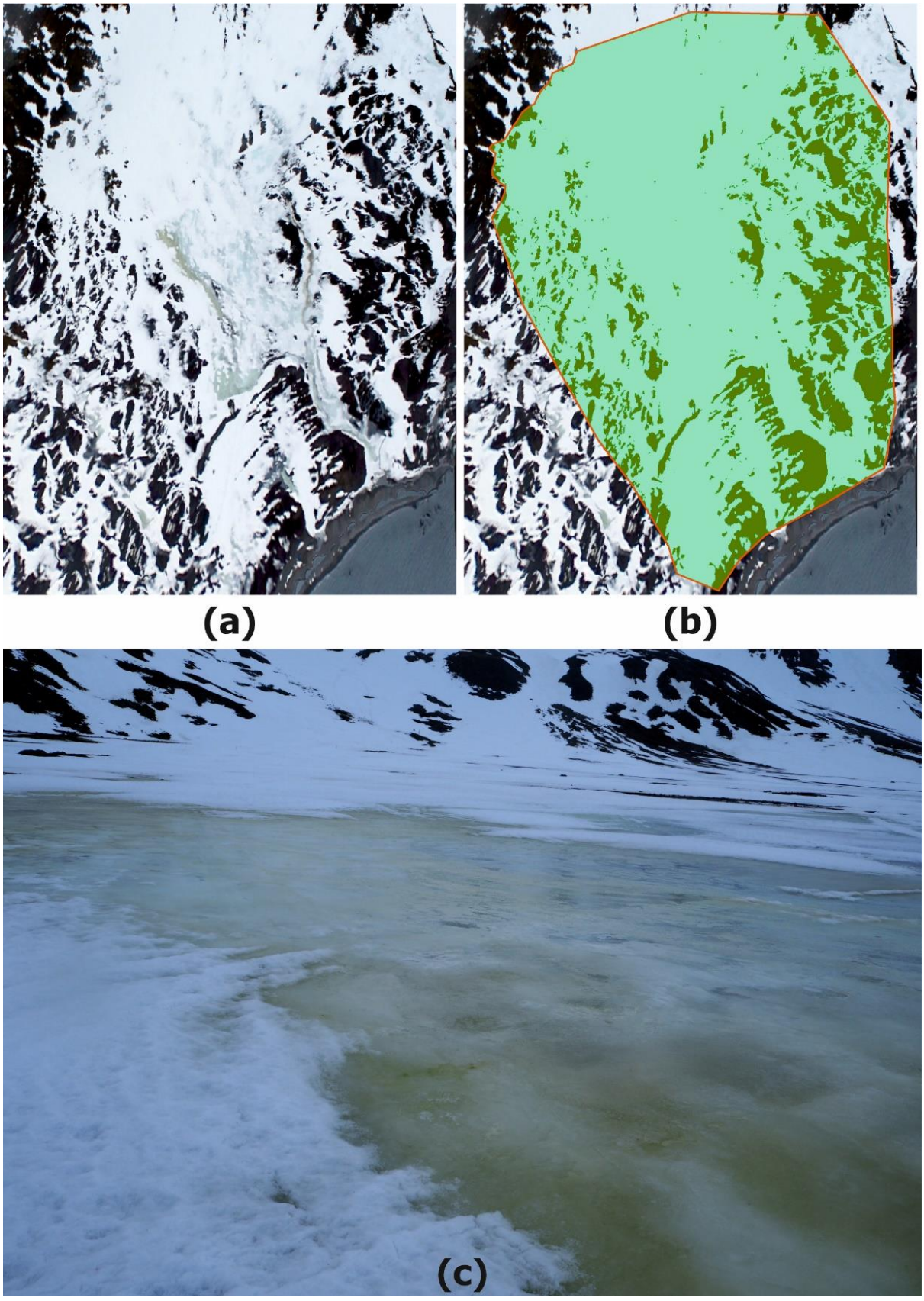

Fig. 36. Classification example for May 23, 2016: (a) orthoimage zoomed to classification area with dark meltwater visible; (b) classification result with threshold value in blue band lowered to 92; (c) photography from the field.

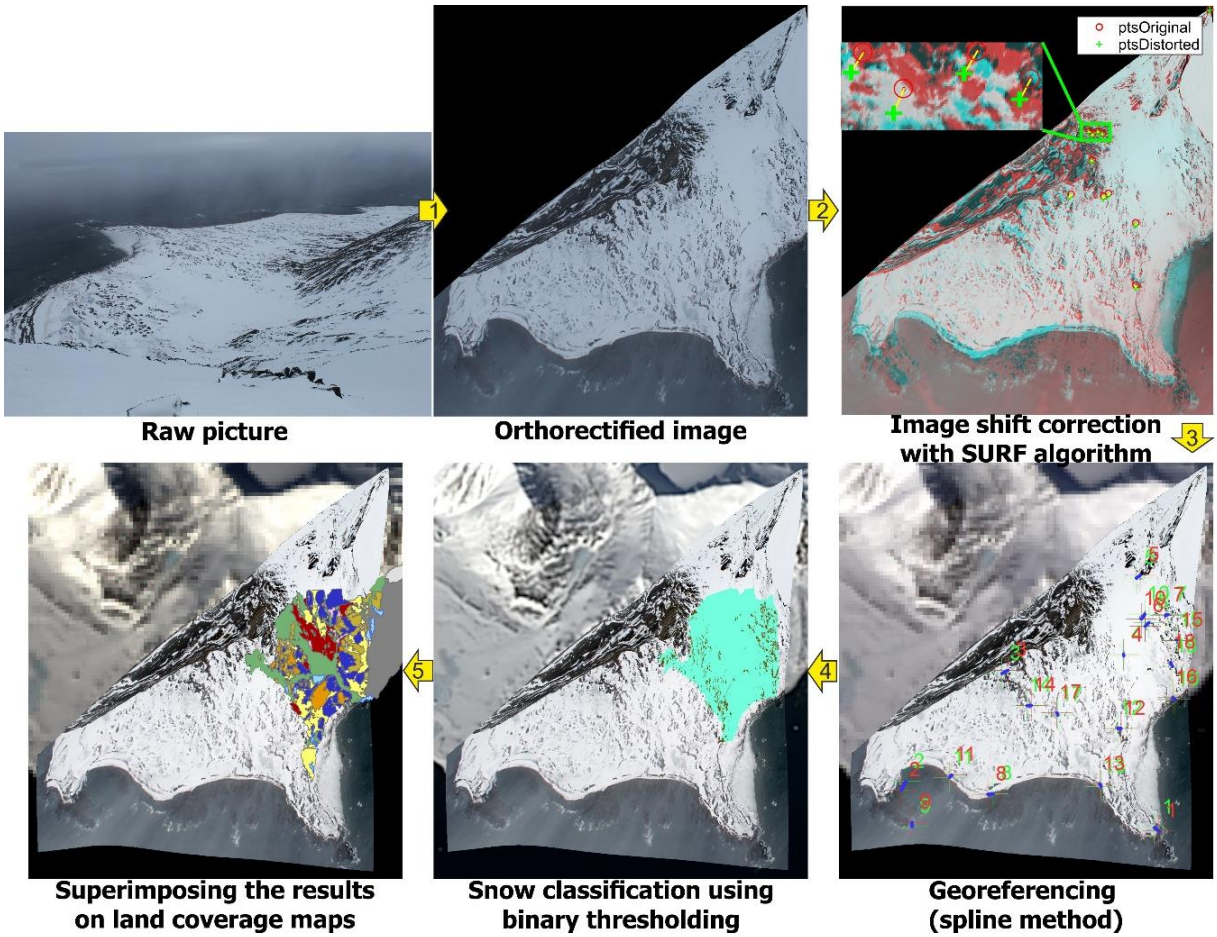

Fig. 37. Workflow for the images obtained from the time-lapse camera. Modified after Kępski et al. (2017a).

cess was masked. That was mostly terrain in greater distance from the camera, e.g. west of the Wilczek Peninsula. Information about tundra vegetation types was in the form of ready-to-use shape file used in the GIS software (Migała et al. 2014). The geomorphological (Traczyk and Kasprzak 2008) and soil type (Szymański et al. 2013) maps were georeferenced and vectorised by the author of the present study before further processing.

The variability of snow coverage on different terrain surfaces in the catchment was checked by comparing the results of image classification with the information from digitized geomorphological, soil, and tundra vegetation maps (Fig. 37). For each terrain class, the percentage of snow coverage on a given day was calculated. Then, using the Kruskal-Wallis test, it was checked whether the differences in snow coverage between particular landforms were statistically significant. The procedure was performed in R environment (Pohlert 2021) using post hoc Dunn test with Bonferroni's *p* adjustment method (Dunn 1964) to quantify the differences between individual land cover types. Such tests were used due to distribution of values not meeting the normal distribution criterium, which did not allow the use of the analysis of variance (ANOVA) method (Conover 1999). The same procedure was repeated for a series of snow cover thickness and SWE measurements in the Fuglebekken catchment. Date of snow cover disappearance and information about terrain type were assigned to all 20 measurement points in the catchment using set of georeferenced data. The date of snow disappearance was considered to be the first day when the pixel with the measurement site and all 8 surrounding cells were snow free (Fig. 38). Comparison of measured SWE and snow thickness values with quan-

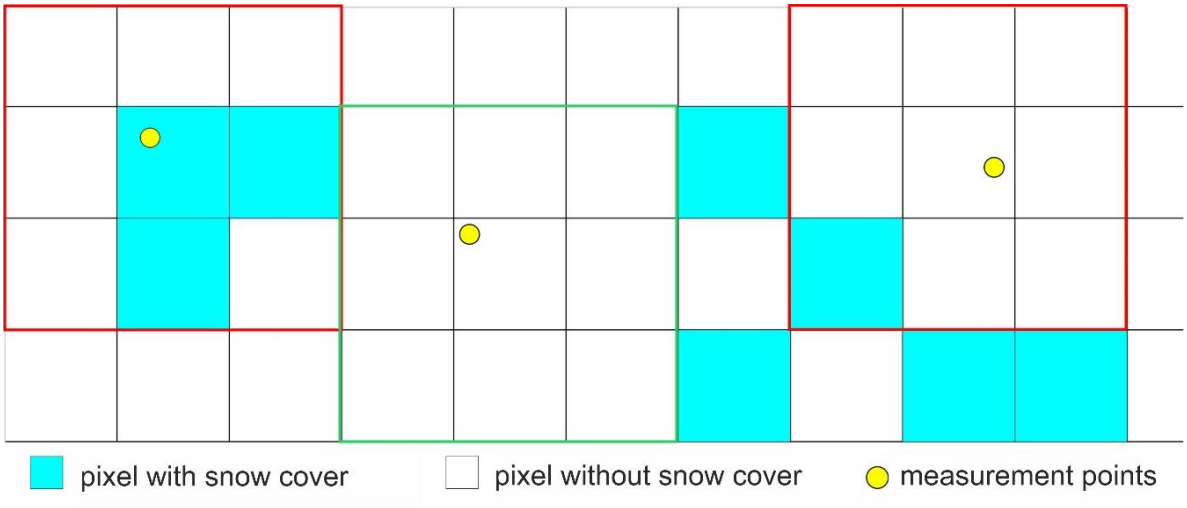

Fig. 38. The principle of determining the date of snow disappearance at the measurement site. In the above case, the middle point is considered snow-free.

titative data like topographical indices, modelled meteorological elements (air temperature, potential sunshine duration etc.) was performed using standard Pearson correlation coefficient (Fotheringham and Brunsdon 1999; Hauke and Kossowski 2011). The relationships with *p* value not exceeding 0.05 were assumed as statistically significant (Dallal 1999).

The differences in snow cover ablation process was illustrated by the superimposition of the binary classification results of photos from the 2014–2016 seasons. Each year, ablation begins at a slightly different time. Therefore, the course of snow disappearance between consecutive years was compared using pictures with the same share of snow coverage, instead of those from specific dates. Images from the days when the SCE was approximately 72%, 33%, and 4.5% were superimposed. Such a share of snow surface was present in the processed images in all analyzed seasons, while more intuitive values, such as 50%, were unavailable in pictures from at least one year due to, e.g., fog occurrence (see Fig. 32). The result of superimposing images from three ablation periods representing the same SCE is a raster composed of pixels ranging from 0 to 3, where 0 means snow free in all seasons, and 3 is snow present in all 3 years.

5.2.2 Satellite imagery

In addition to time-lapse images characterized by high spatial-temporal resolution, four Landsat 8 satellite images from the 2014 ablation season were analyzed. This satellite has been collecting data since 2013, imaging the Earth's surface in 11 spectral channels. First 9 channels are provided by the Operational Land Imager (OLI) sensor, while channels 10 and 11 are provided by the Thermal Infrared Sensor (TIRS) sensitive to thermal infrared wavelength bands. In this study, only the data from the OLI sensor were used. They are characterized by a 30-meter spatial resolution, except for the panchromatic band with a higher, 15-meter resolution. The use of satellite images was intended to rank unglaciated coastal regions in terms of snow cover duration, with reference to more accurate results obtained in the Fuglebekken catchment area. For this purpose, the analysis area was divided into sectors for which the share of the snow covered area was calculated (Fig. 39). However, while the time-lapse camera provided information on the SCE in over 200 days in 3 ablation seasons, for the same time period it was possible to find only 7 satellite images with a little cloud cover allowing for SCE recognition on the shores of the Hornsund Fiord. These were images from 07.04.2014, 25.05.2014, 03.06.2014, 15.06.2014, 26.04.2015, 12.05.2015, 19.04.2016. Scenes showing the early and late ablation stages were

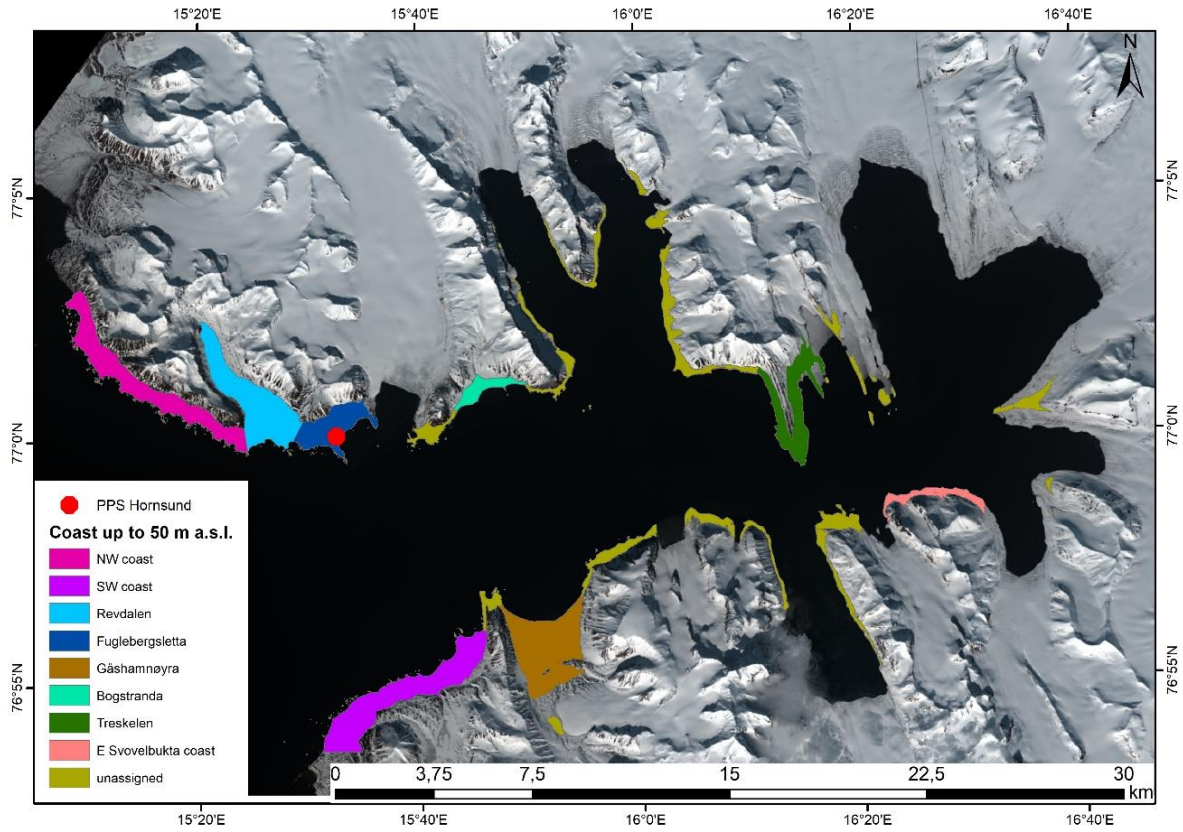

Fig. 39. Division of the Hornsund Fiord coast on sectors for which the snow coverage was calculated.

obtained for 2014 only, so only this season was taken into account. Satellite scenes were downloaded from the https://earthexplorer.usgs.gov/ portal administered by the United States Geological Survey (USGS). The acquired images were already radiometrically and *geometrically* corrected (USGS 2016), but required additional processing before classification. Raw pixel values in the form of digital number (DN) were converted to the reflectance at the top of the atmosphere (TOA reflectance) with correction for the angle of incidence of sunlight according to the formula (USGS 2016):

$$\rho\lambda = \frac{M\rho Q\text{cal} + A\rho}{cos\,(\theta\text{sz})}$$

where $M\rho$ and $A\rho$ are multiplicative (M) and additive (A) rescaling factors specific to certain Landsat spectral bands, Qcal is the quantized and calibrated standard product pixel values (DN) and θsz is the local solar zenith angle (90° – the angle of incidence of the sun's rays at given location and time). All the values required in the formula are provided in the metadata of the downloaded satellite image.

Before starting the analyzes, efforts were made to minimize the effects of different atmospheric scattering on the compared satellite images. The images were atmospherically corrected using the so-called Dark Object Subtraction (DOS) method. This technique assumes that it is possible to get rid of the atmosphere haze component in the images by finding their darkest part with the lowest pixel values and assuming that they only represent atmospheric scattering, without which the object would be perfectly black and thus have a brightness of 0. The DOS method can be used manually by finding a hypothetical perfectly black surface in the image, usually a deep water reservoir, and subtracting its lowest pixel value from all scene cells (Teillet and Fedosejevs 1995). In the Arctic, this approach can be problematic due to the highly variable

optical properties of seawater (which is usually the darkest object) as it can freeze or carry large amounts of suspended particles (Matsuoka et al. 2011). In this study, DOS was applied in the same way as in the work of Gilmore et al. from 2015, so by using the tool from ENVI software, which automatically subtracts the darkest component from the satellite image (Gilmore et al. 2015).

The last step before classifying satellite images into snow covered and snow free surfaces was to mask problematic areas unsuitable for analysis. Despite the selection of almost cloudless photos, the local cloudiness in some places obscured part of the Hornsund Fiord shores (Table 4). In the affected scenes, these places were masked using CFMask product (Zhu and Woodcock 2012; Zhu et al. 2015) available from https://espa.cr.usgs.gov/ website.

Table 4

Cloud cover on the analyzed satellite images

Image acquisition date	The share of cloudiness over the area of analysis excluded by the CFMask algorithm	Scene cloud cover (from metadata)
07.04.2014	1.0%	7.7%
25.05.2014	0.0%	7.6%
03.06.2014	0.0%	26.9%
15.06.2014	9.8%	58.7%

The classification of the processed satellite images was performed applying thresholding technique in a similar way as for time-lapse pictures. One of the most frequently used indices for differentiating the snow from other surfaces on satellite scenes is the *normalized difference snow index (NDSI)* (Dozier 1989; Hall et al. 1995; Hall and Riggs 2011). For the Landsat 8 imagery it is obtained by combining the values from green (band 3; EM wavelength 0.53–0.59 μm) and short-wave infrared (band 6; EM wavelength 1.57–1.65 μm) spectral bands (Ke et al. 2015):

$$\mathrm{NDSI} = \frac{\mathrm{Band\ 3} - \mathrm{Band\ 6}}{\mathrm{Band\ 3} + \mathrm{Band\ 6}}$$

In order to calculate area covered by snow on available Landsat 8 images, two different methods were tested. The first and most frequently used in scientific studies (i.a. Hall et al. 1995; Xiao et al. 2002; Sibandze et al. 2014) assumes that all pixels with an NDSI value greater than 0.4 represent the snow covered surface. The second approach was to manually adjust the NDSI threshold to each scene separately. This method is recommended for processing a small number of images as it is the most accurate and reliable (Racoviteanu et al. 2009; Burns and Nolin 2014). The evaluation of the classification results was made on the basis of visual analysis of the panchromatic channel. It is worth mentioning that it is possible to distinguish snow cover directly from the panchromatic channel with a higher resolution (Vogel 2002). However, such approach requires performing the classification separately for shaded and sunny places (Vogel 2002). By analyzing satellite scenes with different angles of incidence of sunlight, this would mean a time-consuming manual vectorization of areas with variable lightning conditions. At high latitudes, satellite scenes for the same area are captured more often. However, the analysis of additional images is problematic due to variable local acquisition time and scene orientation (Bindschadler 2003), which further complicates the problem with terrain shadows. For this reason, the classification in the panchromatic band was carried out only in an evenly lit area for

the purpose of validating the results obtained with the NDSI index, and it was not used independently in spatial analyzes. The workflow of satellite imagery processing is briefly presented in Fig. 40.

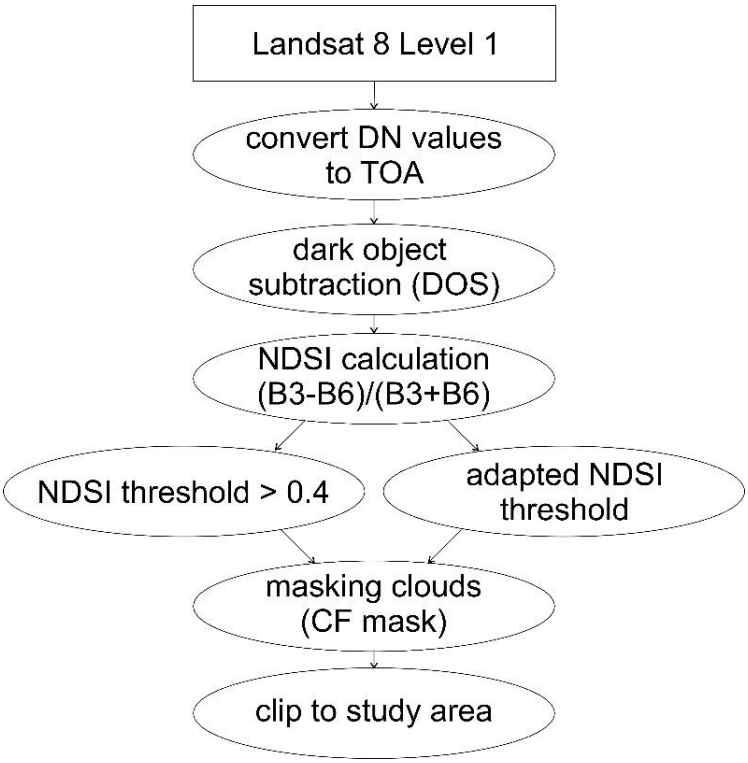

Fig. 40. Workflow of satellite imagery processing.

5.2.3 Topographical indices

Relation of snow cover with terrain features was investigated using topographic indices calculated in GIS software (SAGA, QGIS, and ArcGIS) on the basis of available DEMs. In the case of the Fuglebekken catchment, DEM with a resolution of 1 m was used, derived from laser scanning performed in summer 2016 (Pętlicki 2016). The 20 m Norwegian model was used for the Hornsund Fiord coast area (Norwegian Polar Institute 2014). The analyzes took into account: altitude a.s.l., terrain slope and aspect, ruggedness (Terrain Ruggedness Index (TRI); calculation radius 1 m) (Riley 1999), Topographic Position Index (TPI; calculation radius 10 m) (Guisan et al. 1999), Convergence Index (calculation radius 10 m) (Kiss 2004), Topographic Wetness Index (TWI) (Böhner et al. 2002), General Curvature Index (Heerdegen and Beran 1982), amount of incoming solar energy and an wind exposition index to cardinal and ordinal directions (N, NE, E, SE, S, SW, W, NW).

Analyzes using topographic indices make sense when they are related to spatial information provided, for example, by a laser scanner (Revuelto et al. 2014), a large amount of point data obtained traditionally (Hosang and Dettwiler 1991) or from GPR (Grabiec 2017). Studies that use only the information about the SCE are less common (Kirnbauer and Blöschl 1992). However, in the present study, the classified satellite and time-lapse images constituted the largest resource of spatial data. In order to relate these data to the terrain features, a mosaic of images from the Fuglebekken catchment area was prepared, presenting the snow cover duration as the sum of all classified images from spring 2014. The 2013/2014 season was selected due to the greatest data completeness and the best quality of georeferencing expressed by the lowest

RMSE. For a larger area of the Hornsund Fiord coast, the classified satellite scene from June 15, 2014 and the snow thickness measurement results from 2016 were used. The relationship between topographic indices and snow depth measured at fixed points was also checked.

5.3 Snow stratigraphy representation in SNOWPACK Model

Today, there are many models focusing on snow cover created for different purposes. Some of them were developed solely for hydrological purposes in order to predict the amount of runoff from the catchment area. In such cases, a simplified approach linking the snowmelt rate only with the air temperature is often sufficient. History of temperature index models reaches the nineteenth century (Finsterwalder 1887) and consists in long-term adjustment of water runoff volume during ablation to the contemporary air temperatures. For this purpose, both the amount of runoff from the entire catchment area as well as changes in the SWE observed on a smaller scale can be used. Based on the measurements, the snowmelt rate is averaged and given in, e.g., mm/day/°C for a specific location. These values are often adjusted to the season of the year (Arendt and Sharp 1999), thus taking into account indirectly the change in surface albedo and insolation conditions. Attempts have been made over time to improve the simple simulations by taking into account additional parameters, such as wind speed and relative humidity (e.g. Kustas et al. 1994). More sophisticated than the aforementioned temperature models are those based on the energy balance. In such models, instead of temperature, measurements of sensible and latent heat fluxes as well as shortwave and longwave radiation are required to simulate snow cover ablation (Braithwaite 1995). Although theoretically better, they often do not take into account, for example, the cooling of snow cover, so that some of the energy absorbed by it is first used to warm it to 0 °C. Ignoring this effect usually leads to an overestimation of the melting rate in energy balance models (Kane et al. 1997; Bruland et al. 2001). In the Svalbard region, the empirical temperature index models assume ablation of snow cover on the tundra (Ny-Alesund region) at the level of 3 to 7 mm/day/°C (Bruland and Sand 1994; Killingtveit and Saelthun 1995; Bruland et al. 2001).

Simple methods of modeling the snow ablation rate can be effective and do not require much input information. Therefore, they are readily used in areas with poorly known meteorological conditions (see Hock (2003) and references cited there). However, much better results are achieved with the use of complex physical models requiring a large amount of batch data with very high time resolution, which has been confirmed by a few studies using them in the Svalbard area (Bruland et al. 2001). The most recognizable numerical physical models taking into account the internal structure of snow cover include: SNTHERM developed by Cold Regions Research and Engineering Laboratory (CREEL) in United States (Jordan 1991), French CROCUS from *Centre d'Etudes de la Neige* and SNOWPACK created by Swiss Federal Institute for Forest, Snow and Landscape Research (SLF WSL). Each of them has been used at least once in the Svalbard region (Bruland et al. 2001; Winther et al. 2003; Obleitner and Lehning 2004). Currently, the most advanced CROCUS and SNOWPACK models are further developed. The SNOWPACK model was chosen for the purpose of this study, mostly due to the open GNU *Lesser General Public License* and the extensive documentation available on-line. Important was also the format of meteorological data collected by the Institute of Geophysics, Polish Academy of Sciences and the Faculty of Earth Sciences of the University of Silesia allowing for the preparation of input files with an appropriate structure and resolution for the model developed in SLF WSL.

The history of SNOWPACK dates back to the end of the twentieth century, when it was developed together with the expansion of automatic weather stations network in the Swiss Alps (Lehning et al. 1998,1999). Originally, it was primarily used to predict avalanche danger. Its detailed description is contained in a series of papers published in Cold Regions Science and

Technology journal (Bartelt and Lehning 2002; Lehning et al. 2002a,b). The model is one-dimensional, meaning that it simulates the vertical structure of snow cover only at a specific point for which meteorological data was provided. To run the SNOWPACK simulation, it is required to provide information about (the abbreviation identifying the variable in SMET format is given in parentheses):

- Air temperature (TA),
- Relative humidity (RH),
- Wind speed (VW),
- Incoming shortwave radiation (ISWR) and/or reflected shortwave radiation (RSWR),
- Incoming longwave radiation (ILWR) and/or (snow) surface temperature (TSS),
- Precipitation sum (PSUM) and/or snow height (HS),
- Ground temperature (TSG).

Additional variables that can be given as inputs are ground and snow temperature at different depths. This data must be provided **at least at hourly intervals**, preferably in the **SMET format** developed and used by SLF WSL (Bavay 2017). Preparation of meteorological data, as well as their interpolation or generation in case of missing files is facilitated by a special MeteoIO library written in C++ (Bavay and Egger 2014). The MeteoIO is integrated with SNOWPACK and required for its correct operation. In addition, it is necessary to provide an **SNO** file as input. It contains information about the **soil structure**: the number of layers, their thickness, density, porosity, free water content, size and shape of soil grains, and their temperature just before the start of the simulation. If the model is run when there is already snow on the ground, the SNO file should contain a similar description of the vertical snow cover profile. Additionally, in the file header, the following should be specified: **aspect and slope** of the terrain, the **height of vegetation** together with leaf area index and the **albedo of the snow-free surface**. This file is required, but it may not contain any information other than the header if the model is started during the snow-free period and the soil module is turned off in the settings.

The SNOWPACK outcome is information about the snow vertical structure in a given time span, taking into account all the meteorological data provided. The software forecasts the thickness of each snow layer, its density, humidity and the shape, size and form of grains, along with a full temperature profile, also in the soil medium if it is included in the SNO file. On their basis, the model also calculates additional parameters such as albedo and temperature of the snow surface, heat fluxes directed to the atmosphere or soil, and many others. Output saved is in the form of MET (snow "meteorology" – information about heat fluxes, etc.), PRO (data about snow vertical structure), and HAZ (the calculated thickness of new snow layers and/or the increase of rime) files. SNOWPACK also returns SMET and SNO files with data gaps filled in by MeteoIO. The module update those files with modified snow and soil properties until the simulation is completed. In the model settings it is possible to define the output format to CAAML [http://caaml.org/]. Such files are used inter alia by mountain search and rescue groups to create simplified vertical snow profiles, opened by software such as SnowPilot [https://snowpilot.org/] (Chabot et al. 2004). The MET, SMET and, above all, PRO files thus created can be visualized using NiViz software (Fierz et al. 2016), available both in standalone and online version [https://niviz.org/]. Its advantage is the full interactivity achieved with the use of JavaScript language and the ability to export the obtained results to the JSON format commonly used by web browsers. The SNOWPACK profiles presented in Chapters 8 and 9 of this work were created with the NiViz software.

The input data for the SNOWPACK model were prepared for the location of the meteorological measurement site of the PPS Hornsund (77,00070N; 15,53943E) based on the readings from the Vaisala Automatic Weather Station (AWS) (see Table 5). One of the variables required

in the model is the ground surface temperature (TSG) that is not registered in PPS Hornsund. As a substitute for TSG, a ground temperature measurement at a 5 cm depth was used. The information recorded by automatic sensors of the WMO 01003 station does not include measurements of shortwave and longwave radiation components. For this reason, the prepared SMET files were supplemented with the readings of the Kipp & Zonen CNR1 net radiometer mounted on a nearby mast standing in front of the PPS Hornsund building (77,00138N, 15,54179E). The SNOWPACK model also requires a higher temporal resolution of precipitation and snow thickness data than those recorded at the station (see Chapter 3). In addition to the standard precipitation measurements with the Hellman rain gauge, the following automatic devices work at the PPS: the Geonor T200B weighing precipitation gauge and the OTT Parsivel laser disdrometer. Both devices provide data in real time, with a measurement record every two (Geonor) or one minute (Parsivel). Due to problems with the correct estimation of the precipitation intensity during strong winds by Parsivel devices, the data from weighing gauge was used. Measurements with the Geonor device are, however, sensitive to changing thermal and wind conditions, which cause "noise" in the precipitation weight reading (Duchon 2008). The values were corrected by comparing them with the measurements obtained from the Hellman rain gauge. In this way, cases where Geonor indicated an increase in precipitation totals, while no form of precipitation was recorded at the station were excluded. Negative rain gauge readings generated mostly during strong winds have also been eliminated. The total annual precipitation measured by Geonor after taking into account all corrections amounted to 713.4 mm from June 2013 to June 2014. At the same time, the annual sum obtained from Hellman was 564.4 mm, so 149 mm (21%) less. The increased sum results from the application of the so-called Alter shield in Geonor that reduces the wind effect affecting precipitation measurements and brings them closer to the real values. For the SNOWPACK model needs, data from snow depth measurements carried out at the PPS were specially prepared. Although they are performed only twice a day, it was decided to interpolate them to hourly values due to the low temporal variability of snow height. The increase of snow thickness between the observation times depended on the course of the precipitation data. The snow depth decrease during ablation was adjusted to the course of positive temperature. The SNO file with information on the structure and properties of the soil was prepared on the basis of published data from the Hornsund region (Migała et al. 2014) and Svalbard tundra areas (Putkonen 1998; Askaer et al. 2008).

SNOWPACK was run for the winter seasons 2013/2014 and 2015/2016. Due to gaps in the radiation measurement series, no simulation was performed for winter 2014/2015. In the 2015/2016 season, apart from modeling the snow cover at the PPS Hornsund, SNOWPACK was used to simulate snow conditions at sites in the Revdalen valley and the Fuglebekken catchment where snow pit surveys were performed (see Chapter 5.4). The model results were compared with periodically repeated in situ measurements. On their basis the simulation accuracy was evaluated. The field measurements were also used to improve the model performance during the ablation period. For this purpose, the SNOWPACK simulation was run several times for each site with different initial dates. These were the days with measurements in snow pits, for which SNO files containing information about the current snow cover structure were prepared. The required by model SMET files with meteorological data for each measurement site were obtained thanks to the Alpine3D simulation carried out for the entire winter season.

The modeling results in the 2013/2014 and 2015/2016 season were additionally used to simulate the snow depths measured in the field in different periods of spring 2014 and 2016 (see Table 2). The surveys took place in different days in each region. However, for the comparison of snow amount at various sites, the environment state was presented on April 18, i.e. the day with an approximate maximum thickness of snow cover in 2016, referring to results of

regular measurements carried out in Fuglebekken catchment. In 2014, the maximum accumulation occurred a little later; however, April 18 was roughly the middle day of the field measurements. The ideal situation would be to use the model for corrections for each point separately, but due to the range of calculations and the availability of meteorological data, the results of modeling snow cover at PPS Hornsund were used. It was presumed that the snow melted everywhere at the same pace and if, for example, on May 1 the snow cover decreased by 5 cm at the PPS compared to April 18, it was assumed that in all measurement points on April 18 snow cover was 5 cm higher than that measured on May 1.

5.4 Spatially distributed snow model Alpine3D

The usability of the point models is quite limited in the terrain with a complicated topography. Meteorological conditions can change to a large extent even in a small area, which is reflected in the observed properties of the snow cover. One-dimensional models do not take into account topographical relief, which, together with wind distribution, is the most important factor determining the local distribution of snow. For this reason, attempts have been made for a long time to model the snow cover in a spatial manner.

One of the first models that included snow transportation by wind was Prairie Blowing Snow Model (PBSM). The PBSM was developed in Canada to determine the snow mass fluxes in saltation or suspension processes and, above all, snow mass losses due to sublimation during drifting or blowing snow episodes (Pomeroy 1989, 1991; Pomeroy et al. 1993). Over time, the model has been improved to take into account snow transportation by wind in a spatial manner. This is how the Distributed Blowing Snow Model (DBSM) was born, which requires, in addition to meteorological data, information on the topography and land cover in order to function properly (Pomeroy et al. 1997). Similar physical assumptions were used in the American SnowTran-3D model (Liston and Sturm 1998), which also requires spatial information about the wind field to operate. The SnowTran-3D was quickly adopted worldwide (Liston et al. 2007) and tested, e.g., on Svalbard (Bruland et al. 2004). However, the most advanced models of snow spatial distribution are: French Meso-NH/CROCUS (Vionnet et al. 2014), which is combination of CROCUS snow model with Meso-NH atmospheric model (Lafore et al. 1998), and Alpine3D (Lehning et al. 2008), which is a three-dimensional extension of SNOWPACK. Both solutions require accurate wind field information computed by advanced external software as input. The Meso-NH/CROCUS is based on the results of the MM5 (5th generation Mesoscale Model) model developed at the National Center For Atmospheric Research (NCAR) in Boulder, Colorado (Grell et al. 1995), while Alpine3D uses wind fields obtained from the Advanced Regional Prediction System (ARPS) originally compiled by the University of Oklahoma (Xue et al. 2000, 2001). In this dissertation, the Alpine3D model was used due to the similar requirements in terms of the input data as in the integrated SNOWPACK module. Model popularity was also taken into account. The Alpine3D is an open yet advanced software, used inter alia for forecasting snow conditions during the last three Winter Olympics in Vancouver, Sochi and PyeongChang (Schlögl et al. 2016; Rhyner 2018). However, according to the author's knowledge, this is the first attempt to use Alpine3D in Svalbard and one of the first ever in the polar regions.

Outcome of the Alpine3D model is a matrix with the same spatial resolution as the input DEM and land cover layer. The output parameters can be selected by changing the configuration file. The most important spatial information returned from the model is the snow depth and SWE for the desired time step. In addition to the result in the raster form, the model saves the SNOWPACK calculations in its characteristic formats (HAZ, MET, PRO, SMET, SNO) for points defined by geographic coordinates in a separate POI file (if these are included in the simulation domain). Additionally, the Alpine3D is able to calculate the water runoff from any

catchment fully within the calculation range with an hourly time resolution. This will only be computed if the input data contains a file with the boundaries of these catchments.

The Alpine3D model cannot be run without first compiling the SNOWPACK and MeteoIO tools. In addition to meteorological data, soil and snow properties, it operation requires the information on **topographical relief (DEM) and land coverage**, by default in the form of ASCII files. The land cover must be coded according to the classification system of the PREVAH (Precipitation-Runoff-Evapotranspiration Hydrotope *Model*) hydrological model (Viviroli et al. 2009). The calculation range of Alpine3D will be the same as the extent of the provided files. In the area of the PPS Hornsund (Fig. 41), 4 terrain classes were distinguished on the basis of maps from the Norwegian Polar Institute (NPI) at a scale of 1:100 000. These were, according to the applicable code in PREVAH: water (code 01), bare ice (14), rock (15), and bare soil vegetation (26) class that corresponded to the tundra plants. In the PREVAH system, each pixel contains also encoded information about soil depth and the so-called "Field capacity" which were always set to 1, except for water and glacier surfaces where these values have been changed to 0. The DEM with a spatial resolution of 20 m was used for the calculations (Norwegian Polar Institute 2014). A simulation with a 1 m resolution DEM was also tested, but such settings turned out to be too computationally demanding to run a model for the entire winter seasons. The Alpine3D model needs also **data from more than one weather station**. For the Fuglebekken catchment area, data from the AWS of WMO 01003 synoptic station, AWS in front of the PPS Hornsund building and AWS on the 4th ablation stake on the Hansbreen glacier, located outside the Alpine3D computing domain, were used (Fig. 41; Table 5). Additionally, a series of temperature and air humidity measurements from a HOBO sensor at the top of the Fugleberget mountain were used. Wind speed measurements from Vaisala PPS Hornsund station have been recalculated to a height of 2 m according to the formula (Van Ulden and Holtslag 1985):

$$V_2(h_2) = V_1(h_1) * \frac{\log\left(\frac{h_2}{z_0}\right)}{\log\left(\frac{h_1}{z_0}\right)}$$

Table 5

Meteorological data used in snow cover modelling

Station name	Height [m a.s.l.]	Used meteorological variables	Time interval
AWS WMO 01003	7.3	TA, TSG[1], RH, VW_MAX, VW, DW, ISWR, OSWR, PSUM[2], HS[3]	1 min
AWS US front PPS	8.2	TA, RH, VW, DW, ISWR, OSWR, ILWR, OLWR, PSUM[2]	1 min
AWS Hansbreen4	184.6	TA, TSG[4], RH, VW, DW, ISWR, OSWR, ILWR, OLWR, HS[5]	10 min
Hobo Fugleberget	569.0	TA, RH	10 min / 1 h[2]

[1] Ground temperature at a depth of 5 cm
[2] The same precipitation sums from Geonor measurements was assigned to two stations near the PPS
[3] Interpolated from 2 measurements per day
[4] Assumption of a constant temperature under the snow [268.85 K]
[5] SR-50 measurements populated with interpolated values from weekly depth soundings in case of data gaps

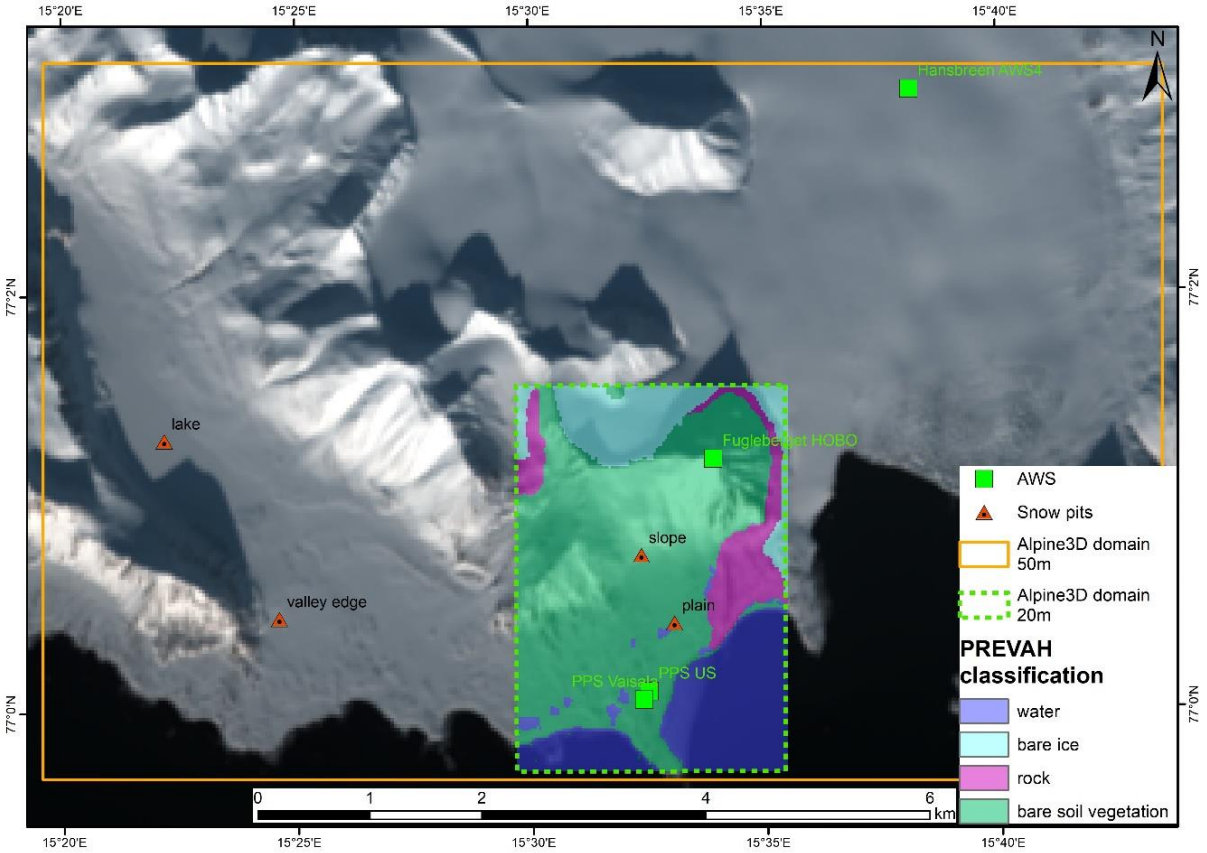

Fig. 41. The domain extents of the Alpine3D model used in the present study together with the presentation of the land cover classification according to the PREVAH system.

where h is the height above the ground in m), V is the wind speed (in m/s), and z_0 is the surface roughness coefficient (in m). This has been set at 0.01 cm, which corresponds to the roughness of the tundra covered with snow (Lewis and Callaghan 1976; Hansen 1993). The purpose of rescaling the wind speed was to standardize all available data to the same format. In AWS on the Hansbreen Glacier, snow height is measured with the SR50 acoustic sensor and once a week by a glaciological observer. Due to gaps in readings from the automatic device, data interpolation was performed. It was assumed that an increase in snow cover is proportional to the amount of rainfall measured in the PPS Hornsund. When missing records appeared during the ablation period, a temperature-dependent decrease in snow cover depth was presumed. In May, ablation at the level of 5.2 mm/day/°C was adopted, which corresponded well with the volume decreases observed between weekly measurements. For the needs of the Alpine3D model, the ground surface temperature (TSG variable) was also prepared. It has been assumed that on a glacier its value from the moment of the snow cover formation is constant and equal to the approximate average annual air temperature measured in this place in recent years (–4.3 °C). Such an assumption should be true when there is a sufficiently thick snow cover to compensate the atmosphere influence on the surface temperature and applies to the glaciated areas of southern Spitsbergen (Kosiba 1978).

In the present study, the Alpine3D simulation was performed for the 2013/2014 and 2015/2016 winter seasons. Due to significantly greater than assumed requirements for the computing power of the ARPS model necessary to map the wind field in the study area, it was not possible to launch Alpine3D with the snowdrift module turned on. On a computer with 32 cores, it took about a month to simulate the wind field for just one case (easterly wind speed of 10 m/s)

with a spatial resolution of 20 m. It was estimated that a reliable mapping of the wind situation, similar to that obtained in studies from Austria or Switzerland (Mott et al. 2008; Dadic et al. 2010), would last about a year, not taking into account the subsequent calculations in the Alpine3D. Instead, the wind field 10 m above ground level was calculated in the WindNinja program (Forthofer et al. 2017). It was used for spatial analysis, but it was not possible to implement it in the Alpine3D model. It requires airflow data in the form of a three-dimensional matrix and currently only ARPS files are supported (Mott, personal communication in 2018). The simulation results were compared with observations of snow cover in the Fuglebekken catchment. The model was launched with a resolution of 20 m for the Fuglebekken catchment area and, additionally, with a resolution of 50 m in 2016, in order to include snow survey sites in the Revdalen valley (Fig. 41).

Alpine3D and SNOWPACK models with modified meteorological parameters were also used to simulate snow conditions at PPS Hornsund at the end of the twenty-first century. For this purpose, a simulation was carried out using hourly data provided in the Polar-CORDEX initiative, resulting from the high-resolution COSMO-CLM model nested in the global model with a lower resolution: MPI-ESM-LR (LR – Low Resolution). The projection of the conditions at the end of the century was made with the assumption of an extremely pessimistic scenario of carbon dioxide emission RCP 8.5. This scenario is commonly known as "business as usual" due to the expectation that no action will be taken to limit greenhouse gases emissions and the belief that energy technologies will not change compared to the present day. It assumes an increase in the magnitude of the radiative forcing of 8.5 W/m^2 by 2100 compared to the one adopted for year 1750 (Riahi et al. 2011). This would mean an increase in the average temperature on Earth by about 4 °C (Stocker et al. 2013).

Projections available from the Polar CORDEX project for 2089–2100 for the southern Spitsbergen area with a spatial resolution of 0.022° (approx. 2.5 km × 2.5 km) was obtained courtesy of the Norwegian Meteorological Institute (Dobler and Haugen 2016). While virtually every meteorological factor is modeled within this initiative, only the air temperature and precipitation data presented in Chapter 3 (Figs. 13–16) are used for the dissertation purposes. It was assumed that the actual measurements better reflect the local anemological and radiation conditions than simulations in which the topography is poorly represented by a spatial resolution of 2.5 km. This means that the climate projection does not take into account possible changes in cloud cover or wind speed related to global warming. Data on temperature and precipitation from the appropriate grid node of the climate model were inserted into SMET files prepared for the 2013/2014 season. In order to avoid conflicting situations that may arise with this approach, for example, occurrence of precipitation simultaneously with cloudless weather (high values of short-wave radiation), the following processing has been undertaken. In case of precipitation, the radiation data was replaced with the lowest values measured in a given month. The ground temperatures were obtained from the formula proposed by Leszkiewicz and Caputa, assuming that it is equal to the average air temperature from the last 4 days (Leszkiewicz and Caputa 2015). For the site on the Hansbreen glacier, it was additionally assumed that the ground temperature cannot be higher than 0 °C. The wind data did not require any changes, because without the use of the snowdrift module in Alpine3D, they are only used to correct the precipitation measurement error. Correction was not applied as the data from the Polar-CORDEX project takes this effect into account and does not require additional modification (see Fig. 16 and Chapter 3). Due to the fact that the climate model overestimated the air temperature for the grid with PPS Hornsund by about 1.8 °C in the re-analysis for 1991–2000 (Fig. 15), the parameters of snow cover formation were slightly modified. This was supposed to compensate to some extent for the effect of the temperature increase. In the default settings of SNOWPACK/Alpine3D, snowfall cannot occur when the air temperature exceeds 1.3 °C. It was decided to

raise this threshold to the level of 2.3 °C, at which solid precipitation in Hornsund still occurs quite often (Łupikasza 2008).

6. SPATIAL AND TEMPORAL VARIABILITY OF SNOW COVER IN THE NEIGHBOURHOOD OF THE POLISH POLAR STATION

6.1 Pattern of snow cover disappearance in Fuglebekken catchment

Regular snow depth and density measurements carried out in the Fuglebekken catchment in three winter seasons (2013/2014, 2014/2015, 2015/2016) prove that in this site conditions for snow accumulation are better than at the meteorological site of PPS Hornsund (Fig. 42). For most of the winter season, all points located in the catchment area are characterized by a higher snow thickness than at the weather station (Fig. 43). The deepest snow can be found in the upper part of the study area, under the slopes of Fugleberget mountain. Additionally, snow accumulation conditions are generally better in the western part of the catchment (Fig. 44). The **measurement points are located in a small area (<1 km^2); however, the differences in the obtained snow cover depths and SWE are significant**. During the period of maximum accumulation, which fell in April in each of the analyzed seasons, snow depths ranging from about 20 cm in the lower part of the catchment to over a meter under the slopes of Fugleberget were recorded. This corresponds to the SWE in the range of about 60 to 400 mm in the snowiest season 2014/2015 (Figs. 42 and 45). The least snowy year occurred in 2015/2016, when the thinnest snow cover was measured both at the PPS site and in the catchment area. It is worth noting, however, that the 2013/2014 season turned out to be the most snowy at the PPS site, while the catchment measurements indicate a deeper snow cover in 2014/2015. In general, the

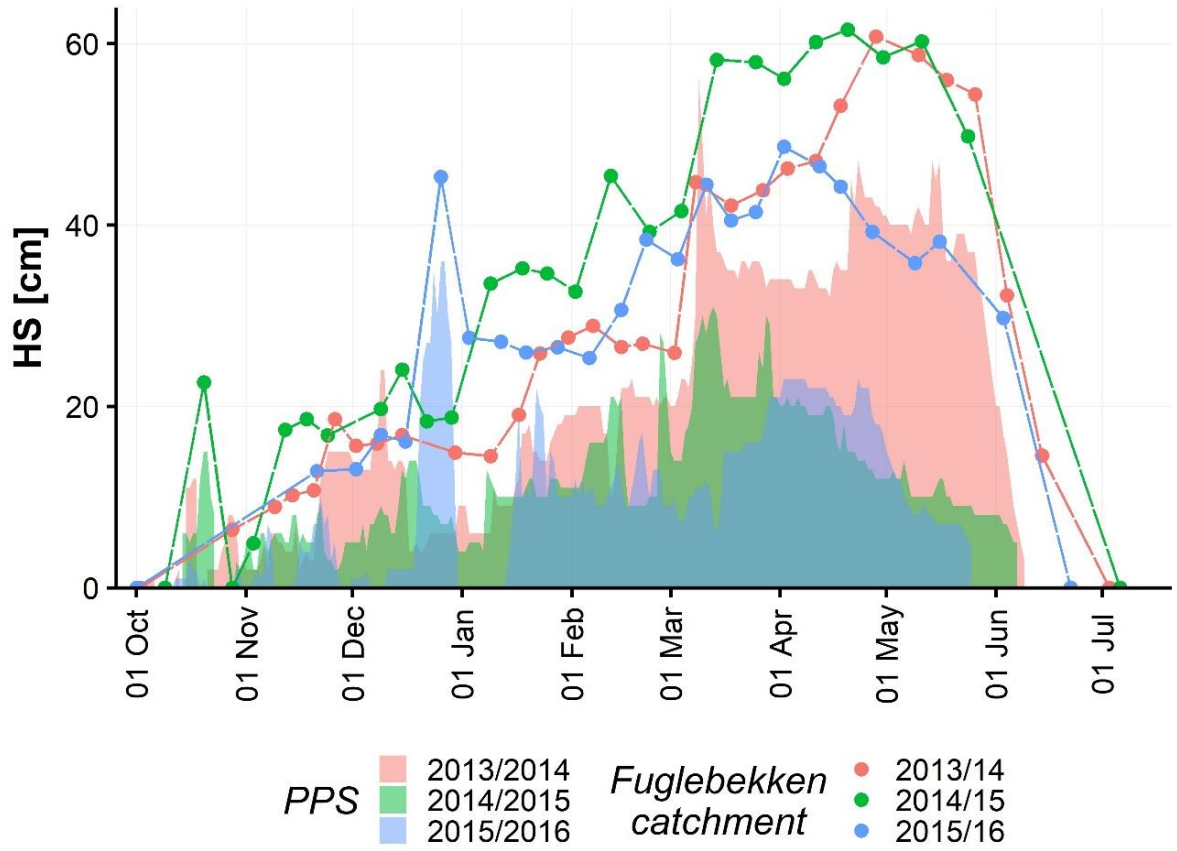

Fig. 42. Mean snow cover depths measured in the Fuglebekken catchment area and PPS Hornsund in individual winter seasons.

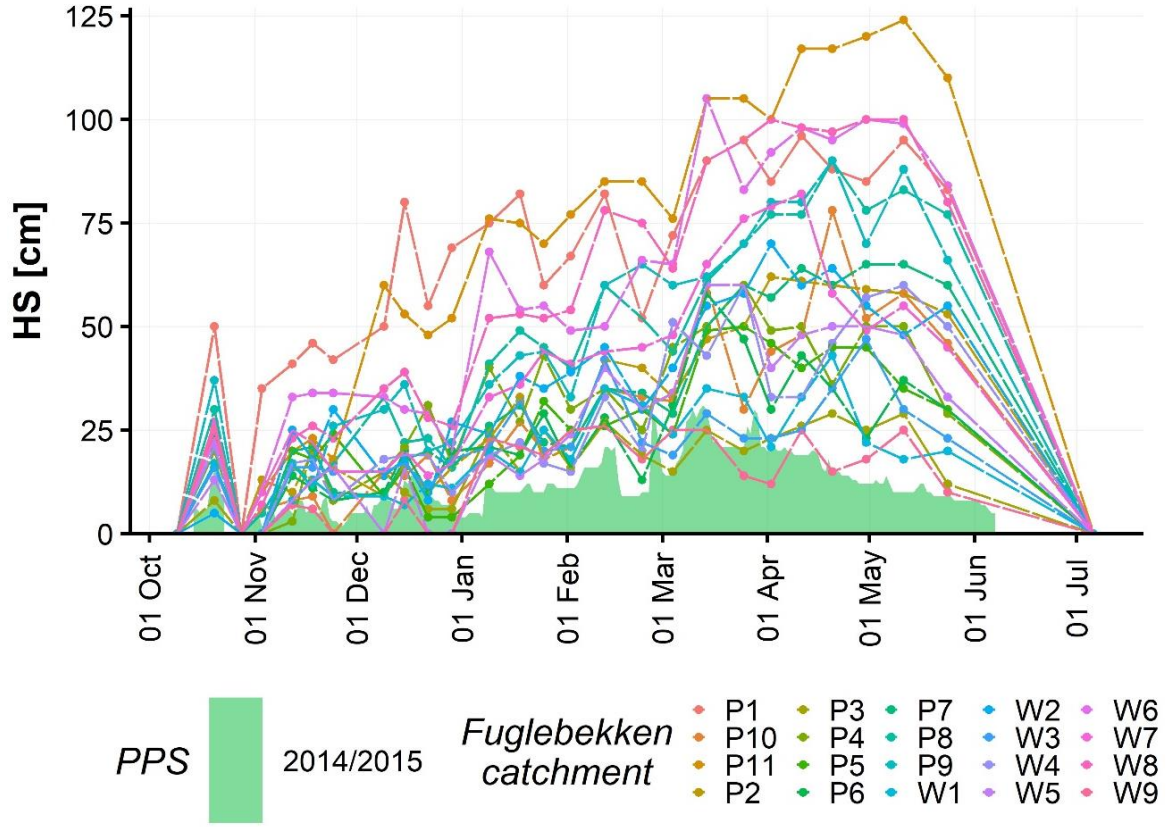

Fig. 43. Snow cover depths measured at points in the Fuglebekken catchment area and PPS Hornsund in winter season 2014/2015.

course of the snow cover depth in the catchment area is characterized by smaller inter-season differences compared to the values recorded at the PPS site. This suggests that the depths recorded at the Hornsund WMO site do not always accurately reflect what is happening in the tundra. Much depends on the snow ability to bind to the ground. Heavy snowfall in early March, which occurred at temperatures close to 0 °C, was the cause of high snow thickness in the 2013/2014 season. Episodes of efficient precipitation followed by sunny weather in late April and May have also contributed to this effect. The slight snow melting that accompanied the above-mentioned situations hindered the subsequent redistribution and erosion of snow cover by the wind activity. Probably for this reason, a relatively large snow thickness was found in the wind-exposed measuring site at PPS (see Fig. 19) compared to the Fuglebekken catchment area. In the following seasons, snow could be easily removed by the wind near the station.

The maximum SWE is usually measured in Fuglebekken catchment in May (Fig. 46). Due to the lack of significant spatial differentiation of snow density, the highest SWE is recorded in places with the greatest amount of snow. The maximum average SWE reaches values close to 200 mm in each of the three seasons: 196 mm in 2013/2014, 236 mm in 2014/2015, and 175 mm in 2015/2016. Depending on the year, this means that the aforementioned average value is from 30% (2013/2014) to 300% (2015/2016) higher than that measured at the same time at the point at PPS (Fig. 46). The snow cover density in the catchment just before the start of ablation was usually in the range of 350–400 kg/m^3. The maximum SWE occurs later than the maximum snow cover thickness. This must be caused by additional water retention coming either from spring rainfalls or from snow ablation taking place in the higher parts of the catchment area. Due to the small precipitation sums in the ablation periods of the analyzed seasons, the latter explanation is more likely.

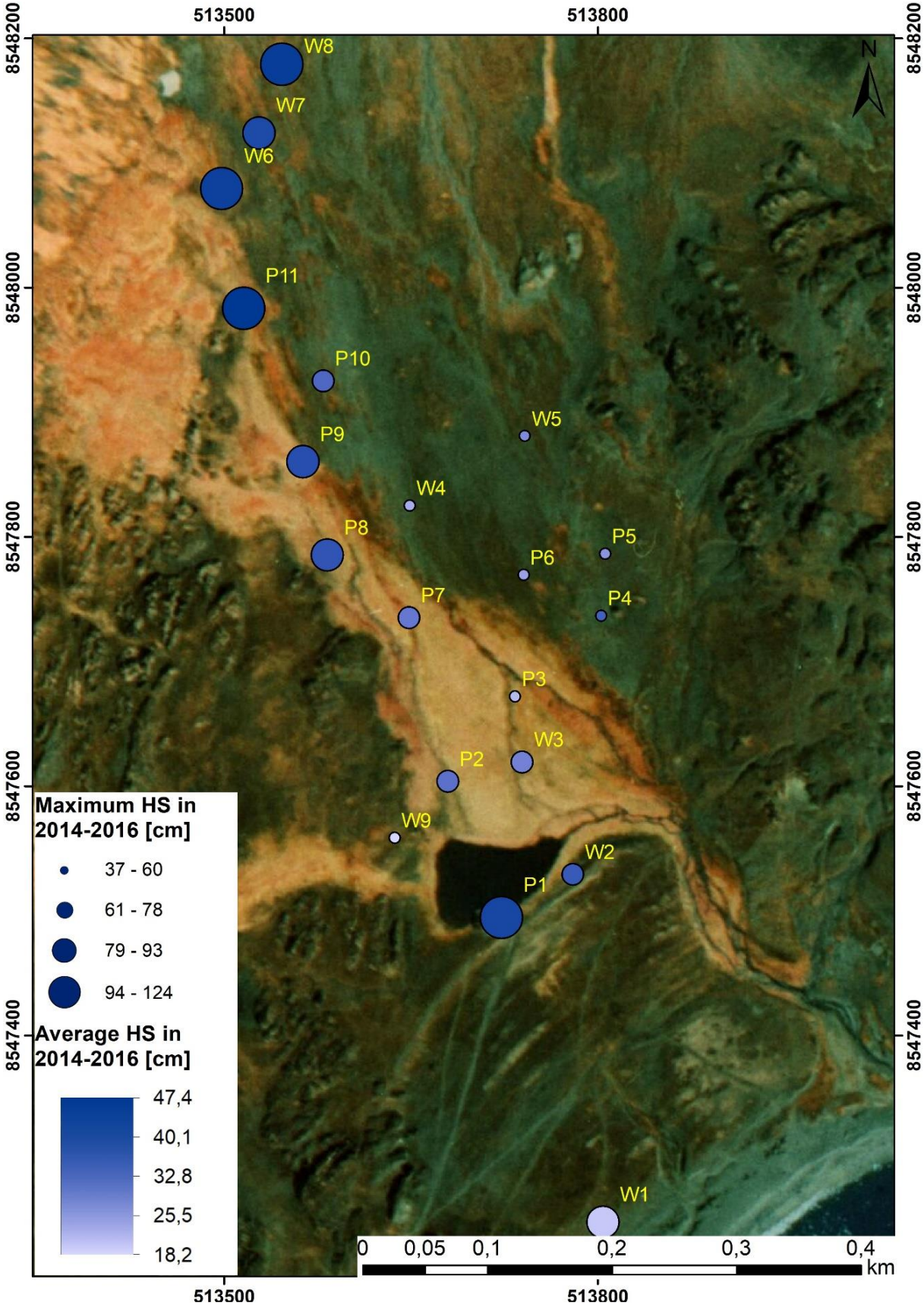

Fig. 44. Average and maximum snow depths at the measuring points in the Fuglebekken catchment area obtained at three winter seasons.

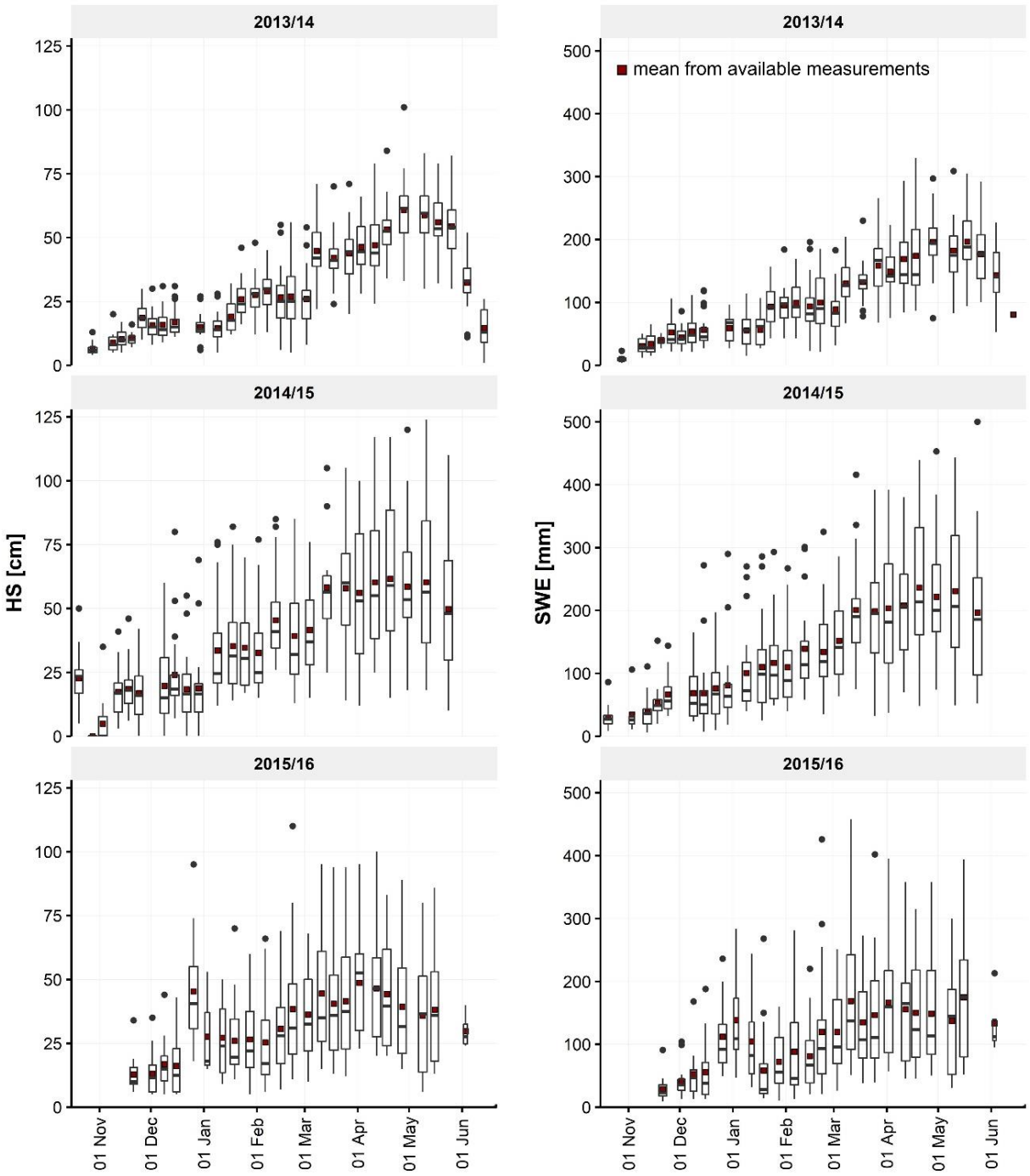

Fig. 45. Distribution of measured snow cover depths and SWE in Fuglebekken catchment in the seasons 2013/2014, 2014/2015, and 2015/2016. Modified after Kępski et al. (2017a).

Twenty measuring points in the catchment area provide some information on the snow cover distribution. However, due to its large variation on the tundra, the number of probing sites is not sufficient to reflect the real situation. This can be better illustrated by analyzing the available time-lapse imagery, assuming that the snow cover spring ablation pattern reflects also its spatial distribution throughout the winter season.

The analysis of images from three years (Kępski et al. 2017b) proves, first of all, a very **uneven melting of snow in the catchment area with significant repeatability of the ablation pattern from year to year** (Fig. 47). The superimposition of photos representing the same SCE

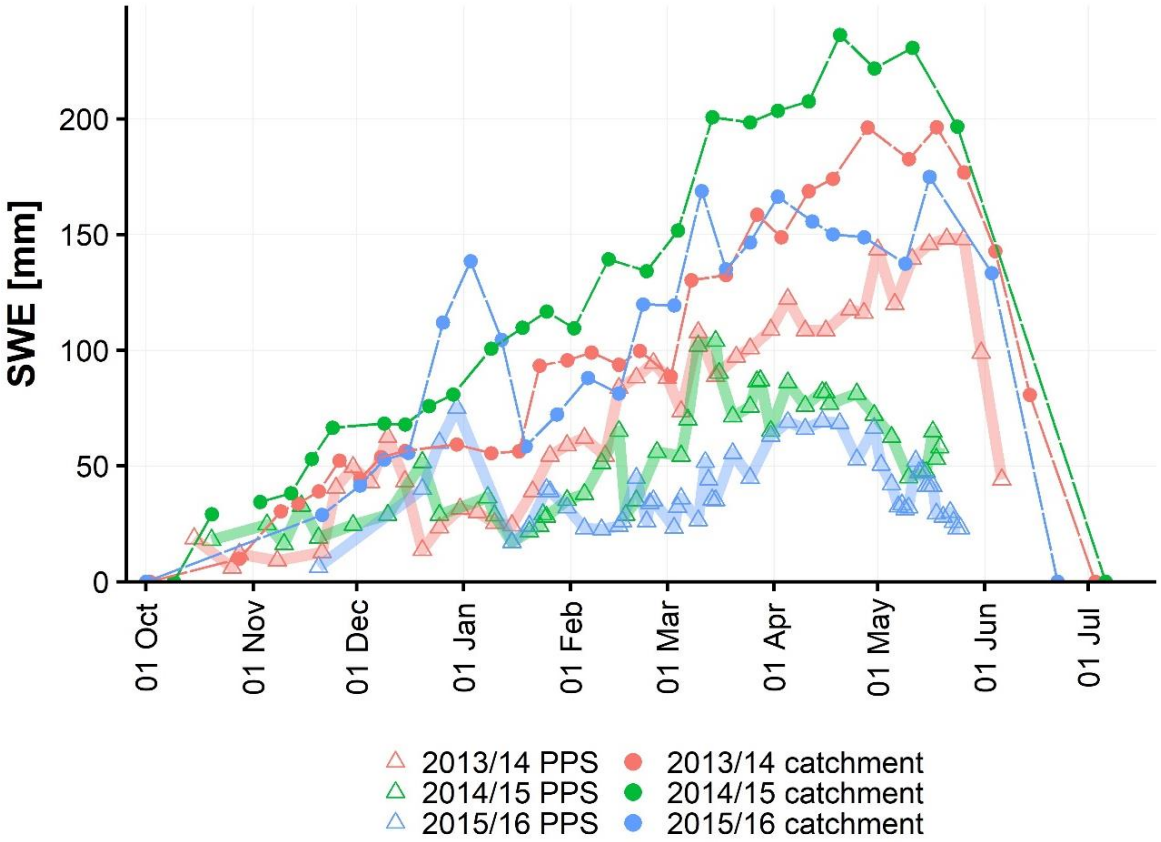

Fig. 46. Course of average SWE values measured in the Fuglebekken catchment area and PPS Hornsund weather site in the seasons 2013/2014, 2014/2015, and 2015/2016.

in the 2014–2016 seasons shows that the rock formations are always the first to emerge from under the snow. In fact, some rocky outcrops are snow-free most of the year. The first photos from 2014 that were processed are from the first decade of April, when negative temperatures and solid precipitation still prevailed. Despite this, a small fraction of the area in the images (<1%) representing the protruding rocks was always snow-free. During the early ablation phase, when 72% of the analyzed surface was still under the snow cover, in each season the snow-free areas were the protruding forms: rocks, their immediate vicinity, and storm ridges. At this stage, also small fragments of flat land were snowless: mainly the western part of the catchment covered with mosses and partly the southern region near the coast and the lake. On the other hand, the central and upper part of the catchment area was completely snow-covered each time. Characteristic is the snow distribution in the advanced ablation stage (33% of the surface under snow). Then the central sector of the area is already snow-free, while the snow patches form a long strip along the western part just in front of the protruding rock formations (Fig. 47b). This shows the decisive influence of the wind from the eastern sector which is responsible for the transport and accumulation of snow in front of the obstacle. On the eastern side, there was also a snow strip in each of the analyzed seasons, but it was definitely narrower and located between the protruding rock forms, not in front of them. Depressions of this type *surrounded by* elevated terrain can effectively accumulate snow in winter. During the late ablation phase (4.5% snow coverage), snow patches occur only locally between the rocks and under the Fugleberget slope. The dates of each ablation stage occurrence are presented in Table 6. It is worth noting here that **the entire process of snow cover disappearance in the catchment area takes a relatively long time**. In exposed areas, the snow cover duration is up to 50 days shorter than in places where snowdrifts form.

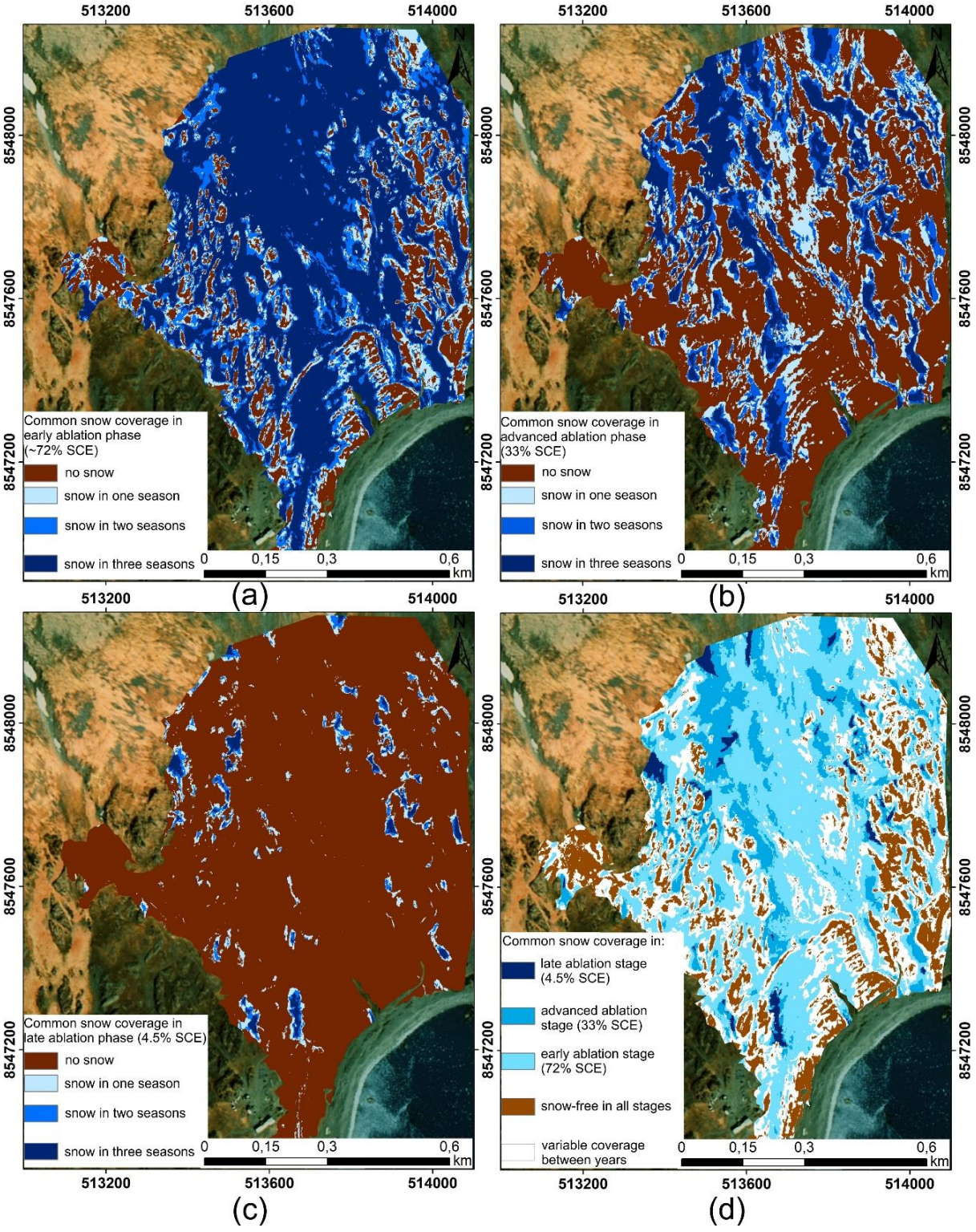

Fig. 47. Snow distribution in the Fuglebekken catchment in the years 2014–2016 presented in the form of superimposing classified images from a time-lapse camera: (a) effect of superimposition of 3 images from early ablation stage in 2014, 2015, and 2016; (b) effect of superimposition of 3 images from advanced ablation stage in 2014, 2015, and 2016; (c) effect of superimposition of 3 images from late ablation stage in 2014, 2015, and 2016; (d) synthesis of 3 obtained images (a, b, and c): superimposition of 9 images representing the early, advanced and late stages of ablation in years 2014, 2015, and 2016.

Table 6

Dates of the ablation phases occurrence in individual years together with snow cover percentage in the analyzed area

Snow cover stage	The precise snow coverage in 2014	Date of occurrence in 2014	The precise snow coverage in 2015	Date of occurrence in 2015	The precise snow coverage in 2016	Date of occurrence in 2016
Early (~72% SCE)	70.22%	09.06.2014	73.35%	12.06.2015	72.53%	24.05.2016
Advanced (~33% SCE)	32.5%	17.06.2014	32.33%	19.06.2015	33.08%	05.06.2016
Late (~4.5% SCE)	4.91%	29.06.2014	3.68%	02.07.2015	4.47%	18.06.2016

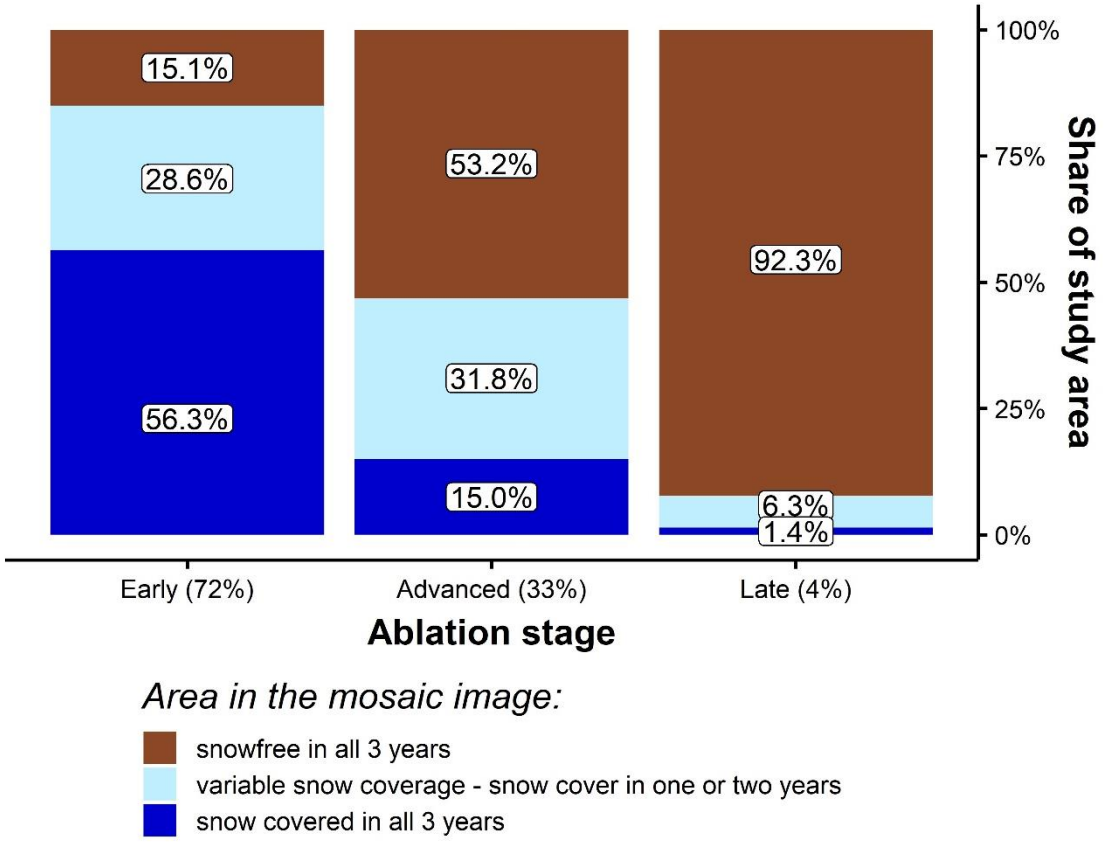

Fig. 48. The share of common and divergent areas on the mosaic of photos from early (Fig 47a), advanced (Fig 47b), and late (Fig 47c) ablation stage.

In the corresponding stages of ablation (Table 6), the surface area covered with snow or snow-free in all 3 years prevails over the area with variable coverage. This is also visible in Fig. 47 and was quantified in Fig. 48. Land with variable snow coverage between the analyzed years accounted for 28.6%, 31.8%, and 6.3% of the total surface area in the early, advanced, and late ablation stages, respectively. It is worth noting that due to minor shifts in classified

images caused by camera movements, the "common" part on superimposed images may even be understated. This means a high repeatability of the snow disappearance pattern in the analyzed area, proving that ablation is each time controlled by similar and rather unchanging factors.

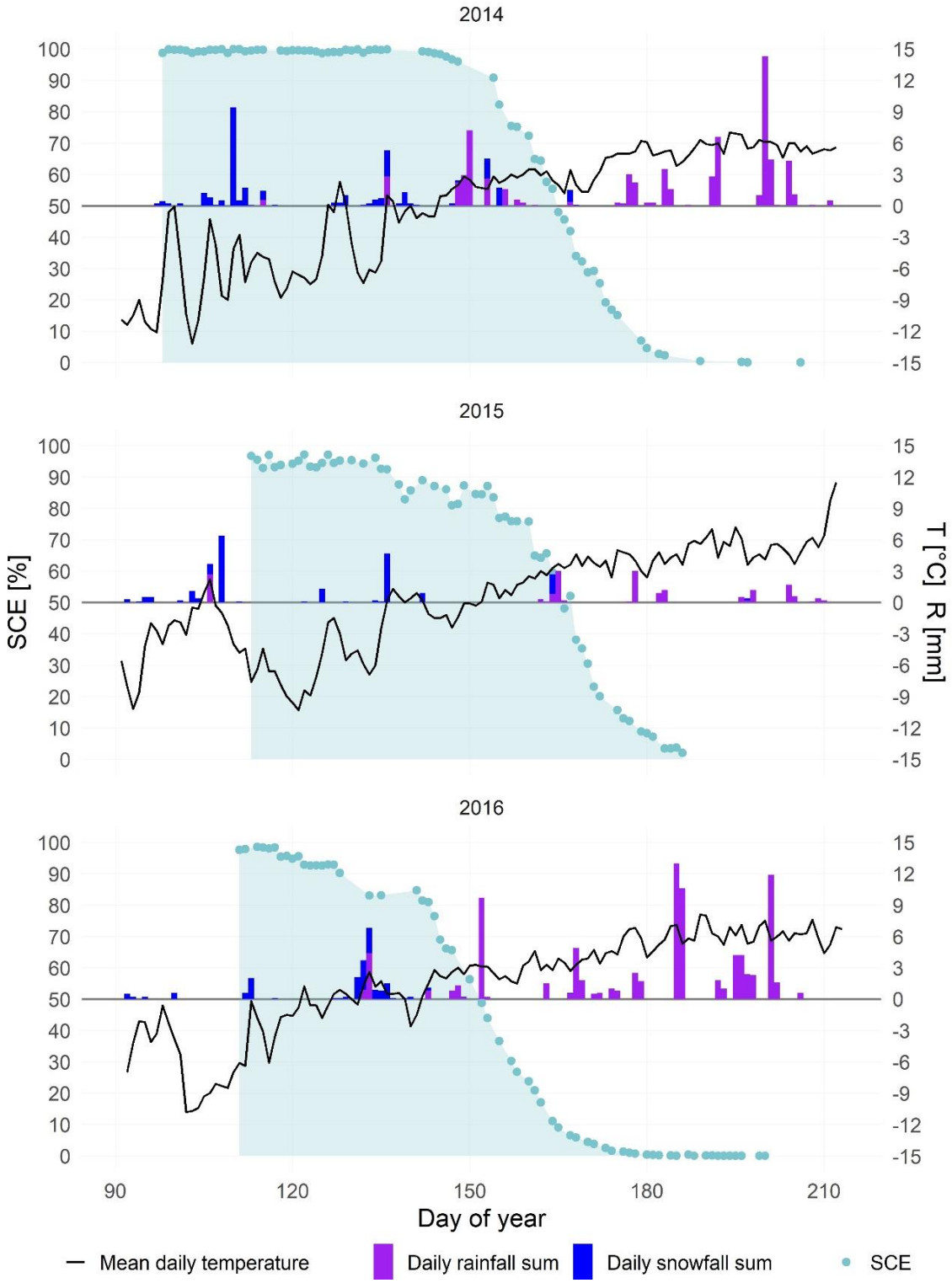

Fig. 49. The SCE in Fuglebekken catchment during ablation seasons 2014–2016 in combination with the meteorological background: mean daily temperatures and precipitation totals measured in PPS Hornsund. Modified after Kępski et al. (2017a).

The rate of snow disappearance in the analyzed area is presented in Fig. 49. Each point on the chart corresponds to one processed picture from the time-lapse camera (see Fig. 37). Despite the desirable temporal resolution of one day, some data gaps appeared due to unfavorable meteorological conditions (see Fig. 32). Usually, the gaps do not exceed 3 days. Overall, the data completeness provided by the time-lapse camera is high. However, the analysis of the images from 2015 revealed some problems. In Figure 49 visible are small peaks in SCE value that cannot be explained by the weather conditions prevailing in Hornsund. They occurred due to the loss of focus by the camera, which resulted in a significant reduction in classification accuracy during photo processing. Nevertheless, the obtained classification error did not exceed 3 percentage points, which the author found acceptable for the spatial analyzes presented in the dissertation.

Regardless of the snow depth measured in individual winter seasons, the fastest reduction in the SCE took place when positive daily air temperatures begin to predominate (Fig. 49). The snow cover disappeared the earliest in 2016. That was caused by the lower snow thickness (see Fig. 42), but also the earlier predominance of air temperatures above 0 °C, from the first days of May. The analysis of classified orthophotos allows for the quantification of the SCE and precise determination of the moment when it drops below 50% on a selected area. In meteorology records, such a moment will be defined as the last day with snow cover. It occurred in the catchment area on June 14, 2014, June 15, 2015, and May 30, 2016. At the WMO station in PPS Hornsund, the last day with snow cover was recorded each time about a week earlier, i.e. June 9, June 7, and May 25 in 2014, 2015, and 2016, respectively. However, this does not necessarily mean a human error in observations, but only confirms the subsequent snow disappearance in the Fuglebekken catchment. The closest vicinity of the station is characterized by earlier ablation, which can be seen in the time-lapse imagery. The characteristic dates illustrating the rate of snow cover disappearance are presented in Table 7. At the latest, the complete disappearance of snow occurred in 2015, on July 6. At the earliest in 2016, on June 22.

Table 7

Dates of occurrence of specific SCE in the Fuglebekken catchment. Dates were interpolated in case of missing photos with the given SCE value

Snow cover extent (SCE)	First occurrence time in 2014	First occurrence time in 2015	First occurrence time in 2016
90%	3.06	17.05	8.05
75%	5.06	10.06	24.05
50%	14.06	15.06	30.05
25%	21.06	20.06	7.06
10%	27.06	27.06	13.06
< 2%	3.07	6.07	22.06

The data contained in Table 7 show that, regardless of the winter season, the transition from the 75% SCE to 10% SCE took about 3 weeks. The last stage of ablation takes an additional week. However, the initial phase is often the longest, i.e. the transition from 90% of snow coverage to 75%. The rationale behind this is that the decrease to 75% is mainly due to operation of the sun and early snowmelt from protruding rocks with a thin snow cover. Snowfalls are still likely at this stage, which could increase the SCE and delay the further melting. The final ablation phase can also take a long time, as only the thickest snowdrifts melt then, often in places sheltered from direct sunlight.

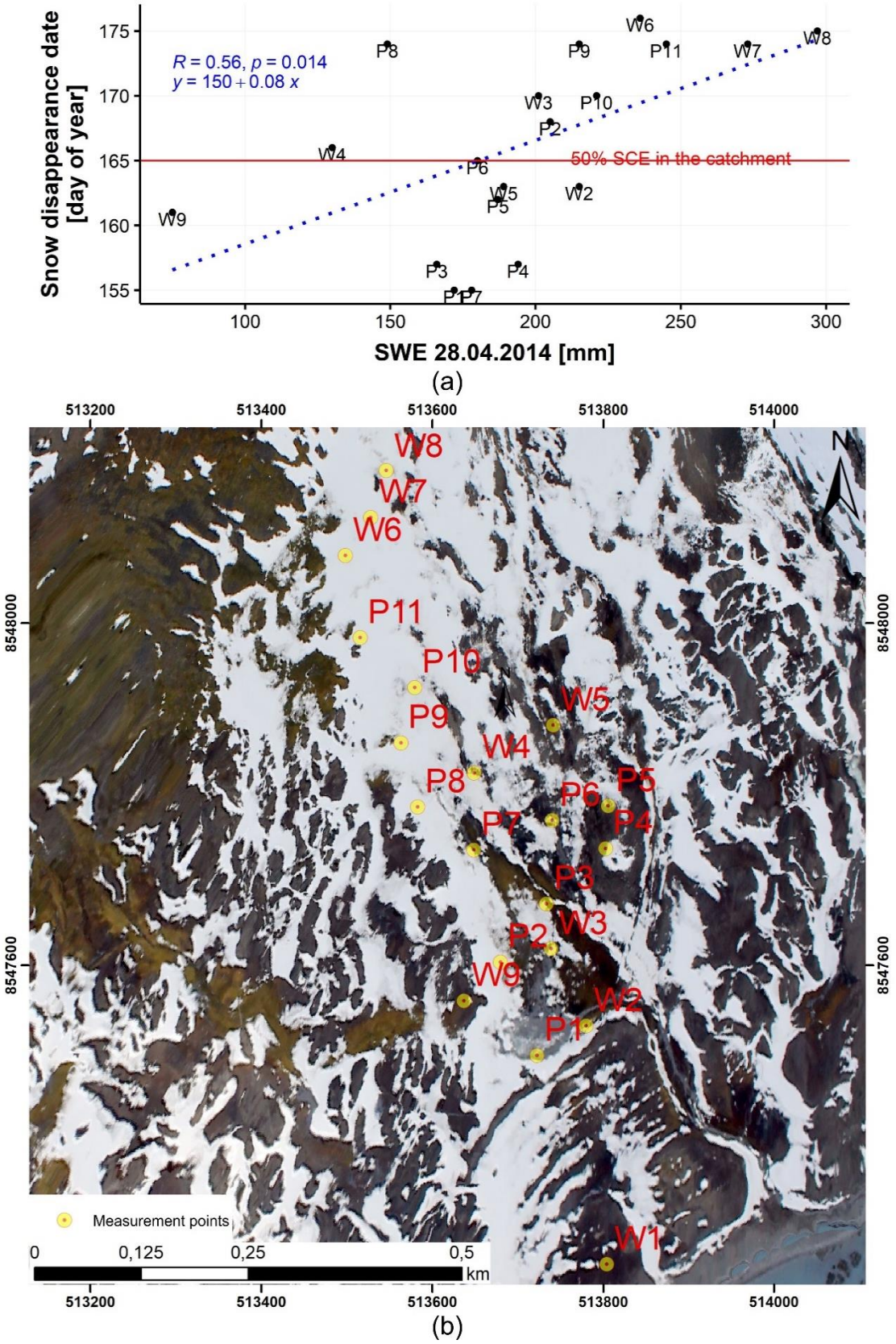

Fig. 50: (a) Relationship between the date of snow disappearance at the measuring site and the SWE during the maximum accumulation in 2014 (28.04.2014). Linear regression and 50% SCE occurrence date (15.06.2014) were specified; (b) Zoomed orthoimage from June 15, 2014 with the location of the measurement points marked.

The relationship between the time of snow disappearance and its maximum seasonal thickness can be easily tested by comparing the information from the time-lapse images with in situ measurements in the Fuglebekken catchment area. The linear correlation between SWE measured in the period of maximum accumulation and day of snow disappearance gives a Pearson correlation value equal to 0.56 (Fig. 50a). After rejecting 3 outliers (points P8, W4, and W9), the value of the correlation increases to 0.81. The sites where the snow had not disappeared until the late ablation phase were characterized by about 60 mm greater SWE measured at the time of maximum accumulation, compared to the locations where the snow had melted earlier. However, the graph shows that there were points where the SWE during the maximum accumulation time was similar, while the ablation date differed by up to 10 days. This may result from the adopted methodology, as the day of snow disappearance at a point was determined on the basis of coverage also in its immediate vicinity. However, this also proves that the rate of snow loss can vary significantly even in a small area.

6.2 Variability of snow cover on different land coverage types

The superimposition of the obtained information about the disappearance of snow cover on maps showing the vegetation, soil and geomorphological forms of the terrain (Fig. 2) allowed to determine the ablation course for each of the types distinguished in them. The analysis omitted only the classes with the smallest share of the area: ornitocoprophilus (0.5% of coverage) and geophytic initial tundra (0.2%) among vegetation and regosols and leptosols with less than 1% coverage among soils. In the years 2014–2016, ablation of snow cover from various landforms proceeded in a similar way (Fig. 51), additionally confirming the previous findings from overlapping photos from the 3 spring seasons (Fig. 47). Each time, snow cover duration was the shortest on lichen-herb-heath tundra, while **longest snow persistence was observed on rock debris formation without** any **vegetation**. Snow cover disappearance between these two terrain types occurs with a time lag of almost two weeks. The late melting of the snow on rock debris was associated with the fact that this formation is located near rocks that favor the formation of snowdrifts. The presence of late disappearing snowdrifts may be one of the reasons why vegetation did not develop in these places. On the other hand, the epilithic tundra occupying protruding rocks in the catchment area was characterized by a low SCE value at the beginning of the ablation season. This is due to their greatest exposure to wind, which does not allow this plant formation to be completely covered with snow in winter. Therefore, it should be assumed that the presence of certain types of vegetation did not affect the snow distribution. However, the opposite relationship is likely and the **snow cover duration could have influenced the development (or total absence) of specific vegetation types. Nevertheless, the primary factors affecting snow accumulation would be the topography and wind field distribution**.

The distribution of vegetation is closely related to the soil type (Fig. 2). The diversity of soils, however, is smaller than that of vegetation and the vast majority of the studied area is covered by cryosols (Fig. 52). The disappearance of snow cover does not show any characteristic pattern in relation to underlying soils. Only slightly less snow coverage can be found at the beginning of the ablation season on lithic soils that coincide with the epilithic tundra occurrence (Fig. 53). However, in the final ablation phase, the differences in SCE between soil formations were minimal and statistically insignificant.

The disappearance of snow cover in the Fuglebekken catchment area turned out to be the most strongly correlated with the geomorphology of the area (Fig. 54). In the early ablation period, the beaches are already snow-free. This is due to the tidal activity that extensively shapes the coast as long as Isbjørnhamna Bay remains free of sea ice. On the other hand, the longest snow cover duration is observed on talus cones. Such forms can have an exceptionally thick

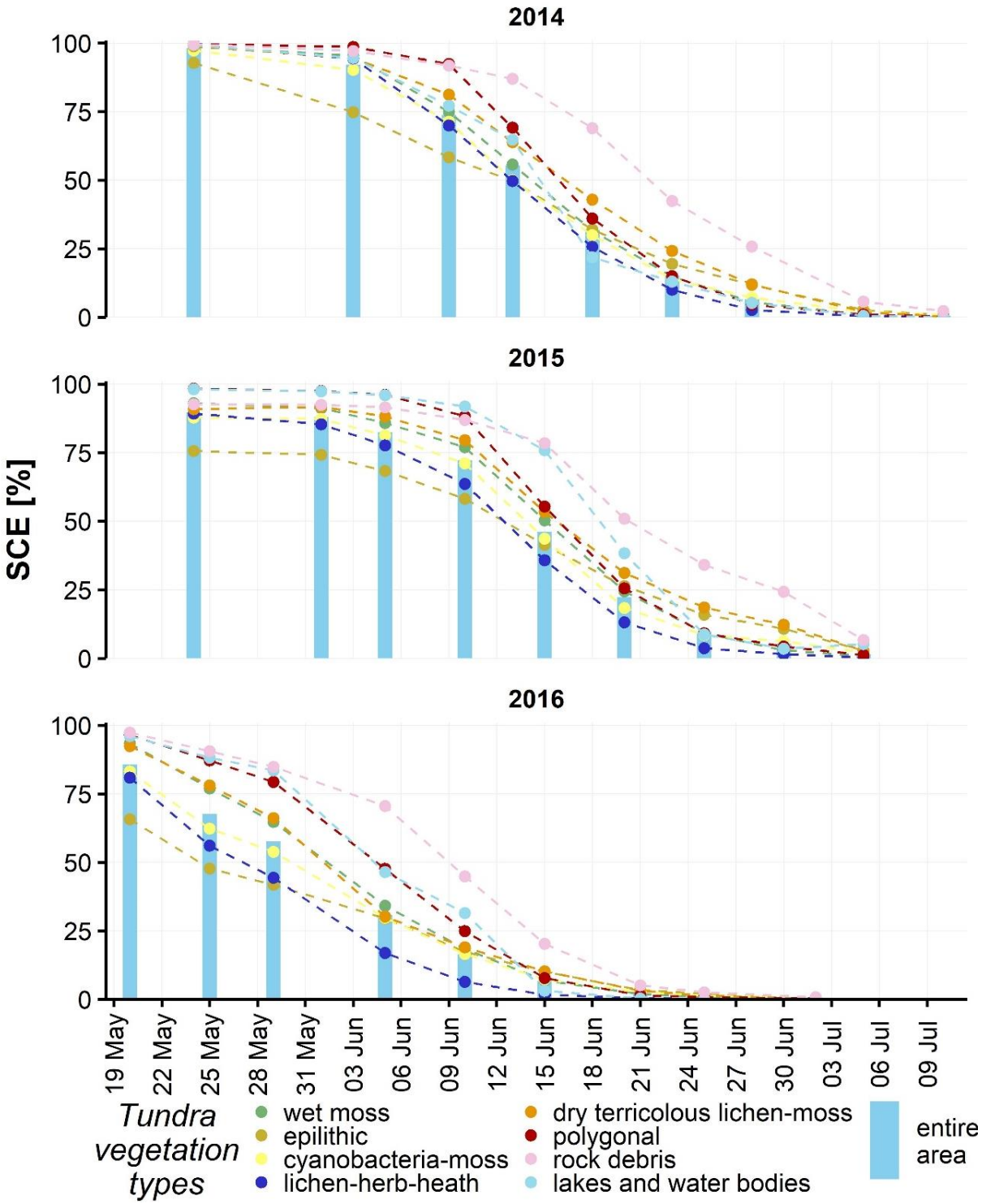

Fig. 51. The disappearance of snow cover from individual types of tundra vegetation presented in a five-day time interval (if possible). The blue bars represent SCE in the whole study area on a given day; points mark SCE on different land cover types. Modified after Kępski et al. (2017a).

snow cover due to additional material supply through avalanches and snow creep from the upper parts of the slope. This also results in an extended snow cover duration on talus cones. It is also visible that the snow on the moraines disappears slightly earlier in relation to the surroundings.

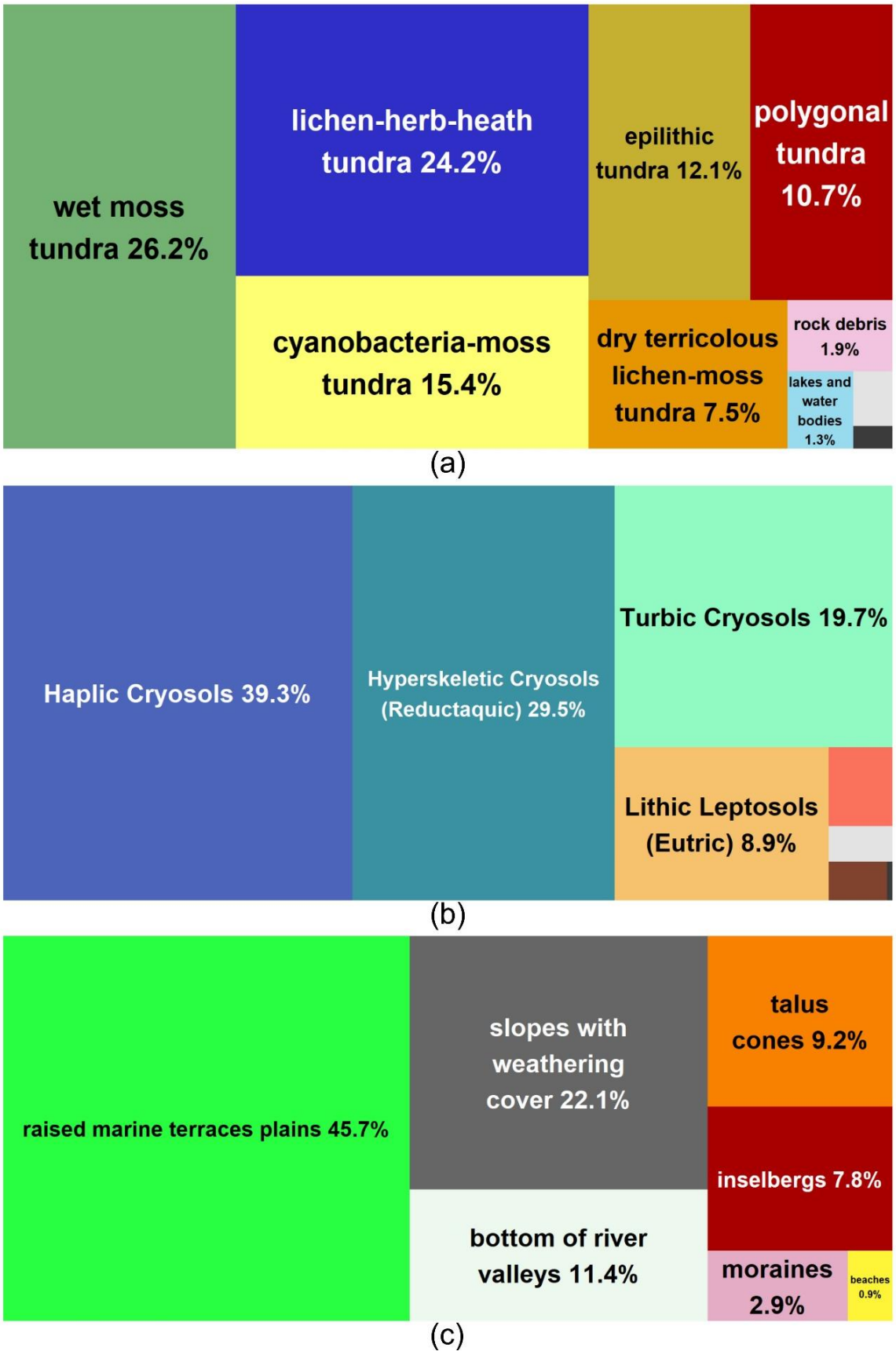

Fig. 52. Share of land cover in the area of analysis divided into: (a) vegetation types, (b) soils, and (c) geomorphological forms.

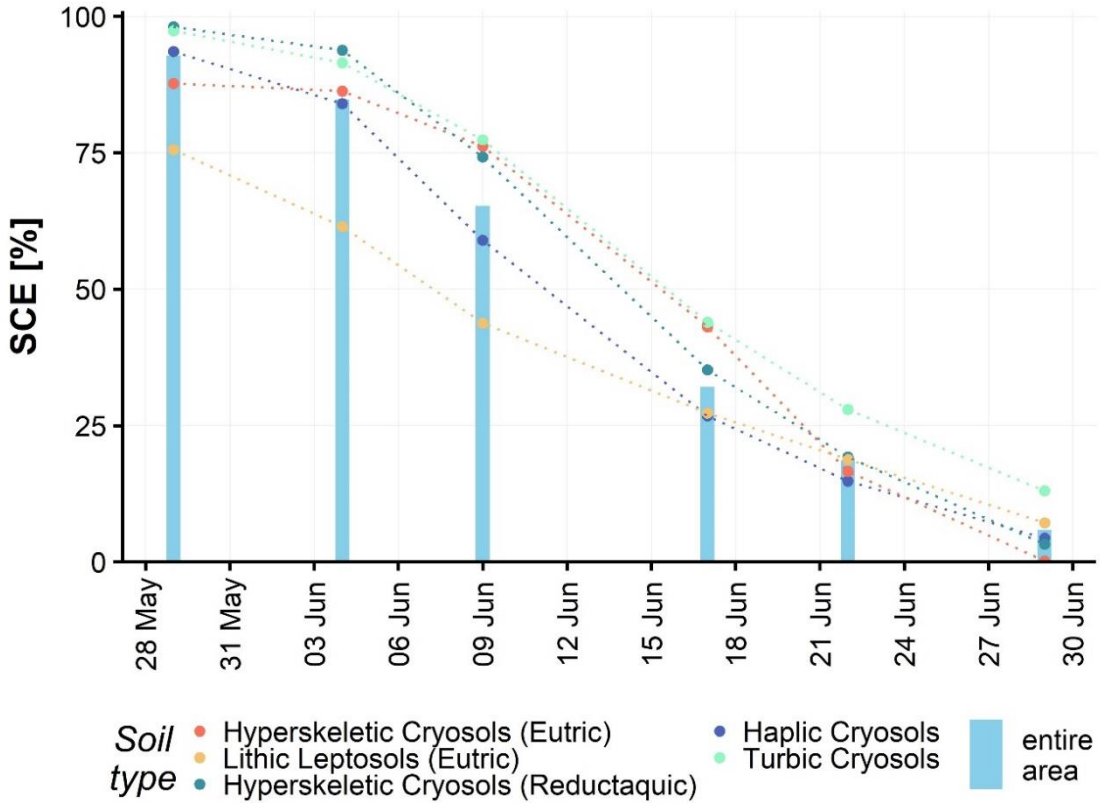

Fig. 53. Changes in SCE on individual soil types occurring in the Fuglebekken catchment during the 2014 ablation season.

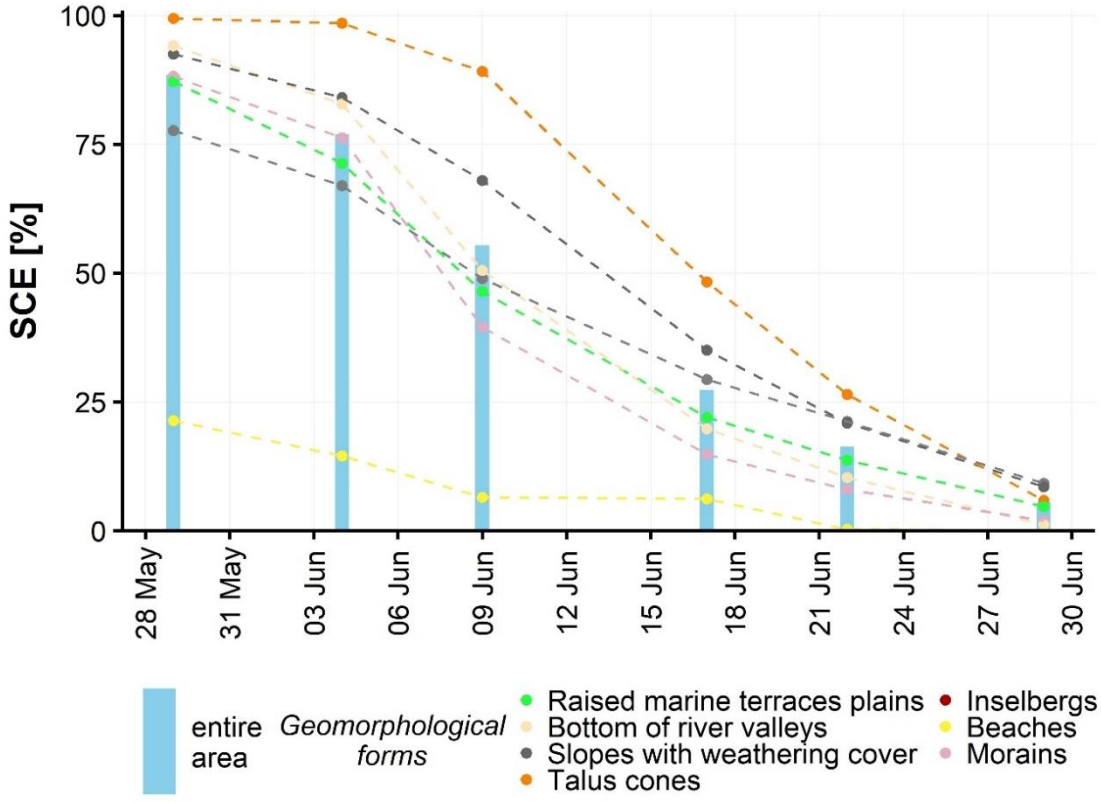

Fig. 54. Snow cover disappearance from different geomorphological forms during the 2014 ablation season.

The Kruskal-Wallis test showed that the differences in the time of snow cover disappearance from distinct vegetation and geomorphological formations were statistically significant. However, this does not apply for soils, where the variability turned out to be insignificant. A later post hoc Dunn's multiple comparison test revealed that only some of the differences were statistically significant. Scarce snow cover on beaches from geomorphological formations and longer snow cover duration on the rock debris surface in the case of vegetation types turned out to be statistically relevant. However, the classification area is covered to a different extent by separate land cover types (Fig. 52), which undoubtedly influences the results of the analysis. Although the method used is not perfect, it allows for at least approximate determination of the variable disappearance of snow from various land cover types.

The Kruskal-Wallis test used on a data series containing snow depth and SWE measurements from the Fuglebekken catchment allowed to quantify the differences in snow cover properties on distinct surfaces (Tables 8 and 9). It should be remembered here that the number of measurement points was different for each of the analyzed surfaces (see Fig. 2), which may affect the result of calculations. Nevertheless, certain relationships are clearly visible and should also be representative of a larger area. The much higher SWE and snow depth values on talus cones in relation to marine terrace plains may be easily explained by the higher altitude and the under-slope location favoring the accumulation of snow. However, **the most interesting in the winter season is the higher snow thickness on wet moss tundra and associated soils** (Hyperskeletic Cryosols (Reductaquic)) (Migała et al. 2014), by a few or over a dozen centimeters, on average. When discussing the statistical test results, it is worth bearing in mind that

Table 8

Statistically significant (p <0.05) interrelationships between SWE on different land types. The analysis was carried out for all points in the catchment area and the entire 2014–2016 season (cases with high uncertainty are marked in red)

	Coverage type 1	Coverage type 2	Mean difference [mm]	p-value significance code
Geomorphological forms	talus cones	bottom of river valleys	+34.3	$p < 0.001$
	slopes with weathering cover	bottom of river valleys	–18.2	$p < 0.05$
	talus cones	plains of raised marine terraces	+48.2	$p < 0.001$
	slopes with weathering cover	talus cones	–52.5	$p < 0.001$
Vegetation types	rock debris	polygonal tundra	–38.4	$p < 0.01$
	wet moss tundra	rock debris	+52.9	$p < 0.001$
	wet moss tundra	lichen-herb-heath tundra	+30.9	$p < 0.05$
	wet moss tundra	cyanobacteria-moss tundra	+39.7	$p < 0.05$
Soil types	Hyperskeletic cryosols (Eutric)	Haplic cryosols	–53.0	$p < 0.001$
	Hyperskeletic cryosols (Reductaquic)	Hyperskeletic cryosols (Eutric)	+43.2	$p < 0.001$
	Turbic cryosols	Hyperskeletic cryosols (Eutric)	+42.8	$p < 0.01$

Table 9
Statistically significant (p <0.05) interrelationships between snow depths on different land types. The analysis was carried out for all points in the catchment area and the entire 2014–2016 season (cases with high uncertainty are marked in red)

	Coverage type 1	Coverage type 2	Mean difference [mm]	p-value significance code
Geomorphological forms	talus cones	bottom of river valleys	+10.2	$p < 0.001$
	slopes with weathering cover	bottom of river valleys	–4.6	$p < 0.05$
	talus cones	plains of raised marine terraces	+13.9	$p < 0.001$
	slopes with weathering cover	talus cones	–14.8	$p < 0.001$
Vegetation types	rock debris	polygonal tundra	–8.8	$p < 0.05$
	wet moss tundra	rock debris	+12.8	$p < 0.001$
	wet moss tundra	lichen-herb-heath tundra	+9.1	$p < 0.01$
	wet moss tundra	cyanobacteria-moss tundra	+11.1	$p < 0.01$
Soil types	Hyperskeletic cryosols (Eutric)	Haplic cryosols	–12.4	$p < 0.01$
	Hyperskeletic cryosols (Reductaquic)	Hyperskeletic cryosols (Eutric)	+10.2	$p < 0.01$
	Turbic cryosols	Hyperskeletic cryosols (Eutric)	+10.0	$p < 0.05$

some of the presented relationships were obtained on the basis of only one measurement point. Such cases with a high level of uncertainty are marked in red in Tables 8 and 9. The results show, for example, lower snow depth on rock debris formation, which is in contradiction with the results of snow cover disappearance obtained from processed time-lapse pictures, which indicates a much longer duration of snow cover in this type of terrain. The result is likely due to the specifics of this single sampling point. It is located in the central part of the catchment, while most of the rock debris area occurs around protruding rock formations in the eastern part, where large amounts of snow accumulate (see Fig. 47). A similar situation occurs in the case of Hyperskeletic Cryosols (Eutric) soils, which are represented by one measurement point only.

6.3 Snow cover relationships with terrain

The relationship between the snow cover duration in the Fuglebekken catchment area (Fig. 55) and the relief characteristics in the form of topographic indices is presented in Fig. 56. The basis for the analysis was a mosaic of classified orthoimages from 2014 (Fig. 55). The obtained dependencies are rather weak, but it is worth noting that the mosaic of images represents the distribution of snow cover in an indirect way, and minor shifts of the classified images that form it result in an error that may affect the correlation value with the topographical relief. Nevertheless, certain regularities are visible. The strongest Pearson correlation ($r = 0.291$) is found between the snow cover duration and the roughness of the terrain represented by the TRI index. The wind exposition index also has a significant influence on snow cover. The strongest negative impact ($r = –0.236$) was related to the exposure to the north-eastern direction (Wind Effect 225; 225 is the direction in degrees towards which the wind is blowing, as opposed to meteorology which determines the direction from which the wind is blowing). Among the wind

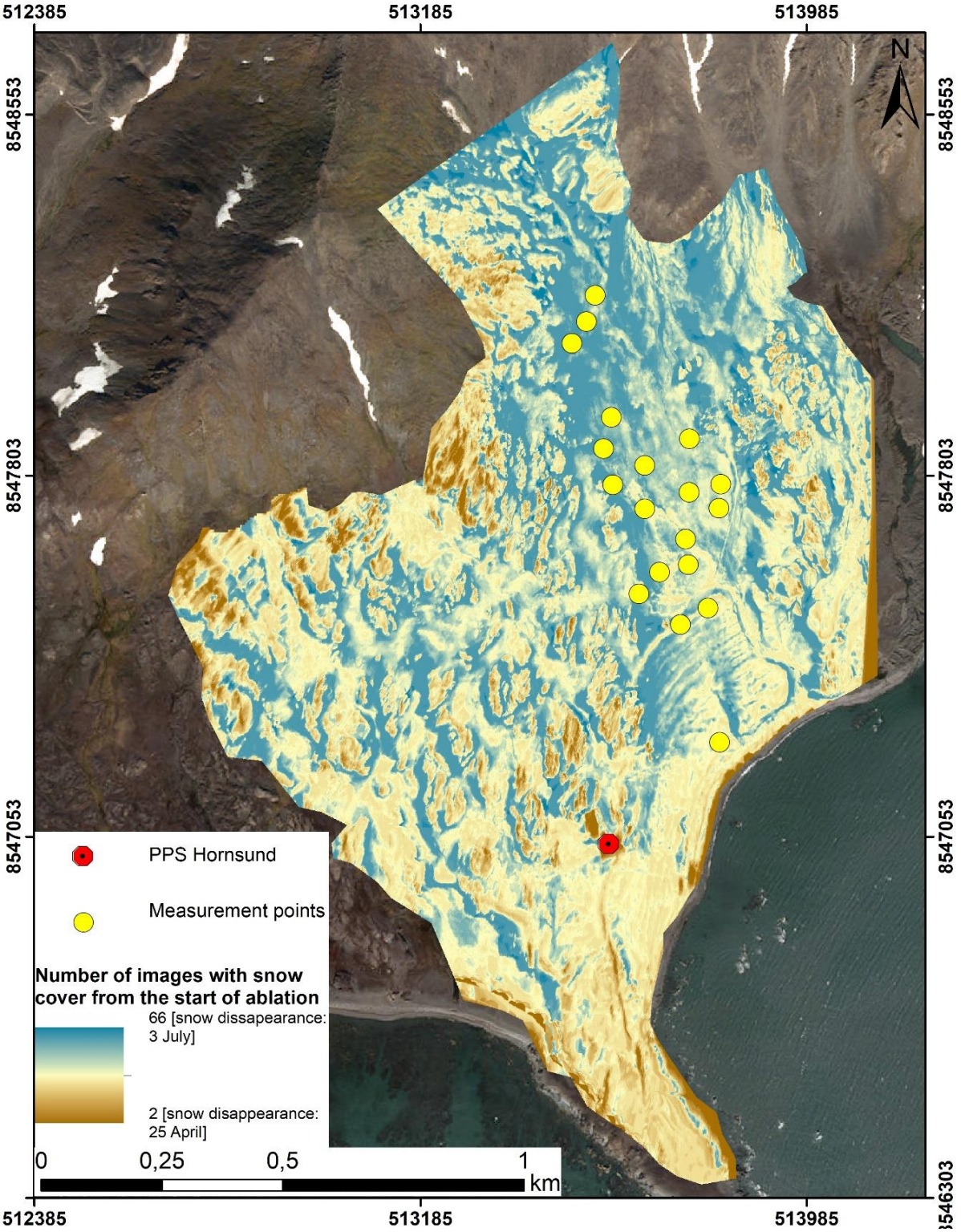

Fig. 55. Mosaic of time-lapse pictures presenting a day of snow cover disappearance as the sum of classified orthoimages from 2014.

exposures, the southern (Wind Effect 0) and south-eastern (Wind Effect 315) directions are the least important, which are the only ones to show an exceptionally weak correlation (r <0.1). It is worth noting that in PPS Hornsund, the inflow of air from these directions practically does not occur (see Fig. 10). From the other factors, the height above sea level, insolation and slope

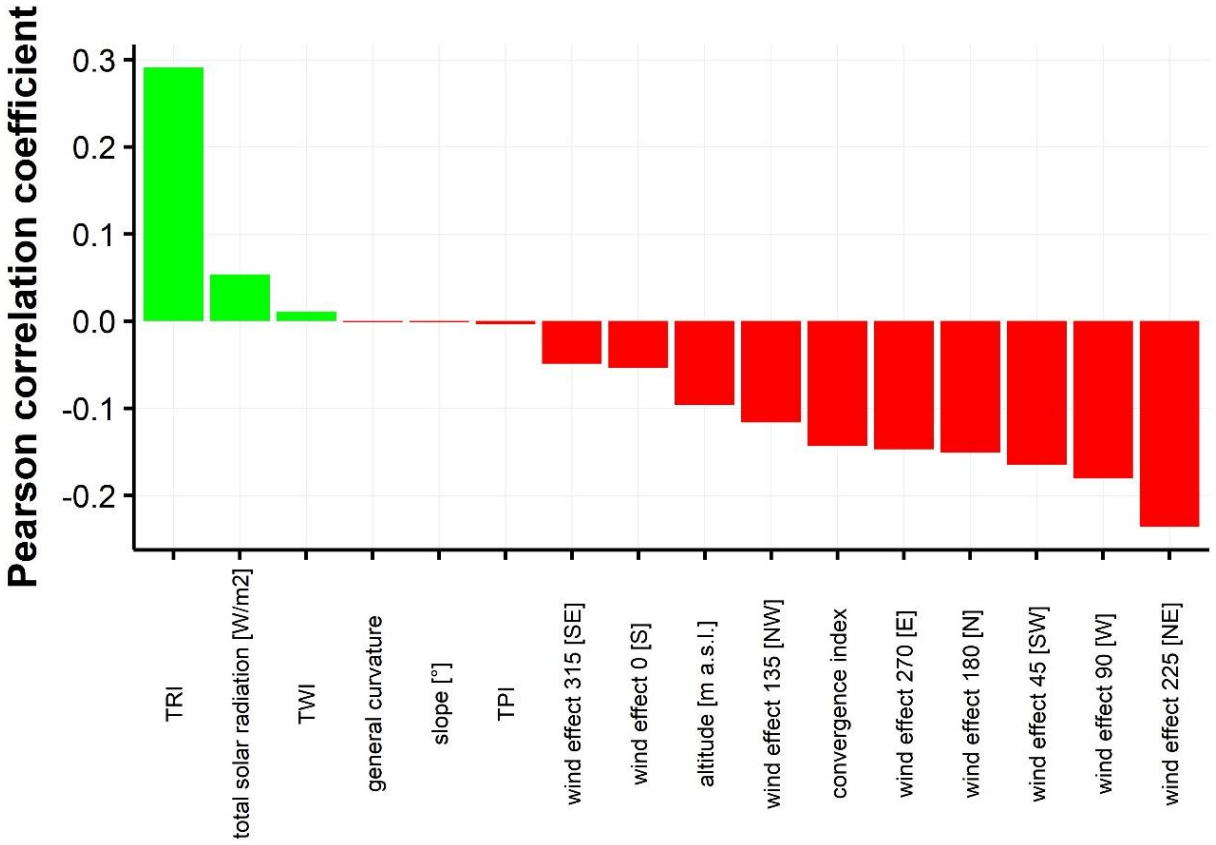

Fig. 56. Pearson's correlation coefficient between snow cover duration in the catchment and selected topographic indices.

do not matter. This is due to their low variability associated with the relatively flat nature of the analyzed area. For the above-mentioned parameters, the obtained dependencies were even quite opposite to the expected ones. The solar irradiance showed a slight positive effect on the snow cover duration, while the altitude above sea level had a negative effect, which of course cannot be true. This indicates that the **snow cover distribution in the vicinity of PPS is strongly related to the wind activity**, which in the analyzed scale prevails over the influence of, e.g., solar radiation. However, the applied methodology does not allow for the determination of clear relationships with the topography. The obtained correlation values would probably be greater if the basis for the comparisons were direct information about the snow cover distribution in space, obtained, e.g., from a series of measurements with a terrestrial laser scanner. Such kind of data will be available for the neighborhood of PPS Hornsund in the near future. At the time of writing the dissertation, the best currently available set of spatial information from the time-lapse camera and field measurements was used.

Stronger relationships between the snow cover distribution and the topography were obtained by assigning values of topographic indices to 20 measurement points. Then, their values were compared with the average and maximum snow depths, as well as SWE values recorded over the three-year period (see Fig. 44). The dependencies are presented in Fig. 57. The snow cover thickness measured in points is most strongly correlated with altitude a.s.l. (r = 0.70), easting coordinate (r = –0.65), northing coordinate (r = 0.6), as well as exposure to the north-east wind direction (Wind Effect 225; r = –0.55). The correlation is also quite strong with the TRI index representing the roughness of the terrain (r = 0.41) and the TWI (r = 0.35) parameter, characterizing the ability of a surface to store water. However, these two relationships turned

out to be statistically insignificant. The negative impact of exposure to wind from various directions is also visible, except for the south and south-east directions, which are rare in PPS Hornsund. The influence of radiation is not visible in the data, as each measuring site receives a similar amount of energy. Overall, the results confirm the pattern of snow disappearance obtained from the analysis of time-lapse imagery (Fig. 47) **indicating the highest snow thickness in the western part of the Fuglebekken catchment**. However, the dependence of the snow cover depth from the Easting coordinate is almost certainly disturbed by a small number of measurements. The measurement points are located closer to the rock outcrops in the western part of the catchment than in the eastern part. If it were otherwise and a snow survey would be carried out closer to the protruding rock formations also in the eastern part, the relationship would certainly not be so clear. In turn the increasing amount of snow together with northing coordinate is associated with an increase in altitude a.s.l. Additionally, the northernmost measurement points are located just below the steep slope, which facilitates the accumulation of snow. Very similar correlations to those for snow thickness were found for SWE.

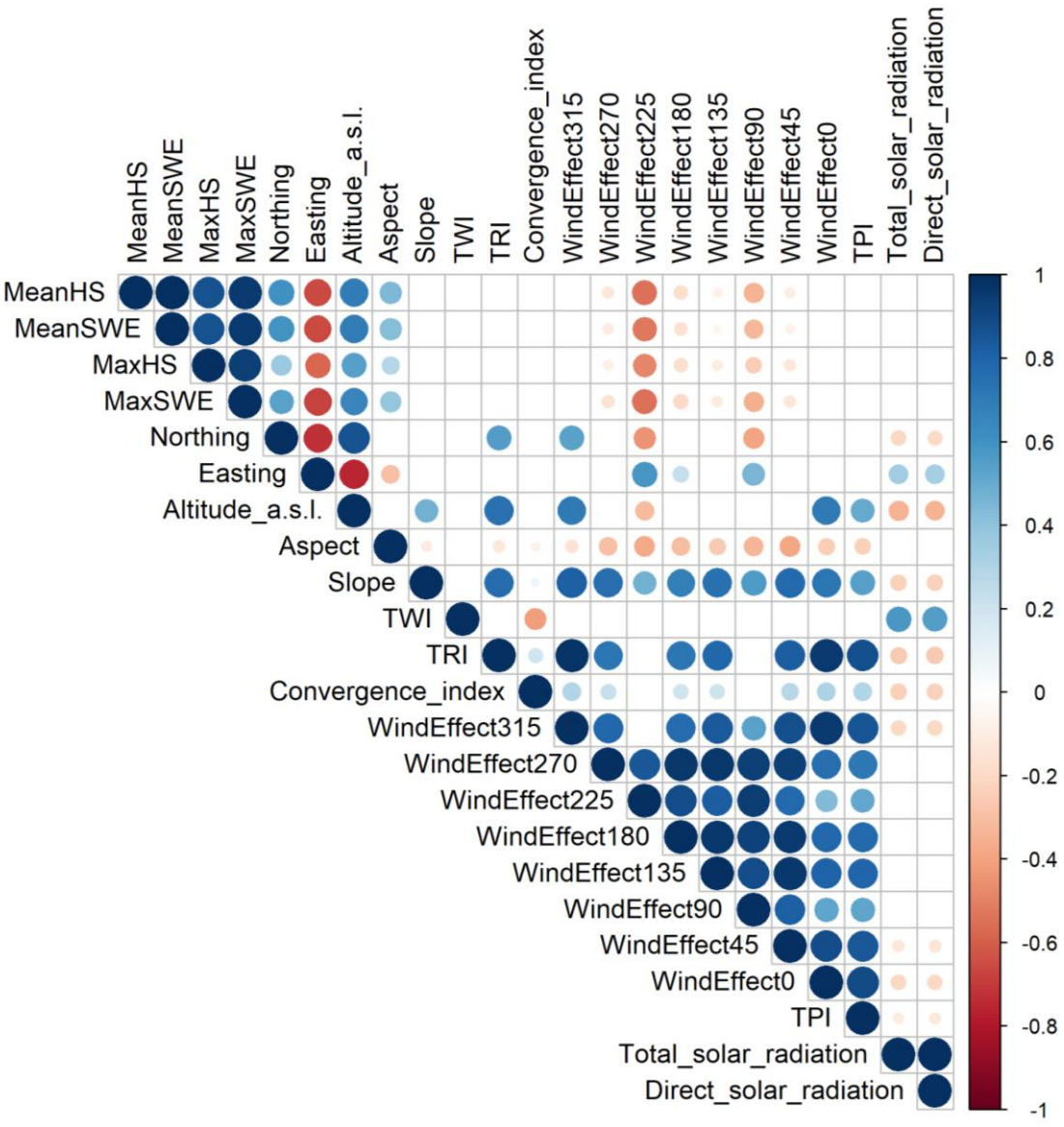

Fig. 57. Pearson's correlation *coefficient* matrix for terrain and snow cover properties characterizing 20 measurement points in the Fuglebekken catchment.

6.4 Result of snow cover distribution model

As the wind redistribution was not taken into account and the model spatial resolution was limited to 20 m, the Alpine3D did not reflect the snow distribution on the ground in correct way. Under such settings, snow depth and SWE in outcome are mainly a function of altitude above sea level (Fig. 58a), because with its increase, the sum of precipitation grows and the air temperature decreases. Zones with a comparable elevation a.s.l. are characterized with very similar snow thickness and SWE values in the model result (Figs. 58 and 59). In model outcome, comparable snow depths were indicated during the maximum accumulation in both 2014 and 2016 (Figs. 58a and 59a), despite the fact that in reality spring 2014 turned out to be a bit more snowy in the catchment area (see Fig. 42). The modelled values in both seasons are much closer to those measured in the field at accumulation points in the catchment area (Figs. 58b and 59b) than to those recorded at the PPS Hornsund weather site (Figs. 58c and 59c). This once again proves the huge impact of snow redistribution by wind on the snow cover observed at the PPS meteorological site.

Tests of various model settings have shown that soil parameters have practically no influence on the results obtained in the analyzed area. Switching off the soil module changed the modeled course of the snow cover depth by at most 1 cm and had some meaning only in the first stage of snow deposition, as well as during its disappearance in late spring. This is because the snow cover in Hornsund usually forms when air and ground temperatures are already below zero (see Chapter 3.2); therefore, the ground is normally frozen and does not transfer heat to the snow. Theoretically, some solar radiation may pass through thin and dry snow cover and heat the ground above 0 °C (Kosiba 1949). In such cases, the type of the soil under the snow can make a difference. However, due to the fact that the snow cover forms in Spitsbergen usually in October, when the solar radiation is already very weak, this effect does not occur in practice. In the ablation period, the type of ground is more important as it determines, e.g., albedo of the terrain emerging from under the snow. However, the differences between the model results with and without including soil properties were practically imperceptible. The model results depended primarily on the selected atmosphere stability settings, which determine the flux of latent and sensible heat between the atmosphere and the surface (Hicks and Martin 1972). The simulated snow cover thickness could differ by several dozen centimeters in the analyzed area, depending on the selected atmospheric stability settings; however, due to the considerable differences between the model and field measurements, it was difficult to determine which option best reflects the real conditions. For example, during the maximum accumulation period (April 18) in 2016, the modeled snow cover was characterized by depths from 53 cm on the coast to 289 cm at the mountain summit using the Monin-Obukhov similarity theory to determine the state of the atmospheric surface layer (Stearns and Weidner 1993; Michlmayr et al. 2008), while for a neutral atmosphere the depths ranged from 76 cm to 249 cm (Fig. 60). Therefore, the result was closer to the actual values observed in the field using the first method, with a greater gradient of snow depths between the coast and mountain peaks. However, due to large differences in calculation requirements, the simulation for the entire winter seasons was carried out for the simplest case, assuming the existence of a neutral atmosphere above the ground, and these results are presented in Figs. 58 and 59. Regardless of the setting used, the snow cover duration and spatial distribution were far from those observed in reality, due to the lack of consideration of snow redistribution by wind in the simulation (Fig. 60; Chapter 8).

Despite the significant overestimation of the snow cover thickness and SWE in the obtained Alpine3D results, the course of the simulated parameters is consistent with those observed in the field (Fig. 58b,c). The model shows that in both seasons the highest snow depths during the maximum accumulation (for the catchment area) occur in the top parts of the Fugleberget-

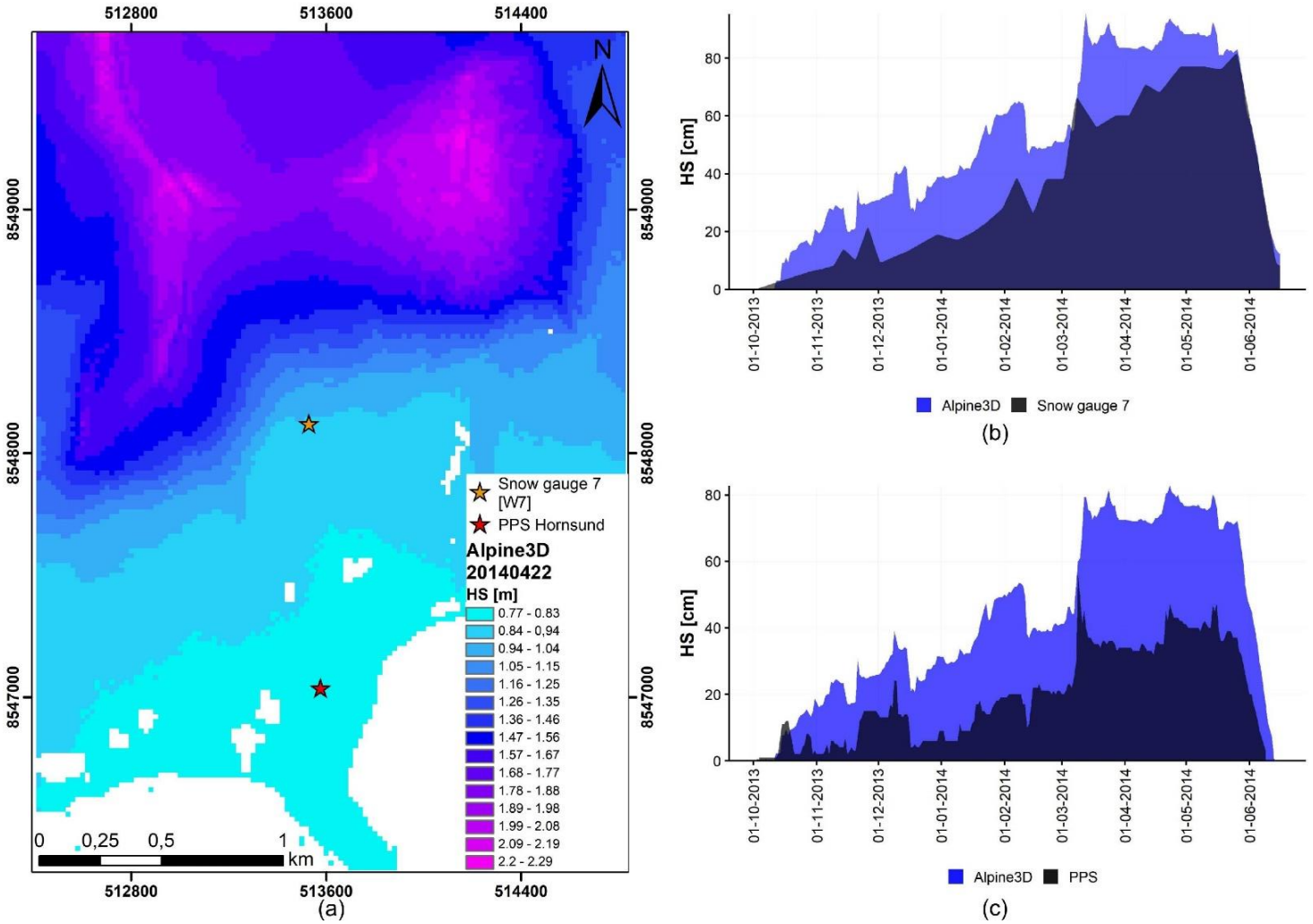

Fig. 58. Alpine3D results: (a) snow cover spatial distribution for the maximum accumulation period in 2014 (22.04) with manual measurement points marked. Actual and predicted by model snow cover depths in 2013/2014 winter season at the (b) measuring site near snow gauge 7 (W7 in Fig. 44); (c) PPS Hornsund meteorological site.

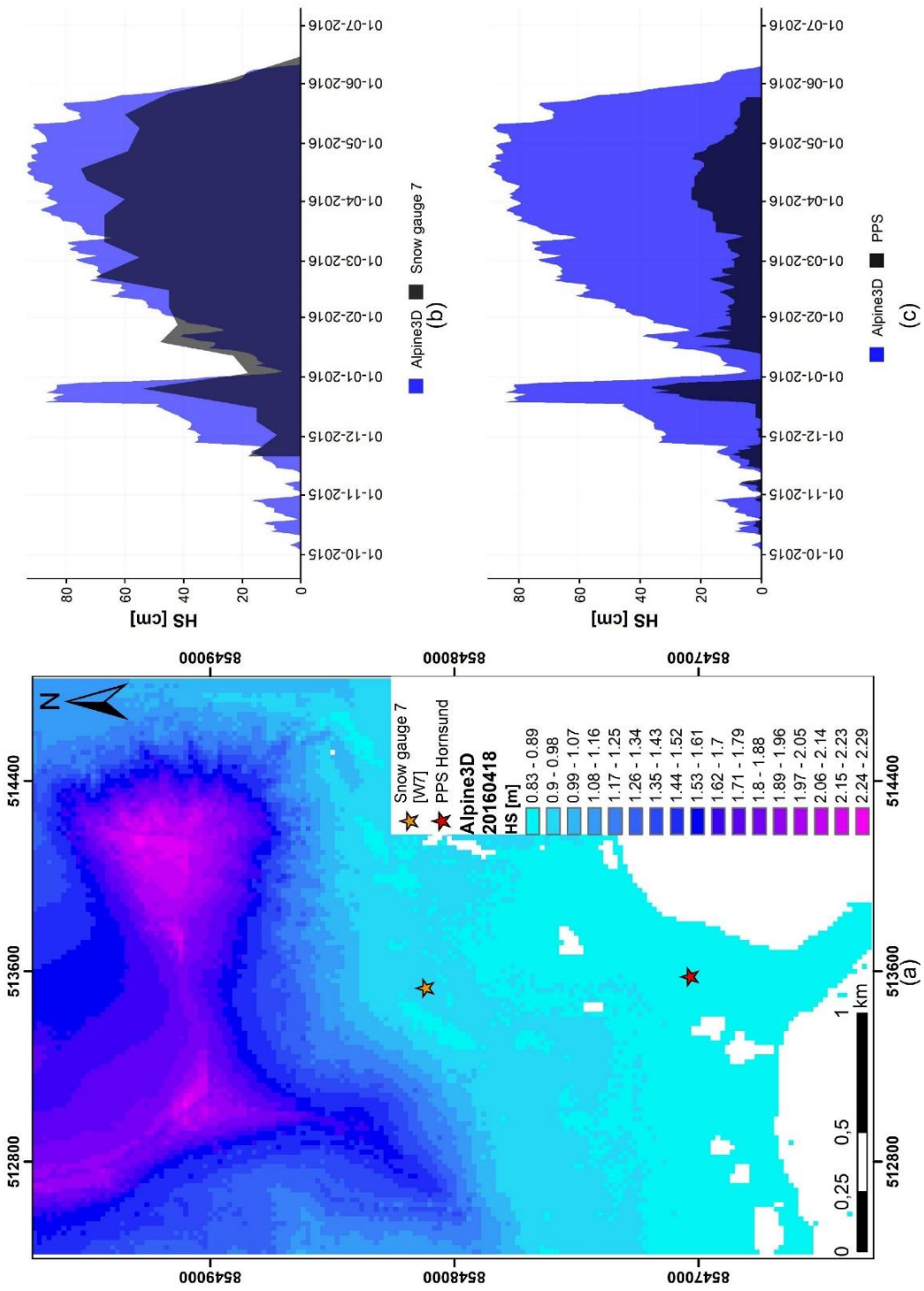

Fig. 59. Alpine3D results: (a) snow cover spatial distribution for the maximum accumulation period in 2016 (18.04) with manual measurement points marked. Actual and predicted by model snow cover depths in 2015/2016 winter season at the (b) measuring site near snow gauge 7 (W7 in Fig. 44); (c) PPS Hornsund meteorological site.

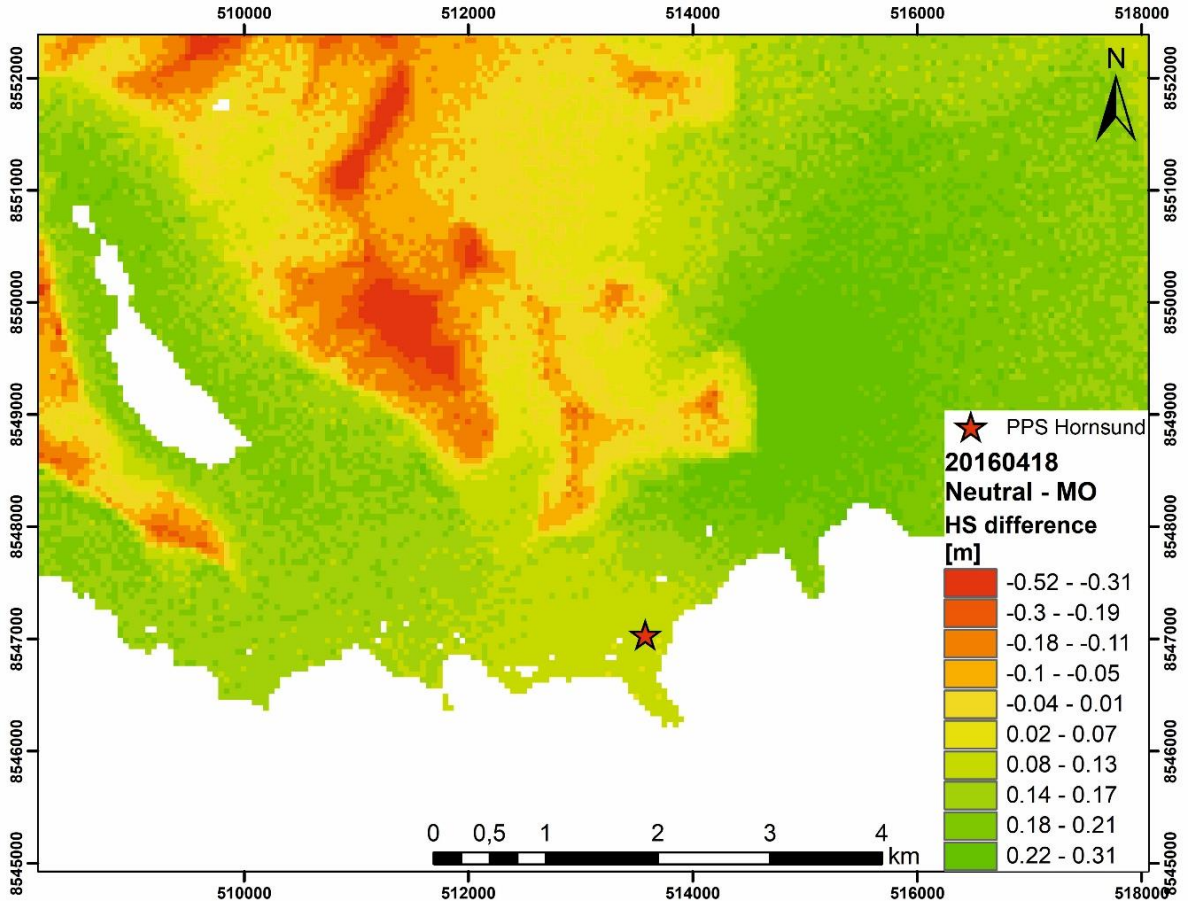

Fig. 60. The difference in the modeled snow cover thickness for the maximum accumulation of the 2015/2016 season (18.04.2016) between the Alpine3D result obtained for the neutral atmosphere (minuend) and the Monin-Obukhov method (subtrahend) to determine the atmosphere above the snow surface.

Ariekammen massif. There, the simulated snow depth exceeds 2 m, which corresponds to about 700 mm of SWE. The smallest values, in the range of 80–90 cm, translating into nearly 300 mm of SWE, were calculated for the lowest part of the catchment. Interestingly, the modeled minima correspond approximately to the maximum values actually recorded in the Fuglebekken catchment, at the accumulation points under the Fugleberget slope (see Fig. 45). Due to the large general discrepancy between the measured values and those obtained from the model, the obtained results cannot be used, e.g., to determine the meltwater runoff from the catchment. However, it can be assumed that the Alpine3D calculations indicate the amount of snow that would accumulate in a given area without wind-driven sublimation and redistribution processes. This would mean that **blowing and drifting snow processes are responsible for approximately 40 to 50% of the snow mass loss in Fuglebekken catchment. In the case of the PPS Hornsund meteorological site, these losses can be as high as 80%** (2015/2016 winter season).

7. SPATIAL VARIABILITY OF SNOW COVER ON THE TUNDRA IN THE SURROUNDINGS OF THE HORNSUND FIORD

7.1 Pattern of snow cover disappearance on the coasts of the Hornsund Fiord

The analysis of satellite images allows, at least partially, to relate the snow cover disappearance in the Fuglebekken catchment to other coastal areas of the Hornsund Fiord. Figure 61 shows

the snow coverage percentage obtained from the satellite images with the division of the surveyed area into sectors (Fig. 39). For ease of comparison, the figure also shows the SCE on these days in the Fuglebekken catchment. The result obtained from the April scene (07.04.2018) was omitted in the graph, because on that day all areas were characterized by SCE exceeding 99% and only single pixels represented the snow-free terrain. The SCE from the Fuglebekken catchment fits well to the SCE acquired from processed LANDSAT scenes for Fuglebergsletta plain. However, it should be remembered that the study areas had a different spatial extent and it is difficult to relate information from the dataset with 1 m resolution with that characterized by 30 m resolution without loss of information. The biggest differences when comparing datasets with such contrasting resolutions can be expected at the beginning and end of snow cover ablation. In the initial phase, it is possible to recognize small individual rocks protruding from snow cover on the high-resolution data, which will not be captured on a less accurate set, thus overestimating the actual SCE. On the other hand, in the final stage of snow disappearance, it becomes impossible to identify small snow patches on satellite images, which leads to an underestimation of actual snow coverage. Nevertheless, comparing the SCE obtained from the time-lapse camera to the SCE from the Landsat data, it is possible to define the **ablation in the Fuglebekken catchment as slightly delayed in relation to the entire Fuglebergsletta area**. At the same time, in relation to the Hornsund coasts taken as a whole, SCE in Fuglebekken basin is within average values. It means that the ablation in the catchment quite well illustrates the snow disappearance also on larger coastal tundra area of southern Spitsbergen.

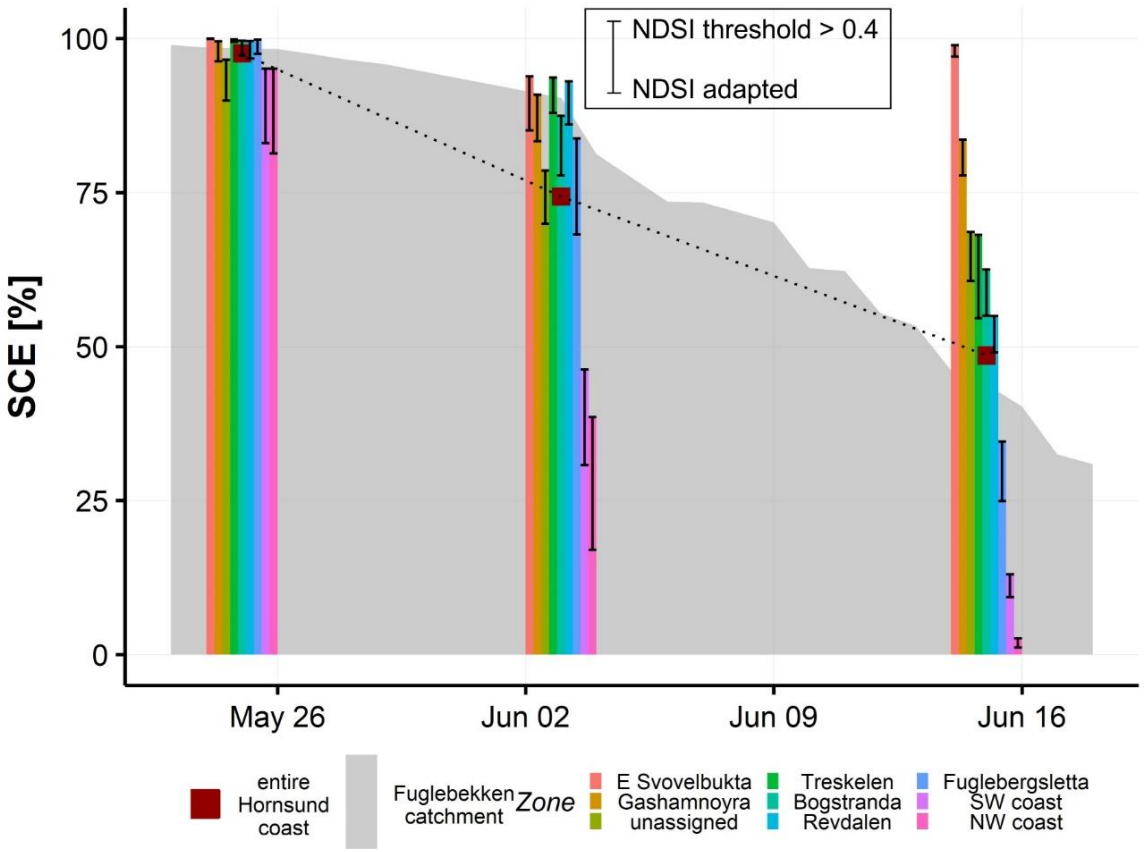

Fig. 61. Disappearance of snow cover in individual coastal zones of the Hornsund Fiord in 2014 (color bars). Presented are also average SCE for the entire analysis area (squares) and daily SCE in Fuglebekken catchment (grey ribbon). Error bars illustrate the differences in SCE results obtained between two classification methods: using adapted for individual scene and fixed threshold (> 0.4) in NDSI value.

Figure 61 proves that the **snow cover disappearance occurs at different times on the shores of the Hornsund Fiord**. On June 15, the total SCE (red square) calculated using the NDSI threshold > 0.4 fell below 50%. On the same day, however, almost 100% of the eastern coast of Svovelbukta was under snow, while the NW Hornsund shore was almost completely snow-free. The chart shows, however, that on June 15, the SCE in the south-eastern part of the fiord (E Svovelbukta) increased compared to the scene from June 3. It is possible because in the period of June 3–15, the average daily temperatures on PPS Hornsund were in the range of 1.2–3.5 °C and rainfalls were noted. In the slightly cooler eastern part of the fiord, this could have translated into snowfall episodes. However, analysis of the panchromatic images revealed that on June 15, the SCE was in fact lower than on June 3. This was caused by the disturbance of classification results based on NDSI by specific lighting conditions and the presence of a fine cloud over part of the E Svovelbukta area not captured by the CFMask algorithm (see its efficiency in Fig. 63). Nevertheless, on June 15, the greatest snow cover was undoubtedly recorded on the eastern coast of Svovelbukta from selected coastal zones. Considering the result from that day as representative, which, due to the high repeatability of the snow ablation pattern in the Fuglebekken catchment (Fig. 47), seems to be appropriate, it can be said that **the snow cover on the Hornsund coasts disappears at the earliest in the northwest, and at the latest in the southeast** (Fig. 62). Snow cover duration in non-glaciated areas up to 50 m above sea level would therefore be as follows: (earliest snowmelt) northwestern shore < southwestern shore < Fuglebergsletta < Revdalen < Bogstranda < Treskelen < Gåshamnøyra < Svovelbukta coasts (latest snow disappearance). This order results from the analysis of the last available satellite image for the 2014 ablation period, but the sequence is generally also maintained on June 3, suggesting that further snow disappearance also follows the scheme above.

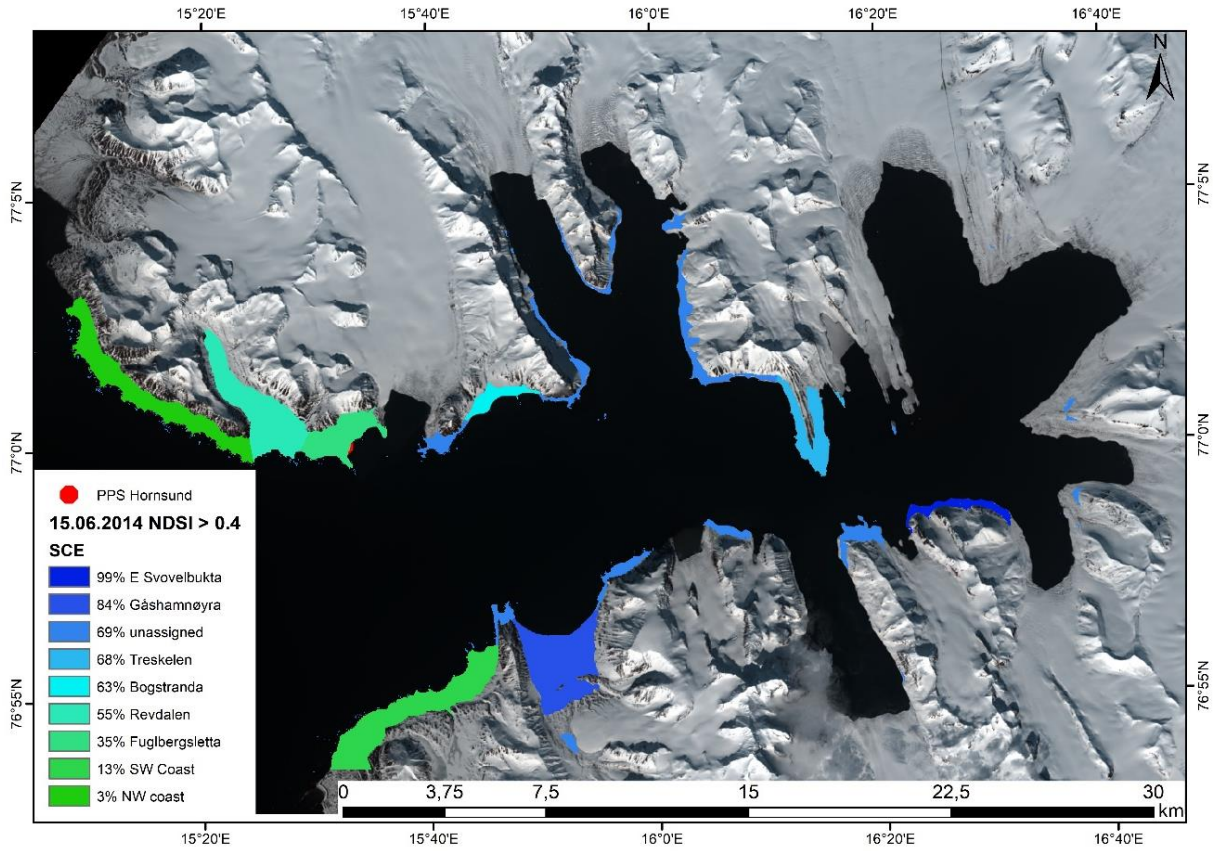

Fig. 62. Snow coverage by zones of Hornsund coasts on June 15, 2014. SCE was obtained using the NDSI threshold of 0.4.

Snow classification in satellite images has been performed not only using a fixed NDSI threshold value of 0.4, but also a threshold adjusted for each scene separately (using the panchromatic band to verify the results – see Chapter 5.2). The NDSI threshold > 0.4 was adequate for the identification of snow surface on satellite scenes, only slightly overestimating the surface area covered by it in relation to that obtained with the manually adjusted thresholds. They were set to 0.56 for April 7, 0.7 for May 25, 0.5 for June 3, and 0.56 for June 15. In Fig. 61, the classification results using fixed NDSI threshold > 0.4 are shown by the bars, while error bars indicate the area that was classified as snow-free using a manually adapted threshold. The most problematic was the correct determination of SCE on the coast in the north-western part of the study area, due to the very irregular terrain with a large number of protruding rocks between the snow cover (Fig. 63). Figure 63 shows differences in the classification results obtained

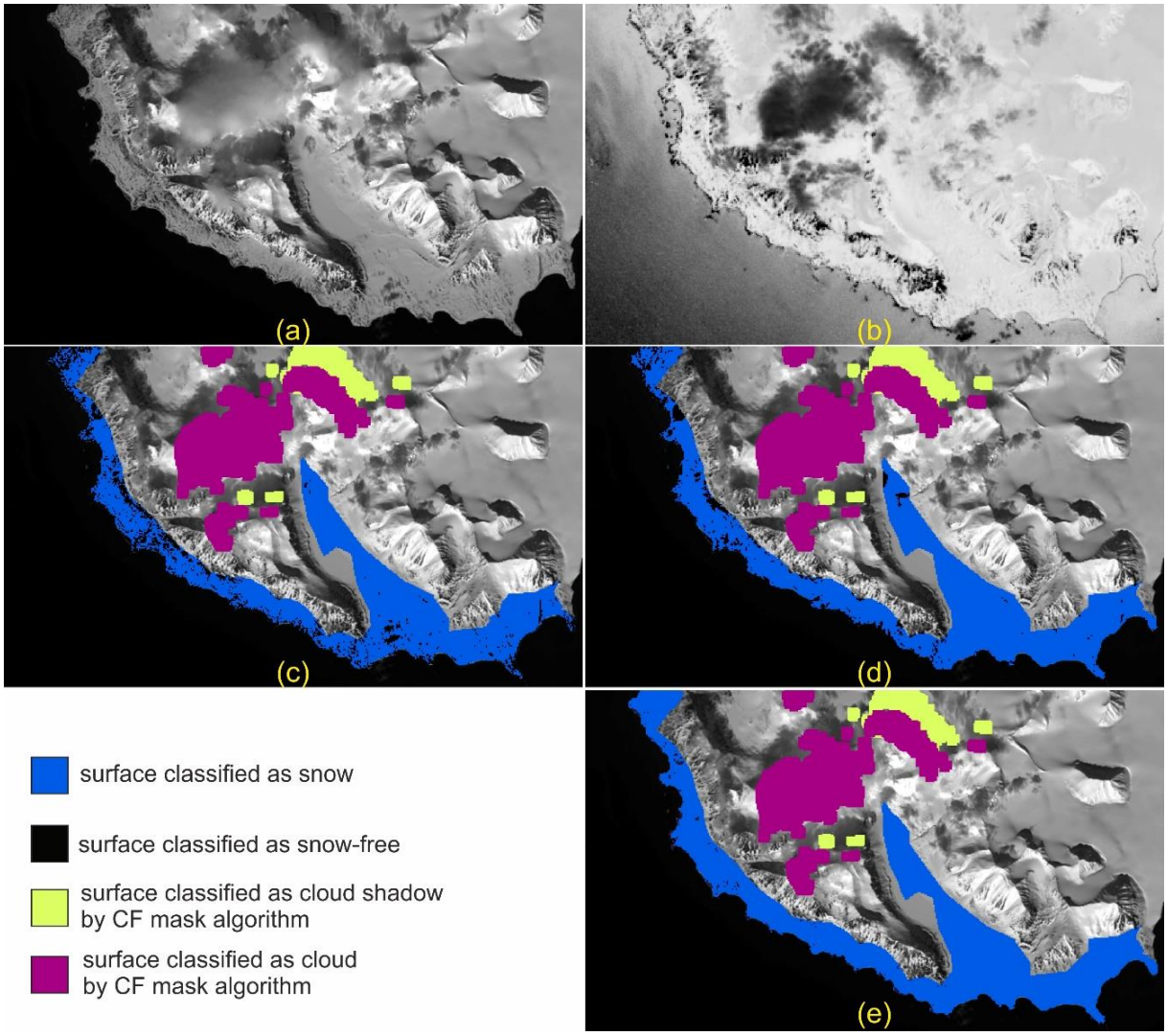

Fig. 63. Zoomed satellite image presenting north-western part of the Hornsund coast on 25.05.2014: (a) raw panchromatic band, (b) NDSI calculated after applying the atmospheric correction, (c) classification result performed on the panchromatic band using thresholding technique, (d) classification result performed on NDSI image using (adapted) threshold value of 0.7, and (e) classification result performed on NDSI image using fixed threshold value of 0.4. On subimages (c), (d) and (e), results of CF cloud mask algorithm are shown.

using various approaches and divergent thresholds as well as the problems caused by the cloud coverage. Clouds are not always identified correctly by the detection algorithms and can both overestimate and underestimate (casting shadows on land) the real SCE. Shreds of clouds are present in the southern part of the image (noticeable over the sea on the NDSI image in Fig. 63) near the Revelva river mouth. They cast a shadow visible in the panchromatic band as a dark object that has been classified as a snow-free terrain. The shaded area is imperceptible at the NDSI image, but the clouds themselves become dark spots there. These properties facilitate the identification of clouds and their shadows. The latter lowers the NDSI values in relation to the surrounding area (Kulkarni et al. 2006), which may affect the resulting SCE too. Despite the problems, the results obtained from the analysis of satellite images using the NDSI classification are of good quality. The differences in SCE between the application of the fixed threshold of 0.4 and the one adjusted to each scene separately do not generally exceed 10%, excluding the problematic north-western coast of Hornsund (Fig. 63) with complex topography.

7.2 Spatial distribution of the snow cover and its properties

Snow cover probing in spring 2016 was carried out at the same locations as in 2014 (Nawrot et al. 2015). That allowed to check the repeatability of snow distribution in a larger area than the nearest vicinity of the PPS. Due to the large area covered by the study and the difficulty of accessing some places, the successive measurements were separated by significant time intervals. In order to compare the obtained results with each other, corrections to compensate for snow melting or accumulation between soundings were applied (Table 10). The adjustments were made using the indications of the SNOWPACK model. As the wind redistribution was not taken into account in its simulations, this method allowed to determine changes in snow depth caused only by ablation or a new snowfall deposition. That was intentional. The use of actual measurements, e.g. from PPS, could give unreliable corrections due to the strong local influence of wind activity (see Chapters 6.1 and 6.4). The obtained result shows that the **snow thickness in the Fuglebekken catchment is average compared to other non-glaciated areas** (Fig. 64). The snow depths recorded here are higher than in Gåshamnøyra, similar to the values measured in the Revdalen valley and the Treskelen peninsula, but significantly lower than in the easternmost Svovelbukta coast and higher elevated areas of Ariedalen and Bogstranda. However, it should be remembered here that the selected measurement sites do not necessarily have to be representative for the zones mentioned as a whole. This applies primarily to Gåshamnøyra, which is a large area, but soundings were carried out only in the coastal strip. Similarly, only a few measurements have been made on the Treskelen peninsula. Nevertheless, an intercomparison of results from two snow surveys proves that **the snow cover distribution in spring 2016 repeated the pattern from 2014**. The highest and the lowest snow depths were usually recorded in the same places, both in individual sampling points and in the entire investigated coastal areas. Measurements in 2016 show generally slightly lower values than those from 2014, although the maximum accumulation period in 2014 was achieved much later than the field studies took place. Only in the Gåshamnøyra and Ariedalen areas somewhat higher snow cover was recorded in 2016. However, there are very large differences on the Svovelbukta coast, even though the measurements were made in the same number and at the same locations. Apart from this location, the obtained results were characterized by high convergence, even despite the fact that the number of soundings in distinguished zones sometimes varied significantly. It is also worth to mention that the detection of measurement points was carried out only on the basis of portable GPS indications with an accuracy of several meters, which did not allow repeated measurements at exactly the same points.

Table 10

The correction values from the SNOWPACK model used to normalize snow thickness measurements from different days in the spring seasons of 2014 and 2016. The benchmark for corrections in both seasons was the snow thickness reported in PPS Hornsund on April 18 (both for 2014 and 2016)

Year	Date of field measurements	Study area	Applied correction [cm]	Number of soundings
2014	13.04	Bogstranda	+1.0	59
	15.04	Revdalen	+2.4	55
	18.04	Fuglebekken	0	19
	19.04	Gåshamnøyra	0	24
	22.04	Treskelen	–6.0	1
	22.04	Svovelbukta coast	–6.0	16
	24.04	Ariedalen	–6.5	46
2016	15.04	Revdalen	+1.4	45
	18.04	Fuglebekken	0	32
	01.05	Ariedalen	+4.8	26
	03.05	Treskelen	+8.4	8
	03.05	Svovelbukta coast	+8.4	16
	10.05	Gåshamnøyra	+7.6	24
	24.05	Bogstranda	+34.3	31

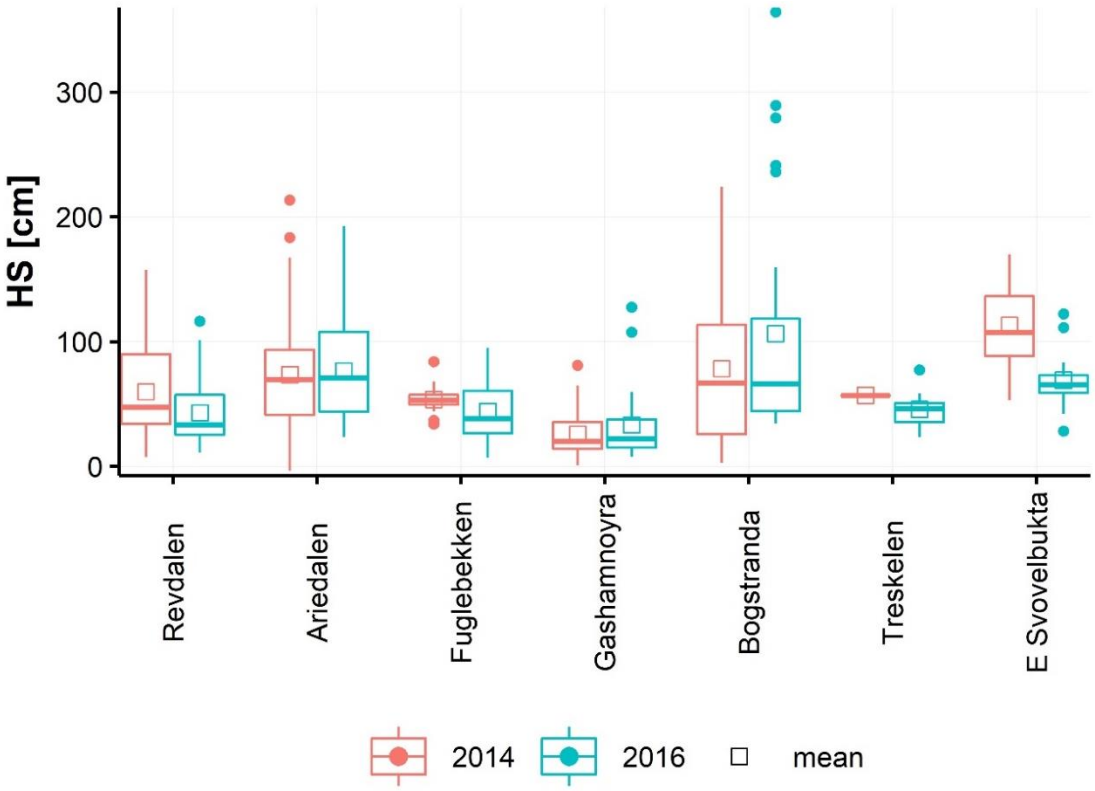

Fig. 64. Comparison of snow depths measured in spring 2014 and 2016 in different parts of the Hornsund Fiord taking into account corrections for snow melting or accumulation (Table 10).

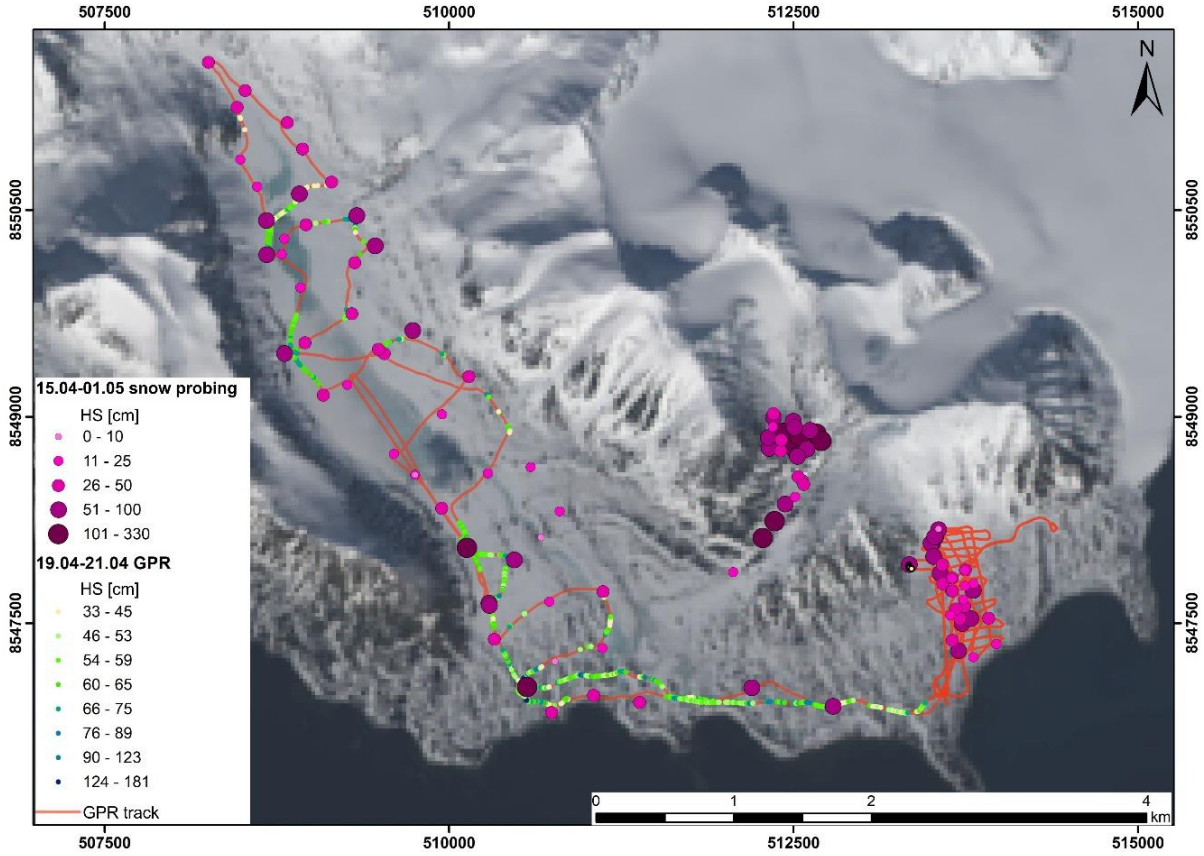

Fig. 65. Snow depths measured from April 15 to May 1, 2016, in the area of Revdalen, Ariedalen and Fuglebergsletta.

The spatial presentation of the measurement results shows that **the highest snow cover depths occur in the western parts of the valleys** (Figs. 65 and 66). This is particularly evident in the Sofiedalen valley: near the western edge of the area, the snow thickness can exceed 2 or 3 meters despite a relatively low altitude a.s.l. This indicates a **significant influence of the prevailing eastern wind on snow cover distribution**. The results from Revdalen and Fuglebekken also suggest **slightly greater snow accumulation on the eastern edges of the plains, while the central parts have the lowest snow thickness**. This should also be explained by the formation of snowdrifts in front of a more elevated terrain. However, GPR soundings did not allow for full recognition of the snow distribution in Fuglebekken and Revdalen areas because the frequency of the device's antenna was too low (see Chapter 5.1). Figure 65 presents only the most reliable results from the entire GPR sounding route. Snow depths that did not match the manual measurements on the trail were discarded. The parts of measurements where the snow depth from GPR was consistent with the manual soundings should be interpreted as the places with the thickest snow cover on the GPR track. In other locations, the snow thickness was either smaller than the near-field effect on the GPR profile, or it could not be confirmed by the avalanche probe measurements. The vast majority of verified readings from radargrams were in the range of 46–65 cm. The GPR measurements from May have not been presented due to the great difficulty in interpreting the profiles obtained at that time.

A specific site covered by the field measurements is the Ariedalen valley. It is a more elevated terrain with generally greater snow thickness (Fig. 67). Additionally, the longitudinal course and the mountains surrounding on three sides make Ariedalen a sheltered place (Fig. 18) with limited snow removal by wind. Interestingly, in this valley the snow cover is thicker in the eastern, not the western, part of the area.

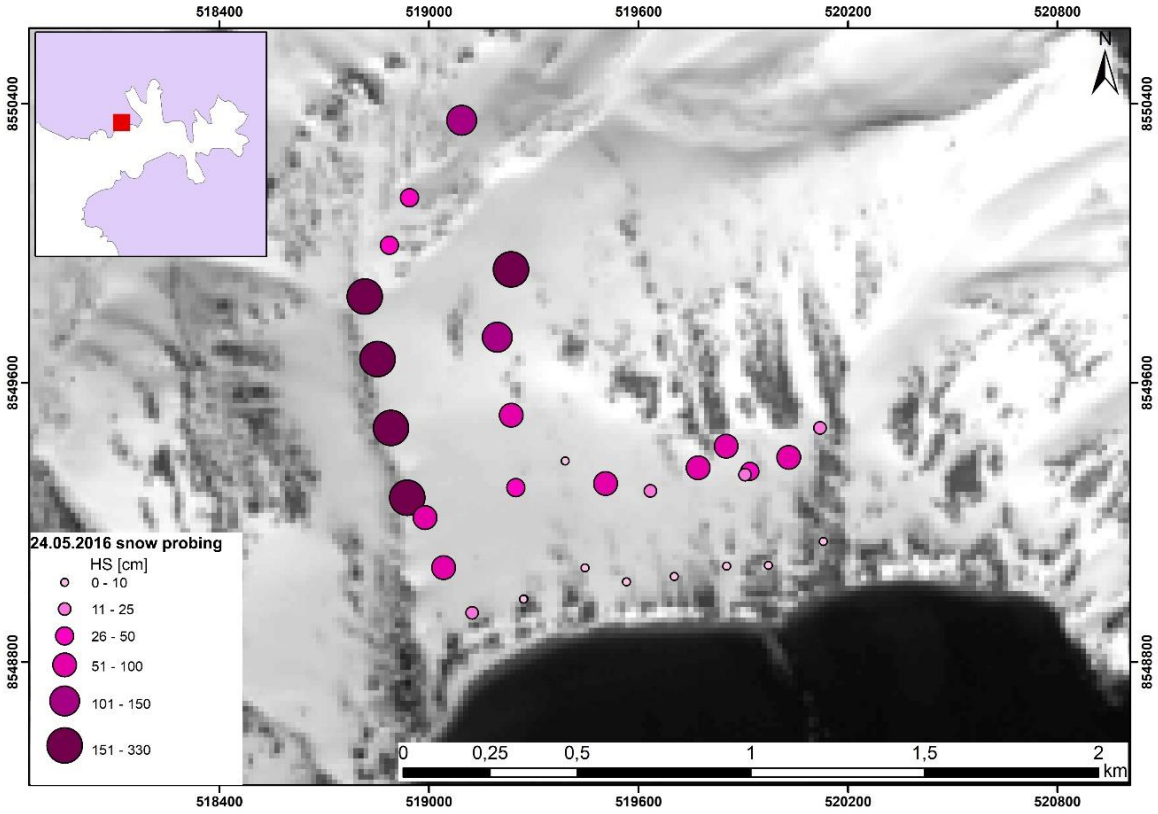

Fig. 66. Snow depths measured on May 24, 2016, in the Bogstranda area.

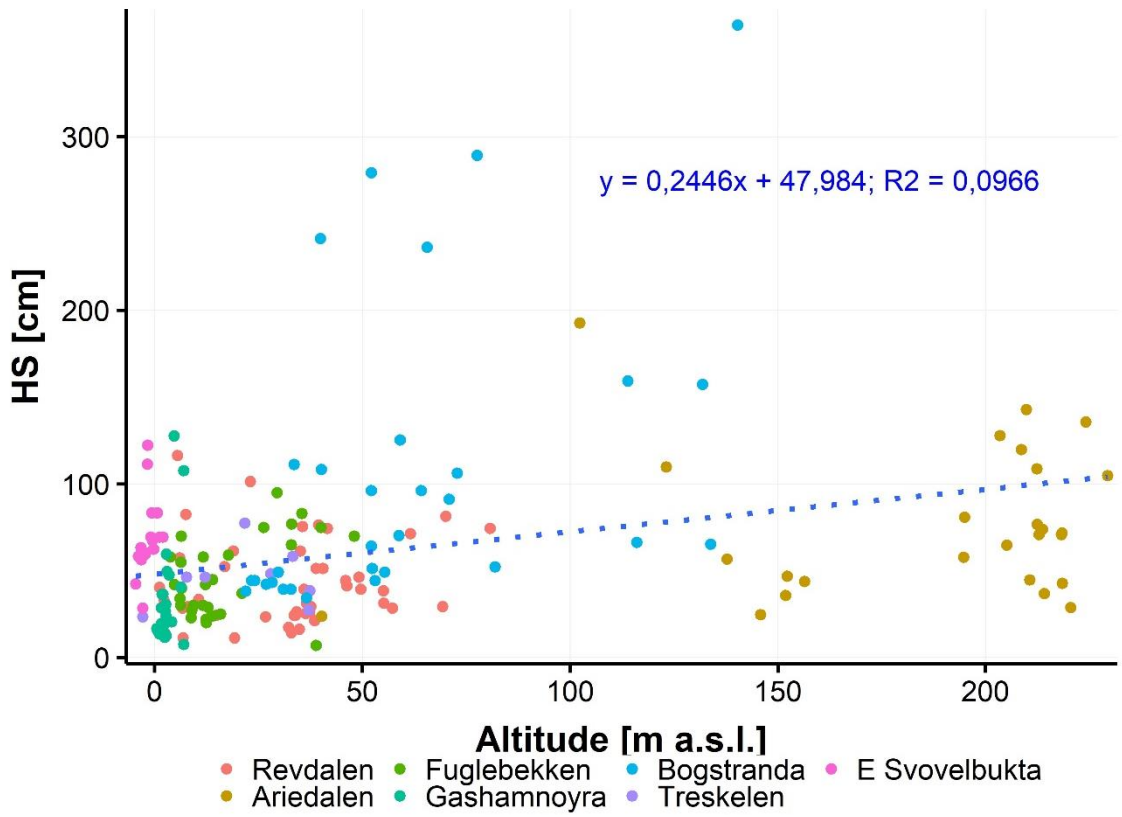

Fig. 67. Snow cover thickness distribution on the tundra in relation to the altitude a.s.l. Negative altitudes are the result of GPS inaccuracy.

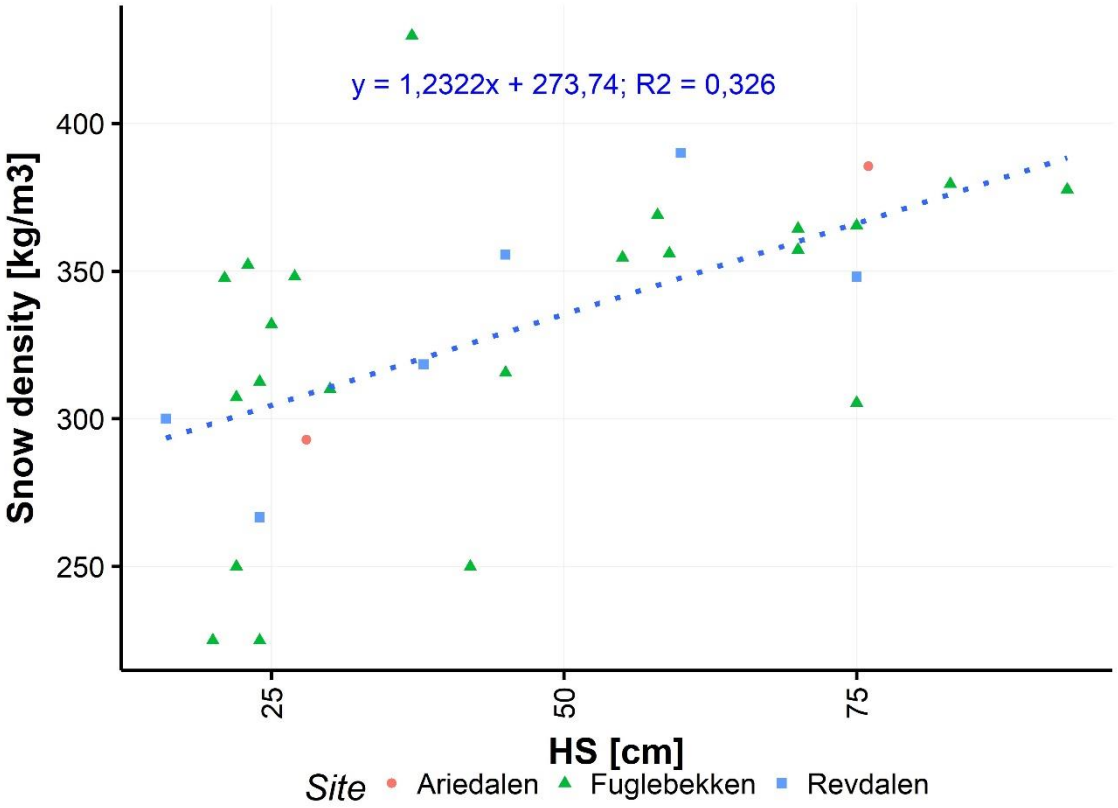

Fig. 68. Relationship between snow density and thickness based on measurements carried out on April 15 – May 1, 2016.

The physico-chemical properties of snow obtained from snow pits carried out in different tundra locations are difficult to compare due to the large time intervals between such measurements and the rapid changes in the internal snow cover structure during ablation. However, the presence of two ice layers was visible in most of the measurement sites. The exceptions were profiles in Ariedalen and on Lake Revvatnet, where snow thickness was generally low at chosen snow pit locations (< 30 cm).

Snow cover density was presented on the basis of measurements performed before the ablation period started in spring 2016 (before the 1st of May). Typically, the values were in the range of 300–400 kg/m^3. Snow density was similar in all analyzed places, but generally, when the snow cover thickness was greater, a slightly higher density was recorded (Fig. 68). No spatial pattern was found in data, similarly as in the measurements from 2014 (Nawrot et al. 2015).

7.3 Snow cover relationships with topography and meteorological conditions

The superimposition of the SCE obtained from the classification of satellite image from June 15, 2016 on the calculated terrain indices and modeled meteorological elements proved a high dependence of snow cover duration on weather conditions (Fig. 69). A very strong Pearson correlation, amounting to –0.78, was obtained between SCE and average annual air temperature from the climatological reanalyses (1991–2000). A slightly smaller positive relationship (r = 0.57) was found for the annual precipitation totals. Worth mentioning is also the potential insolation with obviously negative correlation (–0.24) and elevation a.s.l. with a positive impact (r = 0.22) on SCE. The topographic indices were less important for snow cover duration. Interestingly, the wind exposition index was positively correlated with SCE on June 15, 2016 (r from 0.11 to 0.18, depending on wind direction) but negatively with the TWI index, while the exactly opposite effect would be expected. This may indicate that while the wind exposition is very

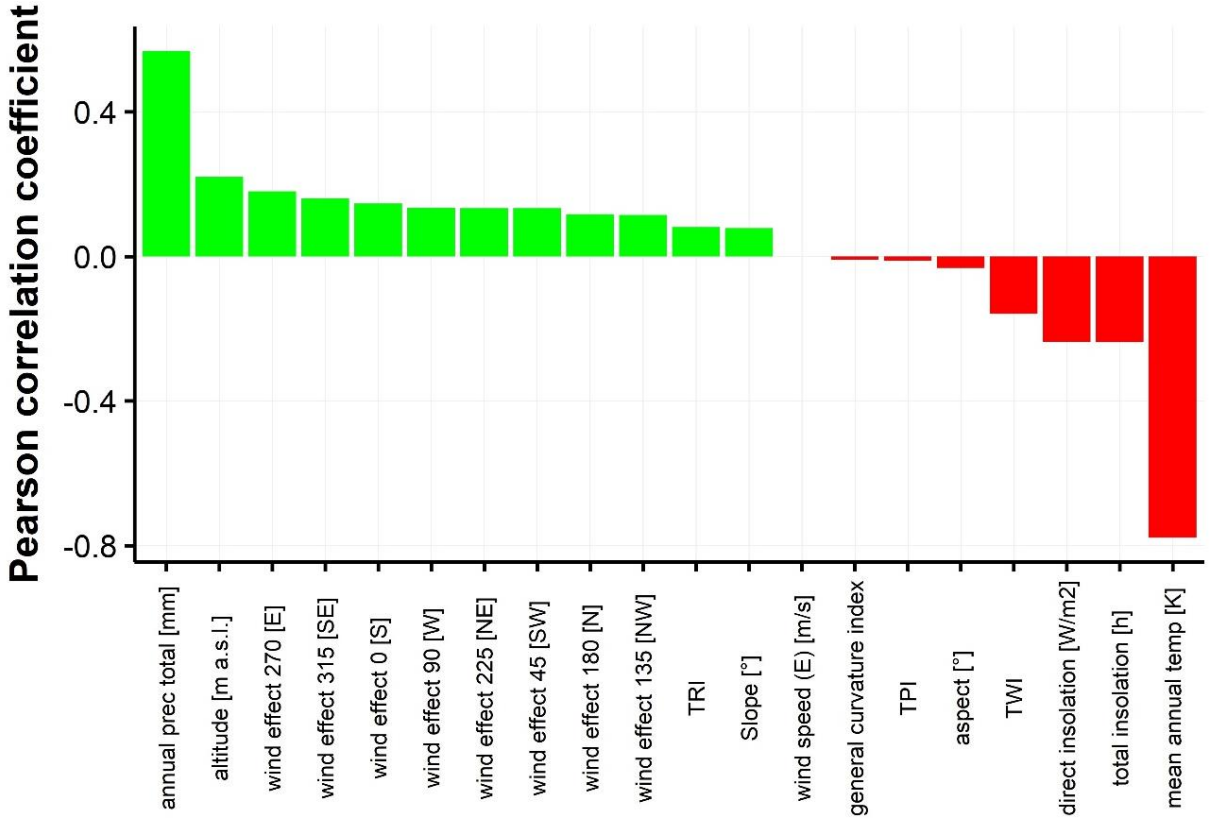

Fig. 69. Pearson's correlation coefficient between SCE on 15.06.2014 and the topographical indices or spatially modeled climatic elements.

important on the micro and meso scale, leading to the formation of snowdrifts near natural terrain barriers, it ceases to be meaningful on the macro scale and gives way to the influence of other meteorological factors. The correlations with the average annual temperature and the precipitation totals are related to the fact that according to the climate model, the warmest and driest are the western shores of the Hornsund Fiord, which on June 15 were almost snow-free. Although the annual values were compared, not those from the winter season only, the variability of temperature and precipitation in the fiord is similar throughout the year, at least according to the model indications. The amount of solar radiation reaching the ground also turned out to be significant, as snow on the northern shores of the fiord melt earlier due to better insolation conditions (see Fig. 17). The influence of altitude on the snow cover is obvious because as it rises the temperature decreases and the precipitation increases. However, the analysis took into account the area located only up to 50 m a.s.l. and for such setting the impact of spatial variability of temperature and precipitation in the Hornsund Fiord region turned out to be much more related with SCE than the altitude a.s.l.

The correlation between snow depth and topographical indices and climatic components did not give such unambiguous results as for SCE from June 15. Snow thickness was positively correlated with terrain roughness (TRI; $r = 0.31$), altitude a.s.l. ($r = 0.32$), and total precipitation sum ($r = 0.33$). Negative influence was found for potential and real insolation ($r = –0.42$), mean annual air temperature ($r = –0.29$), TPI ($r = –0.22$), TWI ($r = –0.27$), and General Curvature Index ($r = –0.15$) (Fig. 70). The results also show that among the measuring points, slightly

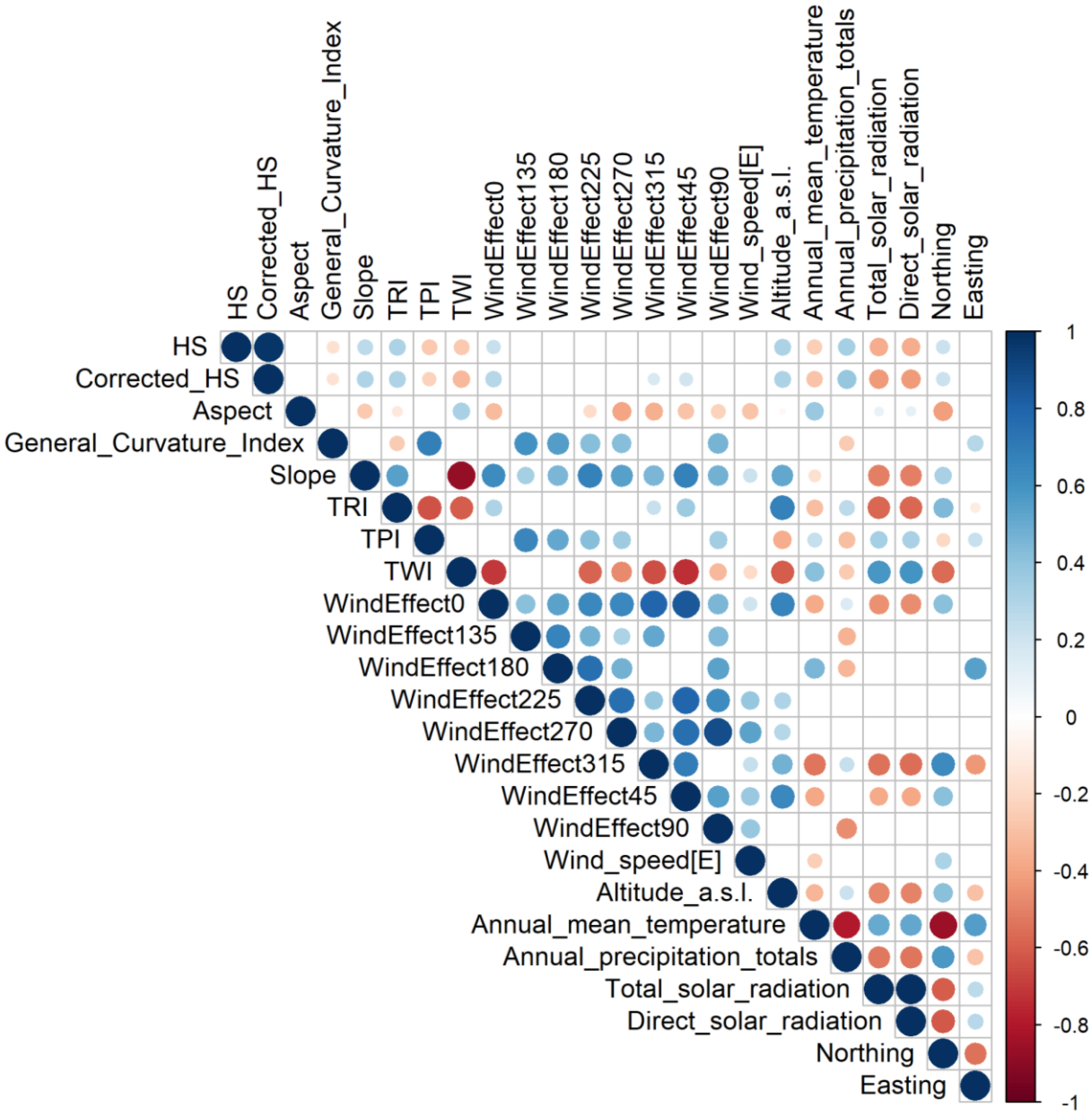

Fig. 70. Pearson correlation matrix between snow cover thickness measured in 2016 in non-glaciated areas, along with topographical indices and modeled climatic elements.

greater snow depths are noted in sites located farther to the north (Northing; $r = 0.22$). The relationships with other indices turned out to be statistically insignificant. While the influence of air temperature, precipitation sum, or altitude seems clear, the explanation is needed for the negative relationship of snow thickness, e.g. with the TWI. This index describes the tendency of an area to accumulate water and thus indirectly also the snow cover. The high values of this index are found, among other places, in Gåshamnøyra, which significantly lowered the average snow depth, being the area with the lowest altitude above sea level. On the other hand, the TWI is low on convex slopes or in the immediate vicinity of, e.g., protruding rocks that facilitate snowdrifts formation. These factors determine the negative correlation of snow thickness with TWI.

8. DYNAMICS OF CHANGES IN SNOWPACK STRATIGRAPHY ON VARIOUS LAND COVER TYPES

In the spring of 2016, the snow cover structure was measured at regular intervals in the same locations. This made it possible to trace the changes taking place in the snow cover during the ablation period. Such information was also used to validate the SNOWPACK model results from the 2016 ablation season. As the simulation was run with a spatial resolution of 50 m for the measurement area (Fig. 41) and the influence of blowing or drifting snow was not taken into account, the outcome shows a similar SWE and snow thickness in locations of snow pits (Fig. 71), which have been dug in the coastal zone at a similar altitude above sea level. Noteworthy is the lack of model results for the lake area, which as a water body was excluded from the calculations. For the maximum accumulation period in spring 2016, the model predicted SWE not exceeding 300 mm stored in a 75–90 cm thick snow cover in the coastal zone. In the field, such values were recorded at that time only in places highly conducive to snow accumulation (see Figs. 65 and 45). Along with the uniform mapping of the snow cover distribution by the model, its internal structure in the simulation also shows no significant variability for points located at the same altitude above sea level (Fig. 73). However, actual field observations reveal serious differences in snow stratigraphy (Fig. 72).

The SWE obtained from measurements in snow pits carried out during the maximum accumulation period (21–23.04.2016) ranged from about 70 mm on a flat plain exposed to wind (68 mm) and a frozen lake (77 mm), through nearly 200 mm (187 mm) at the edge of the river valley (Revdalen) up to 350 mm under the slopes of Fugleberget mountain. This water was accumulated in the snow cover with a depth of 22, 28, 60, and 93 cm, respectively, which translates into an average snow density of 310, 275, 310, and 380 kg/m^3. Therefore, snow was the densest where it had the greatest thickness, being efficiently compacted under the influence of its own weight. The lowest density was observed on the lake. In such a place, thick snow cover cannot form as lake ice sinks under the weight of snow together with its bottom layer. Thus, the snow flooded with water (slush) transforms into lake ice (Duguay et al. 2003; Kirillin et al. 2012). Additionally, the lake ice surface is also less rough than the bare or snow-covered tundra (Berry 1981; Sturm and Liston 2003), which facilitates snow removal by wind in the initial stage of the cover formation.

The internal structure of the snow cover at selected measurement sites was exceptionally diverse. Snow with a generally uniform structure, with density increasing with depth occurred under the slopes of Fugleberget mountain. In turn, low-density depth hoar layers were found in the middle of the profile at the Revvatnet lake site. The only place where distinct, approximately 1 cm thick, ice layers were formed was the western part of the Revdalen valley. Thus, **the internal structure of snow varies depending on the relief and land cover, and these factors, influencing the snow distribution, also indirectly determine the processes of its metamorphism**.

The snow cover metamorphism during the ablation season was best documented at the measurement site in the Revdalen valley. The structure of snow before the beginning of ablation and in its late stage is presented in Fig. 74. Characteristic for this place were two distinct ice layers separated by about 2 cm thick level of metamorphosed snow in the central part of the profile. The first measurement carried out on April 15, 2016, revealed the clear depth hoar layer, with a much lower density than the overlying and underlying snow crystals. Such grains are the result of a large temperature gradient in the snowpack associated with the predominance of low air temperatures for a long time. The snow cover structure found on April 15 remained largely unchanged in the following days, as evidenced by the measurement from April 21. At that time, an experiment was carried out to examine the percolation of water through the snow cover, by

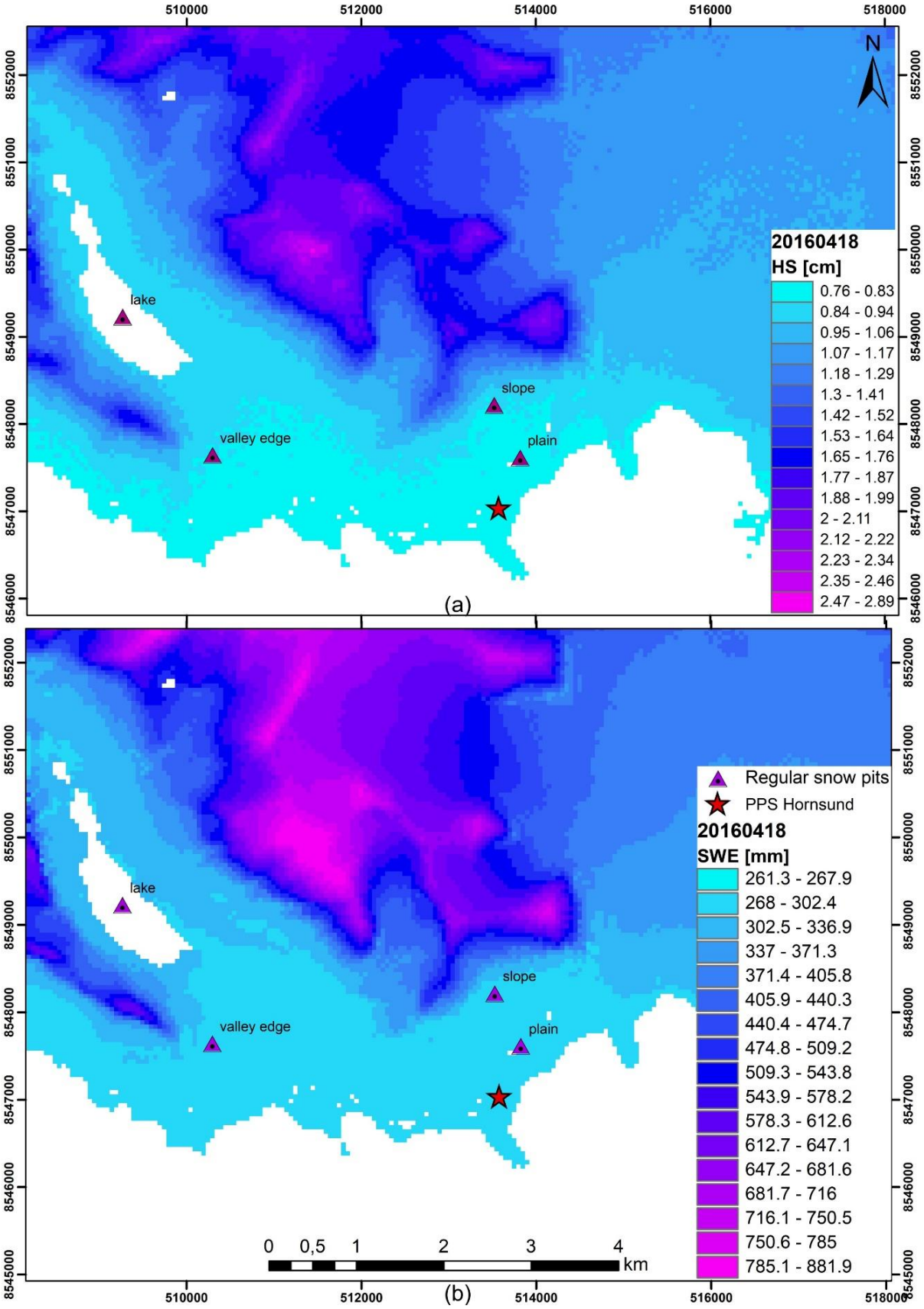

Fig. 71. Alpine3D result (50 m resolution) for the maximum accumulation period in the coastal zone in 2016 (18.04): (a) snow depth, (b) SWE.

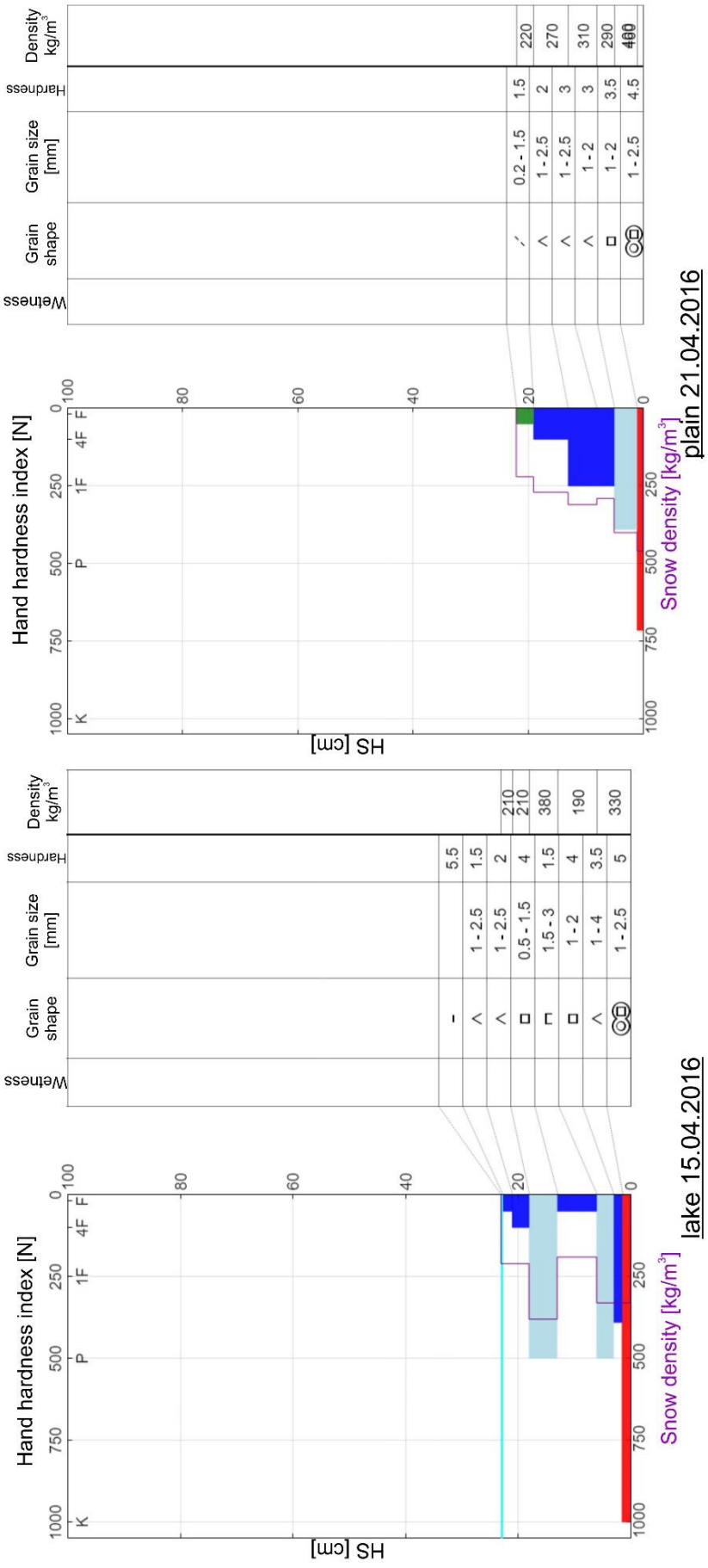

Fig. 72. Snow cover stratigraphy observed in snow pits before the start of ablation period in spring 2016 at 4 measurement sites.

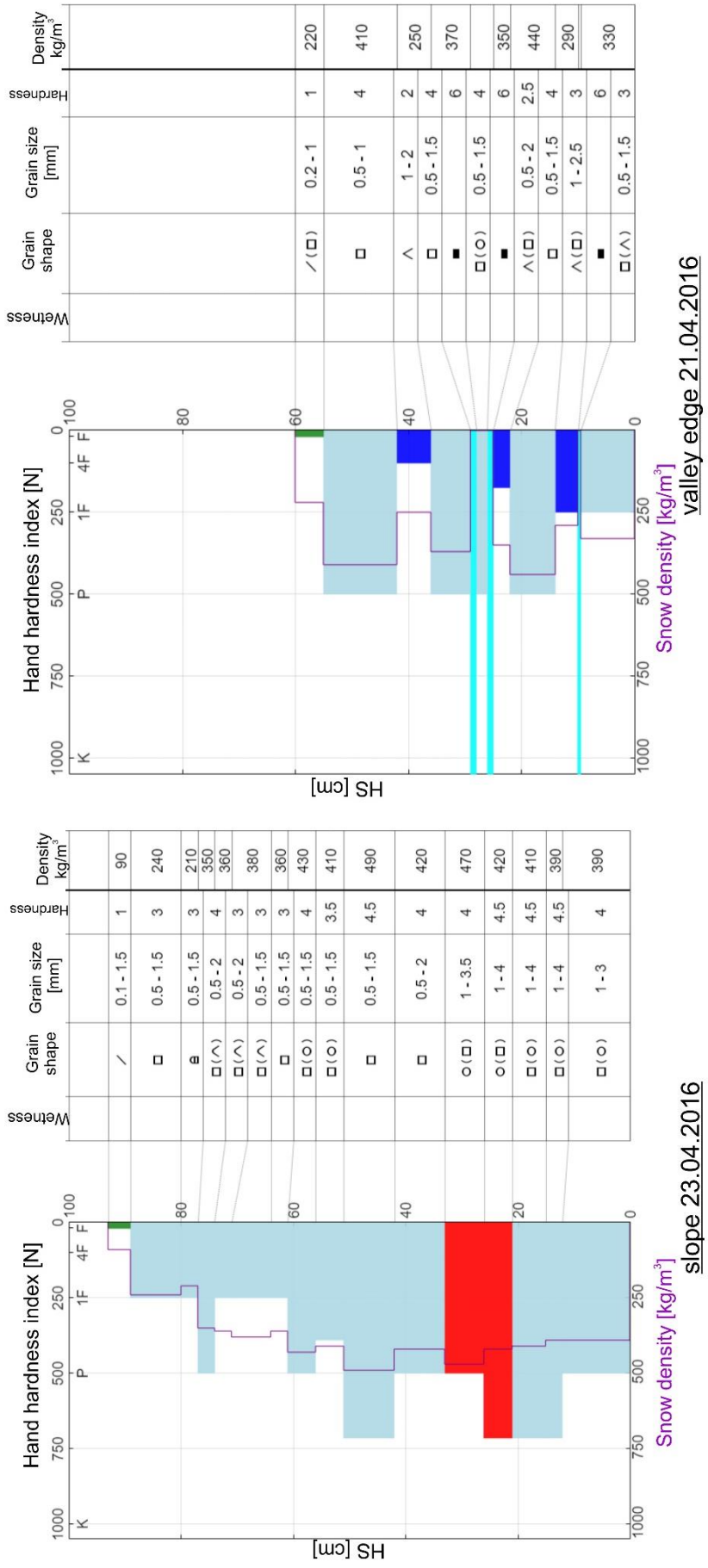

Fig. 72 (contd). Snow cover stratigraphy observed in snow pits before the start of ablation period in spring 2016 at 4 measurement sites.

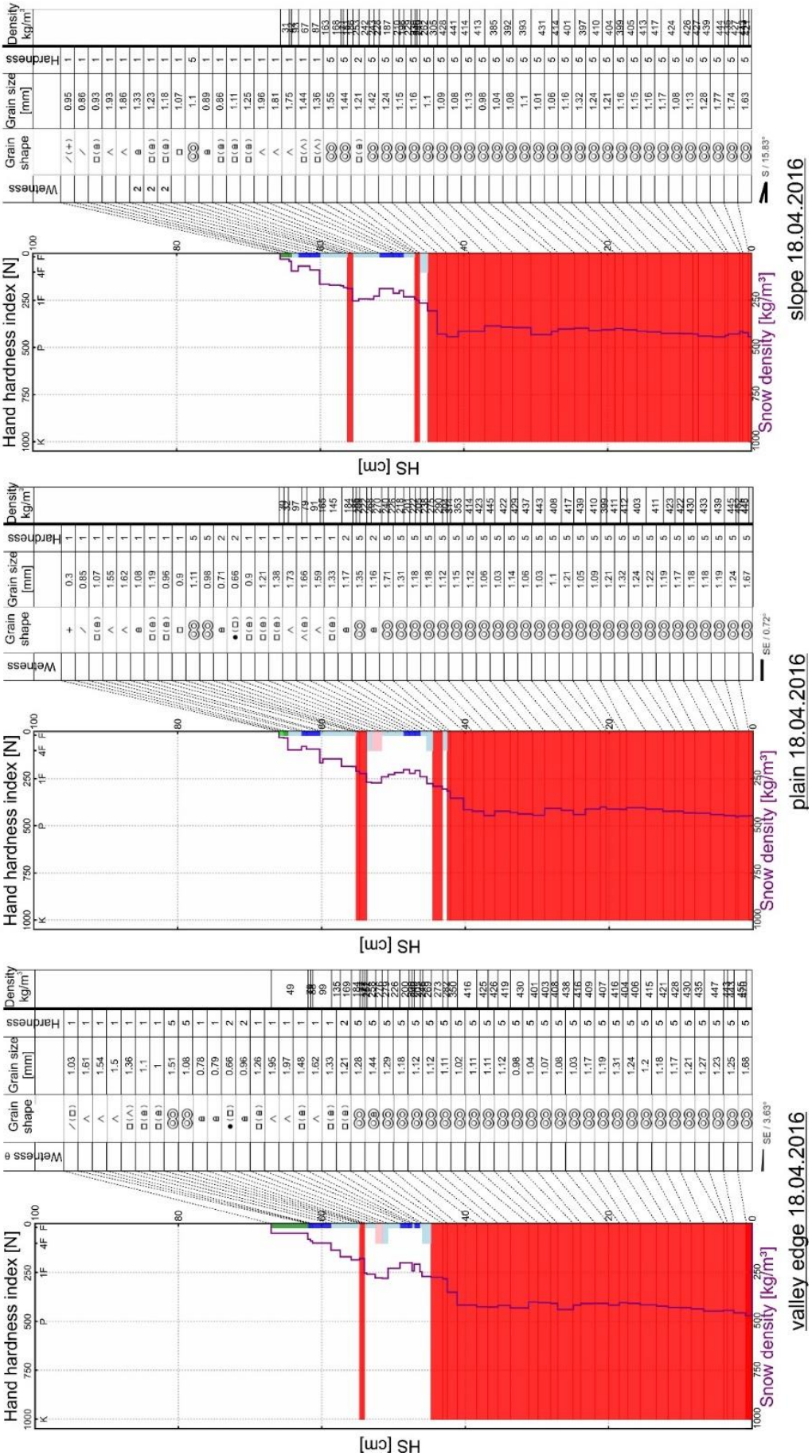

Fig.73. Snow cover stratigraphy obtained from SNOWPACK/Alpine3D model presenting the state before the start of ablation period (18.04.2016) in spring 2016 at the measurement sites.

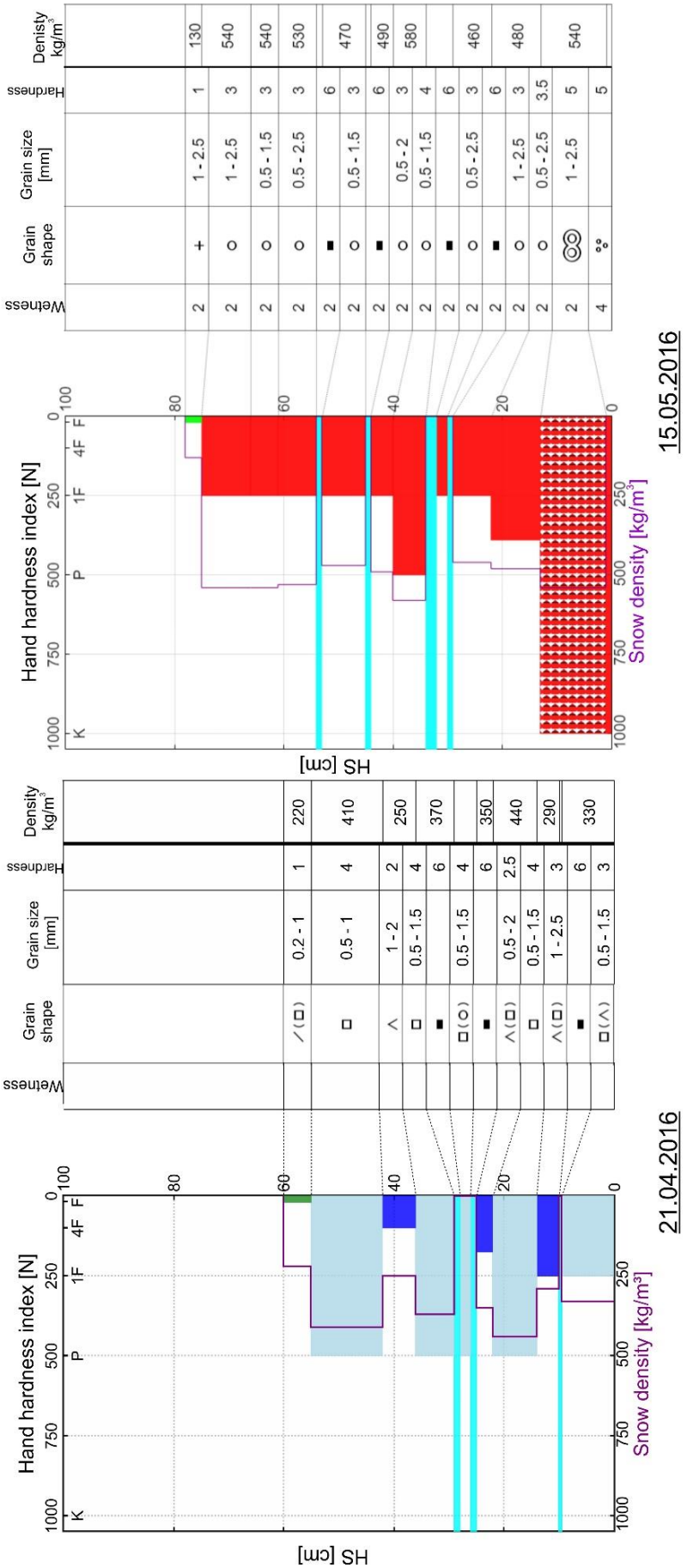

Fig. 74. Changes in the snow cover structure during the 2016 ablation season at the site in the western part of the Revdalen valley.

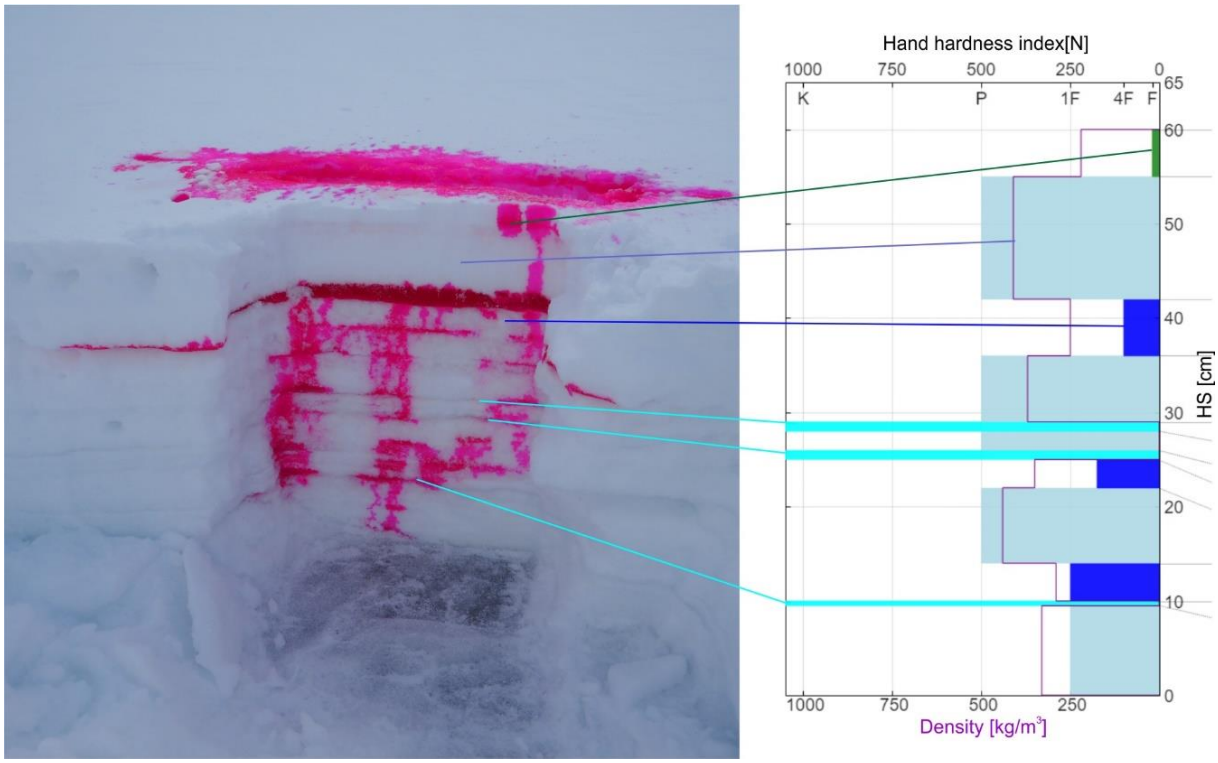

Fig. 75. A photograph of a snow pit in Revdalen valley from 21.04.2016 juxtaposed with its internal structure profile. Visible stratification of snow cover was highlighted by the dye experiment.

pouring diluted dye (rhodamine) onto the snow surface. The colored water briefly lingered at the boundary of each snow layer making them easier to identify, but some barriers were less permeable than others. The water stayed especially in the upper part of the profile, at the border between the denser snow, made of relatively fine grains lying above the depth hoar level, with a large diameter of crystals and small compactness (Fig. 75). This arrangement of layers creates the so-called capillary barriers due to differences in the capillary force in the pores between snow crystals, which is higher between fine grains than coarse ones (Jordan 1995). During the consecutive observation in the same site, an ice layer was found in the place of the most water-impermeable boundary from the previous measurement. It probably formed when meltwater or rainwater stopped on such a capillary barrier and froze when the temperature dropped again or when it came into contact with the cold snow lying below. At other measuring points, with a more homogeneous snow structure, the percolation of dyed water through the layers was more uniform and the barriers were less noticeable. Knowledge of the internal structure of the snow cover and the course of the percolation process taking place in it is important for the ablation rate, because in locations where water penetrates more easily into the cover, melting as well as metamorphosis of snow occurs faster (Marsh and Woo 1984; Tseng et al. 1994; Kępski et al. 2016). It is also worth noting that when positive temperatures dominate, the snow cover becomes homogeneous, transforming all grains into large and round melt forms of similar size, but the ice layers retain their properties (Fig. 74).

The SNOWPACK model indicated much higher snow cover depths and SWE than actually measured in the field. The overestimated values translated into longer snow cover duration in simulation than in reality and incorrect representation of snow layers thickness (Table 11). Nevertheless, the structure of the top of the profile, which was not affected by wet metamorphism,

Table 11

Comparison of SWE values in given days of 2016 from snow pit measurements and various variants of SNOWPACK simulations tuned with actual observation data. The values come from a flat area in the Fuglebekken catchment

Date	SWE from snow pit	SWE in SNOWPACK output [mm]					
		Without corrections	Tuning 23.04.2016	Tuning 30.04.2016	Tuning 09.05.2016	Tuning 16.05.2016	Tuning 22.05.2016
11.04	90	323	–	–	–	–	–
23.04	67.6	332	67.6	–	–	–	–
30.04	81.3	337	66.1	81.3	–	–	–
09.05	134.2	347	77.6	96	134.2	–	–
16.05	96.6	321	33	51.9	57.2	96.6	–
22.05	51	327	41	58.5	64	90.9	51
Snowmelt date	~26.05	13.06	26.05	27.05	27.05	28.05	26.05

was correctly reproduced in the model (Fig. 76). On the other hand, the simulation overestimated the snow density and, above all, the hardness of the layers previously affected by melting and refreezing cycles. It should be assumed that the model correctly predicted when the snow melting occurred, but at none of the measuring points the thick layers with the highest hardness, as predicted by the SNOWPACK simulation, have formed.

Assuming that the low accuracy of the model was mainly due to the fact that the winddrift module was turned off, the SNOWPACK indications were additionally checked by initiating simulation after the ablation has started. This is because in the period with positive temperatures, the phenomenon of blowing or drifting snow is initiated at much higher wind speeds (Li and Pomeroy 1997) and thus has a smaller impact on the snow properties. The modified simulation results of the SNOWPACK model are presented in Fig. 76. The applied approach allowed for a significant increase in the results' quality and, after such model tuning, the predicted date of snow cover disappearance was close to the real one (Table 11). Nevertheless, the simulation still greatly overestimated the snow layer density affected by wet metamorphism. The hardness of melt form grains turned out to be moderate in field measurements (Fig. 74), while the model often showed that they are as hard as ice (see Fig. 73). Additionally, model tuning with real data introduced a new problem with snow cover thickness. Due to the fact that snow pits were performed in a slightly different place each time (in order not to examine the structure affected by the previous measurements), the snow depth fluctuates to a certain level between successive measurements, and increases may happen even when only ablation has occurred. As a result, modeled snow cover development shows distinct "steps" on the chart (Fig. 76). Another problem is the inflow of meltwater from the upper part of the catchment area, which increases the SWE at lower elevations, but cannot be reproduced in the one-dimensional SNOWPACK simulation. However, the correction of the model indications with even one field measurement significantly improved the quality of further simulation and reduced the difference between the modeled and actual SWE and snow cover duration (Table 11). SNOWPACK without corrections predicted even several times higher SWE values than in reality due to the fact that the snow redistribution by wind was not taken into account and the snow density was overestimated. Model tuning was crucial for its indications, especially in places exposed to wind, such as a flat plain (Fig. 76b, Table 11).

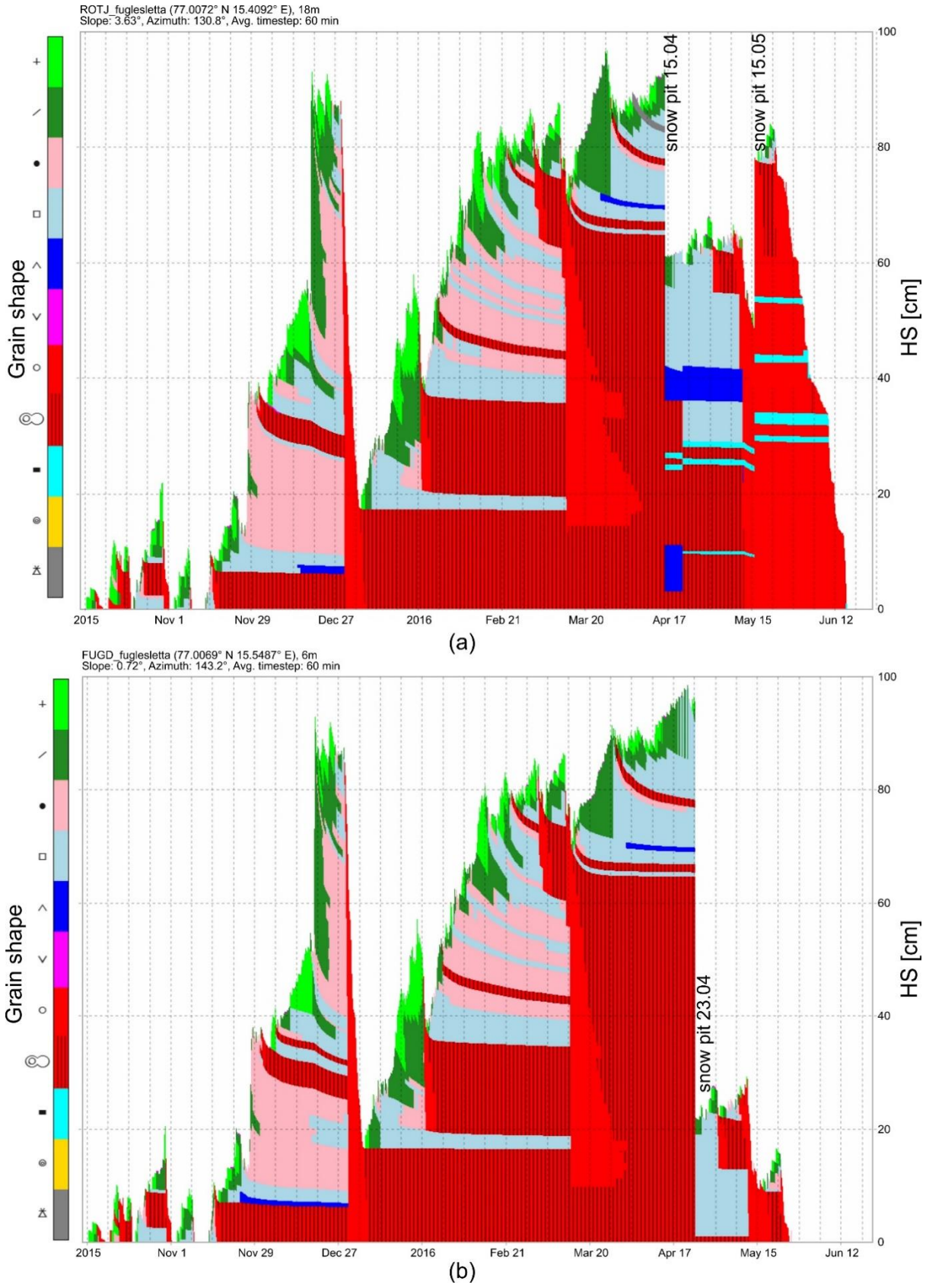

Fig. 76. The SNOWPACK simulation results in the season 2015/2016 for the site: (a) At the mouth of the Revdalen valley. Model tuning with observational data from snow pits carried out on 15.04.2016, 21.04.2016, and 15.05.2016; (b) On a flat plain in the Fuglebekken catchment. Model tuning with observational data from the snow pit carried out on 23.04.2016.

9. FORECAST OF SNOW CONDITIONS IN THE AREA OF THE POLISH POLAR STATION AT THE END OF THE TWENTY-FIRST CENTURY

Climate projection for the southern Svalbard area (Dobler and Haugen 2016; Isaksen et al. 2017) allowed to simulate the snow cover development under changed climatic conditions. The data presented here are based on the assumption of the most severe greenhouse gas emissions scenario RCP8.5. The climate projection itself simulates the snow cover thickness, but only for pixels representing land. Its spatial resolution of approximately 2.5 km does not allow for satisfactory reproduction of the rather narrow coasts of Hornsund, which in this resolution are considered a sea area and thus devoid of snow. Furthermore, the presence of high mountains and glaciers in close proximity to the fiord does not allow the use of modeled data from adjacent land areas. For this reason, only the predicted air temperature and precipitation sum were implemented in the SNOWPACK and Alpine3D models to simulate how the snow season in the vicinity of the PPS Hornsund would look like at the end of twenty-first century.

According to the climate model, **the average annual air temperature in the years 2089–2100 will increase by 6.5 °C compared to the reference data 1991–2000** and will amount to +4.1 °C (Fig. 77, Table 12). However, it is worth noting that the Polar CORDEX data overstate the average air temperature for a PPS cell by 1.8 °C for the period 1991–2000 (see Chapter 3.2 and Fig. 15). Taking into account this measurement error, **the average annual temperature at the end of the century would be +2.3 °C in PPS in the RCP8.5 emissions scenario**. The climate projection also predicts an **increase in the annual precipitation sum by approxi-**

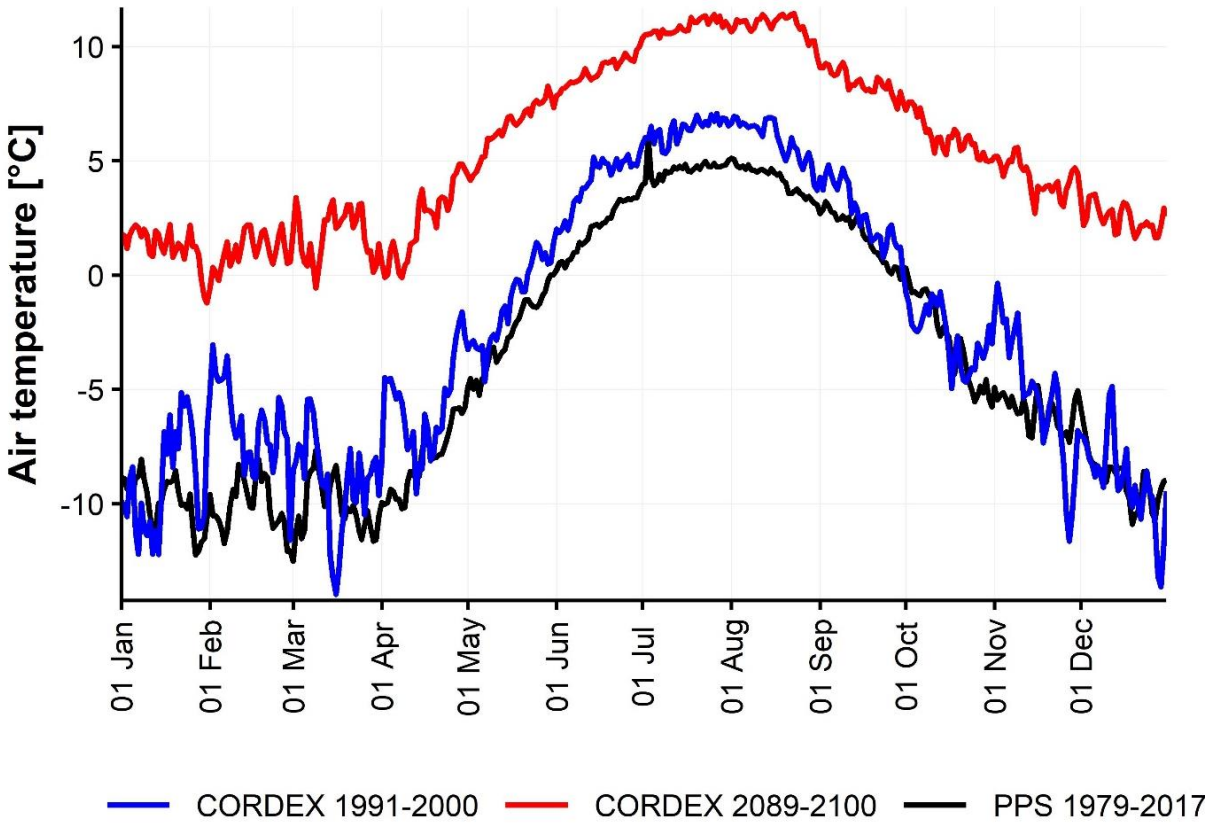

Fig. 77. Air temperature in Polar CORDEX climate reanalysis for the years 1991–2000 and the projection for the years 2089–2100 assuming the RCP8.5 emission scenario for the cell with PPS Hornsund in relation to the long-term average from the years 1979–2017 measured in the PPS meteorological garden.

Table 12

Comparison of average air temperatures and precipitation totals between the Polar CORDEX climate projection for the cell with PPS and the actual PPS Hornsund observation data

	Obervational data 1978–2017		POLAR Cordex reanalysis 1991–2000		POLAR Cordex simulation 2089–2100	
	Air temperature [°C]	Precipitation sum [mm]	Air temperature [°C]	Precipitation sum [mm]	Air temperature [°C]	Precipitation sum [mm]
Jan	–9.8	48.2	–9.1	87.5	–1.2	100.0
Feb	–9.9	31.6	–6.6	76.3	–1.5	68.7
Mar	–10.1	37.5	–9.0	70.6	–0.4	92.1
Apr	–8.1	29.6	–5.8	56.2	0.7	63.7
May	–2.6	30.2	–1.2	48.2	6.0	57.7
Jun	2.1	58.8	4.1	38.0	9.4	48.1
Jul	4.6	78.7	6.4	54.3	11.3	46.7
Aug	4.2	101.6	5.9	67.2	10.7	72.2
Sep	1.7	106.5	2.7	97.2	7.3	92.6
Oct	–2.7	59.4	–2.7	66.7	4.3	103.0
Nov	–5.9	61.6	–5.2	71.7	2.2	85.9
Dec	–8.8	62.7	–9.0	62.4	0.1	73.0
YEAR	**–3.8**	**454.0**	**–2.4**	**796.2**	**4.1**	**903.7**

mately 100 mm (i.e. by 15%) compared to the reference period and **their greatest growth is expected in the cold months**. However, as with air temperature, precipitation totals are also overestimated in the climate reanalysis (see Chapter 3.2 and Fig. 16). According to the climatic model, at the end of the century, a higher precipitation sum will be recorded in winter than in summer. These projections should be treated with caution as high winter totals have already been obtained for the reference period 1991–2000 in the Polar CORDEX reanalysis. Even assuming a 70% underestimation of solid precipitation measurements in Spitsbergen due to strong winds (Hanssen-Bauer et al. 1996), such high sums in the cold months are not confirmed by the observational data (see Fig. 16).

The temperatures modeled for the end of the twenty-first century indicate a **gradual shift of the coasts of Spitsbergen from the present tundra climate (ET) to the subpolar oceanic climate (Cfc)** (according to the Köppen classification). It is characterized by an average temperature of the coldest month above 0 °C, while the average temperature of 1–3 months a year exceeds 10 °C. The climatic conditions predicted for the end of the century in southern Svalbard are analogous to those currently found on the coasts of Iceland.

Data from climate projections were used in the SNOWPACK and Alpine3D models to test the possibility of snow cover development in a warmer environment with higher precipitation totals. The obtained results indicate a significant shortening of the snow season on the coasts of southern Spitsbergen (Fig. 78). Under changed climatic conditions, snowfall does not occur earlier than at the beginning of November. Furthermore, due to the rise in spring air temperatures, the snow cover would completely disappear in the second half of May at the latest. This means an **almost twofold extension of snow-free period from the current 3 months (July–September) to almost 6 months. The projection also shows a reduction in the maximum snow cover depth in the coastal zone, despite a significant increase in precipitation totals**. On the other hand, the results of the Alpine3D model indicate increased depths in the summit

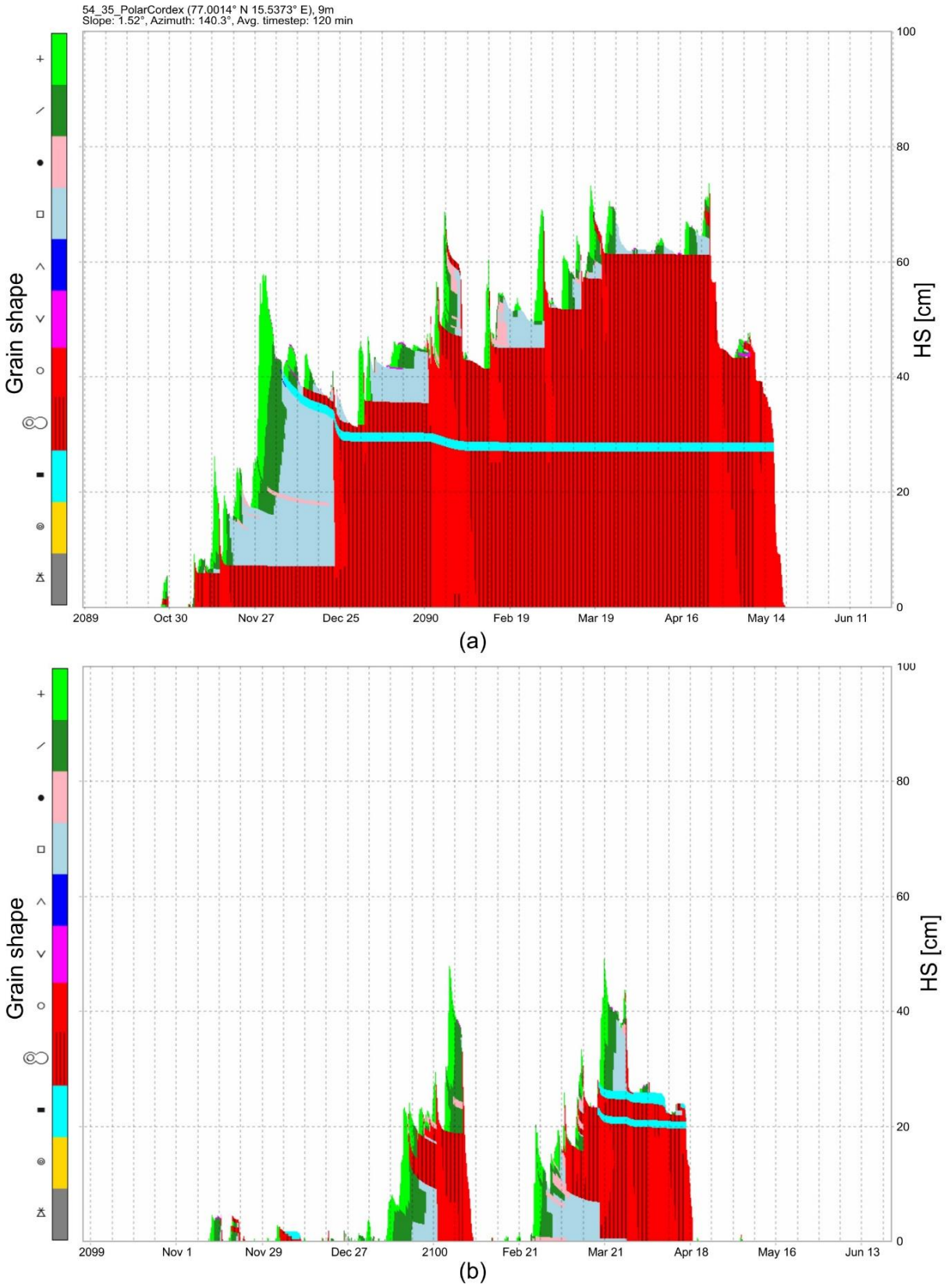

Fig. 78. The SNOWPACK simulation results for the PPS Hornsund location: (a) for the winter season 2089/2090, (b) for the winter season 2099/2100.

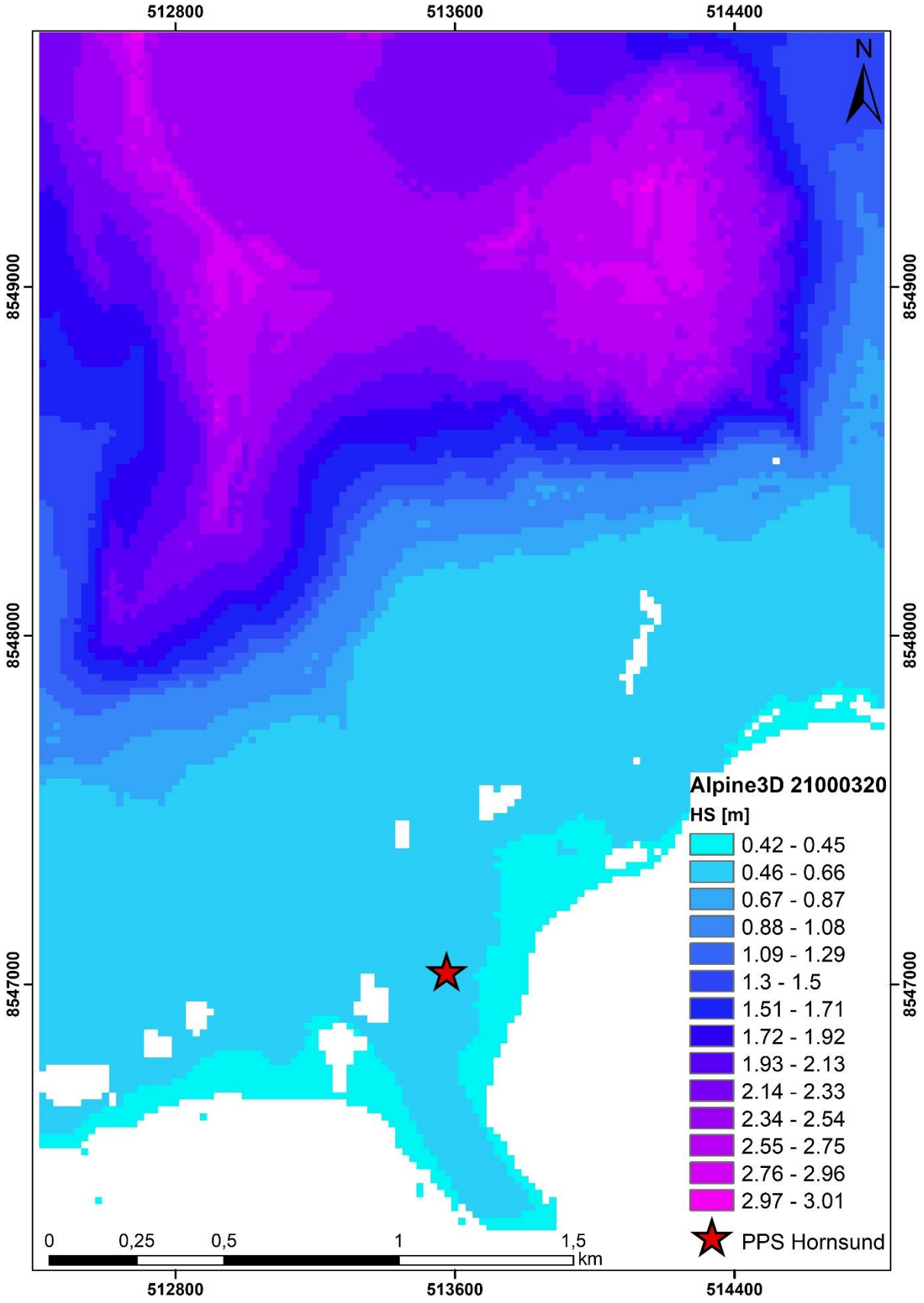

Fig. 79. The results of the Alpine3D model for the PPS Hornsund surroundings in the period of maximum accumulation (20.03 in the coastal zone) of the 2099/2100 season.

parts of the Fugleberget massif under changed climatic conditions compared to the accumulation maxima obtained for the 2014 and 2016 seasons (Figs. 79, 58, and 59). According to the predictions presented here, the maximum snow thickness on the coast will be occurring in the second half of March in the years 2089–2100, when it may exceed 50 cm. However, these values are much lower than those achieved by the SNOWPACK model for the 2014 and 2016 seasons. It should also be remembered that the model does not take into account the redistribution by wind, therefore modeled snow depth from 2014 and 2016 were in extreme cases even four times higher than actually measured in the PPS meteorological garden (see Fig. 59). Consequently, such a large snow thickness should be expected only at accumulation sites, while in most of the tundra area the values would be considerably lower. Obviously, the changes in climatic conditions will affect the internal microstructure of the snowpack. The simulations for the 2089/2090 and 2099/2100 seasons (Fig. 78) indicate the formation of thick ice layers in the snow cover. In turn, model results from 2014 and 2016 did not anticipate ice layers existence, even if they actually occurred in the field (see Chapter 8). The significantly higher temperatures projected for the period 2089–2100 will prevent the formation of high temperature gradients in the snowpack. These, in turn, are required for the development of specific snow grains forms, especially depth hoar crystals (Sommerfeld and LaChapelle 1970) that are now relatively common in the tundra (see e.g. Fig. 74). In predictions for the end of century, snow cover is no longer continuous throughout the whole winter season and snowfree episodes may be introduced even in the middle of the winter. Such situations happened only incidentally in the current records of the PPS Hornsund weather station (see Fig. 21), e.g. in 2011/2012 season. The inter-

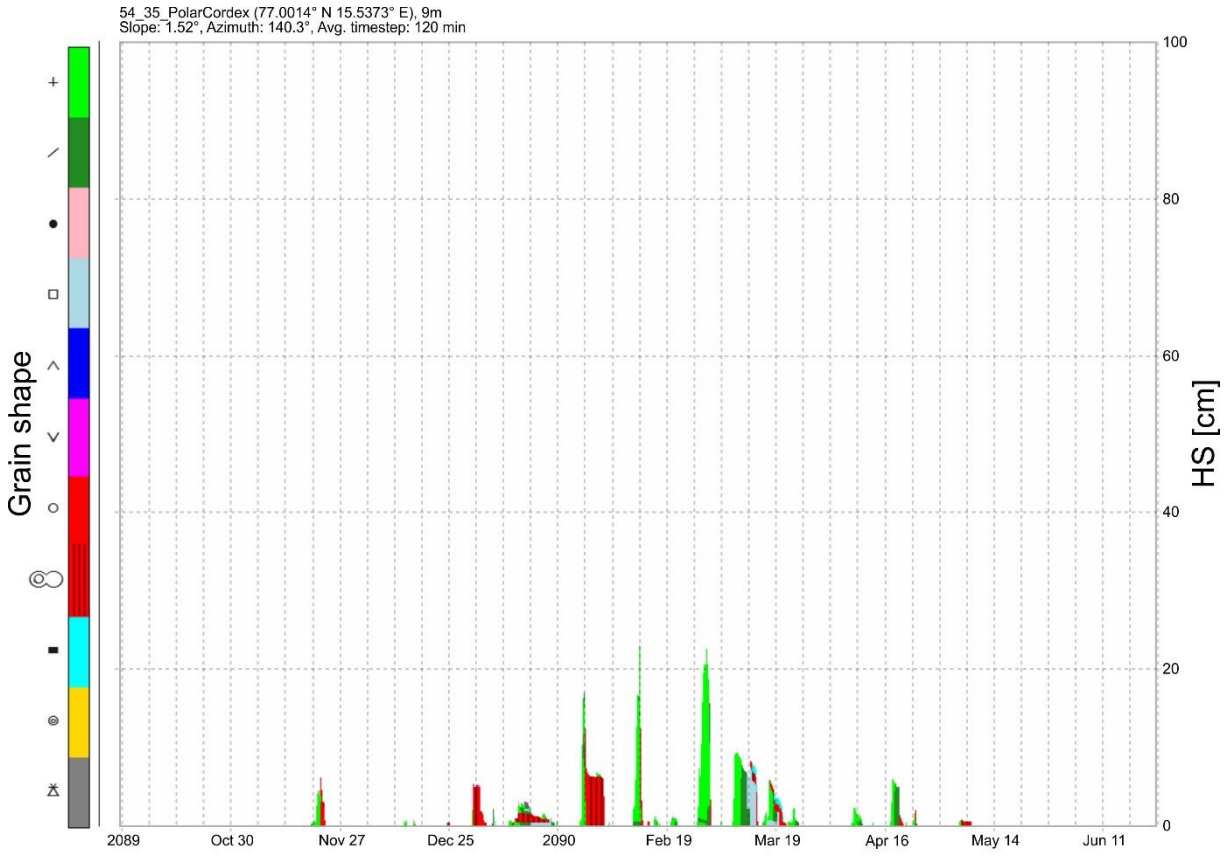

Fig. 80. The SNOWPACK simulation results for the season 2089/2090 with the substitution of Polar CORDEX data from the PPS cell with the data from the cell located entirely above the waters of the Hornsund Fiord (adjacent to the PPS cell from the south).

ruption of the continuous snow cover period is clearly visible in the SNOWPACK simulation for the 2099/2100 season (Fig. 78b).

Noteworthy, the projected climatic conditions for the end of the twenty-first century indicate the occurrence of average air temperatures only slightly lower than 0 °C in the winter months (Table 12). Model predictions were also tested with input data coming from a Polar CORDEX simulation, but from the neighboring southern cell to that with PPS Hornsund. They were characterized by an average annual air temperature equal to +5.4 °C, where the coldest February had already a positive mean monthly temperature (+1.1 °C). These conditions are 1.7 °C warmer than the annual average for the end of the century in the PPS cell. However, this is enough to completely change the snow cover duration and its characteristics. With the dominance of positive temperatures, continuous snow cover has no chance to develop during the winter; however, snowfalls are still possible from November to May. In such conditions, snow depth would not exceed 20 cm and the cover cannot persist on the ground for more than a month (Fig. 80). This means that while the modeled climatic conditions for the PPS at the end of the century does not indicate the disappearance of permanent snow cover in the winter, a further increase by approximately 2 °C is enough to completely change the functioning of the ecosystem, in which snow will appear only periodically.

10. DISCUSSION

The results obtained in this work confirm the previous findings regarding the snow cover distribution obtained from studies based on point measurements. As in the work of Migała et al. (1988), the Fuglebekken catchment turned out to have better snow accumulation conditions than the measurement site at the PPS, with the deepest snow in the lower catchment area on its western side. Average snow thicknesses recorded in the lower part of the catchment in 1979/1980, 1981/1982, and 1982/1983 were 30–60 cm (Migała et al. 1988), which did not differ from the results from the analyzed here years 2013/2014, 2014/2015, and 2015/2016 (see Fig. 42). Average values from the coastal part of Gåshamnøyra (30 cm) and Revdalen (35 cm; varying from 30 cm in the lower part to 80 cm in the upper part of the valley) obtained in the 1980s (Migała et al. 1988) are also in line with the results obtained in spring 2014 and 2016. The differences between the studies concern mainly snow density, which in the 1980s were supposed to be 400–500 kg/m^3, while now such values were recorded in the catchment rather in the late ablation stage. At the moment of maximum accumulation, densities ranging from 350–400 kg/m^3 were dominant. However, the comparative analysis of the results from the 1980s to those developed in this work is difficult. During the first snow measurements campaigns, the probing was done without recording the GPS position, and the sounding dates were not always precisely defined. Nevertheless, comparable values were obtained in the same regions in the 1980s and spring 2014 (Nawrot et al. 2015) and 2016, which confirm the seasonal repeatability of snow cover distribution. The areas with extended snow cover duration found in the Fuglebekken catchment, but not covered by regular measurements, may, however, be associated with depths exceeding 2 m, found here by Dolnicki (Dolnicki 2002, 2015).

The regularities found in the southern part of Svalbard in the glacial area are also valid in the tundra. In a series of works, Grabiec (2017) proved, among others, that better conditions for the snow cover accumulation exist in the western parts of glaciers. This rule was disturbed only in places characterized by a relief perpendicular to the prevailing wind directions (Grabiec 2017; Grabiec et al. 2006, 2011). An example of a location perpendicular to the dominant zonal flow is the Ariedalen valley, where greater snow thickness was found in the eastern than in the western part (Fig. 65). However, the correlation coefficients between the snow depth and the topographic indices on the Hansbreen glacier were much higher (Grabiec 2017) than those presented in this work. This is probably due to the much larger amount of data used to study the

interrelationship provided by GPR soundings. Differences may also come from a less complex glacier relief, which is much easier to characterize by means of topographic indices. The wind velocities that initiate blowing snow in glacial areas are able to move snow in the tundra as well. On the Waldemarbreen glacier, the snow transport by the wind began when its speed exceeded 4 m/s (Grześ and Sobota 2000). The data collected in the PPS showed that drifting snow events occurred at wind speeds higher than 6 m/s. Due to the fact that the air flow is measured at a height of 10 m above the ground, it can be calculated from the wind profile equation (Van Ulden and Holtslag 1985) that the wind speed near the surface is about 2 m/s lower. Thus, both in the tundra and on the glaciers, the near-surface wind speed of 4 m/s is a minimum threshold needed to move snow deposited on the ground. On the Svalbard glaciers treated in the macroscale, greater snow depths occurs in its eastern parts, which is associated with higher precipitation sums there (Winther et al. 1998). The same can be seen on unglaciated coastal areas, both in model outcome (Fig. 14) as well as in the results of snow soundings carried out during the ablation season (Figs. 62 and 64).

The snow cover disappearance dates obtained in this work can be compared to the results of studies carried out in other parts of the Svalbard archipelago. A study conducted in the Bayelva catchment in 2002 using a time-lapse camera showed that snow cover ablation lasted about 50 days there (Hinkler et al. 2003), which is consistent with the results from the Fuglebekken catchment area (see Table 7). As in the results presented in this study, the overwhelming majority of the tundra in Bayelva was snow-free at the turn of June and July (Hinkler et al. 2003). On a larger scale of the Svalbard archipelago, the analysis of MODIS scenes allowed for differentiation of coastal zones in terms of the snow cover duration (Malnes et al. 2010). Between 2005 and 2009, the snow in unglaciated areas disappeared before June 1 at the earliest, e.g. in the Adventdalen valley near Longyearbyen (Malnes et al. 2010). On the coasts of Hornsund, such early disappearance of snow practically does not occur (see Fig. 61). The western shores of the Hornsund Fiord are the first to be snow-free. In the case of 2014, this took place in the first days of June. A little later, the snow cover melts in the Fuglebergsletta area, where PPS is located. In 2014, the snow disappeared on the eastern coasts of the fiord after June 15, which was the last day from the snow season when a satellite image suitable for analysis was available. As about 50% of the unglaciated area of Hornsund was still under snow on that day, this means that the vegetation season is shorter there than in the central Svalbard coastal zone, where most of the shores were snow-free, on average, before June 15 (Malnes et al. 2010). Since the snow cover duration and thickness in the period 2005–2009 and in 2014 were similar (see Figs. 20 and 24), the results from these years should be comparable.

The data presented in this work prove that the conditions for the snow cover development on the eastern coasts of the Hornsund Fiord are better than in its western part. The recorded differences in snow cover duration should be also reflected in the state of vegetation. Satellite studies indicate the highest bioproductivity of flora expressed by the NDVI at the mouth of the fiord (Karlsen et al. 2014; Vickers et al. 2016), i.e., in the place with the shortest snow season. This would suggest a negative impact of snow cover in the analyzed region on the vegetation development. The aforementioned assumption is partially confirmed by the results relating the snow disappearance time in the Fuglebekken catchment with the tundra vegetation type. This is because the snow persists the longest on rock debris that is devoid of any plants. The shortest snow cover duration occurred each time on the lichen-herb-heath tundra, the formation with the highest vascular plants in the study area, represented, e.g., by polar willow (*Salix Polaris*). On the other hand, the deepest snow during the winter season was measured on wet soils and accompanying wet moss tundra. This formation is characterized by the highest NDVI value (Hobbler 2011) as well as nitrogen content in the substrate (Skrzypek et al. 2015) necessary for plant growth. However, it should be remembered that due to the different spectral characteristics of

mosses, lichens, and vascular plants (Bubier et al. 1997), comparing the NDVI values in the tundra environment is subject to a large degree of uncertainty (Williams et al. 2001). The **results obtained in this study indicate an ambiguous impact of snow cover on the condition of vegetation**. They generally confirm the conclusions of previous studies conducted in other regions of the world and **indicate the decisive influence of snow cover in the Arctic on soil moisture and, consequently**, the availability of water for plants and the **occurrence of specific plant formations** (Bliss et al. 1984; Walker et al. 1989,1999).

The modeled snow cover spatial distribution did not represent the actual one, mainly due to the problems with taking into account the snowdrift module. Alpine3D predicted a snow depth of 80–90 cm during the period of maximum accumulation in both 2014 and 2016. This corresponded to a SWE peak of less than 300 mm. At the same time, the average snow thickness from the measurements in the catchment was approximately 60 cm (240 mm SWE) in 2014 and less than 50 cm (175 mm SWE) in 2016. This means that in an area with a relatively good ability to accumulate snow, its depth was overstated by about 50%. Part of this overestimation can be explained by the use of simplified assumptions. Calculations for the entire winter seasons were carried out with the assumption of a neutral atmosphere. However, such model settings indicated greater snow thickness in the low-lying area (see Fig. 60). In addition, studies from alpine and polar regions indicate a significant overestimation of heat fluxes in the Alpine3D model, mainly in strong wind conditions, when using a neutral atmosphere (Schlögl et al. 2017). Nevertheless, such large disproportions between the model and the actual snow distribution are difficult to explain only with this. Field measurements in the Canadian Arctic show that 48 to 58% of snow on the ground is removed before ablation begins (Pomeroy and Li 2000). The results of the PBSM model for the same area show that the snow mass losses due to sublimation are comparable to the losses caused by wind transport (approximate ratio 1:1) (Pomeroy and Li 2000). Other studies from Canada, showing the amount of sublimation at 4 measuring stations, estimate its impact on SWE reduction at 15–41% (Pomeroy and Gray 1995). However, this value is difficult to measure directly and depends largely on local conditions, especially wind speed and relative humidity. Hence, the estimates are very different and, e.g., SnowTran-3D model indicates 10–25% reduction of snow mass during blowing snow episodes (Liston and Sturm 1998) and the PBSM used in the Canadian Rockies suggests a 17–19% weight loss due to the same process (MacDonald et al. 2010). On the other hand, the results of Alpine3D from Switzerland indicate that the reduction of SWE caused by sublimation during the winter season may reach even 400 mm on mountain ridges, while on less elevated terrain it does not exceed 100 mm (Groot Zwaaftink et al. 2013). All the above studies point out significant snow mass losses caused by wind activity, even at negative air temperatures. For this reason, the obtained Alpine3D results seem rational and suggest that the wind in the tundra environment of southern Spitsbergen is responsible for removing even more than half of the snow mass supplied by precipitation.

The SNOWPACK simulation, like the Alpine3D model, greatly overestimated the actual snow thickness. Especially problematic was the representation of bottom layers, where the model indicated the presence of snow heavily transformed by wet metamorphism. In reality, the layers beneath thick ice layers are rather protected from the effects of meltwater and may be the last to be modified during the ablation period (Kępski et al. 2016). However, the model turned out to be generally sufficient to simulate snow metamorphism and ablation in the period with a predominance of positive temperatures. Then, the blowing and drifting snow processes appear rarely and have a smaller impact on the shape of the snowpack (see Fig. 76; Table 11). Therefore, SNOWPACK calculations were used to interrelate the snow depths measured at various locations on different days during the spring season (Fig. 64). It should be remembered that attempts to model the snow cover in Svalbard, mainly in the Ny-Alesund region, have

always been characterized by considerable errors (Brun et al. 1989; Martin 1996). None of the models used there was able to correctly reproduce the snowmelt rate in the tundra, but the results obtained by CROCUS (analogous to SNOWPACK used in this work) were closest to those measured in the field (Bruland et al. 2001).

Due to the strong relationship of the climate with other components of the natural environment, the observed and forecasted warming will cause severe changes in the entire southern Spitsbergen tundra ecosystem. These will include hydrology (Rouse et al. 1997; Adam et al. 2009), vegetation (Wang and Overland 2004; Elmendorf et al. 2012), permafrost and soils (Hinzman et al. 2005; Isaksen et al. 2007), as well as animal populations (Aanes et al. 2002; Jensen et al. 2007; Fuglei and Ims 2008). The rise in temperatures and the associated shortening of the snow cover duration will undoubtedly affect the land cover. Currently, for example, an improvement of vegetation condition and an increase in tundra biomass in Svalbard are observed, but these processes seem to be slowing down (Park et al. 2016; Vickers et al. 2016). It is predicted that in the future, thinner snow cover and more frequent rain on snow episodes initiating the ice layers formation may eventually lead to deterioration of plant growth conditions and the so-called tundra browning (Phoenix and Bjerke 2016). It is also expected that the tundra plant species composition will change. A decrease in the number of mosses and moisture-loving flora is anticipated, with a simultaneous increase in the share of vascular plants (Elmendorf et al. 2012). However, the overall number of species is projected to decline due to the rapid expansion of plants best adapted to changing conditions, which will replace a variety of organisms specialized in living under long persisting snow cover and frost (Chapin et al. 1995). One of the effects of global warming will also be a reduction in soil moisture, even despite the increase in precipitation totals (Houghton et al. 1992; Oechel and Vourlitis 1994). This will be the result of a faster snow cover disappearance and thus a deeper thawing of permafrost (Hinzman et al. 2005). The availability of water for plants seems to be the most important factor for their development in the vicinity of the PPS; therefore, a warmer climate with shorter snow cover duration does not necessarily improve the conditions for the local flora (Opała-Owczarek et al. 2018). In southern Svalbard, negative changes in vegetation condition caused by the increase in the reindeer population are currently observed (Olech et al. 2011; Ziaja et al. 2016). The mortality of these animals is, in turn, strongly correlated with the occurrence of rain on snow episodes during the winter season. Such a rainfall can lead to the formation of basal ice or ice layers inside a snowpack, hindering an access to the food for herbivores (Kohler and Aanes 2004). On the other hand, climate projections indicate a significant increase in winter liquid precipitation, which may deplete the reindeer population in Svalbard (Hansen et al. 2011). Thick ice layers are clearly visible in the SNOWPACK simulation for the period 2089–2100 (see Fig. 78). Overall, the projected global warming will undoubtedly have an impact on the southern Spitsbergen ecosystem. However, due to the number of possible effects of the temperature increase and the shortening of snow cover duration presented above, it is very difficult to determine whether this impact will be positive or negative.

11. SUMMARY AND CONLUSIONS

The aim of the study was to identify the snow cover distribution on the tundra in the vicinity of the Polish Polar Station, to determine the dynamics of its changes during the ablation season and to define their relationship with the relief and land cover on the basis of the cartographic materials available. The presented methodology of processing time-lapse and satellite images allowed to successfully present the temporal and spatial variability of the snow cover occurrence in the unglaciated catchment and relate it to the wider area of the fiord coast. The conclusions coming from remote sensing data were confirmed by the results of field measurements.

The tasks set in the study were successfully completed, although the initially assumed relationships between the snow cover duration and the topography and land cover turned out to be weaker than expected. The spatial variability of the snow cover on the coasts of Hornsund had not been well recognized before, which, due to its crucial environmental importance, was a major research gap that prevented understanding the functioning of the area's ecosystem. The extensive study presented here addresses these shortcomings, and the most important results are briefly discussed below.

1. On the basis of data from the PPS Hornsund, the seasonal and long-term variability of meteorological conditions influencing the snow cover were presented. The average annual air temperature in 1979–2017 was –3.7 °C and the mean annual precipitation total amounted to 450 mm. However, the determined trends indicate the occurrence of significant climatic changes: an increase in air temperature, the strongest in the winter period (+2.16 °C per decade in case of winter months), growth of precipitation sums (+55.5 mm per decade) with a simultaneous decrease in the share of snowfall. Data from the PPS and the period 1983–2017 show that the snow cover lasts, on average, 235 days, from mid-October to mid-June. However, observed climate warming results in the shortening of that period by 10 days per decade. Additionally, reduction of the snow cover thickness is observed (–3.8 cm per decade). The spatial variability of the climate was presented using the WindNinja software (anemological conditions), GIS tools (potential solar radiation), and climate projections from the Polar CORDEX initiative, verified with data from AWS located at various locations in the Hornsund Fiord. They show that the average annual air temperature decreases towards the east (with growing distance to the open Greenland Sea), with a simultaneous increase in annual precipitation totals. The northern shores of the fiord have better insolation conditions and are also more exposed to the most common eastern wind.

2. The results of field measurements carried out since the winter season 2013/2014 in the Fuglebekken catchment indicate much better conditions for snow accumulation in this place compared to the measurement point in the meteorological garden of the Polish Polar Station Hornsund. The Fuglebekken catchment is also characterized by smaller fluctuations in snow thickness from year to year compared to measurements carried out at PPS. The considerable variability of snow cover at the PPS site can be attributed to the greater wind exposure, while the catchment area is partially sheltered from direct wind action. This means greater representativeness of data from the catchment area.

3. The comparison of data from field measurements with changes in snow cover extent revealed a strong relationship between snow thickness during maximum accumulation and its persistence duration. The pattern of snow disappearance turned out to be repeatable and snow patches formed in the same places every year. Similarly, the same parts of the area have the shortest snow cover duration each year. Zones near the rock outcrops, both at the eastern and western edges of the catchment accumulated the greatest amount of snow. On the other hand, the prominent terrain features, such as the storm ridges, are characterized by the shortest snow cover duration. This implies that wind plays a decisive role in the snow cover distribution in the tundra. The strongest and most frequently observed eastern wind has the greatest influence on the snow distribution. Deeper snow was found at the western edges of the studied areas, not only in the Fuglebekken catchment, but also in the Revdalen valley and the Bogstranda region. The comparison of measurements from 2014 and 2016 confirmed the repeatability of the snow cover distribution along the entire coast of the Hornsund Fiord.

4. The snow cover thickness in the Fuglebekken catchment area is average compared to values measured elsewhere along the Hornsund Fiord coast. This is also confirmed by the moderate snow cover duration. The snow cover extent in the catchment area drops below 50% at a similar time as on the shores of the Hornsund Fiord treated as a whole. This means that the

results of the monitoring conducted since the 2013/2014 season are representative of the larger coastal region. Snow cover duration is the longest at the south-eastern part of the fiord, while the fastest disappearance is observed in the north-western part. This is also reflected in snow depth. At comparable altitude, the deepest snow has been found on the eastern shores of Svovelbukta (SE Hornsund), while, upon excluding the problematic area of Gåshamnøyra, snow is the thinnest in the Revdalen Valley (NW Hornund). The snow thickness is strongly correlated with the modeled average air temperature values ($r = –0.78$) and annual precipitation totals ($r = 0.57$). Statistically significant, although definitely weaker, is the correlation with the sum of potential solar radiation ($r = –0.24$), which explains the slightly earlier disappearance of snow cover on the northern coasts.

5. The snow cover duration and its thickness depend to some extent on the type of land cover. The performed statistical analyzes indicate that during the winter season the snow is several centimeters deeper in the area covered by wet tundra mosses. On the contrary, on lichen-herb-heath tundra, the snowpack is on average thinner. It is also a type of vegetation that is generally first exposed from under the snow in spring. There, the snow disappears completely two weeks earlier than on rock debris that is devoid of vegetation. However, it should be assumed that it was the snow cover that influenced the occurrence of certain vegetation types and, for example, its extended duration prevented the development of flora on areas classified as rock debris. On the other hand, the tundra type cover, most likely, does not influence on the snow cover distribution in the study region, because due to the very low variation in plants' height, it could not significantly affect the surface roughness, and thus the accumulation conditions. Among the landforms, the shortest occurrence of snow was found on beaches and the longest on talus cones. There, during the winter season, snow is on average at least a few centimeters deeper than on other geomorphological formations.

6. The snow cover occurrence in the ablation period is poorly correlated with topographic indices. In the Fuglebekken catchment, a positive relationship with the snow cover duration was found for the TRI index (Pearson's $r = 0.29$) representing the surface roughness. Terrain exposure to wind had a negative impact, especially for the one from the north-eastern direction ($r = –0.24$). For the entire area of the Hornsund Fiord coasts, these relationships were even weaker and much less correlated than with the meteorological parameters. Similar conclusions were also obtained after analyzing the relationship between the topography and the measured snow cover depths. This may indicate the dominant influence of wind activity on the snow distribution on the micro and meso scale, while air temperature and precipitation totals play a leading role on a larger scale.

7. The spatial modeling of snow cover distribution was performed using the advanced physical model Alpine3D. To the author's knowledge, this is the first attempt to use this software in Svalbard and one of the first ever used in the high Arctic environment. Due to the enormous computing power requirements, it was not possible to implement the snowdrift module in the simulations. Therefore, the model output did not reflect the actual snow cover distribution and predicted a fairly uniform snowpack shape in the Hornsund coastal zone. However, the simulated snow cover development in the season was highly consistent with the observational data, although the modeled thickness was significantly overstated. In the accumulation sites sheltered from the wind, the differences between the modeled and actual snow depth turned out to be much smaller than at the PPS weather station measurement point. The result of the Alpine3D model may indicate the amount of snow that would be stored in the tundra without wind redistribution and associated sublimation processes. This would mean a reduction in snow cover depth and SWE caused by wind activity by 40–50% in the Fuglebekken catchment and even 80% at the PPS measurement point. However, due to the troublesome measurements of snow transport by wind, this statement is difficult to prove. The performance of the Alpine3D model

has been tested using various settings. The chosen atmospheric stability correction method had the greatest impact on the results in the study area. On the other hand, the soil parameters settings did not have a significant effect on the model output.

8. The one-dimensional SNOWPACK model coupled with Alpine3D did not correctly reflect the development of the vertical snowpack structure during winter mostly due to problems with taking into account the wind redistribution. However, running the model on the data acquired in the field just before the start of ablation period allowed to obtain a reliable course of snow cover metamorphism and the melting rate in the following days. The model had also problems with correct snow hardness representation. All layers affected by wet metamorphism were characterized by maximum hardness in the SNOWPACK output, which, of course, was not confirmed in the field.

9. The Polar CORDEX climate projections for 2089–2100 allowed for the implementation of simulated precipitation totals and air temperatures for the SNOWPACK and Alpine3D models. In these years, the air temperature will increase by 6.5 °C and the precipitation total will grow by almost 100 mm compared to the end of the twentieth century under the most severe greenhouse gas emission scenario (RCP8.5). The tundra climate (ET in the Köppen classification) currently prevailing on the coasts of southern Spitsbergen will therefore change into a subarctic oceanic climate (Cfc), that is now characteristic for Iceland shores. As a result of these changes, the simulations show a shortening of the period with snowfall to November–May. Under such conditions, the occurrence of the maximum accumulation period will shift from the turn of April and May to late March or early April. This means an almost twofold extension of the snow-free period in the tundra in the Hornsund region. The simulation results in modified climate show that despite the increase in precipitation totals, the snow thickness will decrease. Moreover, at the end of the twenty-first century, the period with permanent snow cover may be interrupted by snowless episodes related to the occurrence of strong thaws even in the middle of winter. A further increase in air temperature by about 2 °C will completely change the course of snow cover development and ablation on the tundra. The positive air temperatures prevailing in this case for most of the winter period will not allow for the formation of a permanent snow cover, but will only lead to temporary episodes with snow on the ground. Climate warming, although apparently conducive to the development of life in the tundra area, may turn out to be unfavorable to both vegetation and animals. Plants may suffer drought stress due to shortened snow cover duration and associated lowering of groundwater levels. On the other hand, more frequent rain-on-snow events may lead to the formation of ice layers hindering, e.g., reindeer access to food.

APPENDIX

Explanation of symbols and values used in graphs showing the vertical structure of snow. Modified after Fierz et al. (2009)

Grain shape class	Symbol	Code	Color on schemes
Precipitation **P**articles	+	PP	
Machine **M**ade snow	◎	MM	
Decomposing and **F**ragmented precipitation particles	/	DF	
Rounded **G**rains	●	RG	
Faceted **C**rystals	□	FC	
Depth **H**oar	Λ	DH	
Surface **H**oar	V	SH	
Melt **F**orms	○	MF	
	∞	MFcr	
Ice **F**ormations	■	IF	

Hardness in hand test

0 - 20 N	Fist (F)	
20 - 100 N	Four fingers (4F)	
100 - 250 N	One finger (1F)	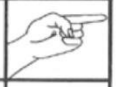
250 - 1000 N	Pencil (P)	
>1000 N	Knife (K)	

Liquid water content

Wetness index	Class	Free water content [%]
1	dry	0
2	moist	0-3
3	wet	3-8
4	very wet	8-15
5	soaked	> 15

References

Aalstad, K., S. Westermann, T.V. Schuler, J. Boike, and L. Bertino (2018), Ensemble-based assimilation of fractional snow-covered area satellite retrievals to estimate the snow distribution at Arctic sites, *The Cryosphere* **12**, 247–270, DOI: 10.5194/tc-12-247-2018.

Aanes, R., B.-E. Saether, F.M. Smith, E.J. Cooper, P.A. Wookey, and N.A. Oritsland (2002), The Arctic Oscillation predicts effects of climate change in two trophic levels in a high-arctic ecosystem, *Ecol. Lett.* **5**, 445–453, DOI: 10.1046/j.1461-0248.2002.00340.x.

Aas, K.S., T. Dunse, E. Collier, T.V. Schuler, T.K. Berntsen, J. Kohler, and B. Luks (2016), The climatic mass balance of Svalbard glaciers: a 10-year simulation with a coupled atmosphere–glacier mass balance model, *The Cryosphere* **10**, 1089–1104, DOI: 10.5194/tc-10-1089-2016.

Adam, J.C., A.F. Hamlet, and D.P. Lettenmaier (2009), Implications of global climate change for snowmelt hydrology in the twenty-first century, *Hydrol. Process.* **23**, 962–972, DOI: 10.1002/hyp.7201.

Affek, A. (2013), Georeferencing of historical maps using GIS, as exemplified by the Austrian Military Surveys of Galicia, *Geogr. Pol.* **86**, 375–390, DOI: 10.7163/GPol.2013.30.

Ahlmann, H.W. (1933), Scientific results of the Swedish-Norwegian Arctic expedition in the summer of 1931. Part VIII, *Geogr. Ann.* **15**, 161–216, DOI: 10.2307/519460.

Ahlmann, H.W. (1935), Scientific results of the Norwegian-Swedish Spitsbergen Expedition in 1934. Part I. The stratification of the snow and firn on Isachsen's Plateau, *Geogr. Ann.* **17**, 29–42, DOI: 10.1080/20014422.1935.11880589.

Araźny, A., R. Przybylak, P. Wyszyński, T. Wawrzyniak, A. Nawrot, and T. Budzik (2017), Spatial variations in air temperature and humidity over Hornsund fjord (Spitsbergen) from 1 July 2014 to 30 June 2015, *Geogr. Ann. A* **100**, 27–43, DOI: 10.1080/04353676.2017.1368832.

Arendt, A., and M. Sharp (1999), Energy balance measurements on a Canadian high Arctic glacier and their implications for mass balance modelling. **In:** M. Tranter, R. Armstrong, E. Brun, G. Jones, M. Sharp, and M. Williams (eds.), *Proceedings of the IUGG Symposium "Interactions between the Cryosphere, Climate and Greenhouse Gases", Birmingham 1999*, IAHS Publication, No. 256, 165–172.

Askaer, L., L.B. Schmidt, B. Elberling, G. Asmund, and I.S. Jónsdóttir (2008), Environmental impact on an Arctic soil–plant system resulting from metals released from coal mine waste in Svalbard (78° N), *Water Air Soil Poll.* **195**, 99–114, DOI: 10.1007/s11270-008-9730-z.

Baranowski, S. (1968), *Termika Tundry Peryglacjalnej SW Spitsbergen*, Acta Univ. Wratislav., No. 68, 74 pp. (in Polish).

Bartelt, P., and M. Lehning (2002), A physical SNOWPACK model for the Swiss avalanche warning: Part I: numerical model, *Cold Reg. Sci. Technol.* **35**, 3, 123–145, DOI: 10.1016/S0165-232X(02)00074-5.

Bavay, M. (2017), Format specification for the SMET Weather Station Meteorological Data Format – version 1.1, available from: https://models.slf.ch/p/meteoio/source/tree/1004/trunk/doc/SMET_specifications.pdf.

Bavay, M., and T. Egger (2014), MeteoIO 2.4.2: a preprocessing library for meteorological data, *Geosci. Model Dev.* **7**, 3135–3151, DOI: 10.5194/gmd-7-3135-2014.

Bay, H., A. Ess, T. Tuytelaars, and L. Van Gool (2008), Speeded-up robust features (SURF), *Comput. Vis. Image Und.* **110**, 346–359, DOI: 10.1016/j.cviu.2007.09.014.

Benson, C.S., and M. Sturm (1993), Structure and wind transport of seasonal snow on the Arctic slope of Alaska, *Ann. Glaciol.* **18**, 261–267, DOI: 10.3189/S0260305500011629.

Bernard, E., J.-M. Friedt, C. Marlin, F. Tolle, S. Schiavone, M. Griselin, and A. Prokop (2016), Investigating snowcover volumes and icings dynamics in the moraine of an Arctic catchment using UAV/photogrammetry and LiDAR. **In:** *Virtual Geosciences Conference, Sep 2016, Bergen,*

Norway, available from: https://hal.archives-ouvertes.fr/hal-01670093/file/Investigating%20snowcover.pdf.

Berry, M.O., (1981), Snow and climate. **In**: D.M. Gray, and D.H. Male (eds.), *The Handbook of Snow. Principles, Processes, Management and Use*, Pergamon, Toronto, 51–60.

Bindschadler, R. (2003), Landsat coverage of the earth at high latitudes, *Photogramm. Eng. Rem. Sens.* **12**, 1333–1339, DOI: 10.14358/PERS.69.12.1333.

Bivand, R., and N. Lewin-Koh (2017), Maptools: Tools for reading and handling spatial objects, available from: https://CRAN.R-project.org/package=maptools.

Bivand, R., T. Keitt, and B. Rowlingson (2018), rgdal: Bindings for the "Geospatial" Data Abstraction Library, available from: https://CRAN.R-project.org/package=rgdal.

Błaszczyk, M., J.A. Jania, and L. Kolondra (2013), Fluctuations of tidewater glaciers in Hornsund Fjord (Southern Svalbard) since the beginning of the 20th century, *Pol. Polar Res.* **34**, 4, 327–352, DOI: 10.2478/ popore-2013-0024.

Błażejczyk, K. (2004), *Bioklimatyczne Uwarunkowania Rekreacji i Turystyki w Polsce*, Monografie IGiPZ PAN, Prace Geograficzne nr 192, 291 pp. (in Polish).

Bliss, L.C., J. Svoboda, and D.I. Bliss (1984), Polar deserts, their plant cover and plant production in the Canadian High Arctic, *Ecography* **7**, 3, 305–324, DOI: 10.1111/j.1600-0587.1984.tb01136.x.

Böhner, J., R. Köthe, O. Conrad, J. Gross, A. Ringeler, and T. Selige (2002), Soil regionalisation by means of terrain analysis and process parameterisation, *Gott. Geogr. Abh.* **115**, 13–28.

Borysiak, J., and H. Ratyńska (2004), Stan badań nad szatą roślinną Spitsbergenu ze szczególnym uwzględnieniem rejonów Bellsundu, Hornsundu i Kaffiøyry. **In:** A. Kostrzewski, M. Pulina, and Z. Zwoliński (eds.), *Warsztaty Glacjologiczne Spitsbergen 2004. Glacjologia, Geomorfologia i Sedymentacja Środowiska Polarnego Spitsbergenu*, Stowarzyszenie Geomorfologów Polskich, Sosnowiec-Poznań-Longyearbyen, 248–260 (in Polish).

Bouguet, J.-Y. (2015), Camera Calibration Toolbox for Matlab, available from: http://www.vision.caltech.edu/bouguetj/calib_doc/.

Bradford, J.H., J.T. Harper, and J. Brown (2009), Complex dielectric permittivity measurements from ground-penetrating radar data to estimate snow liquid water content in the pendular regime, *Water Resour. Res.* **45**, 8, W08403, DOI: 10.1029/2008WR007341.

Braithwaite, R.J. (1995), Positive degree-day factors for ablation on the Greenland ice sheet studied by energy-balance modelling, *J. Glaciol.* **41**, 137, 153–160, DOI: 10.3189/S0022143000017846.

Bruland, O., and E. Cooper (2001), Snow distribution and vegetation. **In**: *Proc. Arctic Feedbacks to Global Change*, Rovaniemen Paintuskeskus Oy, Rovaniemi, Finland, 110.

Bruland, O., and K. Sand (1994), The Nordic HBV-model applied to an Arctic watershed. **In**: *Proc. Tenth International Northern Research Basins Symposium and Workshop*, 594–608.

Bruland, O., D. Maréchal, K. Sand, and Å. Killingtveit (2001), Energy and water balance studies of a snow cover during snowmelt period at a high arctic site, *Theor. Appl. Climatol.* **70**, 53–63, DOI: 10.1007/s007040170005.

Bruland, O., G.E. Liston, J. Vonk, K. Sand, and Å. Killingtveit (2004), Modelling the snow distribution at two high arctic sites at Svalbard, Norway, and at an alpine site in central Norway, *Hydrol. Res.* **35**, 3, 191–208, DOI: 10.2166/nh.2004.0014.

Brümmer, B., S. Thiemann, and A. Kirchgäßsner (2000), A cyclone statistics for the Arctic based on European Centre re-analysis data, *Meteorol. Atmos. Phys.* **75**, 233–250, DOI: 10.1007/s007030070006.

Brun, E., E. Martin, V. Simon, C. Gendre, and C. Coleou (1989), An energy and mass model of snow cover suitable for operational avalanche forecasting, *J. Glaciol.* **35**, 121, 333–342, DOI: 10.3189/S0022143000009254.

Bubier, J.L., B.N. Rock, and P.M. Crill (1997), Spectral reflectance measurements of boreal wetland and forest mosses, *J. Geophys. Res. – Atmos.* **102**, D24, 29483–29494, DOI: 10.1029/ 97JD02316.

Budzik, T., S. Sikora, and A. Araźny (2009), Przebieg roczny salda promieniowania powierzchni czynnej w Hornsundzie (V 2008 – IV 2009), *Probl. Klimatol. Polar.* **19**, 233–246 (in Polish).

Burns, P., and A. Nolin (2014), Using atmospherically-corrected Landsat imagery to measure glacier area change in the Cordillera Blanca, Peru from 1987 to 2010, *Remote Sens. Environ.* **140**, 165–178, DOI: 10.1016/j.rse.2013.08.026.

Callaghan, T.V., M. Johansson, R.D. Brown, P.Ya. Groisman, N. Labba, V. Radionov, R.S. Bradley, S. Blangy, O.N. Bulygina, T.R. Christensen et al. (2011), Multiple effects of changes in arctic snow cover, *AMBIO* **40**, 32–45, DOI: 10.1007/s13280-011-0213-x.

Chabot, D., M. Kahrl, K.W. Birkeland, and C. Anker (2004), SnowPilot: A "new school" tool for collecting, graphing, and databasing snowpit and avalanche occurrence data with a PDA. **In:** *International Snow Science Workshop*, Jackson Hole, Wyoming, 19–24.

Chapin, F.S., G.R. Shaver, A.E. Giblin, K.J. Nadelhoffer, and J.A. Laundre (1995), Responses of arctic tundra to experimental and observed changes in climate, *Ecology* **76**, 3, 694–711, DOI: 10.2307/1939337.

Chmal, H., J. Klementowski, and K. Migała (1988), Thermal currents of active layer in Hornsund area. **In:** *Proc. 5th International Conference on Permafrost, Trondheim*, 44–49.

Christiansen, H.H., B. Etzelmüller, K. Isaksen, H. Juliussen, H. Farbrot, O. Humlum, M. Johansson, T. Ingeman-Nielsen, L. Kristensen, J. Hjort, P. Holmlund, A.B.K. Sannel, C. Sigsgaard, H.J. Åkerman, N. Foged, L.H. Blikra, M.A. Pernosky, and R.S. Ødegård (2010), The thermal state of permafrost in the nordic area during the international polar year 2007-2009, *Permafrost Periglac. Process.* **21**, 2, 156–181, DOI: 10.1002/ ppp.687.

Cimoli, E., M. Marcer, B. Vandecrux, C.E. Bøggild, G. Williams, and S.B. Simonsen (2017), Application of low-cost UASs and digital photogrammetry for high-resolution snow depth mapping in the Arctic, *Remote Sens.* **9**, 11, 1144, DOI: 10.3390/rs9111144.

Claremar, B., F. Obleitner, C. Reijmer, V. Pohjola, A. Waxegård, F. Karner, and A. Rutgersson (2012), Applying a mesoscale atmospheric model to Svalbard glaciers, *Adv. Meteorol.* **2012**, ID 321649, DOI: 10.1155/2012/321649.

Conover, W.J. (1999), *Practical Nonparametric Statistics*, 3rd ed., John Wiley & Sons, New York, 350 pp.

Cooper, E.J., S. Dullinger, and P. Semenchuk (2011), Late snowmelt delays plant development and results in lower reproductive success in the High Arctic, *Plant Sci.* **180**, 1, 157–167, DOI: 10.1016/j.plantsci.2010.09.005.

Dadic, R., R. Mott, M. Lehning, and P. Burlando (2010), Parameterization for wind–induced preferential deposition of snow, *Hydrol. Process.* **24**, 14, 1994–2006, DOI: 10.1002/hyp.7776.

Dallal, G.V. (1999), Confidence intervals and tests of signficance. **In:** G.V. Dallal (ed.), *The Little Handbook of Statistical Practice*, Boston, USA.

de Kleijjn, C. (2016), *Soil Formation in Central Spitsbergen – Framework for Process Integration*, MSc thesis, Wageningen University and Research Centre, Wageningen, Holandia.

de Mendiburu, F. (2021), agricolae: Statistical Procedures for Agricultural Research, available from: https://CRAN.R-project.org/package=agricolae.

Dobler, A., and J.E. Haugen (2016), Convection resolving climate simulations over Svalbard, Bergen.

Doesken, N., and A. Judson (1997), *The Snow Booklet. A guide to the Science, Climatology and Measurements of Snow in the United States*, 2nd ed., Colorado Climate Center, Colorado State University Publications & Printing.

Dolnicki, P. (2002), Wpływ pokrywy śnieżnej na termikę i grubość warstwy czynnej zmarzliny w obszarze tundrowym rejonu Polskiej Stacji Polarnej (SW Spitsbergen), *Probl. Klimatol. Polar.* **12**, 107–116 (in Polish).

Dolnicki, P. (2005), Rozkład przestrzenny poziomu wieloletniej zmarzliny i jego związek z nierównomiernym zanikiem pokrywy śnieżnej na obszarze Fuglebergsletty (SW Spitsbergen). **In:** *Polish Polar Studies, XXXI Sympozjum Polarne, Kielce* **34**, 45 (in Polish).

Dolnicki, P. (2015), Zmienna grubość pokrywy śnieżnej na tundrze jako przyczyna zróżnicowania przestrzennego grubości warstwy czynnej na przykładzie wschodniej Fuglebergsletty (SW Spitsbergen), *Probl. Klimatol. Polar.* **25**, 191–200 (in Polish).

Dolnicki, P., M. Grabiec, D. Puczko, Ł. Gawor, T. Budzik, and J. Klementowski (2013), Variability of temperature and thickness of permafrost active layer at coastal sites of Svalbard, *Pol. Polar Res.* **34**, 4, 353–374, DOI: 10.2478/popore-2013-0026.

Dozier, J. (1989), Spectral signature of alpine snow cover from the Landsat Thematic Mapper, *Remote Sens. Environ.* **28**, 9–22, DOI: 10.1016/0034-4257(89)90101-6.

Duchon, C.E. (2008), Using vibrating-wire technology for precipitation measurements. **In:** S. Michaelides (ed.), *Precipitation: Advances in Measurement, Estimation and Prediction*, Springer-Verlag, Berlin, 33–58, DOI: 10.1007/978-3-540-77655-0_2.

Duguay, C.R., G.M. Flato, M.O. Jeffries, P. Ménard, K. Morris, and W.R. Rouse (2003), Ice-cover variability on shallow lakes at high latitudes: model simulations and observations, *Hydrol. Process.* **17**, 17, 3465–3483, DOI: 10.1002/hyp.1394.

Dunn, O.J. (1964), Multiple comparisons using rank sums, *Technometrics* **6**, 3, 241–252, DOI: 10.1080/00401706. 1964.10490181.

Earle, C.J. (1993), Forest dynamics in a forest-tundra ecotone, Medicine Bow Mountains, Wyoming, PhD thesis, University of Washington, Seattle, 141 pp., available from: https://www.fs.fed.us/rm/pubs_exp_for/glees/exp_for_glees_1993_earle.pdf

Elmendorf, S.C., G.H.R. Henry, R.D. Hollister, R.G. Björk, N. Boulanger-Lapointe, E.J. Cooper, J.H.C. Cornelissen, T.A. Day, E. Dorrepaal, T.G. Elumeeva et al. (2012), Plot-scale evidence of tundra vegetation change and links to recent summer warming, *Nat. Clim. Change* **2**, 453–457, DOI: 10.1038/nclimate1465.

Elvebakk, A., and P. Prestrud (eds.) (1996), *A Catalogue of Svalbard Plants, Fungi, Algae and Cyanobacteria*, Norwegian Polar Institute, Oslo, 395 pp.

Essery, R., and J. Pomeroy (2004), Vegetation and topographic control of wind-blown snow distributions in distributed and aggregated simulations for an arctic tundra basin, *J. Hydrometeorol.* **5**, 5, 735–744, DOI: 10.1175/1525-7541(2004)005<0735:VATCOW>2.0.CO;2.

Essery, R., J. Pomeroy, J. Parviainen, and P. Storck (2003), Sublimation of snow from coniferous forests in a climate model, *J. Climate* **16**, 11, 1855–1864, DOI: 10.1175/1520-0442(2003)016 <1855: SOSFCF>2.0.CO;2.

Fang, J., and F. Porté-Agel (2016), Intercomparison of terrain-following coordinate transformation and immersed boundary methods in large-eddy simulation of wind fields over complex terrain, *J. Phys.: Conf. Ser.* **753**, 8, 082008, DOI: 10.1088/1742-6596/753/8/082008.

Fierz, C., R.L. Armstrong, Y. Durand, P. Etchevers, E. Greene, D.M. McClung, K. Nishimura, P.K. Satyawali, and S.A. Sokratov (2009), The international classification for seasonal snow on the ground, IHP-VII Technical Documents in Hydrology N83, UNESCO/IHP Paris.

Fierz, C., T. Egger, M. Gerber, F. Techel, and M. Bavay (2016), SnopViz, An interactive visualization tool for both snow-cover model output and observed snow profiles. **In:** *Proc. International Snow Science Workshop, ISSW, Breckenridge, Colorado, 2016*, 637–641.

Finsterwalder, S. (1887), Der Suldenferner, *Z. Deut. Osterreich. Alpenver.* **18**, 72–89 (in German).

Forthofer, J., K. Shannon, N. Wagenbrenner, B. Butler, L. Malott, and C. Posey (2017), WindNinja. US Forest Service Missoula Fire Sciences Laboratory, Missoula, Montana, USA.

Fotheringham, A.S., and C. Brunsdon (1999), Local forms of spatial analysis, *Geogr. Anal.* **31**, 4, 340–358, DOI: 10.1111/j.1538-4632.1999.tb00989.x.

Fuglei, E., and R.A. Ims (2008), Global warming and effects on the arctic fox, *Sci. Prog.* **91**, 2, 175–191, DOI: 10.3184/003685008X327468.

Gagolewski, M. (2018), R package stringi: Character string processing facilities, available from: http://www.gagolewski.com/software/stringi/.

Gallet, J.-C., M.P. Björkman, C. Larose, B. Luks, T. Martma, and C. Zdanowicz (eds.) (2018), Protocols and recommendations for the measurement of snow physical properties, and sampling of snow for black carbon, water isotopes, major ions and microorganisms, Brief Report no. 046, Norwegian Polar Institute, Tromsø.

Gamon, J.A., C.B. Field, M.L. Goulden, K.L. Griffin, A.E. Hartley, G. Joel, J. Penuelas, and R. Valentini (1995), Relationships between NDVI, canopy structure, and photosynthesis in three Californian vegetation types, *Ecol. Appl.* **5**, 1, 28–41, DOI: 10.2307/1942049.

Gilmore, S., A. Saleem, and A. Dewan (2015), Effectiveness of DOS (Dark-Object Subtraction) method and water index techniques to map wetlands in a rapidly urbanising megacity with Landsat 8 data. **In:** B. Veenendaal and A. Kealy (eds.), *Proceedings of the Research@Locate'15, Brisbane, Australia, 10–12 March 2015*, 100–108.

Gisnås, K., S. Westermann, T.V. Schuler, T. Litherland, K. Isaksen, J. Boike, and B. Etzelmüller (2014), A statistical approach to represent small-scale variability of permafrost temperatures due to snow cover, *The Cryosphere* **8**, 6, 2063–2074, DOI: 10.5194/tc-8-2063-2014.

Głowacki, P., and M. Pulina (2000), The physico-chemical properties of the snow cover of Spitsbergen (Svalbard) based on investigations during the winter season 1990/1991, *Pol. Polar Res.* **21**, 2, 65–88.

Głowicki, B. (1975), Snow and firn patches between Hornsund and Werenskiold Glacier, *Acta Univ. Wratislav* **251**, 139–146.

Głowicki, B. (1985), Radiation conditions in the Hornsund area (Spitsbergen), *Pol. Polar Res.* **6**, 3, 301-318.

Grabiec, M. (2005), An estimation of snow accumulation on Svalbard glaciers on the basis of standard weather-station observations, *Ann. Glaciol.* **42**, 269–276, DOI: 10.3189/172756405781812808.

Grabiec, M. (2017), Stan i Współczesne Zmiany Systemów Lodowcowych Południowego Spitsbergenu w Świetle Badań Metodami Radarowymi, Wydawnictwo Uniwersytetu Śląskiego, Katowice, 328 pp. (in Polish).

Grabiec, M., J. Leszkiewicz, P. Głowacki, and J. Jania (2006), Distribution of snow accumulation on some glaciers of Spitsbergen, *Pol. Polar Res.* **27**, 4, 309–326.

Grabiec, M., D. Puczko, T. Budzik, and G. Gajek (2011), Snow distribution patterns on Svalbard glaciers derived from radio-echo soundings, *Pol. Polar Res.* **32**, 4, 393–421, DOI: 10.2478/v10183−011−0026−4.

Grabiec, M., T. Budzik, and P. Głowacki (2012), Modeling and hindcasting of the mass balance of Werenskioldbreen (Southern Svalbard), *Arct. Antarct. Alp. Res.* **44**, 2, 164–179, DOI: 10.1657/1938-4246-44.2.164.

Grabiec, M., D. Ignatiuk, J.A. Jania, M. Moskalik, P. Głowacki, M. Błaszczyk, T. Budzik, and W. Walczowski (2018), Coast formation in an Arctic area due to glacier surge and retreat: The Hornbreen-Hambergbreen case from Spistbergen, *Earth Surf. Proc. Land.* **43**, 2, 387–400, DOI: 10.1002/esp.4251.

Granger, R.J., J.W. Pomeroy, and J. Parviainen (2002), Boundary-layer integration approach to advection of sensible heat to a patchy snow cover, *Hydrol. Process.* **16**, 18, 3559–3569, DOI: 10.1002/hyp.1227.

Grell, G.A., J. Dudhia, and D.R. Stauffer (1995), A description of the fifth-generation Penn State/NCAR mesoscale model (MM5), NCAR Technical Note, Boulder, Colorado.

Groot Zwaaftink, C.D., R. Mott, and M. Lehning (2013), Seasonal simulation of drifting snow sublimation in Alpine terrain, *Water Resour. Res.* **49**, 3, 1581–1590, DOI: 10.1002/wrcr.20137.

Grünewald, T., M. Schirmer, R. Mott, and M. Lehning (2010), Spatial and temporal variability of snow depth and ablation rates in a small mountain catchment, *The Cryosphere* **4**, 2, 215–225, DOI: 10.5194/tc-4-215-2010.

Grześ, M. (1985), Warstwa czynna wieloletniej zmarzliny na zachodnich wybrzeżach Spitsbergenu, *Prz. Geogr.* **57**, 4, 671–691 (in Polish).

Grześ, M., and I. Sobota (2000), Winter snow accumulation and discharge from the Waldemar Glacier, northwestern Spitsbergen in 1996–1998, *Pol. Polar Res.* **21**, 1, 19–32.

Guisan, A., S.B. Weiss, and A.D. Weiss (1999), GLM versus CCA spatial modeling of plant species distribution, *Plant Ecol.* **143**, 107–122, DOI: 10.1023/A:1009841519580.

Guskov, A.S., and L.S. Troitskiy (1984), O kolebaniyach snezhnosti na Shpitzbergene [Snow thickness variability on Spitsbergen], *Mater. Glyatsiolog. Issled. [Data Glaciol. Stud.]* **50**, 185–188 (in Russian).

Hagen, J.O., O. Liestøl, E. Roland, and T. Jørgensen (1993), *Glacier Atlas of Svalbard and Jan Mayen*, Norsk Polarinstitutt, Oslo.

Hall, D.K., and G.A. Riggs (2011), Normalized-difference snow index (NDSI). **In:** V.P. Singh, P. Singh, and U.K. Haritashya (eds.), *Encyclopedia of Snow, Ice and Glaciers*, Springer, Dordrecht, 779–780, DOI: 10.1007/978-90-481-2642-2_376.

Hall, D.K., G.A. Riggs, and V.V. Salomonson (1995), Development of methods for mapping global snow cover using moderate resolution imaging spectroradiometer data, *Remote Sens. Environ.* **54**, 2, 127–140, DOI: 10.1016/0034-4257(95)00137-P.

Hansen, B.B., R. Aanes, I. Herfindal, J. Kohler, and B.-E. Sæther (2011), Climate, icing, and wild arctic reindeer: past relationships and future prospects, *Ecology* **92**, 10, 1917–1923, DOI: 10.1890/11-0095.1.

Hansen, B.B., V. Grotan, R. Aanes, B.-E. Saether, A. Stien, E. Fuglei, R.A. Ims, N.G. Yoccoz, and Å.O. Pedersen (2013), Climate events synchronize the dynamics of a resident vertebrate community in the high Arctic, *Science* **339**, 6117, 313–315, DOI: 10.1126/science.1226766.

Hansen, F.V. (1993), Surface roughness lengths, ARL Technical Report, U.S. Army, White Sands Missile Range, 41 pp.

Hanssen-Bauer, I., E.J. Førland, and P. Nordli (1996), Measured and true precipitation at Svalbard, DNMI Report No. 31/96, Norwegian Meteorological Institute, Oslo, available from: https://www.met.no/publikasjoner/met-report/met-report-1996/_/attachment/download/384542de-1466-4987-b3ff-8c69767b9f2c:016c399a34d2c64618f450ba4819241e0759057e/MET-report-31-1996.pdf.

Harbortronics Inc. (2018), Time-Lapse Camera Package, Products, Harbortronics. Time-Lapse Camera Package, available from: https://www.harbortronics.com/Products/TimeLapsePackage/.

Harding, R.J., and C.R. Lloyd (1998), Fluxes of water and energy from three high latitude tundra sites in Svalbard: Paper presented at the 11th Northern Res. Basins Symposium/Workshop Prudhoe Bay to Fairbanks, Alaska, USA – Aug. 18-22, 1997, *Hydrol. Res.* **29**, 4–5, 267–284, DOI: 10.2166/nh.1998.0016.

Härer, S., M. Bernhardt, J.G. Corripio, and K. Schulz (2013), PRACTISE – Photo Rectification And ClassificaTIon softwarE (v. 1.0), *Geosci. Model Dev.* **6**, 837–848, DOI: 10.5194/gmd-6-837-2013.

Hauke, J., and T. Kossowski (2011), Comparison of values of Pearson's and Spearman's correlation coefficients on the same sets of data, *Quaest. Geogr.* **30**, 2, 87–93, DOI: 10.2478/v10117-011-0021-1.

Heer, O. (1836), Die Vegetationsverhältnisse des südöstlichen Teils des Kanton Glarus. **In:** V.J. Frobel and O. Heer (eds.), *Mittheilungen aus dem Gebiete der theoretischen Erdkunde*, Füssli, Zurich, 279–468 (in German).

Heerdegen, R.G., and M.A. Beran (1982), Quantifying source areas through land surface curvature and shape, *J. Hydrol.* **57**, 3–4, 359–373, DOI: 0.1016/0022-1694(82)90155-X.

Hertenstein, R.F., and J.P. Kuettner (2005), Rotor types associated with steep lee topography: influence of the wind profile, *Tellus A* **57**, 2, 117–135, DOI: 10.1111/j.1600-0870.2005.00099.x.

Hicks, B.B., and H.C. Martin (1972), Atmospheric turbulent fluxes over snow, *Bound.-Layer Meteorol.* **2**, 496–502, DOI: 10.1007/BF00821551.

Hijmans, R. (2017), raster: Geographic Data Analysis and Modeling, available from: https://CRAN.R-project.org/package=raster .

Hinkler, J., J.B. Ørbæk, and B.U. Hansen (2003), Detection of spatial, temporal, and spectral surface changes in the Ny-Ålesund area 79° N, Svalbard, using a low cost multispectral camera in combination with spectroradiometer measurements, *Phys. Chem. Earth A/B/C* **28**, 28–32, 1229–1239, DOI: 10.1016/j.pce.2003.08.059.

Hinzman, L.D., N.D. Bettez, W.R. Bolton, F.S. Chapin, M.B. Dyurgerov, C.L. Fastie, B. Griffith, R.D. Hollister, A. Hope, H.P. Huntington et al. (2005), Evidence and implications of recent climate change in northern Alaska and other arctic regions, *Climatic Change* **72**, 251–298, DOI: 10.1007/s10584-005-5352-2.

Hisdal, V. (1976), Weather in Svalbard in 1974. **In:** *Norsk Polaristitutt Arbok 1974*, 195–198.

Hobbler, A. (2011), Thermal characteristics of tundra, based on satellite data (Fuglebekken Basin, SW Spitsbergen), MSc thesis, University of Wroclaw, Wrocław, 79 pp.

Hock, R. (2003), Temperature index melt modelling in mountain areas, *J. Hydrol.* **282**, 1–4, 104–115, DOI: 10.1016/S0022-1694(03)00257-9.

Hosang, J., and K. Dettwiler (1991), Evaluation of a water equivalent of snow cover map in a small catchment area using a geostatistical approach, *Hydrol. Process.* **5**, 3, 283–290, DOI: 10.1002/hyp.3360050308.

Houghton, J.T., B.A. Callander, and S.K. Varney (eds.) (1992), *Climate Change 1992*, The Supplementary Report to the IPCC Scientific Assessment, Cambridge University Press, Cambridge.

Isaksen, K. (1995), The breeding population of little auk (Alle alle) in colonies in Hornsund and northwestern Spitsbergen. **In:** K. Isaksen and V. Bakken (eds.), *Seabird Population in the Northern Barents Sea*, Norsk Polarinstitutt, Oslo, Norway, 49–57 pp.

Isaksen, K., R.E. Benestad, C. Harris, and J.L. Sollid (2007), Recent extreme near-surface permafrost temperatures on Svalbard in relation to future climate scenarios, *Geophys. Res. Lett.* **34**, 17, DOI: 10.1029/2007GL031002.

Isaksen, K., E. Førland, A. Dobler, R. Benestad, J.E. Haugen, and A. Mezghani (2017), Klimascenarioer for Longyearbyen-området, Svalbard, MET Report No. 15/2017, Norwegian Meteorological Institute, available from: https://www.met.no/publikasjoner/met-report/met-report-2017/_/attachment/download/8932a8b1-17b4-4567-8559-ed4b78d61aee:6fe02353a8212c195f00bd59dc5b2baaa6c4118c/2017-10-METreport_Statsbygg-Svalbard_final.pdf

Janiszewski, F. (1962), *Instrukcja dla Stacji Meteorologicznych*, Wydawnictwa Komunikacji i Łączności, Warszawa, 262 pp.

Jensen, R.A., J. Madsen, M. O'Connell, M.S. Wisz, H. Tømmervik, and F. Mehlum (2007), Prediction of the distribution of Arctic-nesting pink-footed geese under a warmer climate scenario, *Glob. Change Biol.* **14**, 1, 1–10, DOI: 10.1111/j.1365-2486.2007.01461.x.

Johansen, B.E., S.R. Karlsen, and H. Tømmervik (2012), Vegetation mapping of Svalbard utilising Landsat TM/ETM+ data, *Polar Rec.* **48**, Sp. Is. 1, 47–63, DOI: 10.1017/S0032247411000647.

Johansson, M., T.V. Callaghan, J. Bosiö, H.J. Åkerman, M. Jackowicz-Korczynski, and T.R. Christensen (2013), Rapid responses of permafrost and vegetation to experimentally increased snow cover in sub-arctic Sweden, *Environ. Res. Lett.* **8**, 035025, DOI: 10.1088/1748-9326/8/3/035025.

Jónsdóttir, I.S. (2005), Terrestrial ecosystems on Svalbard: heterogeneity, complexity and fragility from an Arctic island perspective, *Biol. Environ.: Proc. Royal Irish Acad. JSTOR*, **105B**, 3, 155–165, DOI: 10.3318/BIOE.2005.105.3.155.

Jordan, R. (1991), A one-dimensional temperature model for a snow cover: technical documentation for SNTHERM. 89, Special Report 91-16, U.S. Army Corps of Engineers, Cold Regions Research and Engineering Laboratory, Hanover, N.H. 49 pp.

Jordan, R. (1995), Effects of capillary discontinuities on water flow retention in layered snow covers, *Def. Sci. J.* **45**, 2, 79, DOI: 10.14429/dsj.45.4107.

Kaempfer, T.U., and M. Plapp (2009), Phase-field modeling of dry snow metamorphism, *Phys. Rev. E* **79**, 031502, DOI: 10.1103/PhysRevE.79.031502.

Kane, D.L., R.E. Gieck, and L.D. Hinzman (1997), Snowmelt modeling at small Alaskan Arctic watershed, *J. Hydrol. Eng.* **2**, 4, 204–210, DOI: 10.1061/(ASCE)1084-0699(1997)2:4(204).

Karczewski, A. (2004), Geomorfologia rejonu fiordu Hornsund, Spitsbergen. Komentarz do mapy. **In:** *Glacjologia, Geomorfologia i Sedymentologia Środowiska Polarnego Spitsbergenu. Warsztaty Glacjologiczne SPITSBERGEN 2004*, Stowarzyszenie Geomorfologów Polskich, Sosnowiec-Poznań-Longyearbyen (in Polish).

Karlsen, S., A. Elvebakk, K. Høgda, and T. Grydeland (2014), Spatial and temporal variability in the onset of the growing season on Svalbard, Arctic Norway — measured by MODIS-NDVI satellite data, *Remote Sens.* **6**, 9, 8088–8106, DOI: 10.3390/rs6098088.

Kasprzak, M., M.C. Strzelecki, A. Traczyk, M. Kondracka, M. Lim, and K. Migała (2017), On the potential for a bottom active layer below coastal permafrost: the impact of seawater on permafrost degradation imaged by electrical resistivity tomography (Hornsund, SW Spitsbergen), *Geomorphology* **293**, B, 347–359, DOI: 10.1016/j.geomorph.2016.06.013.

Ke, L., X. Ding, and C. Song (2015), Heterogeneous changes of glaciers over the western Kunlun Mountains based on ICESat and Landsat-8 derived glacier inventory, *Remote Sens. Environ.* **168**, 13–23, DOI: 10.1016/j.rse.2015.06.019.

Kępski, D., M. Błaś, M. Sobik, Ż. Polkowska, and K. Grudzińska (2016), Progressing pollutant elution from snowpack and evolution of its physicochemical properties during melting period—a case study from the Sudetes, Poland, *Water Air Soil Poll.* **227**, 112, DOI: 10.1007/s11270-016-2797-z.

Kępski, D., B. Luks, K. Migała, T. Wawrzyniak, S. Westermann, and B. Wojtuń (2017a), Terrestrial remote sensing of snowmelt in a diverse High-Arctic tundra environment using time-lapse imagery, *Remote Sens.* **9**, 7, 733, DOI: 10.3390/rs9070733.

Kępski, D., B. Luks, K. Migała, T. Wawrzyniak, S. Westermann, and B. Wojtuń (2017b), Snow melt monitoring at Fugleberget, around Hornsund, Svalbard, 2014-2016. Supplement to: "Kępski, D. et al. (2017): Terrestrial remote sensing of snowmelt in a diverse High-Arctic tundra environment using time-lapse imagery, *Remote Sens.* **9**, 7, 733", *PANGAEA*, DOI: 10.1594/PANGAEA.874387.

Killingtveit, Å., and N.R. Saelthun (1995), *Hydrology, Hydropower Development*, Vol. 7, Norwegian Institute of Technology, Division of Hydraulic Engineering, Trondheim, 213 pp.

Kirillin, G., M. Leppäranta, A. Terzhevik, N. Granin, J. Bernhardt, C. Engelhardt, T. Efremova, S. Golosov, N. Palshin, P. Sherstyankin, G. Zdorovennova, and R. Zdorovennov (2012), Physics of seasonally ice-covered lakes: a review, *Aquat. Sci.* **74**, 659–682, DOI: 10.1007/s00027-012-0279-y.

Kirnbauer, R., and G. Blöschl (1992), An analysis of snow cover patterns in a small alpine catchment, *Hydrol. Process.* **6**, 1, 99–109, DOI: 10.1002/hyp.3360060109.

Kiss, R. (2004), Determination of drainage network in digital elevation models, utilities and limitations, *J. Hung. Geomath.* **2**, 16–29.

Klump, J., T. Leya, and G. Fuhr (2014), Mapping snowfields in the High Arctic by UAV. **In:** *EGU General Assembly Conference Abstracts, 27 April – 2 May 2014, Vienna, Austria*, ID9675.

Kohler, J., and R. Aanes (2004), Effect of winter snow and ground-icing on a Svalbard reindeer population: Results of a simple snowpack model, *Arct. Antarct. Alp. Res.* **36**, 3, 333–341, DOI: 10.1657/1523-0430(2004)036[0333:EOWSAG]2.0.CO;2.

Kolondra, L. (2003), Polish polar station and surrounding areas, Spitsbergen, Orthophotomap 1: 5 000.

Kondo, K., M. Tsuchiya, and S. Sanada (2002), Evaluation of effect of micro-topography on design wind velocity, *J. Wind Eng. Ind. Aerod.* **90**, 12–15, 1707–1718, DOI: 10.1016/S0167-6105(02)00281-7.

Köppen, W., and R. Geiger (1936), *Handbuch der Klimatologie,* Gebrüder Borntraeger, Berlin (in German).

Kosiba, A. (1949), Przenikliwość promieniowania słonecznego wgłąb szaty śnieżnej. **In:** *Częstość Szaty Śnieżnej na Ziemiach Śląskich*, Wrocławskie Towarzystwo Naukowe, Wrocław (in Polish).

Kosiba, A. (1958), Badania glacjologiczne na Spitsbergenie w lecie 1957 roku, *Prz. Geof.* **3**, 95–122 (in Polish).

Kosiba, A. (1960), Some of results of glaciological investigations in SW-Spitsbergen: Carried out during the Polish IGY Spitsbergen Expeditions in 1957, 1958 and 1959, *Zesz. Nauk. Uniw. Wrocł.* **4**, 1–30.

Kosiba, A. (1978), *Śniegi, Lodowce, Lądolody*, Wydawnictwa Szkolne i Pedagogiczne, Warszawa, 184 pp. (in Polish).

Kruszewski, G. (2004), Zmienność temperatury powierzchni morza w rejonie Spitsbergenu (1982–2002) jako przejaw współcześnie zachodzących zmian klimatycznych, *Probl. Klimatol. Polar.* **14**, 79–86 (in Polish).

Kruszewski, G., A.A. Marsz, and S. Zblewski (2003), Wpływ zmian temperatury powierzchni oceanu na Morzu Norweskim na temperaturę powietrza na Svalbardzie i Jan Mayen (1982-2002), *Probl. Klimatol. Polar.* **13**, 59–78 (in Polish).

Kuc, M., and E. Dubiel (1995), The vascular plants of the Hornsund area [SW Spitsbergen], *Fragm. Flor. Geobot.* **40**, 2, 797–824.

Kulkarni, A.V., S.K. Singh, P. Mathur, and V.D. Mishra (2006), Algorithm to monitor snow cover using AWiFS data of RESOURCESAT-1 for the Himalayan region, *Int. J. Remote Sens.* **27**, 12, 2449–2457, DOI: 10.1080/01431160500497820.

Kustas, W.P., A. Rango, and R. Uijlenhoet (1994), A simple energy budget algorithm for the snowmelt runoff model, *Water Resour. Res.* **30**, 5, 1515–1527, DOI: 10.1029/94WR00152.

Lafore, J.P., J. Stein, N. Asencio, P. Bougeault, V. Ducrocq, J. Duron, C. Fischer, P. Héreil, P. Mascart, V. Masson, J.P. Pinty, J.L. Redelsperger, E. Richard, and J. Vilà-Guerau de Arellano (1998), The Meso-NH Atmospheric Simulation System. Part I: adiabatic formulation and control simulations, *Ann. Geophys.* **16**, 1, 90–109, DOI: 10.1007/s00585-997-0090-6.

Lang, C., X. Fettweis, and M. Erpicum (2015), Future climate and surface mass balance of Svalbard glaciers in an RCP8.5 climate scenario: a study with the regional climate model MAR forced by MIROC5, *The Cryosphere* **9**, 945–956, DOI: 10.5194/tc-9-945-2015.

Laska, M. (2017), Zmienność topnienia pokrywy śnieżnej na lodowcach Ziemi Wedela Jarlsberga (SW Spitsbergen), PhD thesis, Uniwersytet Śląski, Sosnowiec (in Polish).

Laska, M., M. Grabiec, D. Ignatiuk, and T. Budzik (2017), Snow deposition patterns on southern Spitsbergen glaciers, Svalbard, in relation to recent meteorological conditions and local topography, *Geogr. Ann.: Ser. A Phys. Geogr.* **99**, 3, 262–287, DOI: 10.1080/04353676.2017.1327321.

Lehning, M., P. Bartelt, and B. Brown (1998), Operational use of a snowpack model for the avalanche warning service in Switzerland: model development and first experiences. **In:** *Proc. NGI Anniversary Conference, Norwegian Geotechnical Institute, May 1998*, No. EPFL-CONF-170344, 169–174.

Lehning, M., P. Bartelt, B. Brown, T. Russi, U. Stöckli, and M. Zimmerli (1999), SNOWPACK model calculations for avalanche warning based upon a new network of weather and snow stations, *Cold Reg. Sci. Technol.* **30**, 1–3, 145–157, DOI: 10.1016/S0165-232X(99)00022-1.

Lehning, M., P. Bartelt, B. Brown, C. Fierz, and P. Satyawali (2002a), A physical SNOWPACK model for the Swiss avalanche warning: Part II. Snow microstructure, *Cold Reg. Sci. Technol.* **35**, 3, 147–167, DOI: 10.1016/S0165-232X(02)00073-3.

Lehning, M., P. Bartelt, B. Brown, and C. Fierz (2002b), A physical SNOWPACK model for the Swiss avalanche warning: Part III: Meteorological forcing, thin layer formation and evaluation, *Cold Reg. Sci. Technol.* **35**, 3, 169–184, DOI: 10.1016/S0165-232X(02)00072-1.

Lehning, M., H. Löwe, M. Ryser, and N. Raderschall (2008), Inhomogeneous precipitation distribution and snow transport in steep terrain, *Water Resour. Res.* **44**, 7, W07404, DOI: 10.1029/2007WR 006545.

Leszkiewicz, J., and Z. Caputa (2004), The thermal condition of the active layer in the permafrost at Hornsund, Spitsbergen, *Pol. Polar Res.* **25**, 3/4, 223–239.

Leszkiewicz, J., and Z. Caputa (2015), Rekonstrukcja brakujących danych temperatury gruntu w Polskiej Stacji Polarnej w Hornsundzie (SW Spitsbergen) w latach 1990-2013, *Probl. Klimatol. Polar.* **25**, 201–210 (in Polish).

Leszkiewicz, J., and P. Głowacki (2001), Metamorfoza pokrywy śnieżnej w rejonie południowego Spitsbergenu w sezonie 1992/1993, *Probl. Klimatol. Polar.* **11**, 41–54 (in Polish).

Leszkiewicz, J., and M. Pulina (1999), Snowfall phases in analysis of a snow cover in Homsund, Spitsbergen, *Pol. Polar Res.* **20**, 1, 3–24.

Lewis, H.W., S.D. Mobbs, and M. Lehning (2008), Observations of cross-ridge flows across steep terrain, *Q. J. Roy. Meteor. Soc.* **134**, 633, 801–816, DOI: 10.1002/qj.259.

Lewis, M.C., and T.V. Callaghan (1976), Tundra. **In:** *Vegetation and the Atmosphere*, Vol. 2, Academic Press, New York, 399–433.

Li, L., and J.W. Pomeroy (1997), Estimates of threshold wind speeds for snow transport using meteorological data, *J. Appl. Meteorol. Climatol.* **36**, 3, 205–213, DOI: 10.1175/1520-0450(1997) 036<0205: EOTWSF>2.0.CO;2.

Liston, G.E. (1995), Local advection of momentum, heat, and moisture during the melt of patchy snow covers, *J. Appl. Meteorol. Climatol.* **34**, 7, 1705–1715, DOI: 10.1175/1520-0450-34.7.1705.

Liston, G.E., and M. Sturm (1998), A snow-transport model for complex terrain, *J. Glaciol.* **44**, 148, 498–516, DOI: 10.3189/S0022143000002021.

Liston, G.E., R.B. Haehnel, M. Sturm, C.A. Hiemstra, S. Berezovskaya, and R.D. Tabler (2007), Simulating complex snow distributions in windy environments using SnowTran-3D, *J. Glaciol.* **53**, 181, 241–256, DOI: 10.3189/17275650778220286.

Lloyd, C.R., R.J. Harding, T. Friborg, and M. Aurela (2001), Surface fluxes of heat and water vapour from sites in the European Arctic, *Theor. Appl. Climatol.* **70**, 19–33, DOI: 10.1007/ s007040170003.

López-Moreno, J.I., J. Boike, A. Sanchez-Lorenzo, and J.W. Pomeroy (2016), Impact of climate warming on snow processes in Ny-Ålesund, a polar maritime site at Svalbard, *Global Planet. Change* **146**, 10–21, DOI: 10.1016/j.gloplacha.2016.09.006.

Lüdecke, C. (2001), Historische Wetterstationen auf Spitzbergen. Ein Besuch im Sommer 2000, *Polarforschung* **71**, 1/2, 49–56 (in German).

Luks, B. (2012), Dynamika zmian pokrywy śnieżnej w rejonie południowo-zachodniego Spitsbergenu, PhD thesis, Institute of Geophysics, Polish Academy of Sciences, Warszawa, 143 pp. (in Polish).

Luks, B., M. Osuch, and R.J. Romanowicz (2011), The relationship between snowpack dynamics and NAO/AO indices in SW Spitsbergen, *Phys. Chem. Earth A/B/C* **36**, 13, 646–654, DOI: 10.1016/ j.pce.2011.06.004.

Luks, B., M. Osuch, and R.J. Romanowicz (2012), A comparison of two approaches to modelling snow cover dynamics at the Polish Polar Station at Hornsund. **In:** *EGU General Assembly Conference Abstracts, 22–27 April 2012, Vienna, Austria*, p. 5110.

Łupikasza, E. (2002), Zmienność opadów atmosferycznych w Hornsundzie (Spitsbergen) w okresie 1978-2000, *Probl. Klimatol. Polar.* **12**, 77–88 (in Polish).

Łupikasza, E. (2003), Zmienność występowania opadów deszczu i śniegu w Hornsundzie w okresie lipiec 1978 – grudzień 2002, *Probl. Klimatol. Polar.* **13**, 93–105 (in Polish).

Łupikasza, E. (2008), Zależność występowania rodzajów opadów od temperatury powietrza w Hornsundzie (Spitsbergen) w okresie 1978-2007, *Probl. Klimatol. Polar.* **18**, 99–112 (in Polish).

MacDonald, M.K., J.W. Pomeroy, and A. Pietroniro (2010), On the importance of sublimation to an alpine snow mass balance in the Canadian Rocky Mountains, *Hydrol. Earth Syst. Sci.* **14**, 7, 1401–1415, DOI: 10.5194/hess-14-1401-2010.

Madsen, J., M. Tamstorf, M. Klaassen, N. Eide, C. Glahder, F. Rigét, H. Nyegaard, and F. Cottaar (2007), Effects of snow cover on the timing and success of reproduction in high-Arctic pink-footed geese Anser brachyrhynchus, *Polar Biol.* **30**, 1363–1372, DOI: 10.1007/s00300-007-0296-9.

Malnes, E., S.R. Karlsen, B. Johansen, J. Haarpaintner, and K.A. Hogda (2010), Monitoring of the snow coverage and its relation to vegetation and growing seasons on Svalbard using Envisat ASAR and Terra MODIS data. **In:** *Proceedings of ESA Living Planet Symposium, 28 June – 2 July 2010, Bergen, Norway*, ESA SP-686, 265 pp.

Marsh, P., and M.-K. Woo (1984), Wetting front advance and freezing of meltwater within a snow cover: 1. Observations in the Canadian Arctic, *Water Resour. Res.* **20**, 12, 1853–1864, DOI: 10.1029/WR020i012p01853.

Marsh, P., J.W. Pomeroy, and N. Neumann (1997), Sensible heat flux and local advection over a heterogeneous landscape at an Arctic tundra site during snowmelt, *Ann. Glaciol.* **25**, 132–136, DOI: 10.3189/S0260305500013926.

Marsz, A.A., and A. Styszyńska (eds.) (2013), *Climate and Climate Change at Hornsund, Svalbard*, Gdynia Maritime University, Gdynia, 402 pp.

Martin, E. (1996), The snow cover model CROCUS, Technical description, Ver. 2.

Matsuoka, A., V. Hill, Y. Huot, M. Babin, and A. Bricaud (2011), Seasonal variability in the light absorption properties of western Arctic waters: Parameterization of the individual components of absorption for ocean color applications, *J. Geophys. Res.* **116**, C2, C02007, DOI: 10.1029/2009JC005594.

Maurer, J.A.I. (2006), Local-scale snow accumulation variability on the Greenland ice sheet from ground-penetrating radar (GPR), Master's thesis, Univ. of Colorado, Boulder.

McFadden, J.P., G.E. Liston, M. Sturm, R.A. Pielke, and F.S. Chapin (2001), Interactions of shrubs and snow in arctic tundra: measurements and models. **In:** A.J. Dolman (ed.), *Soil-vegetation-atmosphere Transfer Schemes and Large-scale Hydrological Models*, IAHS Publ., 317–325.

Meister, R. (1989), Influence of strong winds on snow distribution and avalanche activity, *Ann. Glaciol.* **13**, 195–201, DOI: 10.3189/S0260305500007886.

Ménard, C.B., R. Essery, and J. Pomeroy (2014), Modelled sensitivity of the snow regime to topography, shrub fraction and shrub height, *Hydrol. Earth Syst. Sci.* **18**, 6, 2375–2392, DOI: 10.5194/hess-18-2375-2014.

Michlmayr, G., M. Lehning, G. Koboltschnig, H. Holzmann, M. Zappa, R. Mott, and W. Schöner (2008), Application of the Alpine 3D model for glacier mass balance and glacier runoff studies at Goldbergkees, Austria, *Hydrol. Process.* **22**, 19, 3941–3949, DOI: 10.1002/hyp.7102.

Miętus, M. (1991), Snow depth at the Hornsund Station, Spitsbergen in 1978-1986, *Pol. Polar Res.* **12**, 223–228.

Migała, K. (1988), Snow cover influence on active layer of permafrost (Hornsund region, Spitsbergen). **In:** *XV Sympozjum Polarne*, Wrocław, 19–21.

Migała, K. (1991), Effect of the winter season and snow cover on the active layer of permafrost in the region of Hornsund (SW Spitsbergen). **In:** J. Repelewska-Pękalowa and K. Pękala (eds.), *Wyprawy Geograficzne na Spitsbergen. Materiały Sesji Polarnej „Arctic Environment Research"*, UMCS, Lublin, 241–256.

Migała, K., J. Pereyma, and M. Sobik (1988), Akumulacja śnieżna na południowym Spitsbergenie. **In:** I. Bajerowa, (ed.), *Wyprawy Polarne Uniwersytetu Ślaskiego 1980-1984*, Uniwersytet Śląski, Katowice, 48–63 (in Polish).

Migała, K., B. Wojtuń, W. Szymański, and P. Muskała (2014), Soil moisture and temperature variation under different types of tundra vegetation during the growing season: A case study from the Fuglebekken catchment, SW Spitsbergen, *CATENA* **116**, 10–18, DOI: 10.1016/j.catena.2013.12.007.

Moe, B., L. Stempniewicz, D. Jakubas, F. Angelier, O. Chastel, F. Dinessen, G. Gabrielsen, F. Hanssen, N. Karnovsky, B. Rønning, J. Welcker, K. Wojczulanis-Jakubas, and C. Bech (2009), Climate change and phenological responses of two seabird species breeding in the high-Arctic, *Mar. Ecol. Prog. Ser.* **393**, 235–246, DOI: 10.3354/meps08222.

Montesi, J., K. Elder, R.A. Schmidt, and R.E. Davis (2004), Sublimation of intercepted snow within a subalpine forest canopy at two elevations, *J. Hydrometeorol.* **5**, 5, 763–773, DOI: 10.1175/1525-7541(2004)005<0763:SOISWA>2.0.CO;2.

Moskalik, M., P. Grabowiecki, J. Tęgowski, and M. Żulichowska (2013), Bathymetry and geographical regionalization of Brepollen (Hornsund, Spitsbergen) based on bathymetric profiles interpolations, *Pol. Polar Res.* **34**, 1, 1–22, DOI: 10.2478/popore-2013-0001.

Mott, R., and M. Lehning (2010), Meteorological modeling of very high-resolution wind fields and snow deposition for mountains, *J. Hydrometeorol.* **11**, 4, 934–949, DOI: 10.1175/2010JHM1216.1.

Mott, R., F. Faure, M. Lehning, H. Löwe, B. Hynek, G. Michlmayer, A. Prokop, and W. Schöner (2008), Simulation of seasonal snow-cover distribution for glacierized sites on Sonnblick, Austria, with the Alpine3D model, *Ann. Glaciol.* **49**, 155–160, DOI: 10.3189/ 172756408787814924.

Nawrot, A., T. Wawrzyniak, W. Walczowski, P. Wieczorek, A. Araźny, and W. Mateja (2015), Snow thickness, density and chemical properties distribution around Hornsund Fjord (Svalbard). **In:** *1st Central European Polar Meeting, 10-13 November 2015, Vienna, Austria*.

NOAA (2013), Snow measurement guidelines for national weather service surface observing programs., available from: http://www.nws.noaa.gov/os/coop/reference/Snow_Measurement_Guidelines.pdf.

Nordli, P., I. Hanssen-Bauer, and E.J. Førland (1996), Homogenity analyses of temperature and precipitation series from Svalbard and Jan Mayen, DNMI Klima Report No. 16, Norwegian Meteorological Institute, Oslo, Norway.

Norwegian Polar Institute (2014), Terrengmodell Svalbard (S0 Terrengmodell) [Data set].

Nowak, A., and A. Hodson (2013), Hydrological response of a High-Arctic catchment to changing climate over the past 35 years: a case study of Bayelva watershed, Svalbard, *Polar Res.* **32**, 19691, DOI: 10.3402/polar.v32i0.19691.

Nuth, C., J. Kohler, M. König, A. von Deschwanden, J.O. Hagen, A. Kääb, G. Moholdt, and R. Pettersson (2013), Decadal changes from a multi-temporal glacier inventory of Svalbard, *The Cryosphere* **7**, 1603–1621, DOI: 10.5194/tc-7-1603-2013.

Obleitner, F., and M. Lehning (2004), Measurement and simulation of snow and superimposed ice at the Kongsvegen glacier, Svalbard (Spitzbergen), *J. Geophys. Res. – Atmos.* **109**, D4, D04106, DOI: 10.1029/2003JD003945.

Oechel, W.C., and G.L. Vourlitis (1994), The effects of climate charge on land—atmosphere feedbacks in arctic tundra regions, *Trends Ecol. Evol.* **9**, 324–329, DOI: 10.1016/0169-5347(94)90152-X.

Ojrzyńska, H., M. Blaś, M. Kryza, M. Sobik, and G. Urban (2010), Znaczenie lasu oraz morfologii terenu w rozwoju pokrywy śnieżnej w Sudetach Zachodnich na przykladzie sezonu zimowego 2003-2004, *Sylwan* **154**, 6, 412–428 (in Polish).

Olech, M., M. Węgrzyn, M. Lisowska, A. Słaby, and P. Angiel (2011), Contemporary changes in vegetation of polar regions, *Pap. Global Change IGBP* **18**, 35–51, DOI: 10.2478/v10190-010-0003-8.

Opała-Owczarek, M., E. Pirożnikow, P. Owczarek, W. Szymański, B. Luks, D. Kępski, M. Szymanowski, B. Wojtuń, and K. Migała (2018), The influence of abiotic factors on the growth of two

vascular plant species (Saxifraga oppositifolia and Salix polaris) in the High Arctic, *CATENA* **163**, 219–232, DOI: 10.1016/j.catena.2017.12.018.

Osuch, M., and T. Wawrzyniak (2017), Variations and changes in snow depth at meteorological stations Barentsburg and Hornsund (Spitsbergen), *Ann. Glaciol.* **58**, 75pt1, 11–20, DOI: 10.1017/aog. 2017.20.

Osuch, M., B. Luks, and R. Romanowicz (2010), Stochastic transfer function modelling of snow depth at Polish Polar Station in Hornsund, Spitsbergen. **In:** *EGU General Assembly Conference Abstracts, 2–7 May 2010, Vienna, Austria*, p. 10392.

Owczarek, P. (2010a), Dendrochronological dating of geomorphic processes in the High Arctic, *Landform Anal.* **14**, 45–56.

Owczarek, P. (2010b), Talus cone activity recorded by tree-rings of Arctic dwarf shrubs: a study case from SW Spitsbergen, Norway, *Geologija* **52**, 1–4, 34–39, DOI: 10.2478/v10056-010-0003-3.

Owczarek, P., and M. Opała (2016), Dendrochronology and extreme pointer years in the tree-ring record (AD 1951–2011) of polar willow from southwestern Spitsbergen (Svalbard, Norway), *Geochronometria* **43**, 1, 84–95, DOI: 10.1515/geochr-2015-0035.

Påhlsson, L. (1985), *List of Vegetation Types and Land Forms in the Nordic Countries with the Plant Species of the Vegetation Types in Latin, the Nordic Languages and English*, Nordic Council of Ministers, 69 pp.

Park, T., S. Ganguly, H. Tømmervik, E.S. Euskirchen, K.-A. Høgda, S.R. Karlsen, V. Brovkin, R.R. Nemani, and R.B. Myneni (2016), Changes in growing season duration and productivity of northern vegetation inferred from long-term remote sensing data, *Environ. Res. Lett.* **11**, 8, 084001, DOI: 10.1088/1748-9326/11/8/084001.

Pebesma, E.J., and R.S. Bivand (2005), Classes and methods for spatial data in {R}, *R News* **5**, 2, 9–13, available from: https://cran.r-project.org/doc/Rnews/Rnews_2005-2.pdf.

Pereyma, J. (1981), Pokrywa śnieżna w rejonie Fiordu Hornsund na Spitsbergenie. **In:** *VII Sympozjum Polarne, Sosnowiec*, 7–20 (in Polish).

Pereyma, J. (1983), Climatological problems of the Hornsund area, Spitsbergen, *Acta Univ. Wratislav.* **714**, 134 pp.

Pereyma, J. (1988a), Climatology. **In:** *Results of Investigations of the Geographical Research Expedition Spitsbergen 1985*, Univerzita J.E. Purkyně.

Pereyma, J. (1988b), Termika pokrywy śnieżnej na tundrze w zlewni Fugleberget na Spitsbergenie. **In:** *XV Sympozjum Polarne*, 226–229 (in Polish).

Peterson, K.A., A. Arribas, H.T. Hewitt, A.B. Keen, D.J. Lea, and A.J. McLaren (2015), Assessing the forecast skill of Arctic sea ice extent in the GloSea4 seasonal prediction system, *Clim. Dynam.* **44**, 147–162, DOI: 10.1007/s00382-014-2190-9.

Pętlicki, M. (2012), Modelowanie bilansu masy i energii lodowca Arie na Spitsbergenie, PhD thesis, Instytut Geofizyki PAN, Warszawa (in Polish).

Pętlicki, M. (2016), High-resolution mapping of tidewater glaciers of Hornsund with Terrestrial Laser Scanning, Institute of Geophysics PAS/NORUT Northern Research Institute AS.

Phoenix, G.K., and J.W. Bjerke (2016), Arctic browning: extreme events and trends reversing arctic greening, *Glob. Change Biol.* **22**, 9, 2960–2962, DOI: 10.1111/gcb.13261.

Piechura, J., and W. Walczowski (2009), Warming of the West Spitsbergen Current and sea ice north of Svalbard, *Oceanologia* **51**, 2, 147–164, DOI: 10.5697/oc.51-2.147.

Pierce, D. (2017), ncdf4: Interface to Unidata netCDF (Version 4 or Earlier) Format Data Files, available from: https://CRAN.R-project.org/package=ncdf4.

Pohlert, T. (2021), PMCMRplus: Calculate Pairwise Multiple Comparisons of Mean Rank Sums Extended, available from: https://CRAN.R-project.org/package=PMCMRplus.

Pomeroy, J.W. (1989), A process-based model of snow drifting, *Ann. Glaciol.* **13**, 237–240, DOI: 10.3189/S0260305500007965.

Pomeroy, J.W. (1991), Transport and sublimation of snow in wind-scoured alpine terrain. **In:** *Proc. Symp. "Snow, Hydrology and Forests in High Alpine Areas", August 1991, Vienna, Austria*, IAHS Publ. no. 205, 131–140.

Pomeroy, J.W., and D.M. Gray (1995), Snowcover accumulation, relocation and management, *Bull. Int. Soc. Soil Sci.* **88**, 2, 144.

Pomeroy, J.W., and L. Li (2000), Prairie and arctic areal snow cover mass balance using a blowing snow model, *J. Geophys. Res. – Atmos.* **105**, D21, 26619–26634, DOI: 10.1029/2000JD900149.

Pomeroy, J.W., D.M. Gray, and P.G. Landine (1993), The Prairie Blowing Snow Model: characteristics, validation, operation, *J. Hydrol.* **144**, 1–4, 165–192, DOI: 10.1016/0022-1694(93)90171-5.

Pomeroy, J.W., P. Marsh, and D.M. Gray (1997), Application of a distributed blowing snow model to the Arctic, *Hydrol. Process.* **11**, 11, 1451–1464, DOI: 10.1002/(SICI)1099-1085(199709)11:11 <1451::AID-HYP449>3.0.CO;2-Q.

Promińska, A., M. Cisek, and W. Walczowski (2017), Kongsfjorden and Hornsund hydrography – comparative study based on a multiyear survey in fjords of west Spitsbergen, *Oceanologia* **59**, 4, 397–412, DOI: 10.1016/j.oceano.2017.07.003.

Pruim, R., D.T. Kaplan, and N.J. Horton (2017), The mosaic package: helping students to "Think with Data" using R, *The R J.* **9**, 1, 77–102, DOI: 10.32614/RJ-2017-024.

Przybylak, R. (2016), Air temperature. **In:** R. Przybylak (ed.), *The Climate of the Arctic*, Springer, Dordrecht, 127–136, DOI: 10.1007/978-3-319-21696-6_4.

Pulina, M. (1991), Stratification and physico-chemical properties of snow in Spitsbergen in the hydroglaciological year 1989/1990. **In:** *Wyprawy Geograficzne na Spitsbergen*, 191–213.

Putkonen, J. (1998), Soil thermal properties and heat transfer processes near Ny-Alesund, northwestern Spitsbergen, Svalbard, *Polar Res.* **17**, 2, 165–179, DOI: 10.3402/polar.v17i2.6617.

R Core Team (2018), R: A language and environment for statistical computing, R Foundation for Statistical Computing, Vienna, Austria.

Racoviteanu, A.E., F. Paul, B. Raup, S.J.S. Khalsa, and R. Armstrong (2009), Challenges and recommendations in mapping of glacier parameters from space: results of the 2008 Global Land Ice Measurements from Space (GLIMS) workshop, Boulder, Colorado, USA, *Ann. Glaciol.* **50**, 53, 53–69, DOI: 10.3189/172756410790595804.

Raderschall, N., M. Lehning, and C. Schär (2008), Fine-scale modeling of the boundary layer wind field over steep topography, *Water Resour. Res.* **44**, 9, W09425, DOI: 10.1029/2007WR006544.

Rahmstorf, S., J.E. Box, G. Feulner, M.E. Mann, A. Robinson, S. Rutherford, and E.J. Schaffernicht (2015), Exceptional twentieth-century slowdown in Atlantic Ocean overturning circulation, *Nat. Clim. Change* **5**, 475–480, DOI: 10.1038/nclimate2554.

Raschke, E., T.H. Vonderhaar, M. Pasternak, and W.R. Bandeen (1973), The radiation balance of the earth-atmosphere system from Nimbus 3 radiation measurements, Technical Note D-7249, NASA, Washington, 73 pp.

Raynolds, M.K., D.A. Walker, H.E. Epstein, J.E. Pinzon, and C.J. Tucker (2012), A new estimate of tundra-biome phytomass from trans-Arctic field data and AVHRR NDVI, *Remote Sens. Lett.* **3**, 5, 403–411, DOI: 10.1080/01431161.2011.609188.

Revuelto, J., J.I. López-Moreno, C. Azorin-Molina, and S.M. Vicente-Serrano (2014), Topographic control of snowpack distribution in a small catchment in the central Spanish Pyrenees: intra- and inter-annual persistence, *The Cryosphere* **8**, 1989–2006, DOI: 10.5194/tc-8-1989-2014.

Rhyner, H. (2018), Pyeongchang Snow – Snow and weather forecasts at the Olympics, available from: https://www.slf.ch/en/projects/show/pyeongchang.html.

Riahi, K., S. Rao, V. Krey, C. Cho, V. Chirkov, G. Fischer, G. Kindermann, N. Nakicenovic, and P. Rafaj (2011), RCP 8.5—A scenario of comparatively high greenhouse gas emissions, *Climatic Change* **109**, 33, 33–57, DOI: 10.1007/s10584-011-0149-y.

Riley, S.J. (1999), Index that quantifies topographic heterogeneity, *Intermt. J. Sci.* **5**, 23–27.

Rodzik, J. (1985), Ablacja pokrywy śnieżnej w Hornsundzie (05.-07.83), Spitsbergen, Akademia Rolnicza, Szczecin (in Polish).

Rønning, O.I. (1996), *The flora of Svalbard*, Norsk Polarinstitutt, Oslo, Norway, 184 pp.

Rouse, J.W., R.H. Haas, J.A. Schell, and D.W. Deering (1974), Monitoring vegetation systems in the Great Plains with ERTS. **In:** S.C. Freden, E.P. Mercanti, and M.A. Becker (eds.), *Third Earth Resources Technology Satellite – 1 Symposium, Dec. 10-14, 1973*, Vol. 1, Paper A20, NASA, Washington, DC, 309–317.

Rouse, W.R., M.S. Douglas, R.E. Hecky, A.E. Hershey, G.W. Kling, L. Lesack, P. Marsh, M. McDonald, B.J. Nicholson, and N.T. Roulet (1997), Effects of climate change on the freshwaters of arctic and subarctic North America, *Hydrol. Process.* **11**, 8, 873–902, DOI: 10.1002/(SICI)1099-1085(19970630)11:8<873::AID-HYP510>3.0.CO;2-6.

RStudio Team (2016), RStudio: Integrated Development for R. RStudio, RStudio, Inc., Boston, USA.

Ruckstuhl, C., R. Philipona, J. Morland, and A. Ohmura (2007), Observed relationship between surface specific humidity, integrated water vapor, and longwave downward radiation at different altitudes, *J. Geophys. Res.* **112**, D3, D03302, DOI: 10.1029/2006JD007850.

Rudowski, S., and A. Marsz (1996), Cechy rzeźby dna i pokrywy osadowe we współcześnie kształtujących się fiordach na przykładzie Hornsundu (Spitsbergen) oraz Zatoki Admiralicji (Antarktyka Zachodnia), *Prace Wydziału Nawigacyjnego WSM w Gdyni* **3**, 39–81 (in Polish).

Salvatori, R., P. Plini, M. Giusto, M. Valt, R. Salzano, M. Montagnoli, A. Cagnati, G. Crepaz, and D. Sigismondi (2011), Snow cover monitoring with images from digital camera systems, *Ital. J. Remote Sens.* **43**, 2, 137–145, DOI: 10.5721/ItJRS201143211.

Schlögl, S., C. Marty, M. Bavay, and M. Lehning (2016), Sensitivity of Alpine3D modeled snow cover to modifications in DEM resolution, station coverage and meteorological input quantities, *Environ. Modell. Softw.* **83**, 387–396, DOI: 10.1016/j.envsoft.2016.02.017.

Schlögl, S., M. Lehning, K. Nishimura, H. Huwald, N.J. Cullen, and R. Mott (2017), How do stability corrections perform in the stable boundary layer over snow?, *Bound.-Layer Meteorol.* **165**, 161–180, DOI: 10.1007/s10546-017-0262-1.

Schmidt, R.A. (1982), Vertical profiles of wind speed, snow concentration, and humidity in blowing snow, *Bound.-Layer Meteorol.* **23**, 223–246, DOI: 10.1007/BF00123299.

Semenchuk, P.R., M.A.K. Gillespie, S.B. Rumpf, N. Baggesen, B. Elberling, and E.J. Cooper (2016), High Arctic plant phenology is determined by snowmelt patterns but duration of phenological periods is fixed: an example of periodicity, *Environ. Res. Lett.* **11**, 12, 125006, DOI: 10.1088/1748-9326/11/12/125006.

Serreze, M.C., and J.A. Francis (2006), The Arctic amplification debate, *Climatic Change* **76**, 241–264, DOI: 10.1007/s10584-005-9017-y.

Sibandze, P., P. Mhangara, J. Odindi, and M. Kganyago (2014), A comparison of Normalised Difference Snow Index (NDSI) and Normalised Difference Principal Component Snow Index (NDPCSI) techniques in distinguishing snow from related land cover types, *S. Afr. J. Geomat.* **3**, 2, 197, DOI: 10.4314/sajg.v3i2.6.

Sicart, J.E., J.W. Pomeroy, R.L.H. Essery, and D. Bewley (2006), Incoming longwave radiation to melting snow: observations, sensitivity and estimation in Northern environments, *Hydrol. Process.* **20**, 17, 3697–3708, DOI: 10.1002/hyp.6383.

Sievert, C., C. Parmer, T. Hocking, S. Chamberlain, K. Ram, M. Corvellec, and P. Despouy (2017), plotly: Create Interactive Web Graphics via "plotly.js," *R Package Version*. **4**, 1, 110.

Skrzypek, G., B. Wojtuń, D. Richter, D. Jakubas, K. Wojczulanis-Jakubas, and A. Samecka-Cymerman (2015), Diversification of nitrogen sources in various tundra vegetation types in the High Arctic, *PLOS ONE* **10**, 9, e0136536, DOI: 10.1371/journal.pone.0136536.

Sommerfeld, R.A., and E. LaChapelle (1970), The classification of snow metamorphism, *J. Glaciol.* **9**, 55, 3–18, DOI: 10.3189/S0022143000026757.

Stanton, M.L., M. Rejmanek, and C. Galen (1994), Changes in vegetation and soil fertility along a predictable snowmelt gradient in the Mosquito Range, Colorado, USA, *Arctic Alpine Res.* **26**, 4, 364–374, DOI: 10.2307/1551798.

Stearns, C.R., and G.A. Weidner (1993), Sensible and latent heat flux estimates in Antarctica. **In:** D.H. Bromwich and C.R. Stearns (eds.), *Antarctic Meteorology and Climatology: Studies Based on Automatic Weather Stations*, Vol. 61, Antarctic Research Series, American Geophysical Union, Washington, D.C., 109–138, DOI: 10.1029/AR061p0109.

Stocker, T.F., D. Qin, G.K. Plattner, M.M.B. Tignor, S.K. Allen, J. Boschung, A.Nauels, Y. Xia, V. Bex, and P.M. Midgey (2013), Summary for policymakers. **In:** *Climate Change 2013: The Physical Science Basis. Contribution of Working Group I to the Fifth Assessment Report of the Intergovernmental Panel on Climate Change*, Cambridge University Press, Cambridge, UK / New York, USA, 3–29.

Strzelecki, M.C., M. Kasprzak, M. Lim, Z.M. Swirad, M. Jaskólski, Ł. Pawłowski, and P. Modzel (2017), Cryo-conditioned rocky coast systems: A case study from Wilczekodden, Svalbard, *Sci. Total Environ.* **607–608**, 443–453, DOI: 10.1016/j.scitotenv.2017.07.009.

Sturm, M., and J. Holmgren (1994), Effects of microtopography on texture, temperature and heat flow in Arctic and sub-Arctic snow, *Ann. Glaciol.* **19**, 63–68, DOI: 10.3189/1994AoG19-1-63-68.

Sturm, M., and G.E. Liston (2003), The snow cover on lakes of the Arctic Coastal Plain of Alaska, USA, *J. Glaciol.* **49**, 166, 370–380, DOI: 10.3189/172756503781830539.

Sturm, M., J. Holmgren, and G.E. Liston (1995), A seasonal snow cover classification system for local to global applications, *J. Climate* **8**, 5, 1261–1283, DOI: 10.1175/1520-0442(1995)008<1261: ASSCCS>2.0.CO;2.

Styszyńska, A. (2011), Wpływ zmian temperatury wody powierzchniowej mórz Barentsa, Norweskiego i Grenlandzkiego na trend rocznej temperatury powietrza na Spitsbergenie, *Probl. Klimatol. Polar.* **21**, 115–131 (in Polish).

Swerpel, S. (1985), The Hornsund fiord: water masses, *Pol. Polar Res.* **6**, 4, 475-496.

Szymański, W., S. Skiba, and B. Wojtuń (2013), Distribution, genesis, and properties of Arctic soils: a case study from the Fuglebekken catchment, Spitsbergen, *Pol. Polar Res.* **34**, 3, 289–304, DOI: 10.2478/popore-2013-0017.

Teillet, P.M., and G. Fedosejevs (1995), On the dark target approach to atmospheric correction of remotely sensed data, *Can. J. Remote Sens.* **21**, 4, 374–387, DOI: 10.1080/07038992.1995. 10855161.

Tennekes, M. (2017), treemap: Treemap Visualization., available from: https://CRAN.R-project.org/package=treemap

Tomaselli, M. (1991), The snow-bed vegetation in the Northern Apennines, *Vegetatio* **94**, 177–189, DOI: 10.1007/BF00032630.

Traczyk, A., and M. Kasprzak (2008), Geomorfologia rejonu Revdalen a warunki topoklimatyczne. **In:** *Warsztaty Projektów Badawczych Specjalnych MNiSZW TOPOCLIM, GLACIODYN, KINVIKA, POLARCAT Międzynarodowego Roku Polarnego 2007-2008*, Uniwersytet

Troitskiy, L.S., A.S. Guskov, N.I. Osokin, and V.G. Hodokov (1980), Issledovanija seezhnogo pokrova na Shpitzbergene vesnoi 1979 [Snow cover investigation on Spitsbergen during spring 1979], *Mater. Glyatsiolog. Issled. [Data Glaciol. Stud.]* **39**, 185–192 (in Russian).

Tseng, P.-H., T.H. Illangasekare, and M.F. Meier (1994), Modeling of snow melting and uniform wetting front migration in a layered subfreezing snowpack, *Water Resour. Res.* **30**, 8, 2363–2376, DOI: 10.1029/94WR00764.

USGS (2016), LANDSAT Data Users Handbook 8 Version 2.0, available from: https://landsat.usgs.gov/sites/default/files/documents/Landsat8DataUsersHandbook.pdf.

van Pelt, W.J.J., J. Kohler, G.E. Liston, J.O. Hagen, B. Luks, C.H. Reijmer, and V.A. Pohjola (2016), Multidecadal climate and seasonal snow conditions in Svalbard:, *J. Geophys. Res. – Earth Surf.* **121**, 11, 2100–2117, DOI: 10.1002/ 2016JF003999.

Van Ulden, A.P., and A.A.M. Holtslag (1985), Estimation of atmospheric boundary layer parameters for diffusion applications, *J. Appl. Meteorol. Climatol.* **24**, 11, 1196–1207, DOI: 10.1175/1520-0450(1985)024<1196:EOABLP>2.0.CO;2.

Vestergren, T. (1902), Om den olikformiga snöbetäkningens inflytande på vegetationen i Sarekfjällen, *Bot. Notiser* **1902**, 241–268 (in Swedish).

Vickers, H., K.A. Høgda, S. Solbø, S.R. Karlsen, H. Tømmervik, R. Aanes, and B.B. Hansen (2016), Changes in greening in the high Arctic: insights from a 30 year AVHRR max NDVI dataset for Svalbard, *Environ. Res. Lett.* **11**, 10, 105004, DOI: 10.1088/1748-9326/11/10/105004.

Vionnet, V., E. Martin, V. Masson, G. Guyomarc'h, F. Naaim-Bouvet, A. Prokop, Y. Durand, and C. Lac (2014), Simulation of wind-induced snow transport and sublimation in alpine terrain using a fully coupled snowpack/atmosphere model, *The Cryosphere* **8**, 2, 395–415, DOI: 10.5194/tc-8-395-2014.

Viviroli, D., M. Zappa, J. Gurtz, and R. Weingartner (2009), An introduction to the hydrological modelling system PREVAH and its pre- and post-processing-tools, *Environ. Modell. Softw.* **24**, 10, 1209–1222, DOI: 10.1016/j.envsoft.2009.04.001.

Vogel, S.W. (2002), Usage of high-resolution Landsat 7 band 8 for single-band snow-cover classification, *Ann. Glaciol.* **34**, 53–57, DOI: 10.3189/172756402781818058.

Vovinckel, E., and S. Orvig (1973), Klimat Arkticheskogo baseyna. **In:** *Klimat Polarnykh Reyonov*, Gidrometeoizdat, Leningrad, 170–317 (in Russian).

Wahren, C.-H.A., M.D. Walker, and M.S. Bret-Harte (2005), Vegetation responses in Alaskan arctic tundra after 8 years of a summer warming and winter snow manipulation experiment, *Global Change Biol.* **11**, 4, 537–552, DOI: 10.1111/j.1365-2486.2005.00927.x.

Walczowski, W., and J. Piechura (2011), Influence of the West Spitsbergen Current on the local climate, *Int. J. Climatol.* **31**, 7, 1088–1093, DOI: 10.1002/joc.2338.

Walker, D.A. (1985), Vegetation and environmental gradients of the Prudhoe Bay region, Alaska, CRREL Report 85-14, US Army Cold Regions Research and Engineering Laboratory, Hanover, NH, 240 pp.

Walker, D.A., E. Binnian, B.M. Evans, N.D. Lederer, E. Nordstrand, and P.J. Webber (1989), Terrain, vegetation and landscape evolution of the R4D research site, Brooks Range Foothills, Alaska, *Ecography* **12**, 3, 238–261, DOI: 10.1111/j.1600-0587.1989.tb00844.x.

Walker, D.A., W.D. Billings, and J.G. De Molenaar (2001), Snow-vegetation interactions in tundra environments. **In:** H.G. Jones, J.W. Pomeroy, D.A. Walker, and R.W. Hoham (eds.), *Snow Ecology: An Interdisciplinary Examination of Snow-Covered Ecosystems*, Cambridge University Press, New York, 266–324.

Walker, M.D. (1990), *Vegetation and Floristics of Pingos, Central Arctic Coastal Plain, Alaska*, Dissertationes Botanicae, Vol. 149, Berlin, Germany, 283 pp..

Walker, M.D., D.A. Walker, J.M. Welker, A.M. Arft, T. Bardsley, P.D. Brooks, J.T. Fahnestock, M.H. Jones, M. Losleben, A.N. Parsons, T.R. Seastedt, and P.L. Turner (1999), Long-term experimental manipulation of winter snow regime and summer temperature in arctic and alpine tundra, *Hydrol. Process.* **13**, 14–15, 2315–2330, DOI: 10.1002/(SICI)1099-1085(199910)13:14/15<2315::AID-HYP888>3.0.CO;2-A.

Walker, M.D., C.H. Wahren, R.D. Hollister, G.H.R. Henry, L.E. Ahlquist, J.M. Alatalo, M.S. Bret-Harte, M.P. Calef, T.V. Callaghan, A.B. Carroll et al. (2006), Plant community responses to experimental warming across the tundra biome, *Proc. Nat Acad Sci* **103**, 5, 1342–1346, DOI: 10.1073/pnas.0503198103.

Wang, M., and J.E. Overland (2004), Detecting Arctic climate change using Köppen climate classification, *Climatic Change* **67**, 43–62, DOI: 10.1007/s10584-004-4786-2.

Wawrzyniak, T., M. Osuch, J. Napiórkowski, and S. Westermann (2016), Modelling of the thermal regime of permafrost during 1990–2014 in Hornsund, Svalbard, *Pol. Polar Res.* **37**, DOI: 10.1515/popore-2016-0013.

Wei, T., and V. Simko (2017), R package "corrplot": Visualization of a Correlation Matrix, available from: 1https://github.com/taiyun/corrplot

Wei, T., M. Ding, B. Wu, C. Lu, and S. Wang (2016), Variations in temperature-related extreme events (1975-2014) in Ny-Ålesund, Svalbard, *Atmos. Sci. Lett.* **17**, 1, 102–108, DOI: 10.1002/asl.632.

Westermann, S., J. Boike, M. Guglielmin, K. Gisnås, and B. Etzelmüller (2015), Snow melt monitoring near Ny-Ålesund, Svalbard, using Automatic Camera Systems, University of Oslo, Department of Geosciences, DOI: 10.1594/PANGAEA.846617.

Wickham, H., M. Averick, J. Bryan, W. Chang, L. McGowan, R. François, G. Grolemund, A. Hayes, L. Henry, J. Hester et al. (2019), Welcome to the Tidyverse, *JOSS* **4**, 43, 1686, DOI: 10.21105/joss.01686.

Williams, C.J., J.P. McNamara, and D.G. Chandler (2009), Controls on the temporal and spatial variability of soil moisture in a mountainous landscape: the signature of snow and complex terrain, *Hydrol. Earth Syst. Sci.* **13**, 7, 1325–1336, DOI: 10.5194/hess-13-1325-2009.

Williams, M., E.B. Rastetter, G.R. Shaver, J.E. Hobbie, E. Carpino, and B.L. Kwiatkowski (2001), Primary production of an arctic watershed: an uncertainty analysis, *Ecol. Appl.* **11**, 6, 1800–1816, DOI: 10.1890/1051-0761(2001)011[1800:PPOAAW]2.0.CO;2.

Williamson, D.F., R.A. Parker, and J.S. Kendrick (1989), The box plot: a simple visual method to interpret data, *Ann. Intern. Med.* **110**, 11, 916–921, DOI: 10.7326/0003-4819-110-11-916.

Winther, J.-G., O. Bruland, K. Sand, å Killingtveit, and D. Marechal (1998), Snow accumulation distribution on Spitsbergen, Svalbard, in 1997, *Polar Res.* **17**, 2, 155–164, DOI: 10.3402/polar.v17i2.6616.

Winther, J.-G., O. Bruland, K. Sand, S. Gerland, D. Marechal, B. Ivanov, P. Gøowacki, and M. König (2003), Snow research in Svalbard—an overview, *Polar Res.* **22**, 2, 125–144, DOI: 10.3402/polar.v22i2.6451.

Wipf, S. (2010), Phenology, growth, and fecundity of eight subarctic tundra species in response to snowmelt manipulations, *Plant Ecol.* **207**, 53–66, DOI: 10.1007/s11258-009-9653-9.

Wojciechowska, A., A. Zwolicki, A. Barcikowski, and L. Stempniewicz (2015), The structure of Cochlearia groenlandica population along the bird colony influence gradient (Hornsund, Spitsbergen), *Polar Biol.* **38**, 1919–1930, DOI: 10.1007/s00300-015-1755-3.

Wojtuń, B., A. Samecka-Cymerman, K. Kolon, A.J. Kempers, and G. Skrzypek (2013), Metals in some dominant vascular plants, mosses, lichens, algae, and the biological soil crust in various types of terrestrial tundra, SW Spitsbergen, Norway, *Polar Biol.* **36**, 1799–1809, DOI: 10.1007/s00300-013-1399-0.

WRB Group (2014), World reference base for soil resources 2014 international soil classification system for naming soils and creating legends for soil maps, Food and Agriculture Organization of the United Nations.

Xiao, X., B. Moore, X. Qin, Z. Shen, and S. Boles (2002), Large-scale observations of alpine snow and ice cover in Asia: Using multi-temporal VEGETATION sensor data, *Int. J. Remote Sens.* **23**, 11, 2213–2228, DOI: 10.1080/01431160110076180.

Xue, M., K.K. Droegemeier, and V. Wong (2000), The Advanced Regional Prediction System (ARPS)–A multi-scale nonhydrostatic atmospheric simulation and prediction model. Part I: Model dynamics and verification, *Meteorol. Atmos. Phys.* **75**, 161–193, DOI: 10.1007/s007030070003.

Xue, M., K.K. Droegemeier, V. Wong, A. Shapiro, K. Brewster, F. Carr, D. Weber, Y. Liu, and D. Wang (2001), The Advanced Regional Prediction System (ARPS) – A multi-scale nonhydrostatic atmospheric simulation and prediction tool. Part II: Model physics and applications, *Meteorol. Atmos. Phys.* **76**, 143–165, DOI: 10.1007/s007030170027.

Zdanowicz, C. (2015), Trends in snow research in Svalbard: A look back over the past ~25 years. **In:** *Taking The Next Step In Svalbard Snow Research, Svalbard Science Forum Workshop, 1–4 September 2015, Sosnowiec.*

Zhang, T. (2005), Influence of the seasonal snow cover on the ground thermal regime: An overview, *Rev. Geophys.* **43**, 4, RG4002, DOI: 10.1029/2004RG000157.

Zhu, Z., and C.E. Woodcock (2012), Object-based cloud and cloud shadow detection in Landsat imagery, *Remote Sens. Environ.* **118**, 83–94, DOI: 10.1016/j.rse.2011.10.028.

Zhu, Z., S. Wang, and C.E. Woodcock (2015), Improvement and expansion of the Fmask algorithm: cloud, cloud shadow, and snow detection for Landsats 4–7, 8, and Sentinel 2 images, *Remote Sens. Environ.* **159**, 269–277, DOI: 10.1016/j.rse.2014.12.014.

Ziaja, W., M. Węgrzyn, M. Lisowska, M. Olech, and P. Osyczka (2016), Conclusions and prognosis for environmental change. **In:** W. Ziaja (ed.), *Transformation of the Natural Environment in Western Sørkapp Land (Spitsbergen) Since the 1980s*, Springer International Publishing, Cham, 75–78.

Zuzel, J.F., and L.M. Cox (1975), Relative importance of meteorological variables in snowmelt, *Water Resour. Res.* **11**, 1, 174–176, DOI: 10.1029/WR011i001p00174.

Zwolicki, A., K.M. Zmudczyńska-Skarbek, L. Iliszko, and L. Stempniewicz (2013), Guano deposition and nutrient enrichment in the vicinity of planktivorous and piscivorous seabird colonies in Spitsbergen, *Polar Biol.* **36**, 363–372, DOI: 10.1007/s00300-012-1265-5.

Zwoliński, Z., J. Giżejewski, A. Karczewski, M. Kasprzak, K.R. Lankauf, P. Migoń, K. Pękala, J. Repelewska-Pękalowa, G. Rachlewicz, I. Sobota, W. Stankowski, and P. Zagórski (2013), Geomorphological settings of Polish research areas on Spitsbergen, *Landform Anal.* **22**, 125-143, DOI: 10.12657/landfana.022.011.

Żarnowiecki, G. (2008), *Związek Pomiędzy Pokrywą Śnieżną a Roślinnością na Przykładzie Grądów Białowieskiego Parku Narodowego*, Prace Geograficzne 216, IGiPZ PAN., Warszawa, 215 pp. (in Polish)

Received 1 December 2021
Received in revised form 28 December 2021
Accepted 31 December 2021

"Publications of the Institute of Geophysics, Polish Academy of Sciences: Geophysical Data Bases, Processing and Instrumentation" appears in the following series:

A – Physics of the Earth's Interior

B – Seismology

C – Geomagnetism

D – Physics of the Atmosphere

E – Hydrology (formerly Water Resources)

P – Polar Research

M – Miscellanea

Every volume has two numbers: the first one is the consecutive number of the journal and the second one (in brackets) is the current number in the series.